IFSix - In-flight Simulator

Design the modifications to convert a small business aircraft into a advanced low-cost in-flight simulator, by 10 students in 10 weeks.

T.J.P. Bregt	4106121	W.P. den Ouden	4205618
J.M. Eppink	4290429	A. Pardi	4297083
L. Gooijaers	4096800	K. van Rest	4205758
M.J.J. Linssen	4141830	R.R.M. Schildkamp	4079663
L.P.L. Mac An Bhaird	4048660	V.F. Wilod Versprille	4223675

Final Report

Design Synthesis Exercise

TU Delft Delft University of Technology

Aerospace Engineering

25 January 2017

Revision History

Date	Version	Description	Notes
23/01/2017	0.9	Initial draft	
25/01/2017	1.0	First version	
31/01/2017	1.1	Revision	Feedback from tutors implemented. Additions: section 14.4. Modifications: sections 4.2, 4.3, 4.4, 5.3, 9.4, 9.5, 10.2, Symbols and Acronyms.

Preface

This report presents the final design for the Design Synthesis Exercise of a Modern Electrically Actuated In-Flight Simulator. This project is the final part of the bachelor programme as taught at the faculty of Aerospace Engineering at Delft University of Technology. The Design Synthesis Exercise is a highly valued project by the aerospace students, staff and industry because of its reflection of a real-life design problem as encountered at later stages of the studies or career. The project challenges a group of 10 students to think outside of the box and present innovative solutions to current problems in the aerospace section within a 10 week lasting project. All disciplines that are taught in the bachelor programme will be dealt with during the Design Synthesis Exercise, so it can be regarded as a final wrap-up of the complete aerospace bachelor.

This report is the final report in a series of four reports that describe the design process. In this report the focus is laid upon the detailed design phase for the in-flight simulator. The analyses that were performed to verify and validate the final design will be presented, as well as the post-DSE plan on how to operate and maintain the IFS.

We would like to thank our tutor dr.ir. M.M. van Paassen and our coaches MSc. S.S. Mestry and dr. F. Oliviero for their regular support during the Design Synthesis Exercise and helpful feedback on the design procedure. We also would like to thank the OSCC for their assistance during the project management & systems engineering workshops.

T.J.P. Bregt	4106121
J.M. Eppink	4290429
L. Gooijaers	4096800
M.J.J. Linssen	4141830
L.P.L. Mac An Bhaird	4048660
W.P. den Ouden	4205618
A. Pardi	4297083
K. van Rest	4205758
R.R.M. Schildkamp	4079663
V.F. Wilod Versprille	4223675

Delft, 25 January 2017

Contents

List of Figures

List of Tables

Acronyms and symbols

Acronym	Meaning
A/C	Aircraft
ACS	Aircraft Control System
AoA	Angle of Attack
APU	Auxiliary Power Unit
AVL	Athena Vortex Lattice
BEW	Basic Empty Weight
BFL	Balanced Field Length
CBS	Cost Break-down Structure
CFD	Computational Fluid Dynamics
CG	Center of Gravity
COTS	Commercial Off-The-Shelf
DOF	Degrees Of Freedom
ECEF	Earth-centered, Earth-fixed
EOM	Equation of Motion
FBD	Free Body Diagram
FBS	Functional Breakdown Structure
FBW	Fly-By-Wire
FCS	Flight Control System
FFBD	Functional Flow Block Diagram
FOR	Frame Of Reference
GPS	Global Positioning System
HLD	High-Lift Device
IFS	In-Flight Simulator
L/D	Lift over Drag
MAC	Mean Aerodynamic Chord
MFW	Maximum Fuel Weight
MIT	Massachussets Institute of Technology
MLW	Maximum Landing Weight
MSL	Mean Sea Level
MTBF	Mean Time Between Failures
MTOW	Maximum Take-Off Weight
MTTF	Mean Time To Failure
MTTM	Mean Time To Maintenance
NACA	National Advisory Committee for Aeronautics
NASA	National Aeronautics and Space Administration
PDD	Project Design & Development
RAMS	Reliability, Availability, Maintainability and Safety
S&C	Stability and Control
SCS	Simulation Control System
SPWS	Stall Protection and Warning System
STA	Shuttle Training Aircraft

Acronym	Meaning
TBD	To Be Defined
V&V	Verification and Validation
VLM	Vortice Lattice Method
WBS	Work Breakdown Structure

Symbol	Name	Unit/Value
A	aspect ratio	-
C_l	2D lift coefficient	-
C_d	2D drag coefficient	-
C_L	3D lift coefficient	-
C_D	3D drag coefficient	-
D	drag force	N
e	Oswald efficiency factor	-
g_0	gravitational acceleration	9.81 m/s^2
GB	gigabyte	10^9 bytes
H_h	height of horizontal tail	m
H_v	height of vertical tail	m
Hz	Hertz	1/s
L	lift force	N
M	Mach number	-
N_z	ultimate load factor	-
p	pressure	N/m^2
q	dynamic pressure	N/m^2
S	wing surface	m^2
S_v	vertical fin surface	m^2
V	airspeed	m/s
W_g	flight design gross weight	N
α	angle of attack	degrees
β	angle of sideslip	degrees
Δ	variation	-
Λ	sweep angle	degrees
λ	taper ratio	-
ρ	density	kg/m^3
€	Euro currency	-
$	U.S. dollar currency	-
x_{cg}	centre of gravity position	m
x_{mw}	main wing aerodynamic centre position	m
x_{uw}	upper wing aerodynamic centre position	m
x_h	horizontal tail aerodynamic centre position	m

Summary

An In-Flight Simulator is an aircraft with additional systems and control surfaces that is able to mimic the handling characteristics of other aircraft. Currently, the best product the market for in-flight simulation has to offer is a five degrees of freedom jet-powered IFS or a six degrees of freedom propeller IFS. A jet-powered IFS with six degrees of freedom would fill up the gap in the current IFS-market. This design provides a wider variety of test possibilities than currently available and will therefore be a viable product. The goal of this project is to modify and redesign a business-jet to a six degrees of freedom IFS.

The detailed design of the IFS is performed in this report, based on the final conceptual design. The supposed solution consists of attaching an interconnected vertical and horizontal wing to the main wing and engine nacelle. By doing this, a so-called boxwing is formed. The design itself is based on several requirements with respect to the performance of the IFS, while other aspects such as risk assessment, the operational life of the aircraft and potential market share are extensively analyzed. The shape of the boxwing was first determined based on the forces that it has to produce and the constraints with respect to the original aircraft, the Embraer Phenom 300. The parameters coming from this analysis such as airfoil shape and sweep, served as an input for any further calculations. An aerodynamic analysis was performed that calculated the aerodynamic polars and stability derivatives of the converted aircraft using a numerical Vortex Lattice Method. The structural layout of the boxwing was designed by determining detailed parameters for the boxwing wingbox and its the connections to the aircraft. These parameters included for example cross-sectional area and number of ribs as well as center of gravity locations. These center of gravity locations and the stability derivatives from the aerodynamic analysis were used for the stability & control analysis. This evaluation involved checking the longitudinal and lateral stability of the IFS, checking the center of gravity range, doing calculations on the influence of the added control surfaces for the different simulation types as well as providing equations of motion to describe the aircraft attitude in order to process the data gathered during the simulation flights. Since the aerodynamic, structural and stability & control analyses are highly dependant on their respective outcomes, the input and outputs of each domain were continuously adjusted until the results converged to an optimum solution. This optimum solution was analyzed by means of a sensitivity analysis. Apart from the boxwing itself, additional subsystems such as the Simulation Control System and actuators were designed. Block diagrams showing the architecture of a number of subsytems such as the data-handling system and electrical system were also created. Besides the technical designs, several non-technical aspects were worked out in detail as well. For instance, a design & development plan was made in order to give direction to the trajectory of the project after the detailed design has been finished. A cost-breakdown has been made in combination with a market analysis to verify whether the IFS has a high chance of becoming a profitable investment. This chance was increased by performing a risk assessment, where after the most eminent risks where mitigated. At last, the complete set of requirements originating from the stakeholder analysis was evaluated based on the outcomes on the detailed design and thereby validation of our design was performed.

As discussed in the previous paragraph, the final design consists of the addition of a vertical and a horizontal wing to the aircraft along with a drag parachute in order to mimic other aircraft as well as having the ability of reaching a lift-over-drag ratio of 4. The upper wing will have a sweep angle of -28 degrees, a span of 3.54 m, a mass of 77.2 kg and is defined by the geometry of the NACA0012 airfoil. Two trailing edge flaps with a chord of 0.62 m will be added to provide direct lift control. The vertical wing will have no sweep due to the sweep, a span of 0.96 m, a mass of 15.1 kg and an airfoil profile of the NACA0008. It will feature a single flap at the trailing edge with a chord of 0.5 m. The flaps on both additional wings will have maximum deflection of 20 degrees in both directions and are operated with torsional actuators. Each wing will have a total chord length of 1.34 m, preventing the structural complexity of taper. Low resistance hinges are used to connect these wings to both each other and the aircraft. The vertical wing is attached on the wingbox of the main wing between the aileron and the outer flap. The horizontal wing is attached to the engine nacelle. By making use of hinges the deflection of the main wing is not introducing loads in the boxwing structure. The drag chute will have an area of 3.85 m^2 and has a mass of 6.5 kg. The right side of the cockpit of the IFS will contain a test pilot station, equipped with force feedback controls. In the cabin a test engineer will be placed, equipped with a simulation control panel and monitoring screens. These display both ACS data and data from additional sensors. An SCS will run the simulation and includes a safety trip system to restore the unmodified controls of the safety pilot in case of failure. An overview of the whole system is given using diagrams on hardware, software, data handling and the electric systems.

1 Introduction

An In-Flight Simulator consists of an existing aircraft that is modified to have variable control and stability characteristics. With variable control and stability, the handling qualities and flying experience of other aircraft can be mimicked. An IFS can be used to train or test pilots, or to simulate a new aircraft with new or experimental flight characteristics. Currently, there are a few IFS in use. The most advanced IFS are either a six degree of freedom piston-driven aircraft or a jet-powered aircraft with five degrees of freedom[1]. A new jet-powered model with control over six degrees of freedom would allow for a much larger flight envelope, providing a much wider variety of test possibilities.

The design of the IFS consists of an Embraer Phenom 300 with additional wings, additional control surfaces and a drag parachute to obtain the six degrees of freedom variable stability. The purpose of this report is to present a detailed design of the IFS and show to the stakeholders that the design is indeed feasible. The concept that was chosen in the conceptual phase has been worked out in detail with the emphasis on four domains; aerodynamics, structural integrity, stability & control and actuation of the system. Furthermore it provides the basis for the Final Review and the Symposium. This report was preceded by the Project Plan [8], the Baseline Report [9] and the Mid-Term Report [10]. These reports describe the group and project organization, project approach, design option trees, aircraft trade-off and conceptual design. Several aspects of the previous reports have been updated and integrated in this report as more in-depth knowledge is gathered on each topic.

The report will start off with a more in-depth market analyses following from a deeper understanding of the IFS. This can be found in chapter 2. Chapter 3 holds the sustainable development strategy. This strategy aims to reduce the impact of the IFS on the environment as much as possible by keeping sustainability in mind for each phase of the design process. The following 4 contains the FFBD, the FBS as well as resource allocation and an approach to the systems engineering. In chapter 5 the general configuration of the boxwing design is presented. This includes the sizing and airfoil selection for the horizontal and vertical wing of the boxwing, but also sizing of the drag parachute and spoilers. Once the configuration was known, several analyses in different domains were performed. Chapter 6 shows the findings of the aerodynamic analysis of the IFS. The aircraft was modelled in a program and analyzed on aerodynamic characteristics using the Vortex Lattice Method. This resulted in aerodynamic polars and stability derivatives, which were used in chapter 7. This chapter assesses the stability & control characteristics of the IFS, such as center of gravity range, longitudinal stability, lateral stability and the equations of motion that can describe the behaviour of the aircraft in normal and simulated flight. Chapter 8 consists of the structural analysis of the boxwing. The dimensions and shape of the wings were already set, however the structure itself is still undefined. Therefore a wingbox was designed for the upper and vertical wing. This wingbox ensures that the wings will not collapse under the aerodynamic loading they create. Furthermore the attachment points of the boxwing to the original aircraft were designed. In chapter 9 the way in which the aircraft is controlled and how the system functions is described. This includes all the additional hardware, sensors, the functioning of the safety control system, the new layout of the cockpit and several sub-systems. Chapter 10 shows the system characteristics of the design along with the configuration & layout of the IFS. After that, chapter 11 will elaborate on the operations & logistics of the IFS. For example, procedures for aircraft relocation and manufacture and assembly plans are elaborated upon. In chapter 12 a cost analysis is made based on a top-down and bottom-up approach. After that the findings of the sensitivity analysis and technical risk assessment are presented in chapter 13 and chapter 14 respectively. Now the design is fully determined, it is important to check whether the design meets all the requirements. Therefore a compliance matrix is constructed, which can be found in chapter 15. The report is finalized with a conslusion in chapter 17 and appendices A, B, C containing the stability and control derivatives, the structural loading diagrams and the work distribution respectively.

[1] http://www.in-flightsimulation.com/ [cited 24 January 2017]

2 | Market Analysis

This chapter features a full description of the market situation that the final product will encounter on introduction. It will elaborate on the market analysis presented in the Baseline Report [9]. First a short description on the history of in flight simulation is given in section 2.1 after which a target market is indicated in section 2.2. From this target market the costumer base is extracted on which also the market size for the newly designed IFS is estimated, complying to block *1.9 Design for marketing* in the FBS. After having investigated the potential competition in section 2.3, a market projection is presented in section 2.4 for both the developing company selling the IFS and the customer that operates the aircraft and lends it to the end-users. Finally, also a recap on the different stakeholders is presented in section 2.5.

2.1 Industry description

The industry of in-flight simulation is a specific one. With respect to ground-based simulators, In-Flight Simulators (IFS) have higher costs when it comes to the purchase, operations, maintenance and certification. Though, the facilitation of experiencing the simulation of an aircraft whilst flying under real conditions in real time is unmatched by any other simulator. The in-flight simulation market started in 1947 with the erection of the Calspan Corporation and their first flight in 1949 [6]. In-flight simulation became more realistic by adding more degrees of freedom to existing aircraft through installing extra control surfaces. In 1968 the first in-flight simulator with a six Degree Of Freedom (DOF) control was taken into service, making it possible to simulate forces in all directions and moments around all axes. This aircraft was taken out of service in 2008. Since then no other in-flight simulators with six DOF have been introduced to the market and only in-flight simulators with five degrees of freedom are flying around. The current flight simulator market size is estimated at $ 6.18 billions. The market for in-flight simulators is only a small part of the total simulation market [10], but the total simulation market has an expected growth of 4% per year over the upcoming five years. [1]

2.2 Target market

First of all, the prospects for the IFS market in general are positive. As seen in section 2.1, the overall simulator industry is expected to grow steadily. Within this simulator industry, the need for more advanced in-flight simulators is expected to grow even more. The reason for this expected growth is twofold. Firstly, the technology of in-flight simulation is becoming more and more accessible to a widespread range of companies due to technological advances in in-flight simulation. Secondly, companies developing aircraft are developing more and more complex aircraft and aircraft systems that will implicitly require more complicated in-flight simulator systems as well. Within this growing in-flight simulator market there are two main market segments to be distinguished:

- **Segment 1 - high quality simulation for new aerial vehicles:** this market requires more sophistication in modeling and more capabilities of the simulator system. The main driver of this higher level of sophistication is that very specific aircraft dynamics have to be simulated including non-linear effects and performance limits that constrain these dynamics. Projects in this market often have large budgets, but occur less frequently. Given the fact that Calspan was involved in over 50 large aircraft development programs in their 60 years of existence, a similar frequency can be expected for the developed simulator [6]. Adding to that the long list of future projects in aircraft development improves the forecast for this market segment even further [2].

- **Segment 2 - variable stability simulation and training of flight test pilots:** the flights in this segment are more standard, meaning that the generic adaptations of the aircraft dynamics suffice. These tests do not involve the simulation of an entire aircraft. Even though the individual projects involve much smaller budgets, this part of the market is much larger than the part of segment 1.

The IFS can be operated by a company in both of these segments. It was decided though that the aircraft will be operated by a company that is not the designer and manufacturer of the modified aircraft. So the focus for the designing company will be on selling the IFS. So the potential clients are the operators, that can be both existing companies and new to establish companies. To get an estimation on the viability on operating the IFS also a business plan for the operating company is given in the following sections.

[1] http://www.marketsandmarkets.com/Market-Reports/flight-simulator-market-22246197.html [cited 17 November 2016]
[2] http://www.aerospace-technology.com/projects/ [cited 28 November 2016]

2.2.1 Targeted customer base

Positioning the in-flight simulator as an accessible solution that can be tailored to specific research needs, will open up a lot of opportunities in the markets described in section 2.2. In the current days of cost-cutting, ever-increasing competition and the growing desire for flexibility within the industry, renting from the operator will suit the needs of most end users. Several end user types can be identified within different segments. Below a list is given with the different end user types and the segments from section 2.2 that they are active in. Note that these segments are not definitive.

- **Universities:** segment 1, only end user.
- **Research institutes:** segment 1, potential client and end user.
- **Military test pilot schools:** segment 2, end user.
- **Commercial test pilot schools:** segment 2, end user.
- **Aircraft manufacturers:** segment 1, end user.

These end users are relevant for the operator, so the client, but also for the manufacturer of the aircraft. This because the end users can also decide to buy the product themselves and become a direct client in that way. Other operators will be interested in using the aircraft for both segments, to maximize their operational usage.

2.2.2 Market size

In subsection 2.2.1 several customers are indicated on which will be elaborated on further in this section. There are several research institutes around the world that might be interested in having an IFS themselves. For example the TU Delft operates one toghether with the NLR research institute. [3]

Currently there are 9 test pilot schools operating where aircraft will be certified, of which 2 are located in Europe. One of these schools, the Empire Test Pilot School, already makes use of the variable stability Learjet offered by Calspan[4]. This indicates that they do not fly enough hours on these platforms to make it interesting to buy a variable stability aircraft themselves and so only will be end users renting the aircraft from the operator. This will be assumed for all test pilot schools, since the Empire Test pilot school is one of the largest in its class.

Also the two major aircraft manufacturers, Boeing and Airbus, make use of Calspans services [5]. Apparently the amount of testing for their new to develop aircraft is not enough to operate the IFS themselves. These two and other smaller manufacturers could be a potential end user though.

This leaves one potential type of client for the IFS. These are the operators that are specialized in offering both variable stability training and the testing of aircraft handling characteristics. Currently Calspan is the only real player that operates in this segment. So to compute the size of the in-flight simulator market in terms of operating hours, they are used as a reference. The method used for estimating the size of this market in number of operating hours is mainly based on an extrapolation from the hours that Calspan is making with their aircraft. Table 2.1 shows the operating hours until 2005, giving a total of 1,056 hours that are flown in the in-flight simulators operated by Calspan each year [6]. Given the fact that in-flight simulation is still growing, the number of hours per year today and upon introduction of the in-flight simulator will be even higher. Taking the annual growth rate of the total simulator market from section 2.1, a 4% growth rate would be reasonable. However, it is estimated that the commercial in-flight simulation market will be growing at a rate that is 50% larger than the rate of the total simulation market, since technology in this market is still advancing. Therefore, using a 6% growth rate, a total number of operating hours of 2,005 for 2016 and 2,521 hours for 2020 (estimated year of introduction of the IFS) is calculated.

Table 2.1: Operation details of the Calspan in-flight simulators as per 2005 [6].

Aircraft	Years in operation [yr]	Total hours [h]	Average Annual Use [h/yr]
TIFS	37	4,400	119
Learjet #1	24	13,500	563
Learjet #2	14	3,700	264
VISTA	10	1,100	110
Total	**n.a.**	**22,700**	**1,056**

[3] http://cs.lr.tudelft.nl/facilities/ph-lab/ [cited 18 January 2017]
[4] http://www.etps.qinetiq.com/school/fleet/fixedwing/Pages/Calspan-Learjet.aspx [cited 17 January 2017]
[5] http://www.calspan.com/company/testimonials-customer [cited 24 January 2017]

2.3 Competitive analysis

To see if the design is viable both to built and to operate, a closer look on the competition in the market of in flight simulation has to be performed. First the competition will be identified and then this competition will be assessed on its strengths and weaknesses.

2.3.1 Competition in the targeted market

As already mentioned in subsection 2.2.2 there is one main player present for both developing and operating variable stability aircraft. Although this company, Calspan, could be a potential customer for the Phenom 300 IFS, it will be treated as a competitor in the following section. From the operating perspective they are also both active in the simulation of handling characteristics of aerial vehicles and pilot training in a variable stability environment. On the development side, they currently are not likely to sell their design for a variable stability aircraft. It can be concluded that in the beginning of in-flight simulation Calspan Corporation had a leading market position and it has never given that away.

2.3.2 Competitors strengths and weaknesses

As Calspan Corporation is the main competitor in this field, the company is investigated further. To find out what the best market entry strategy is, the strengths and weaknesses of the company are listed [6].

Strengths:

- Calspan Corporation has much experience in the development of in-flight simulation systems.
- Calspan Corporation has much experience in the implementation of in-flight simulation systems.
- Calspan Corporation has much experience in the certification of in-flight simulation systems.
- Calspan Corporation has a big network of clients.
- Calspan Corporation has many resources available.
- Calspan Corporation is part of Calspan Holdings which makes company processes cheaper.

Weaknesses:

- The in-flight simulation system of Calspan Corporation is limited to 4 degrees of freedom. The control axes that they are missing include the direct side-force and direct lift control that will be fitted on the IFS designed in this project.
- The activities of Calspan Corporation are limited to the United States of America, which gives the IFS a geographical advantage in Europe.

2.4 Market Projections

After analyzing the target market and the competition it is possible to make projections for the market share, pricing and gross margin. This will first be done for the developing company. Thereafter, a projection for operating the aircraft will be elaborated on. Assumptions that are made to come to estimates are listed.

2.4.1 Market share - IFS developer

From the development perspective, the aspect of the product that offers the simulation of aircraft characteristics will be unique to buy of the shelf, meaning that it basically takes up the entire market of potential operators for this in flight simulation segment, albeit this market will be very small. It will most probably mainly consist of universities and research institutes. The numbers of these are difficult to estimate. They are expected to be low, since it is quite a large investment for research purposes only. Companies that are focused on making profit from the characteristic simulation will also operate in the pilot training segment, to maximize usage and revenues. Also on this part of advanced training for pilots there is no real competition and certainly none that offer the six degrees of freedom simulation. Getting back to the numbers in subsection 2.2.2 the current market size will be around 2,500 operating hours in the near future. It is considered that the extra degrees of freedom may attract more end users in the market. Also making in flight simulation more accessible for the European market, can increase the amount of world wide operating hours. It is estimated this will lead to a total market size of 3,500 operating hours. Conservatively estimating this creates a margin for 3 IFS aircraft, flying a total of around 2,250 hours a year. So a part of Calspans market will be taken over and possibly Calspan will also acquire an IFS themselves. So for the IFS the market share will be large, but the market size small.

2.4.2 Pricing and gross margin - IFS developer

To determine how much profit the developer/manufacturer can make the price of the product offered has to be compared with the cost. The price asked depends mainly on to which purchase price the IFS is attractive to invest in, as will be discussed in subsection 2.4.4. The two major cost factors are listed in Table 2.2, in which the modification cost is retrieved from section 12.1.

Table 2.2: Total IFS price.

Part	**Cost (€/year)**
Aircraft purchase cost	8,200,000
Modification cost	621,575
Total	**8,821,575**

For an estimation it is expected that a total of three Phenom 300 in flight simulators will be sold. This is based on the expected market growth described in subsection 2.4.1. In the end the product will simulate more realistically and be around longer than that of Calspan, which also makes them a potential customer. Since this number of total products is small, selling one or two aircraft less will have a large impact on the distribution of the design costs. To account for this a larger gross margin is taken, namely one of 12%, which is slightly higher then the typical 7% for engineering services [6]. This leads to a price of around €9.9 millions per IFS. Also this is still a reasonable purchase price as will be explained in subsection 2.4.4. So for the projected number of three aircraft to be sold an estimated profit of €3.2 millions can be made by the developer of the IFS. With a profit margin of 10% of the total revenue requirement **IFS-SH5-01** can be met, stating that the return of investment should be high.

2.4.3 Market share - IFS operator

In the following sections a business scenario for operating the IFS will be described, to prove it is viable. As was estimated in section 2.2.2 the total size of the commercial in-flight simulator market will be approximately 3,500 operating hours per year. As was stated in the requirements in the project plan, the projected use of the in-flight simulator is 750 hours per year [8]. By the time of its first flight, the market share of one in-flight simulator will be 20% and 30% of the total commercial in-flight simulator market.

2.4.4 Pricing and gross margin - IFS operator

The value of one flight hour of the IFS is determined from all the costs plus a profit margin. The operating costs are conservatively estimated to be €2,470 per/hour as stated in section 12.1 or €1,852,500 a year. Outside of this operating cost for the aircraft, also other company cost are present. These mainly consist of the payroll of the non-flying employees. To make an estimate of these cost, a short overview is made of an example employee composition of the operating company, see Table 2.3.

Table 2.3: Example of employee composition and salary.[7]

Part	**Cost (€/year)**
Director	130,000
Operations manager	85,000
Facility manager	85,000
Total	**300,000**

Table 2.4: Estimated total cost per year.

Part	**Cost (€/year)**
Company cost	600,000
Operational cost (750 hr/year)	1,852,500
Total	**2,875,000**

[6] http://research.financial-projections.com/IndustryStats-GrossMargin.shtml [cited 18 January 2017]
[7] http://www.nationaleberoepengids.nl/beroepen_per_salarisschaal [cited 1 December 2016]

For a typical company offering services payroll can be around 50% of the total revenue [8]. In the case of an IFS operator that would imply a company cost of €600,000 a year, assuming cost equals revenue. Usually the revenue will be higher then cost, leading to higher company cost. However since already a part of the costs are in the operational cost, this rough estimate suffices for preliminary cost calculations. Dividing the total cost mentioned in Table 2.4 by the amount of flying hours per year leads to €3,833 per operating hour.

The price of the IFS is about €9.9 millions and this is basically the only real investment that has to take place, since buildings and maintenance tools are not acquired but rented in this case. If a gross margin of 60% is taken, the investment could be returned in a minimum of around 6 years, while still having a valuable aircraft as an asset. This profit margin could also leave room to invest and let the company grow. When a second aircraft is purchased the total cost will not increase linearly by a factor two. So this leaves even more profit. The 60% profit margin leads to a price of €6,130 per/hour. One has to look if end users are willing to pay this price of course. As described earlier in this chapter, there is not much competition. As a consequence, there is almost no reference on pricing. Keeping in mind that an unique product will be offered, a price of €6,130 per hour seems reasonable. This calculation is an example to show the design is feasible to operate, with the remark it that is a rough estimation since little is known about this market.

To get a better view on the uncertainties in this cost estimation, a risk map is made for the cost in Table 2.5. The various risks are the following are displayed next to the table.
One can see there are two main risks present in the top right corner. These are increasing fuel cost and a lack of market interest. The likelihood of increasing fuel cost cannot be adjusted since it depends on the ever fluctuating oil price. The impact however is manageable by having an aircraft that has a low fuel consumption. In the design there is accounted for this by choosing a modern aircraft with fuel efficient engines and the modifications using an efficient boxwing design. The other main risk is the that there will be low interest for using the IFS. Obviously, this will have a high cost impact. The likelihood this happens is medium because it is known there is an existing market for it, but it is not sure customers will prefer the newly developed IFS over the Learjet Calspan operates with all their experience. To get more insight in this customers that are currently client at Calspan should be asked about their opinion. The remaining risks are considered less are in the lower left corner of the risk map.

Table 2.5: IFS cost estimation risk map.

1: Increasing fuel cost
2: General stagnation in aircraft development
3: No market interest or product not distinctive enough
4: Higher material cost
5: Higher personnel cost
6: Higher maintenance cost

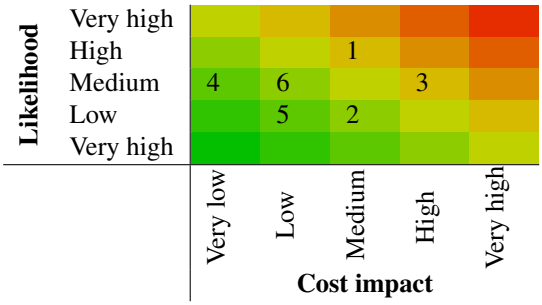

2.5 Stakeholder review

In the Baseline Report several stakeholders were identified [9]. From the needs of the stakeholders several requirements were extracted. In the following section the stakeholders will mentioned again and a short assessment on how their needs are fulfilled is presented.

- **Customers:** they are organisations that want to operate the IFS is meant and therefore they are very important stakeholders. It includes the operations team, ground support, customer support and any other staff that the organization consists of. Since they will be the operator of the aircraft they need a viable business case and a reliable and attractive IFS. In subsection 2.4.4 the viability of operating the aircraft is proved. The reliability has yet to be proven but the IFS certainly is a unique product to offer.
- **End Users:** companies that want to test new aircraft handling characteristics and test pilot schools seeking for training platforms for their students. Their interest lies in the range of possibilities of the IFS and the costs of using it. The requirements on the simulation of force are met as can be read in chapter 15, thereby the desired capabilities are met. Also the cost per hour to make use of the aircraft is reasonable as explained in subsection 2.4.4.

[8] http://secondwindconsultants.com/percent-revenue-allocated-payroll [cited 18 January 2016]

- **Regulators:** these are the authorities with the task to regulate aviation. These are EASA and FAA in Europe and the United states, respectively. The regulator's need is that the IFS complies with existing safety regulations. Although it is not yet tested if the IFS can comply with all these regulations, it is designed to do so. Thereby the regulators needs are probably fulfilled.
- **Suppliers:** they consist of the aircraft manufacturer Embraer, the supplier of the engine Pratt and Whitney and the suppliers of the additional parts for modification. The suppliers of the additional parts are mentioned in chapter 9. Their need is to get the right price for the products sold to the development team. In chapter 12 it is accounted for that the suppliers will get a good, mostly off the shelf, price for their product.
- **Competitors:** they are other parties offering products in the same market. In the case of IFS this equals Calspan. Its interest will be high, since the newly developed IFS can affect their market position. They can also be interested in buying an Embraer IFS to increase their capabilities. In that case care should be taken on still being able to sell the projected number of 3 IFS aircraft.
- **Investors:** with investors, a person or group that commits capital with the expectation of financial returns is meant. Their need is to gain high returns while keeping the expenses low. They will be closely related to the customer, so the eventual operator. Since the operator will have a viable operation, the investors will also be satisfied.
- **Environmental agencies:** they are agencies established to reduce pollution and protect the environment. They have the need to make sure the simulator is developed and operated in the most sustainable way. Since the drag is kept as low as possible by a boxwing design, the use of fossil fuel is also minimized. Also in the production and maintenance processes is accounted for sustainability as can be read in chapter 3 and chapter 11.
- **Unions:** they are organizations that come together to achieve common goals such as a stable and safe working environment for the employees of the suppliers, the end users and the crew. They will be concerned with the operation of the IFS as well as the production. Nevertheless, if no attention is drawn by simply treating all involved staff properly, the interest of unions will remain low.

3 | Sustainable Development Strategy

Nowadays, state of the art technologies break through boundaries of what was previously thought to be impossible. These possibilities come with the big responsibility to keep the environmental impact of developments as small as possible. This is done by making sustainable development a major aspect of the design. At block *1.4* of the FBS, is stated that it IFS shall be designed for sustainability. Being sustainable is not only taking care of the waste after the operational life. On the contrary, sustainability is something that has to be embodied right at the start of the design phase and ends with a well thought out end-of-life destination. Four criteria that play a role in assessing the sustainability during operation are operational power, material type, maintainability and fuel consumption [11].

In this chapter, the relevant requirements set will be discussed per phase, as well as their actual implications for now and considerations for the subsequent design phase. Moreover, sustainability can be seen as a mindset, having a constant role in all choices made during the design. This means that the sustainability is also increased in areas where no requirements have been set.

3.1 Manufacturing process

First of all, choosing an existing business jet instead of designing a jet is considered a sustainable choice. This way, the environmental impact of testing can be reduced. Furthermore, sustainability has been taken into account in the trade-off that yielded the Embraer Phenom 300 as best option. [9]

The addition of the upper wing and side wings are considered the largest difference of the IFS with respect to the original Phenom 300. Its manufacturing will for this reason determine a considerable share of the sustainability of the modification process. Both the upper- and side wings are built of 7075-T6 Aluminum, which is a frequently used alloy in the aerospace industry. The sustainable aspect of choosing an upper wing to be able to fulfil the flight requirements, is that its structural integrity can be assured with relatively little material, since the upper wing is supported by the nacelle and the vertical wing is supported by the main wing.

The exact production techniques that will be used in order to manufacture the designed parts, is beyond the scope of this report and has to be determined in the next phase of the design process. Nevertheless, it has already been decided in section 11.3 that lean manufacturing will be applied during the production process, decreasing the amount of waste [12].

3.2 Aircraft operations

In **IFS-SYS-24** it is stated that the average fuel use of the IFS shall not exceed 3.15 $\times 10^{-4} m^3$/s in a flight with 4 approaches with descent from 3,048 to 0 m, and test sections at 3,048 m and 6,096 m, in which the IFS covers the speed envelope. This has been declared plausible in section 7.4. In **IFS-SYS-27** it is stated that the IFS shall be certifiable in Europe. This includes an operational maximum of 89 EPNdB during a fly-over. This sub-requirement is expected to be met, since the unmodified Phenom 300 passed the FAA's stage 4 external noise requirement with a respectable margin of 24 EPNdB, meaning it will still pass after a considerable increment in noise due to addition of the boxwing. [1]

In section 9.8 it has been decided that electrical actuators will apply the deflections to the extra control surfaces as designed for the IFS. With electrical actuators, no fluids leaks will be present, eliminating environmental hazards.[2] Furthermore, the removal of all unnecessary weight by the ergonomics department as described in subsection 9.2.1, allows that the aircraft to fly at more optimal flight conditions, decreasing fuel burn with respect to the same design with the lavatory, luxury seats and cabinets still installed. Lastly, the fact that the low lift over drag L/D requirement is met by adding the drag chute as designed in section 5.4, means that no excessive amount of speed brakes have to be installed, resulting in a decrease in weight of the aircraft during flight tests.

[1] http://www.embraer.com/en-US/ImprensaEventos/Press-releases/noticias/Pages/EMBRAER-OBTEM-CERTIFICACAO-DO-JATO-PHENOM-300-DA-ANAC.aspx [cited 23 January 2017]

[2] http://machinedesign.com/linear-motion/what-s-difference-between-pneumatic-hydraulic-and-electrical-actuators [cited 23 January 2017]

3.3 End-of-life disposal

According to **IFS-SYS-23**, the aircraft shall have an operational life span of 20 years. This justifies the unavoidable impact on the environment by the modifications. Computing components may be replaced after 10 years, as stated in **IFS-SYS-25**, however two laptops are used by the test engineer. These laptops will likely have a lifespan of 5 years hence a replacement of this has been taken into account. **IFS-SYS-26** says that the design should provide the possibility for mid-life updates. This has been accounted for as much as possible. For instance, most mounting divisions of the added flaps are classified as type-B, meaning they are mounted for regular replacement. When the time has come for the IFS to reach the end of its operational life, usable components present in and on the aircraft will be refurbished and sold, the function in the FBS at block *5.0 dispose of IFS* is fulfilled. The hazardous waste shall be taken care of in such a manner that it does not pollute the environment. The parts that are left, which will be the majority of the aircraft but mainly the structural components, will be donated to a educational facility, such as an university.

4 | Design Principles

This chapter features an introduction of the principles governing the design and the design process of the IFS. The design process, involving mostly the systems engineering approach used in the project, is first explained in section 4.1. Next are the basic foundation of the design itself, starting with the functions that the finished product should have. These functions are therefore visualized in section 4.2, followed directly by the Functional Breakdown Structure in section 4.3. The second part of this chapter involves the initial division of the resources that were available over the course of the project. These resources are specified in section 4.4. The cost and mass budgets belonging to the resource allocation are explained in subsection 4.4.1 and 4.4.2, respectively.

4.1 Systems engineering approach

A focus on systems engineering has been present during the whole project. Starting at the Project Plan [8], charts have been made containing information on the organizational aspects of the work that needed to be done. Charts have been upgraded and added, and in the Mid-Term Report [10] a detailed planning was made for verification and validation procedures. This plan was implemented in the individual chapters of this report. Next to this, systems engineering also involved time spent on integration of the different technical departments that were formed in this detailed design phase of the DSE. Due to the fact that different teams worked on different parts of the design, aligning the common variables was essential. Tools used to align these different departments were extra system-engineering oriented team meetings, but also an online Excel document having all of the common variables in it, that was maintained by the systems engineers. All in all, this systems engineering process went smooth, and all of the variables in the final design have successfully been aligned.

4.2 Functional Flow Block Diagram

The Functional Flow Block Diagram (FFBD) and the Functional Breakdown Structure (FBS) are two diagrams that show the different functions that the IFS needs to fulfill to perform the mission. Different levels of detail are shown from a top down perspective. On the top level in the FFBD in Figure 4.1 one can see that there are 5 main functions to be fulfilled by the IFS from beginning to end of life. Each level a more detailed function description is given. This is demonstrated in Figure 4.1. At various sections in the report where functions are worked out, references to the FFBD are made by calling the identifier of the specific function.

4.3 Functional Breakdown Structure

Because there was a lack of integration between the FBS and the FFBD in the Baseline Report [9], emphasis has been laid on the integration of the two diagrams. Each block from the top level to the third level is integrated in both diagrams Figure 4.1 and autoreffig:FBSA. Naming of each box can be cross referenced in both diagrams, meaning that identifiers of functions throughout the report can also be linked to the FBS.

To increase the readability of the FBS, 4th and 5th levels were added to the functional breakdown of blocks 3.2 and 3.3 as seen in Figure 4.3. This is done in an extra FBS to show the differences in basic flight and simulated flight as the IFS is the main focus of this project.

4.4 Resource allocation

After the resource allocation in the Baseline Report [9] the concept was chosen [10] and preliminary sizing has been done. This gave more knowledge about the system and a more accurate resource allocation. The three budget breakdowns as presented in the Baseline Report will also be discussed in this section, starting with the total cost budget in subsection 4.4.1. After this the mass budget will be presented in subsection 4.4.2. The cost- and mass budget will be taken into account during every relevant design section in this report. Lastly, an overview of the mass of the aircraft is provided in section 7.1, whereas the final estimate for cost is made in chapter 12.

4.4.1 Cost budget breakdown

The current cost budget breakdown has several differences w.r.t. the breakdown as stated in the Baseline Report. First, each difference will be discussed and thereafter the new cost budget breakdown is shown in Table 4.1.

The categories of the breakdown have been changed. First the category *Design and development* was taken out, since the concept design is no longer part of the cost budget. Besides this the *Actuators* and *Sensor* categories are changed to respectively *Control* and *Data gathering*. This is done to include the safety trip system, e.g. clutches, and cabling. Also the *Engineering station* category is renamed to *Ergonomics* and now includes all the interior changes, like implementing a control-loaded stick in the test pilot station. Lastly the *Production and installment* group is renamed to *Structures* with production and installment of other subgroups included in their cost. The new categories are the following:

- **Control:** costs of purchasing and installing COTS actuators and implementing the safety system for the IFS.
- **Data handling:** costs of purchasing and installing COTS sensors, their associated cables, the data collecting devices and data storage for the IFS.
- **Ergonomics:** costs of purchasing and implementing COTS computers and hardware that will be installed in the IFS, both in the test engineer station as in the test pilot station. Also included are costs of removal of redundant aircraft interior.
- **Structures & aerodynamics:** costs for producing and applying the structural modifications to the aircraft, both implementing the boxwing as replacement of existing control surfaces.

The second major difference is the change in cost budget contingency. Since the *Production and installment* costs are divided over the other categories, the contingency for each group changed. The new contingency numbers will be in between the percentages of *Production and installment* and the category in which it is implemented, where the actual percentage is dependent on the relative cost of each group. Also the current design phase is different, hence a more accurate cost estimation is made. The new contingency table is presented in Table 4.2.

Table 4.1: Revised cost budget breakdown.

Sub-group	Maximum budget
Control	€160,000
Data handling	€80,000
Ergonomics	€62,000
Structures & aerodynamics	€450,000
Total	€752,000

Table 4.2: Revised contingency allowances for the cost budget breakdown.

	Control	Data handling	Ergonomics	Structures
Preliminary design	12%	12%	10%	15%
Detailed design	6%	6%	5%	7%
Pre-production stage	2%	2%	1%	3%
Final product	0%	0%	0%	0%

As can be seen in Table 4.1, the *Structures & aerodynamics* department has the highest budget. This is due to the fact an entire extra wing is to be implemented as is explained in chapter 8. The lowest budget still goes to *Ergonomics* since there are only a few critical structural changes necessary for this department, namely the actuator implementation. The removal of lining and addition of instruments and computers is non-critical for structural integrity, hence has different certification cost. The budget of *Data handling* is also low, however slightly higher w.r.t. previous values. This is because the sensors and data gathering system have to be aircraft-grade and new cabling needs to be implemented, which may span the whole aircraft. Lastly the *Control* department has a significant part of the budget since it includes the implementation of the safety trip system, consisting of for example extra clutches and actuators. The costs of the final design are presented in chapter 12, which will inherently serve as a check to see whether the budgets stated in the breakdown are not exceeded.

4.4.2 Mass budget breakdown

As for the cost budget, the mass budget as stated in the Baseline Report is revised. First each difference will be discussed and then the new mass budget breakdown and contingency allowance is shown in respectively Table 4.3 and Table 4.4.

Table 4.3: Mass budget breakdown.

Sub-group	Maximum budget
Control	70 kg
Data handling	30 kg
Ergonomics	90 kg
Structures	224 kg
Total	414 kg

Table 4.4: Revised contingency allowances for the mass budget breakdown.

	Control	Data handling	Ergonomics	Structures
Preliminary design	8%	9%	5%	10%
Detailed design	5%	4%	2%	5%
Pre-production stage	2%	2%	1%	2%
Final product	0%	0%	0%	0%

Differently from the categories of the cost budget breakdown, the mass categories were not changed w.r.t. what was stated in the Baseline Report. This is due to the fact that the existing division of the mass budget breakdown is similar to the new cost budget breakdown, however the naming is changed. *Actuators* category was renamed in *Control*, *Structural modifications* in *Structures & Aerodynamics* and *Electronics & sensors* in *Data handling*. When looking at content changes, the *Control* department is changed, since the safety trip system is added to it. Also the *Ergonomics* will be heavier, since removal of lining is not included any more, but is considered to increase the mass budget. Lastly the total mass budget is now calculated and equal to the total modification weight, as stated in the Mid-Term Report [10], corrected for the mass contingency. The contingency is not changed, as can be seen in Table 4.4. Because of the added parts in *Control* and *Ergonomics* categories these both have a slightly higher budget. Also the structures and total mass estimations are now included.

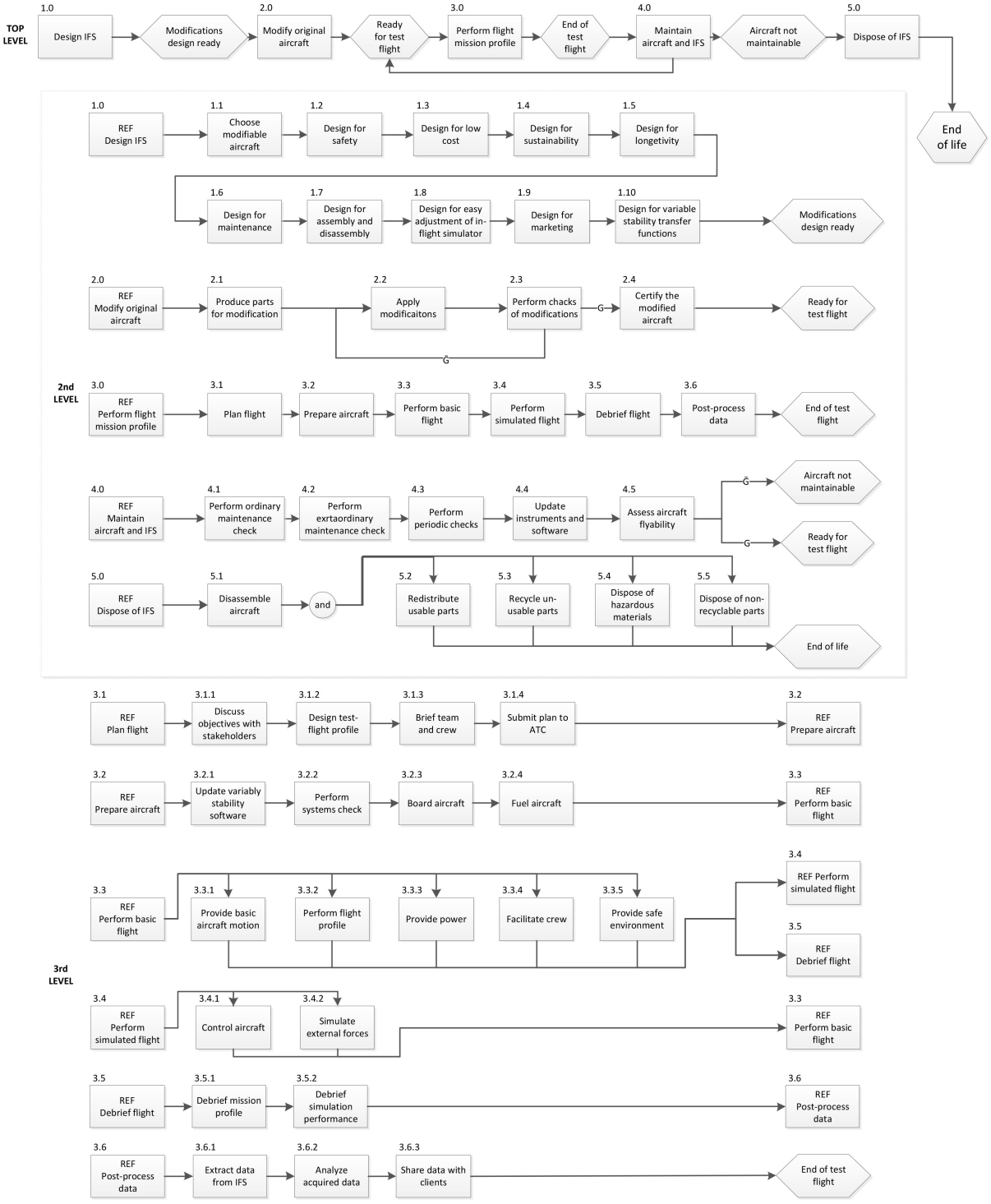

Figure 4.1: Functional Flow Block Diagram update.

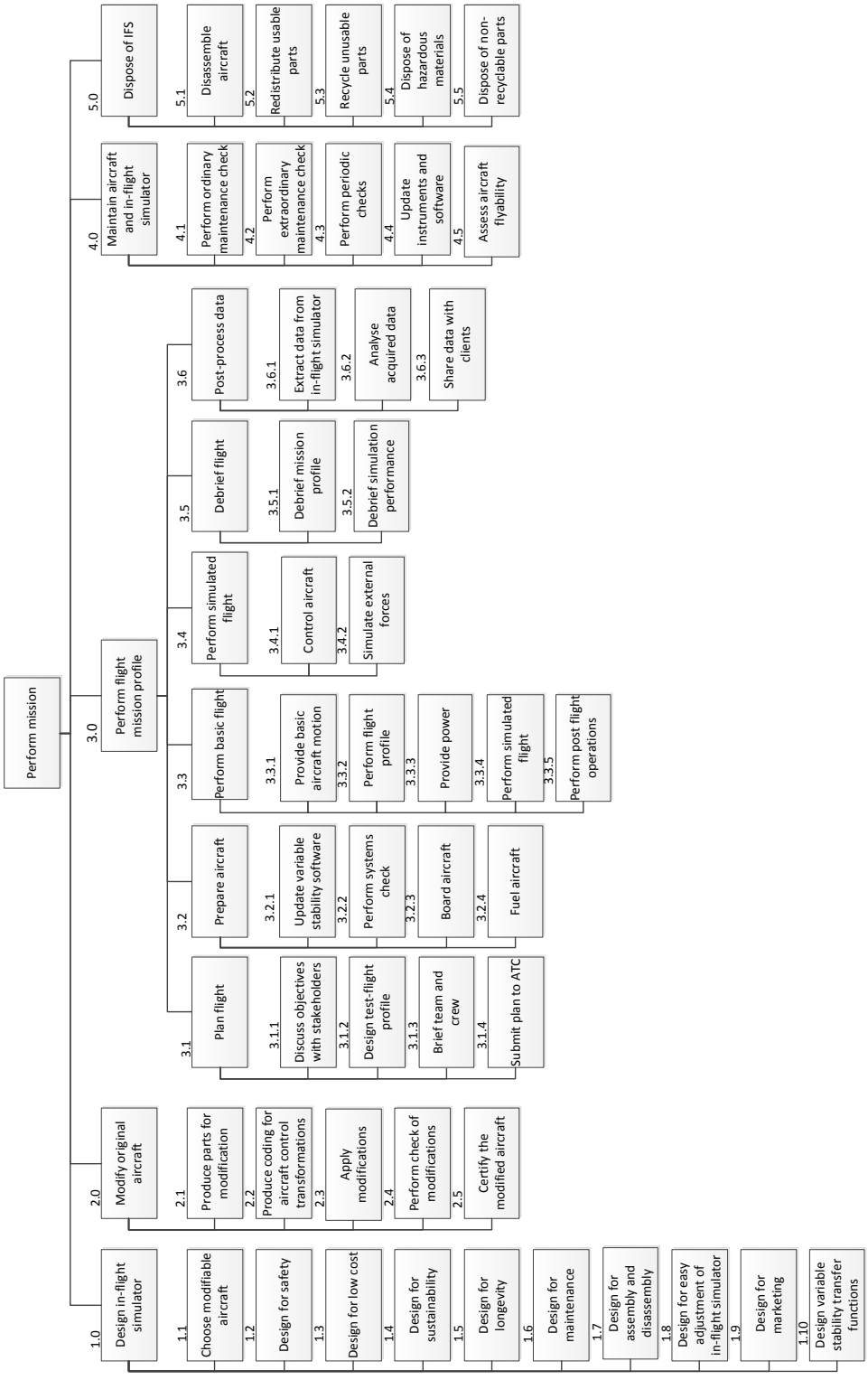

Figure 4.2: Functional Breakdown Structure update.

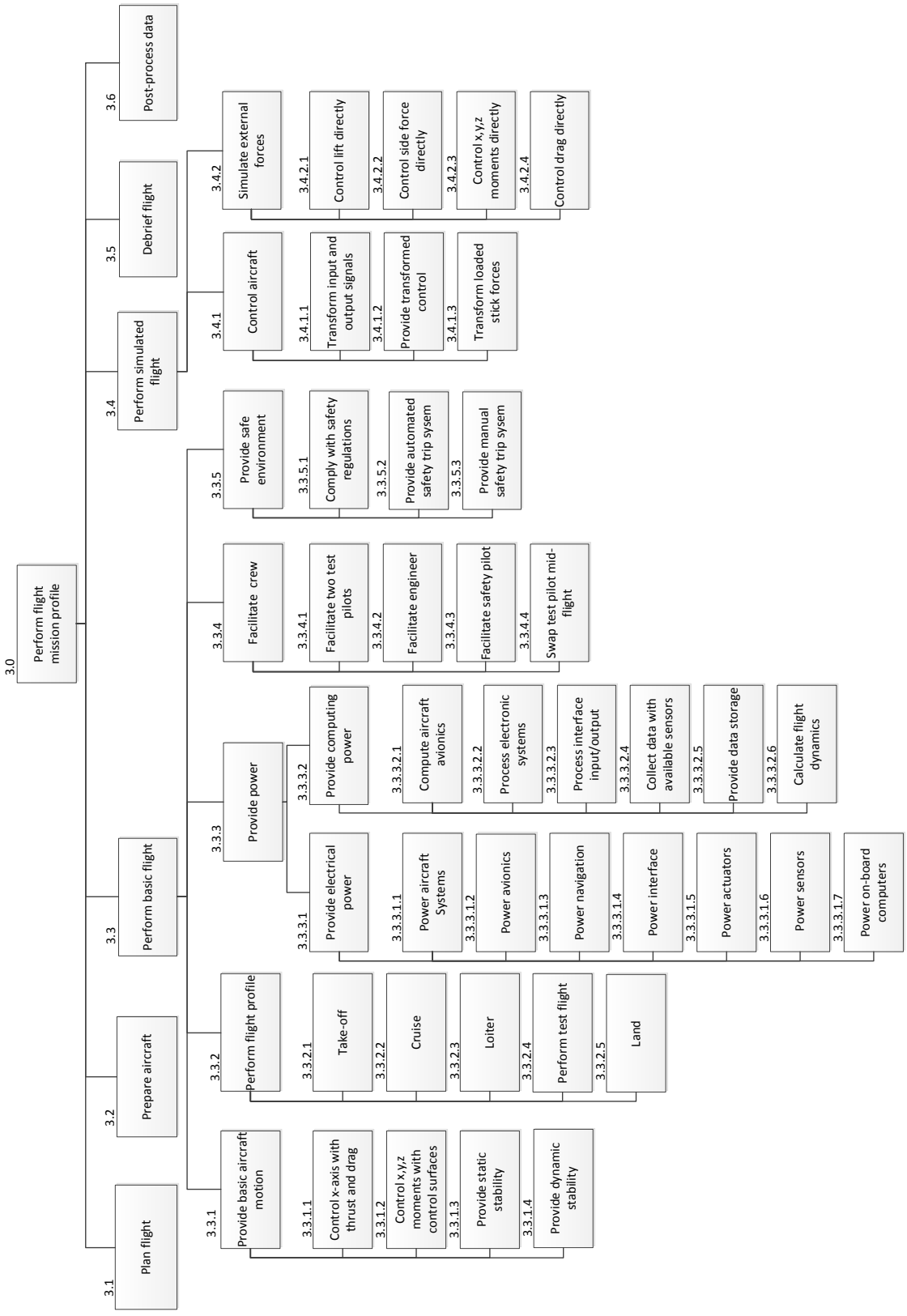

Figure 4.3: Functional Breakdown Structure update with extra detail on the IFS.

5 | Boxwing Design

After the trade-off of all possible design concepts in the Mid-Term Report was performed, it was found that the boxwing configuration was the best possible design concept. This chapter presents the actual design of the boxwing. For the boxwing design the upper wing and vertical wings characteristics had to be defined and optimized. Section 5.1 presents the chosen planform for the boxwing design. Next, the airfoils that are chosen for the boxwing configuration are elaborated upon in section 5.2. Then the design of the flaps will be discussed in section 5.3. Lastly, the characteristics of the design options that enables flights with a low glide ratio will be presented in section 5.4.

5.1 Planform boxwing

The planform of the boxwing design involves the determination of the span, chord length, sweep angle and taper ratio of the new appendages [13]. Due to the fact that a boxwing design is chosen, the vertical wings and upper wing connect at a certain point. This configuration is favourable for reducing drag and transferring structural loads with respect to finite wing aircraft, but it limits the design possibilities opposed to the case where the wings do not have to connect [14]. The actual planform is presented in Figure 5.1.

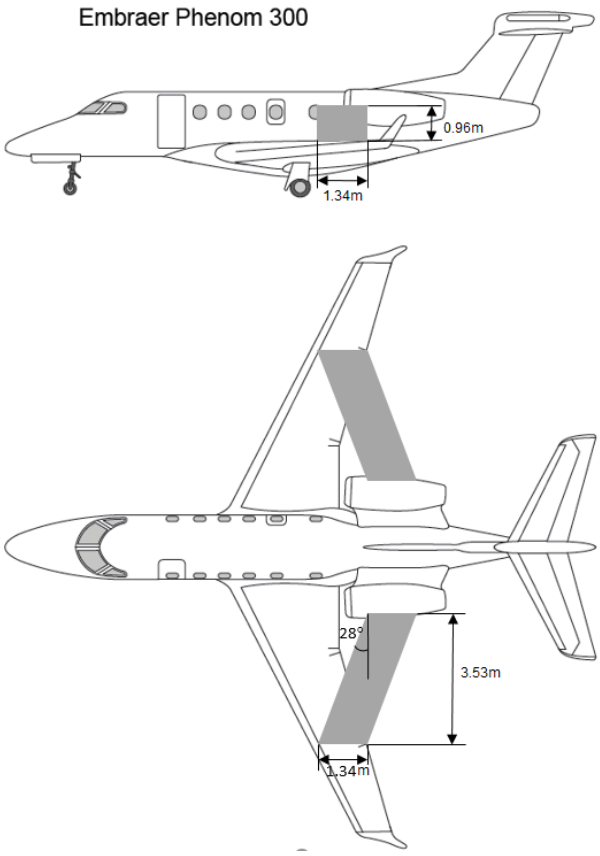

Figure 5.1: The planform of the IFS boxwing.

5.1.1 Span and chord

The span of the boxwing configuration entails the span of the upper wing as well as the span of the vertical wings. It is desirable to attach the wings to the original aircraft at points where no cost-intensive modifications are necessary and the aerodynamic performance of the original aircraft is affected as little as possible, while keeping the span at a maximum. The dimensions are displayed in Figure 5.1.

It was chosen to attach the vertical wings to the main wing at the point in between the outboard flap and aileron. In this way it is possible to install the main wing without altering the original wingbox and control and lifting surfaces of the Embraer Phenom 300, thus minimizing costs. To ensure that the lateral acceleration of 0.5 m/s^2 could be achieved as stated in requirement **IFS-SYS-08-AERO-01** [9], the chord was chosen to be the same length as the chord of the main wing at that point and not a smaller value.

For the upper wing it was chosen to attach the wing to the outer part of the engine nacelle. If the upper wing would have been installed in front of the engine, the airflow that enters the engine would have been distorted, creating a serious risk of malfunction with possible flame-out. If the wing would have been installed aft of the engine, the hot exhaust gases would have changed the material properties of the wing, in this way also affecting the aerodynamic properties.

5.1.2 Sweep

To establish a closed boxwing configuration instead of just two separate wings, the upper wing and vertical wing need to be connected to one another. Therefore it was necessary to apply sweep to the planform. It can either be decided to sweep the vertical wing backwards and connect it to a straight upper wing, apply forward sweep to the upper wing and have a straight vertical wing and every possible combination in between. Regarding longitudinal stability it is favourable for the upper wing to have the aerodynamic center of the wing as close to the center of gravity as possible. Therefore it is chosen to go with the 28 $^\circ$ forward swept upper wing and straight vertical wing.

5.1.3 Taper ratio

For aircraft that have finite wings, taper ratio is applied to generate a more elliptical lift distribution. The generated lift force decreases further outboard near the tip to have a lower load case and less bending of the wing. The upper wing and vertical wing of the IFS are meant for a change in lift and side force, but for the most part of the flight these surfaces should not produce significant lift or side force. Therefore no loads and bending moments are present. Besides that, the upper wing and vertical wing are connected to one another, so the bending of the wings due to the generation of lift or side force is limited. Taper would also increase structural complexity, so it was decided not to apply taper to the vertical wing and upper wing.

5.2 Airfoil selection

With the planform defined, the airfoil selection process can be started. It is important that the airfoil is symmetrical. The difference in lateral acceleration and lift coefficient either has to be equally positive or negative. If a cambered airfoil would have been selected, the lift coefficient would have been higher for one of the two sides, which is inefficient in this case. The thickness ratio then determines the final shape of the airfoil.

5.2.1 Thickness ratio

The design philosophy used to determine the thickness of the airfoil is that it is desirable to have a minimal change in the center of pressure with changing pressure distributions. A small change in the loading configuration of the wing leads to the lightest possible wingbox. Thicker airfoils have a lower change in the center of pressure with changing angles of attack, so it was decided to have the thickest possible airfoil while still complying with the requirements. The thickness ratio of the airfoil depends on the critical Mach number. Requirement **IFS-SYS-01**, stated in the Baseline Report [9], was that the IFS should fly at a maximum speed of Mach 0.65. Thicker airfoils lead to lower critical Mach numbers, so it was decided to use 0.65 as the design critical Mach number. The method used to calculate the maximum thickness ratio is provided by Torenbeek [15]. This is the most accurate method out of eleven possible methods, with a standard estimate of error of only 0.81% for different types of aircraft [1]. The thickness ratio can be calculated using Equation 5.1, where M_{DIV} is the drag divergence Mach number.

$$t/c = 0.30\left(\left[1 - \left(\frac{5 + M_{DIV}^2}{5 + (M^*)^2}\right)^{3.5}\right]\frac{\sqrt{1 - M_{DIV}^2}}{M_{DIV}^2}\right)^{2/3} \tag{5.1}$$

[1] http://www.fzt.haw-hamburg.de/pers/Scholz/arbeiten/TextCiornei.pdf [cited 15 January 2017]

The variable M^* has no physical meaning, but is merely a figure of defining the aerodynamic sophistication employed to obtain supercritical flow at the design condition. For conventional NACA airfoils, M^* is 1.0. Korn found a relation between the drag divergence Mach number and critical Mach number [16], as shown in Equation 5.2.

$$M_{cr} = M_{DD} - \left(\frac{0.1}{80}\right)^{1/3} \tag{5.2}$$

The conversion to another, more accurate drag divergence Mach number M_{DIV} that accounts better for compressibility effects can be done with Equation 5.3 which was presented by Shevell [17][2]. In this case the Mach number only holds for so-called "peaky" airfoils and is later corrected for NACA airfoils. Peaky airfoils have upper-side pressure distributions with a definite "peak" close to the leading edge.

$$M_{DD} = M_{DIV_{peaky}} + 0.02 \tag{5.3}$$

The conversion from peaky airfoils to NACA airfoils as proposed by Torenbeek [15] is shown in Equation 5.4, with ΔM_{DIV} equal to 0.04.

$$M_{DIV_{peaky}} = M_{DIV_{NACA}} + \Delta M_{DIV} \tag{5.4}$$

5.2.2 Vertical wing

After estimation of drag-divergence Mach number for NACA airfoils the thickness ratio can be calculated. For the vertical wing airfoil, the thickness ratio is 0.0843. The NACA profile that was selected for the vertical wing is NACA0008 (maximum thickness is 8% of the chord), the thickest possible airfoil while still achieving a critical Mach number of 0.65.

5.2.3 Upper wing

For the horizontal wing, a correction factor was applied to account for sweep. The thickness ratio for the forward swept, horizontal wing can be found using equation 5.5 [15]. The effective drag divergence Mach number $M_{DIV,eff}$ instead was calculated with Equation 5.6.

$$t/c = 0.30\cos(\Lambda)\left(\left[1 - \left(\frac{5 + M_{DIV,eff}^2}{5 + (M^*)^2}\right)^{3.5}\right]\frac{\sqrt{1 - M_{DIV,eff}^2}}{M_{DIV,eff}^2}\right)^{2/3} \tag{5.5}$$

$$M_{DIV,eff} = M_{DIV} \cdot cos(\Lambda) \tag{5.6}$$

The critical Mach remains the same for the upper wing, but due to the sweep a thicker airfoil can be selected. The thickness ratio for the upper wing is 0.1255. The selected airfoil for the upper wing is NACA0012 (maximum thickness is 12% of the chord length).

5.3 Flap design

After selecting the airfoils it is possible to calculate the flap-to-chord ratios and the flap deflections needed for the lateral acceleration of 0.5 m/s^2 as stated in requirement **IFS-SYS-08-AERO-01** and direct lift force to meet requirement **IFS-SYS-08-AERO-04** [9]. To this purpose the program XFLR5 was used to find optimal values. It was decided to start with a maximum flap deflection of 20° because typically no flow separation phenomena are present up until these angles of deflection [18]. For now it is assumed that the lift coefficient for the 2D situation will be equal to the lift coefficient for the 3D case because the boxwing configuration prevents induced drag. The wings will therefore be modeled as infinite wings. This assumption was checked with results from AVL analysis as presented in section 6.4.

5.3.1 XFLR5

XFLR5 is a software tool created by Mark Drela of MIT and Harold Youngren of Aerocraft Inc [3] that can be used to analyze airfoils. One can select a NACA airfoil and determine the lift, drag and moment coefficients at a particular Reynolds number and Mach number. The program was validated by comparing its generated data with the experimental data from Abbott and Von Doenhoff [1] about the NACA0012. Tests were performed at Reynolds numbers of three, six and nine millions at a Mach number of 0.15. [4]

[2] http://adg.stanford.edu/aa241/drag/mdiv.html [cited 16 January 2017]
[3] http://www.xflr5.com/xflr5.htm [cited 16 January 2017]
[4] https://turbmodels.larc.nasa.gov/naca0012_val.html [cited 18 January 2017]

As can be seen in Figures 5.2 and 5.3 the C_{L_α}-curve provided by Abbott and Von Doenhoff without flap deflection match perfectly with the C_{L_α}-curve provided by XFLR5. At zero angle of attack the lift coefficients are zero for both cases, the only logical solution for symmetric airfoils. At 8° angle of attack the simulation shows a lift coefficient of 0.897 whereas the test data has around 0.87, a percentage difference of only 3% for the C_{L_α} curve.

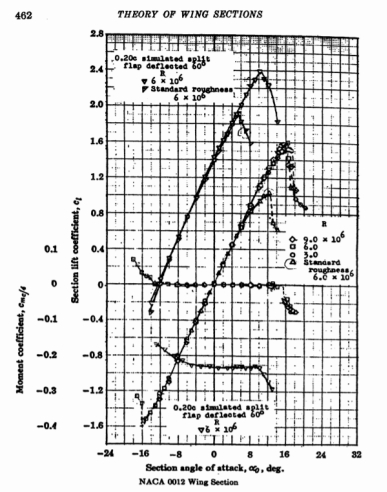

Figure 5.2: NACA0012 C_{L_α} curve as taken from experimental data of Abbott and Von Doenhoff [1].

Figure 5.3: NACA0012 C_{L_α} curve as generated by XFLR5.

5.3.2 Vertical wing

The lift coefficient that the vertical wing has to generate through its flap deflection can be calculated with the lift equation stated in Equation 5.7, with the lift-vector pointing horizontally and not vertically. As a symmetrical airfoil was chosen and no sideslip was assumed, the area of the vertical wing not covered by flaps will not produce any side force. The lift coefficient that needs to be generated to achieve the required lateral acceleration is calculated in Equation 5.7.

$$C_L = \frac{L}{\frac{1}{2}\rho V^2 S} = \frac{MTOW \cdot a}{\frac{1}{2}\rho V^2 S_{flapped}} \tag{5.7}$$

As the COG location is yet unknown, the generated side force is assumed not acting on the line passing through the COG. The side force generated by the tail rudder to prevent a yawing moment has to be taken into account for the total generated side force.Stability and controllability calculations in subsection 7.3.2 produced the exact magnitudes of the forces, with 4,891 N total force for both vertical wings (F_S) and 816 N in the tail rudder (F_r).

In the first iteration it was assumed that 80% of the span would be used to install flaps, as it is not affected by either ailerons (main wing) or upper wing flaps. This margin was included because deflection allowance for the flaps in the upper wing was not available. The span that is flapped is then 0.56 m. This leads to a minimum required lift coefficient of 1.327. The Mach number of the testing conditions were calculated with Equation 5.8:

$$M = \frac{V}{a} = \frac{V}{\sqrt{\gamma RT}} \tag{5.8}$$

The temperature at sea level is 288.15 K, leading to a Mach number of 0.18. The Reynolds number can be calculated with Equation 5.9:

$$Re = \frac{V \cdot c}{\nu} \tag{5.9}$$

In this equation ν is the kinematic viscosity with a value of 1.460 $\cdot 10^{-5}$ for sea level conditions. With a chord of 1.34 m and an airspeed of 61.7 m/s it can be found that the Reynolds number is 5.5 millions. After selecting the proper airfoil and flight conditions in XFLR5 it was found that, with a maximum deflection of 20°, the chord-to-flap ratio had to be at least 0.38. This means that the flap hinge needs to be located at 62 % of the chord length. A schematic representation of the flap dimensions can be found in Figure 5.4. As displayed in the figure, the flap area is divided over two different flaps as a safety measure. If one flap gets stuck in a certain position, the other can counteract the induced forces and moments on the IFS. This is more elaborately explained in section 9.8.

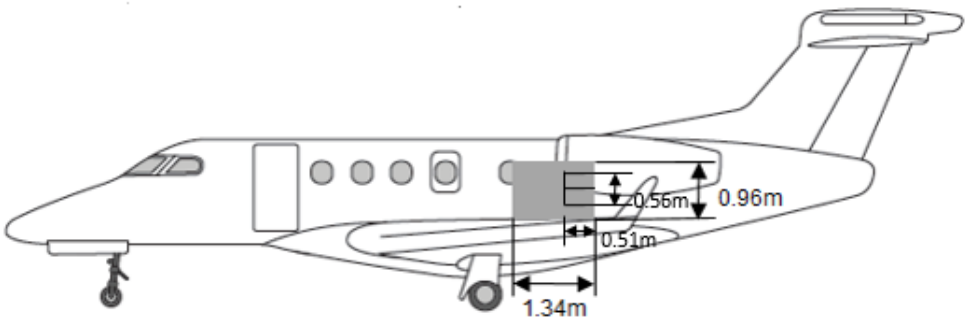

Figure 5.4: A schematic representation of the flap dimensions on the vertical wing.

The pressure distributions for the vertical wing with and without deflection can be found in Figure 5.5. The pressure distributions will be used to define and evaluate the structural design of the wingbox as presented in subsection 8.2.5. As expected for a symmetric airfoils, the pressure distribution without flap deflection sums to zero, thus not producing any lift. It is also logical that the pressure distributions for a positive and negative deflection for the flap of the vertical wing are equal in magnitude because the sideslip angle is zero, which can be clearly be seen by the perfect overlap of the yellow and pink curve. The lift-drag polar, C_{L_α} curve, C_{m_α} curve, the lift coefficient versus transition point and lift-drag ratio versus the angle of attack are presented in Figure 5.6.

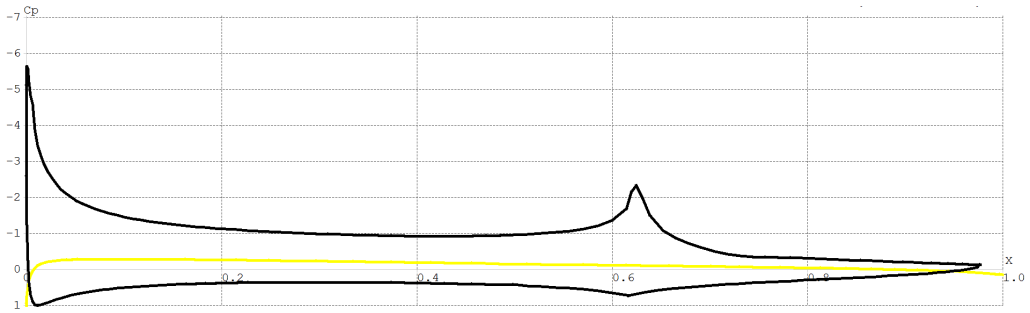

Figure 5.5: Pressure distribution of the vertical wing in clean configuration and flapped configuration.

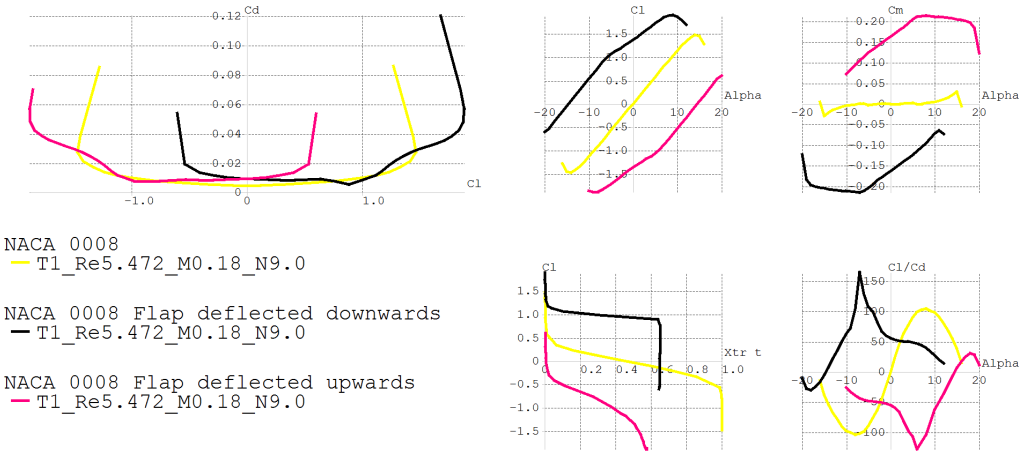

Figure 5.6: Lift-drag polar, C_{L_α} and C_{m_α} curves, lift coefficient versus transition point and lift-drag ratio versus the angle of attack of the vertical wing.

5.3.3 Upper wing

For the upper wing the same approach for calculating the chord ratio of the vertical wing was used as for the vertical wings. In this situation, the extra generated lift force needs to be balanced by the horizontal stabilizer to have a moment equilibrium about the Y-axis. The exact values for these forces were calculated in subsection 7.3.1 as 29,424 N upward for the upper wing and 6,867 N downward for the horizontal tail in the +0.15 ΔC_L case. For the -0.15 ΔC_L case, 4,247 N downward for the upper wing and 4,247 N downward for the horizontal tail was calculated. Both cases are based on the original lift coefficient produced by the main wing. Unlike for the side-force case, it cannot be assumed the incoming airflow has an angle of attack of zero degrees. The angle of attack of the main wing at testing conditions is equal to 10° as derived in subsection 7.3.1. Subsection 6.4 shows that the calculated angle of attack for the 3D model is 9.8°, so the angle of attack of 10° is assumed a valid value for the 2D situation. With the XFLR5 program it was found that the ideal incidence angle for the upper wing would be -5.5°, leading to an angle of attack of the upper wing of 4.5° at testing conditions. If the angle of incidence with respect to the main wing would have been 0°, the angle of attack at testing conditions would have been 10°, making it impossible to reach a ΔC_L of -0.15. If the angle of incidence would have been -10°, the angle of attack at testing conditions would have been ideal, but the upper wing would produce a fair amount of negative lift and extra drag at cruise conditions. For an initial step on the design process, 80% of the upper wing span is assumed to be covered by flaps. That gives a length of 5.41 meters. A schematic representation of the initial flap dimensions can be found in Figure 5.7. As displayed in the figure, the flap area is divided over two different flaps as a safety measure just as was done with the vertical wing. More elaborate information on this safety system is provided in section 9.8.

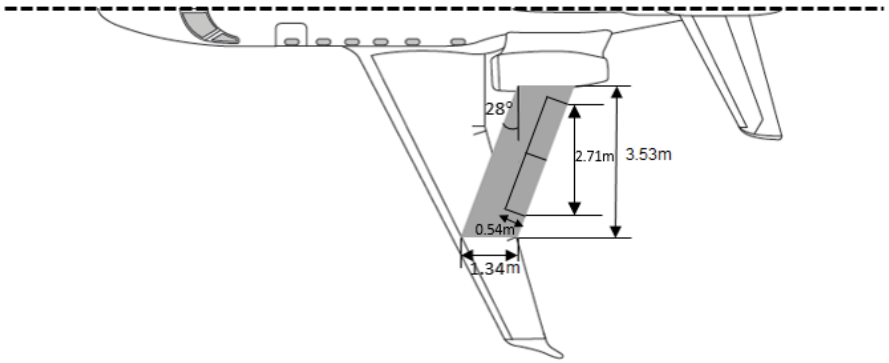

Figure 5.7: A schematic representation of the initial flap dimensions on the upper wing.

For the upper wing the Mach number and Reynolds number change with respect to the vertical wing because of the added sweep angle. Equations 5.8 and 5.9 produced new values for Mach number and Reynolds number resulting in 0.16 and 4.3 million respectively. The airspeed component perpendicular to the wing is 54.5 m/s. The flapped part of the wing generates lift according to Equation 5.7. In the positive and negative ΔC_L the lift coefficients then become 2.53 and -0.36 respectively. It was however found that a deflection of 20° was not sufficient to achieve the required positive lift. Because the maximum lift coefficient with NACA0012 airfoil was 1.61 with flap-to-chord ratio of 0.46 it was decided to increase the span of the flapped part. The minimum clearance for the flap movement was calculated with Equation 5.10 to be 0.19 m.

$$b_{clear} = c_f tan(\delta_{fl_{vw}}) \tag{5.10}$$

Following this estimation the flapped area of the upper wing was extended at both sides with 0.2 m so that 0.02 m clearance is left close to the vertical wings. A schematic representation of the new, final flap dimensions can be found in Figure 5.7.

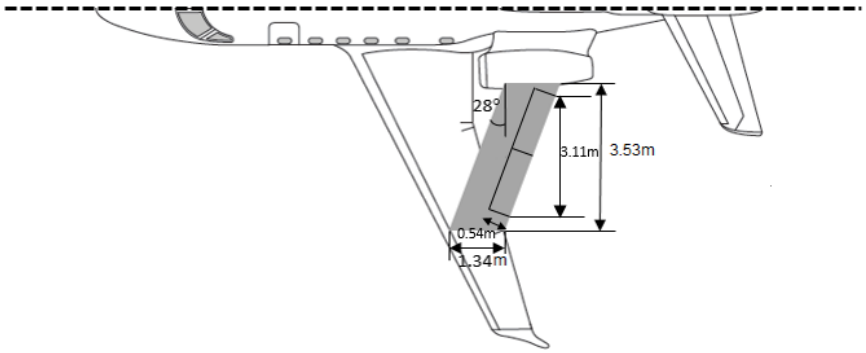

Figure 5.8: A schematic representation of the final flap dimensions on the upper wing.

The lift coefficients of the airfoil that have to be achieved were calculated again with Equation 5.7 and found to be 2.20 and -0.31. Regarding the negative ΔC_L, the 20° deflection upward was found to be creating too much force, therefore after re-calculation a value of 10° was decided upon. Regarding the positive lift case, the 1.61 lift coefficient proved to be less than the required 2.20, leading to the decision to use also the main wing's high-lift devices to achieve the ΔC_L. This is further explained in subsection 7.3.1. The pressure distribution for the upper wing with and without deflections can be found in Figure 5.9. The pressure distributions will be used to define and evaluate the structural design of the wingbox as presented in subsection 8.2.5. The lift-drag polar, C_{L_α} curve and C_{m_α} curve, the lift coefficient versus transition point and lift-drag ratio versus the angle of attack can be found in Figure 5.10.

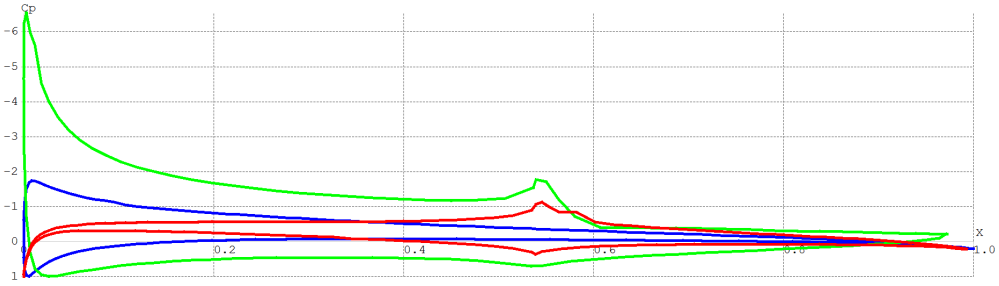

Figure 5.9: Pressure distribution of the upper wing in clean configuration and flapped configuration.

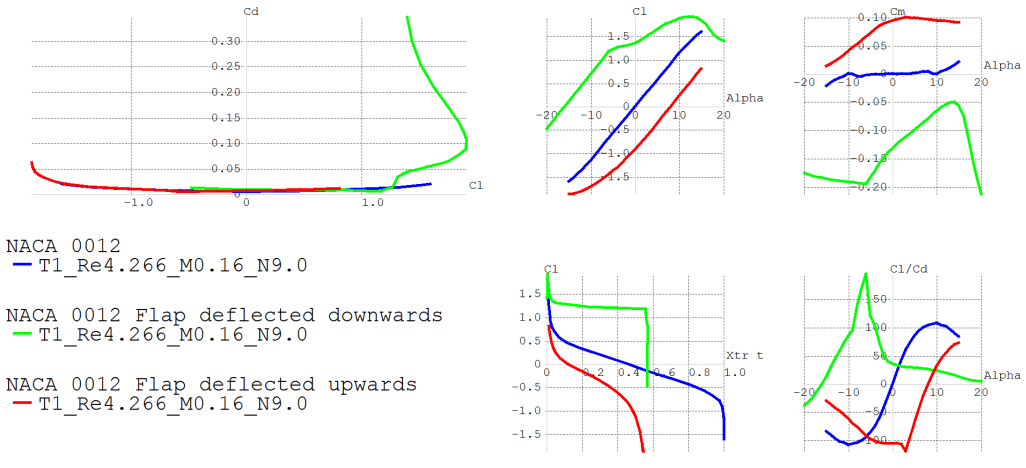

Figure 5.10: Lift-drag polar, C_{L_α} and C_{m_α} curves, lift coefficient versus transition point and lift-drag ratio versus the angle of attack of the upper wing.

5.3.4 Clearance check

It is important to check that the flaps of both wings do not touch each other when fully deflected. The clearance of the flap of the vertical wing was already calculated in section 5.3. In this section also the clearance of the upper wing will be checked.

The flapped areas are placed in the middle of the span and, as was already calculated in the previous subsection, there is a clearance of 0.02 m between the furthest inboard position of the flap of the vertical wing. This means that even if the upper wing exceeds the clearance that was mentioned at the start of section 5.3, the flaps would not hit each other, because the clearance of 0.02 m is independent of the clearance of the flap deflection of the upper wing. Therefore it is clear that all clearances have still been met.

5.4 Drag chute and spoilers design

As already mentioned in the Mid-Term Report [10], the IFS should be able to reach an L/D value of 4 at a flight path angle of 15° downwards as stated in requirement **IFS-SYS-08-AERO-02** [9]. This requirement was included mainly to contribute to the re-entry simulation capabilities of the IFS, therefore the hing-drag mission will be referred to as the 're-entry mission'. The sizing the parachute was done for the design point at which the necessary extra drag is lowest, and apply more drag with spoilers to achieve the L/D value of 4 for the other design point. First the design point is selected for which the parachute will be sized, next the actual sizing is performed and lastly the spoiler sizing is looked into.

5.4.1 Design points

A typical mission during which the IFS will have to reach an L/D of 4, the IFS will be flying with a speed of 144 m/s at 40,000 ft, ending the mission at 61.7 m/s at MSL. The lift and drag coefficients are calculated using Equations 5.11 and 5.12.

$$C_L = \frac{2 \cdot MTOW \cdot g}{\rho V^2 S} \qquad (5.11) \qquad C_D = C_{D_0} + C_{D_i} = C_{D_0} + \frac{C_L^2}{\pi A e} \qquad (5.12)$$

The lift coefficients are 0.695 for the start of the re-entry mission (design point 2) and 0.935 for the end of the re-entry mission at sea level (design point 1). The corresponding drag coefficients are 0.0562 and 0.0769 respectively, leading to starting L/D values of 12.40 and 12.15. It can be seen that extra drag coefficients of 0.118 and 0.157 are necessary to bring both L/D ratios down to 4. This means that the drag chute will be designed for the conditions of design point 2 (starting the re-entry mission) while spoilers will be used as the IFS progresses to design point 1 at sea level.

5.4.2 Drag chute

The drag chute is stored in the back of the aircraft and is released by the test engineer pressing a button so that the re-entry simulation can begin. The parachute system consists of two parts; a pilot chute and a main chute. The pilot chute is used to pull the main chute out of its casing while the main chute is used to achieve the L/D of 4. The complete deployment sequence is shown in Figure 5.11.

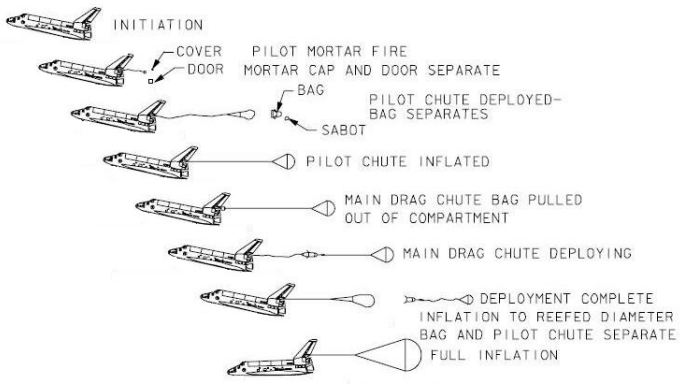

Figure 5.11: Procedure of a chute deployment on the Space Shuttle [5].

[5] http://www.spaceshuttleguide.com/system/landingdeceleration_system.htm [cited 24 January 2017]

At the start of the re-entry simulation the test engineer releases the pilot chute by firing a mortar so that cap and door can separate from the IFS. The pilot chute is then pulled out of its vane and exposed to the airflow, where it inflates, in turn pulling out the main chute as the drag rises. When the main chute starts to inflate, the pilot chute separates from the main chute. The re-entry mission flight plan should be planned ahead to pinpoint the location for easy retrieval of the pilot chute. When the mission reaches sea level altitude, the mission is complete and the parachute is jettisoned, again at a planned location.

The sizing of both parachutes is explained next. It was chosen to use a shallow, conical parachute as these are used more often in modern aerospace applications. These shapes optimize the value of the drag coefficient [6]. The drag force that has to be generated by the main parachute for the static loading case can be calculated with Equation 5.13, where q is the dynamic pressure $1/2\rho V^2$ and the pa subscript denotes parachute-related area and drag coefficient.

$$q \cdot C_{D_{extra}} \cdot S_{IFS} = q \cdot C_{D_{pa}} \cdot A_{pa} \tag{5.13}$$

Because dynamic pressure is not zero and equal in both sides of the equation, it can be left out. The drag coefficient of the parachute was then calculated with Equation 5.14 [19].

$$C_{D_{pa}} = \left(0.854 + 0.044\frac{x}{D_o} - 0.004(\frac{x}{D_o})^2\right) \cdot \left(0.874 - 2.29\lambda_g + 1.953\lambda_g^2 + (0.055 + 1.145\lambda_g)(\frac{L_s}{D_o} - 1) + (0.012 - 0.775\lambda_g)(\frac{L_s}{D_o} - 1)^2\right) \tag{5.14}$$

In Equation 5.14, $\frac{x}{D_o}$ is the ratio between the body-parachute distance (IFS to parachute opening) and the diameter of the parachute, λ_g is the geometric porosity of the canopy and $\frac{L_s}{D_o}$ is the ratio between the suspension line length and the diameter of the parachute. To generate the highest C_D, the individual parameters are inspected. The drag coefficient decreases with increasing geometric porosity, so it is desirable to have a low geometric porosity. The lowest possible porosity is of course zero, id est when the canopy has no vents. However in this case the dynamic loading case would increase dramatically while stability would decrease. It was then decided to use a geometric porosity of 0.20. The drag coefficient increases with increasing ratios of $\frac{x}{D_o}$ and $\frac{L_s}{D_o}$). It is therefore desirable to have these ratios high as possible. Though, to achieve longitudinal stability it is necessary to have the parachute close to the body to take the main wing downwash into account and have a better longitudinal stability. It was decided to use a value of 2.5 for $\frac{x}{D_o}$ and a value of 1.5 for $\frac{L_s}{D_o}$. This leads to an overall drag coefficient for the parachute of 1.158. The frontal area of the parachute is then calculated to be 3.85 m^2, the suspension line length is to be 3.32 m and the distance between the IFS and the parachute is to be 5.53 m. The pilot chute sizing was made using a scaling factor, determined via a second-degree polynomial trendline for different sizes of available canopies [7]. A diameter of 0.53 m was calculated, leading to a parachute frontal area of 0.22 m^2. A schematic visualization of the deployed parachute system is presented in Figure 5.12.

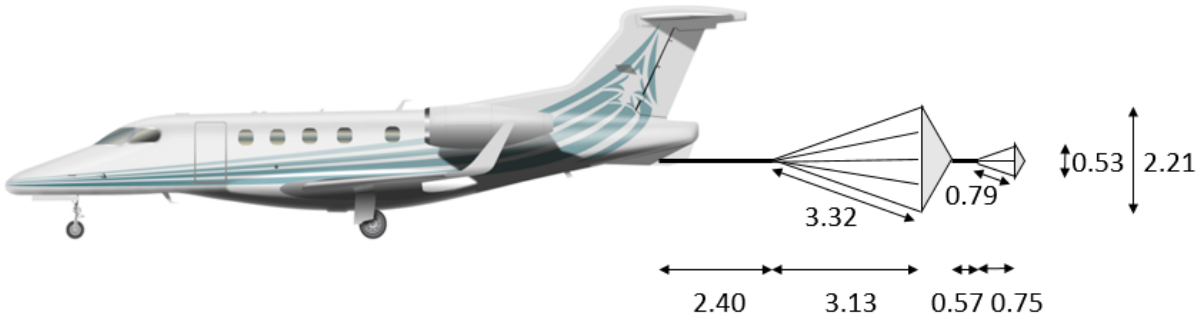

Figure 5.12: Dimensions of the parachute system of the IFS.

[6] http://www.pcprg.com/rounddes.htm [cited 17 January 2017]
[7] http://www.sunpath.com/canopysizing.php [cited 17 January 2017]

The parachute system needs also to be as light as possible. To determine the total mass of the parachute the cables, both main-line and suspension-lines, have to be sized such that no failure occurs. The highest tensions in the cable are calculated by examining the dynamic loading case just after deployment. No useful literature was found to determine the dynamic loads directly, so the static loading cases were used with a safety factor instead. Applying an overall safety factor of 3 to account for the dynamic loads was chosen. The ultimate load that is applied per suspension line is calculated with Equation 5.15.

$$F_{total} = nF_s = \frac{sf_{dl} \cdot D}{\cos(19.6°)} \tag{5.15}$$

In Equation 5.15, n is the number of suspension lines and sf_{dl} is the safety factor of 3 accounting for the dynamic loading case. The actual tension in the suspension lines has to take into account the angle with respect to the main line, so it will be higher than the total drag that is generated. The total tension force for the main line is 44.7 kN. A safety factor, denoted by sf_{fail} of 1.5 is applied to ensure the cable does not fail, so the cables are designed for a load of 67.1 kN. The total mass of all suspension lines is calculated with Equation 5.16.

$$W = \rho A L_s n \tag{5.16}$$

In Equation 5.16 ρ and A_{min} are the density and cross-sectional area of the wire ropes respectively. The minimum cross-sectional area of each suspension line is shown in Equation 5.17.

$$A = \frac{sf_{fail}F_s}{\sigma} = \frac{sf_{fail}F_{total}}{n\sigma} \tag{5.17}$$

The relation between the force that is applied to a cross-sectional area is denoted by the universal stress symbol σ. Though, the failure for wire ropes is not often denoted by the yield stress, but by the breaking strength that increases with increasing cross-sectional area. The relation between the breaking strength and the cross-sectional area is here denoted by σ as shown in Equation 5.18.

$$W = \rho A L_s n = \rho \frac{sf_{fail}F_{total}}{n\sigma} L_s n = sf_{fail}F_{total}L_s\frac{\rho}{\sigma} \tag{5.18}$$

In Equation 5.18 the overall mass of the cables of the parachute is independent of the number of cables, depending only on cable type and material. A higher number of cables would lead to cables with a smaller cross-sectional area, in this way decreasing the mass. To minimize the mass of the set of suspension lines, the ratio between ρ and σ needs to be minimal as presented in Equation 5.19.

$$W_{min} = sf_{fail}F_{total}L_s\left(\frac{\rho}{\sigma}\right)_{min} \tag{5.19}$$

After assessment of all the different wire ropes available it was found that the F-type had the lowest ratio between ρ and σ [8]. The mass of the set of suspension lines is 0.93 kg. It was chosen to have a high number of suspension lines so that if one fails, there are still many suspension lines left to compensate the drag force. If n is set to 20, the corresponding diameter is 2.16 mm. The suspension lines will be evenly spread along the circumference of the parachute.

For the main cable between the suspension lines and the aircraft, the mass is different due to the fact that the cable is not placed at an angle anymore [20]. The length of the main cable is 2.40 m and it bears 63.2 kN of load for the dynamic loading case. The minimum mass of the main cable then becomes 0.63 kg.

The same procedure is applied for the pilot chute. The drag that the pilot chute generates is calculated with Equation 5.13 to be 3.6 kN. The same configuration for the pilot chute is used as for the main chute. The mass of the suspension lines of the pilot chute is 12 gram and the mass of the main line of the pilot chute 8.6 gram. The total mass of the cabling system of both parachutes is 1.58 kg.

The mass of the canopies was also calculated. If one wants to calculate the surface area of a cone-shaped figure, one needs to know the distance from the top of the cone to the bottom, which is the radius of the circle of the open-folded cone. Since it a 20° conical shaped parachute, the radius can easily calculated by trigonometry. The radius of the main chute is 1.179 m and the radius of the pilot chute 0.277 m. The circumference of the parachutes is the circumference of the open-folded cone. To produce the parachutes, including the geometric porosity, a total of 3.53 m^2 of material is needed excluding production-related allowances. Assuming a thickness of 1 mm and Nylon-66 as material [9], the mass of both canopies becomes 4.94 kg. The total mass of the drag chute system is 6.52 kg. The mass of the attachment subsystem and releasing spring subsystem have not been taken into account for the total mass of the drag chute system and is recommended for future research.

[8] http://www.steelwirerope.com/Downloads/AsahiProductGuide.pdf [cited 23 January 2017]
[9] http://www.azom.com/article.aspx?ArticleID=477 [cited 19 January 2017]

5.4.3 Spoilers

As was already stated in the Mid-Term Report [10] it is difficult to predict the airflow characteristics when spoilers are deployed without using extensive CFD tools. Therefore, the same procedure is applied to check if the spoilers that are on the original Embraer Phenom 300 suffice with fully deflected surfaces to achieve the L/D value at design point 1. The procedure relies on finding a ratio between the area of the spoilers and the total wing area of the Embraer Phenom 300 with empirical data of the Boeing 747. When the HLDs of the IFS are fully deflected to 25° and the main wing spoilers are deflected to 45° the difference in lift coefficient can be calculated in Equation 5.20 [21].

$$\Delta C_{L_{sp}} = (k_{\delta_{sp}}) \cdot (\Delta C_{L_{sp}45}) \cdot \frac{(C_{L_{sp}})_M}{(C_{L_{sp}})_{M=0}} \cdot \left(\frac{L_E}{L_R}\right)_{sp} \tag{5.20}$$

In Equation 5.20, $k_{\delta_{sp}}$ is the spoiler effectiveness, $\Delta C_{L_{sp}45}$ is the effect of the spoiler angle, $\frac{(C_{L_{sp}})_M}{(C_{L_{sp}})_{M=0}}$ is the effect of the Mach number and finally $(\frac{L_E}{L_R})_{sp}$ is the effect of aeroelasticity on the lift coefficient. The difference in lift coefficient then becomes -0.137, causing a net reduction in lift force. The difference in drag coefficient of the spoiler only depends on the spoiler angle and the flap angle, with a variation of 0.008, that is an increase in drag force. If the numbers are inserted in Equation 5.21 the ratio of spoiler area that is necessary to achieve this situation can be found.

$$\frac{L}{D} = \frac{C_{L_{DP1}} + N \cdot \Delta C_{L_{sp}}}{C_{D_{DP1}} + C_{D_{extra}} + N \cdot \Delta C_{D_{sp}}} \tag{5.21}$$

With this it can be found that the ratio of spoiler area and total wing area is 0.93, which entails that the spoiler area in combination with the HLD that are currently installed on the Embraer Phenom 300 are enough to achieve the L/D value of 4 in combination with the parachute at design point 1. Requirement **IFS-SYS-08-AERO-05** will be dropped which states that a ΔC_D of +/-<*TBD*>needs to be generated, the requirement is dropped because the amount of drag is formulated with the L/D of four and the other requirement will become obsolete. It is stated that the re-entry vehicles that will be simulated have an L/D of a minimum of four [10]. With the added drag chute and the original control surfaces still functional during this mission, an L/D of 4 can be simulated, meaning requirement **IFS-SH2-07** is met.

6 | Aerodynamic Analysis

This chapter will discuss the aerodynamic analysis of the complete aircraft, both with and without modifications. This aerodynamic analysis was performed with the Vortex Lattice Method (VLM) of which the principals will be discussed in section 6.1. The VLM analysis was performed in Athena Vortex Lattice (AVL). This program, along with the models that were used and the setup of the simulations will be discussed in section 6.2. This is followed by the verification and validation of the aerodynamic analysis in section 6.3. Finally, section 6.4 will present the results obtained from the aerodynamic analysis.

6.1 Vortex Lattice Method

With the Vortex Lattice Method (VLM), a lifting surface is represented by a grid of horseshoe vortices that is superimposed on the intended surface. A typical horseshoe vortex consist of a single bound vortex, paired with trailing vortices on each of its sides, as pictured in Figure 6.1. Every panel has a horseshoe vortex at the quarter chord point of the panel and a control point at the three quarter chord point, as pictured in Figure 6.2. At this point the velocities induced by all vortices is calculated using Equation 6.1, known as the *Biot-Savart law*.

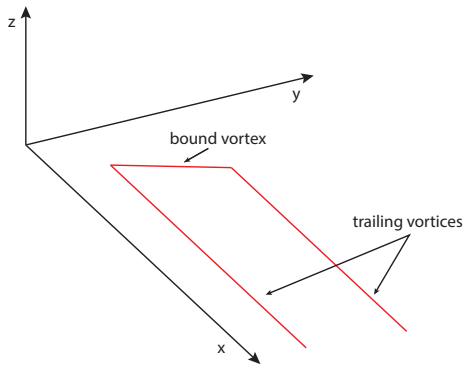

Figure 6.1: Typical horseshoe vortex definition in VLM.

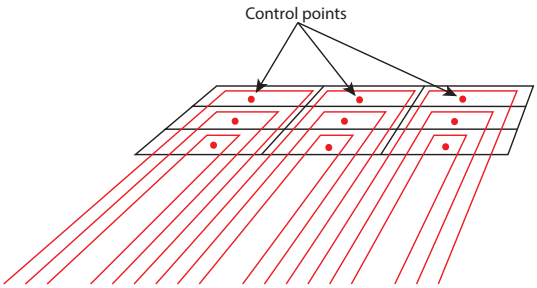

Figure 6.2: 3x3 vortex lattice representation of a lifting surface in VLM.

A set of linear equations for the vortex strengths is obtained when all the control points are summed. For each control point, the total velocity is expressed as the sum of the velocities induced by all points on the grid and the free stream velocity. When this is done for all control points, a system of equations is formed. To solve this system of equations for circulation strength, the boundary condition in the form of Equation 6.2 is applied to the system. This boundary condition implies that no flow exists through the wing. This boundary conditions sets the flow at each control point parallel to the wing, thus making the surface a streamline of the flow.

$$\mathbf{dV} = \frac{\Gamma}{4\pi}\frac{\mathbf{dl}\times\mathbf{r}}{|\mathbf{r}|^3} \qquad (6.1) \qquad\qquad \mathbf{V}\cdot\mathbf{n} = \mathbf{0} \qquad (6.2)$$

For this condition to be satisfied, the sum of the components of the induced velocity and free stream velocity perpendicular to the wing at each control point should be zero. For a 3-dimensional wing with camber and dihedral this results in Equation 6.3, with ϕ the dihedral angle and $\delta = \tan^{-1}\left(\frac{dz}{dx}\right)_m$ the mean camber line slope. Assuming small angles of attack and mean camber line slope, this reverts to Equation 6.4.

$$-u_m \sin\delta\cos\phi - v_m\cos\delta\sin\phi + w_m\cos\phi\cos\delta + V_\infty \sin\left[\alpha-\delta\right]\cos\phi = 0 \qquad (6.3)$$

$$w_m - v_n\tan\phi + V_\infty\left[\alpha - \left(\frac{dz}{dx}\right)_m\right] = 0 \qquad (6.4)$$

This in turn allows the system of equations to be solved for the circulation strengths Γ_n. With the circulation per section known, the lift per section can now by calculated. This is done using the *Kutta-Joukowski theorem* in Equation 6.5. For total lift of a surface, the lift per panel l_n is summed over the entire span following Equation 6.6.

$$l_n = \rho_\infty V_\infty \Gamma_n \qquad (6.5) \qquad\qquad L = \sum_{n=1}^{N} l_n = \rho_\infty V_\infty \sum_{n=1}^{N}\Gamma_n \Delta y_n \qquad (6.6)$$

6.2 Athena Vortex Lattice

Athena Vortex Lattice (AVL) is a software tool provided by Mark Drela of MIT and Harold Youngren of Aerocraft Inc. It can be used for the aerodynamic and flight dynamic analysis of arbitrary configured aircraft. The program performs the analysis of the lifting surfaces by employing the Vortex Lattice Method discussed in the previous section. It can also be used to simulate ground effect, wind tunnel wall interference and influence of other nearby aircraft.

The main input for AVL is an 'xxx.avl' file describing the geometry of the aircraft. Optional input files are the mass and run files, respectively 'xxx.mass' and 'xxx.run'. The mass file gives the mass and inertia values and dimensional units. This file is required for the stability analysis of the aircraft. The run file contains a list of parameters defining any number of run cases. If this file is absent, the variables need to be defined first using the command prompt. Available variables are:

- Roll rate, $\frac{pb}{2V}$
- Pitch rate, $\frac{qc}{2V}$
- Yaw rate, $\frac{rb}{2V}$
- Angle of attack, α
- Angle of sideslip, β
- Control surface deflection, $D1, ..., DN$, for all defined control surfaces

Each variable can either be constrained directly or indirectly. For example, one can set $\alpha = x.x$ or one can set $\alpha \ni C_L = x.x$.

After a run is set up, it is executed. The main outputs of AVL are direct aerodynamic force and moment coefficients and stability derivatives in body and stability axes. An example of the output screen of AVL is shown in Figure 6.3. It is also possible to visualize the load distribution by plotting the loads on the surfaces on which they act. This is seen in Figure 6.4. For a detailed overview of the program the reader is referred to the AVL website[1] and the AVL user guide [22].

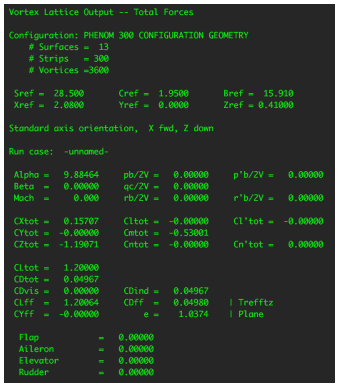

Figure 6.3: Screenshot of the AVL output.

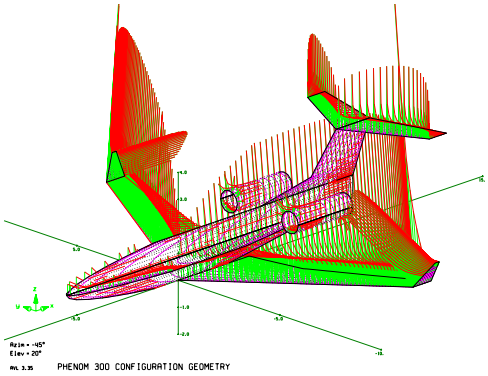

Figure 6.4: 3D visualization of forces acting on the aircraft in AVL.

6.2.1 Limitations

Flow calculations performed with AVL are inviscid. Since the surfaces are modelled as slender bodies and the flow region which is of interest is outside the boundary layer, the assumption of inviscid flow provides a valid representation [23].

Viscous flow however does not provide a valid representation of the flow inside the boundary layer. This means separation of the flow (stalling) does not occur in AVL. Also, the total aerodynamic drag is not accurately represented, as only the lift induced drag is calculated. The skin friction and pressure drag (together called parasite drag) appear due to viscous effects and are therefore not represented in AVL. A separate calculation will be performed to provide a drag estimate in subsection 6.2.4.

[1] http://web.mit.edu/drela/Public/web/avl/ [cited 18 January 2017]

6.2.2 Model

The main input for AVL is a file describing the aircraft. This description includes reference values, aircraft geometry and the grid definition. The reference values are the the x-, y- and z-coordinates of the center of gravity, the wing area, MAC and wingspan. The first three are used as a reference about which the moments are calculated and are taken with respect to the nose, centerline and bottom of the fuselage. The latter three are used to non-dimensionalize the forces and moments. For the model of the IFS, the total wing area, a weighted average of the MAC and the original wingspan were taken. These reference values for both models can be found in Table 6.1.

Table 6.1: Reference values of the Phenom 300 and IFS models used in AVL.

Model	$\mathbf{X_{ref}}$	$\mathbf{Y_{ref}}$	$\mathbf{Z_{ref}}$	$\mathbf{S_{ref}}$	$\mathbf{C_{ref}}$	$\mathbf{B_{ref}}$
Phenom 300	7.58	0.00	0.41	28.5	1.95	15.91
IFS	8.08	0.00	0.41	37.48	1.80	15.91

The geometry is defined by specifying locations of sections of a surface. A new section is defined for each change in geometry or the inclusion of a control surface, in addition to a section at the beginning and end of a surface. Lines are extrapolated between each section to provide the total geometry. The fuselage is approximated by a horizontal and vertical surface resembling the shape of the fuselage. The control surfaces and the high-lift devices defined for the Phenom 300 are ailerons, rudder, elevator and flaps. Additionally, the flaps on the upper wing and the rudders on the vertical wings are defined for the model of the IFS.

Furthermore, the grid is defined in the input file. The grid is specified by the number of chordwise (N_{chord}) and spanwise (N_{span}) horseshoe vortices and their respective spacing (C_{space}, N_{space}). Table 6.2 gives an overview of the grid of the models. The used spacings are defined as follows:

- **Equal:** constant spacing throughout span (| | | | | |)
- **-Sine:** coarse at the root, fine at the tip (| | | ||)
- **Cosine:** fine at the root and tip, coarse in the middle (|| | | | | ||)

Table 6.2: Grid definition of the AVL models.

Surface	**Type**	**Sections**	$\mathbf{N}_{chord}$	$\mathbf{C}_{space}$	$\mathbf{N}_{span}$	$\mathbf{S}_{space}$	**Airfoil**
Wing	Lifting	6	12	Cosine	40	Equal	NACA 63412
Winglets	Lifting	2	12	Cosine	12	-Sine	NACA 0010
Vertical Tail	Lifting	3	12	Cosine	12	Equal	NACA 0010
Horizontal Tail	Lifting	3	12	Cosine	12	Equal	NACA 0012
Fuselage	Non-lifting	7	12	Cosine	10	-Sine	n.a.
Nacelles	Non-lifting	13	12	Cosine	12	Equal	n.a.
Vertical Wing	Modification	4	12	Cosine			NACA 0008
Upper Wing	Modification	5	12	Cosine			NACA 0012

The input file is generated by a MATLAB script. This was done to ensure a consistent layout and provide the ability to change any variable (e.g. wing sweep) and have this changed accurately applied on all defined sections. For both aircraft, two models were made: one model containing the whole aircraft and one model containing only the force producing surfaces. For the complete model, the fuselage was modelled as planar surfaces in the xz-plane and xy-plane. The engine nacelles were modelled as straight cylinders. Both the fuselage and nacelles were assumed to not provide any lift. Therefore the *NOWAKE* command was used to prevent these from being seen as lifting surfaces. The resulting models can be seen in Figure 6.5a through Figure 6.6b.

6.2.3 Simulation

Simulations using the models from the previous section were run for two different cases. The conditions for these cases can be found in Table 6.3. For both cases multiple simulations were run. To gather data for the lift and drag polars, simulations were run with an angle of attack varying from -5 to 15 degrees. For the stability derivatives, simulations were run for steady flight. For steady flight, the required lift coefficient was calculated using Equation 6.7.

$$C_L = \frac{2 \cdot m \cdot g}{q_\infty S} \tag{6.7}$$

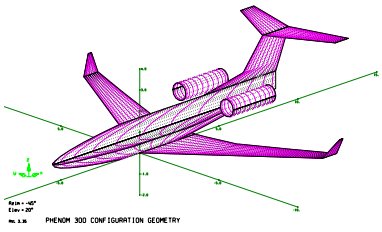

(a) Phenom 300 including non-lifting surfaces.

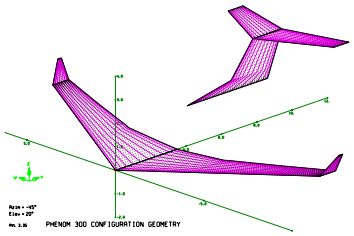

(b) Phenom 300 without non-lifting surfaces.

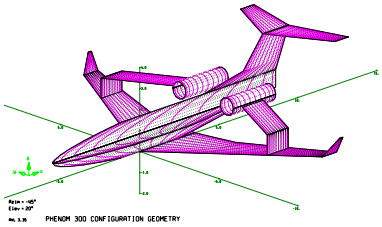

(a) IFS including non-lifting surfaces.

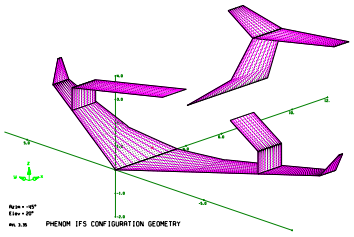

(b) IFS without non-lifting surfaces.

Figure 6.6: AVL models of the Phenom 300 and the IFS, with and without the non-lifting surfaces.

Table 6.3: Flight conditions used in the simulation runs.

Case	Altitude [m]	Speed [m/s]	Density [kg/m^3]	Lift coefficient [-]
Design point 1	0	61.7	1.225	1.2
Cruise	12,192	191.8	0.302	0.51

The following assumptions were used for the simulations:

- The aircraft mass is constant and equal to the MTOW.
- The standard gravity is constant and independent of altitude.
- Angles of attack and sideslip are small.

6.2.4 Drag

The main limitation of AVL is the inviscid flow assumption. This means another, extra method has to be applied to estimate the total drag. For the purpose of this analysis, the total drag is defined by Equation 6.8. A method to estimate the zero-lift drag (Equation 6.9), originally by Shevell (1989) and Schaufele (2000), was provided by Bertins [24].

A separate skin friction coefficient is determined for all different parts of the aircraft. This coefficient is then adjusted for form factor of the component and finally scaled to size. Geometrically, a component is either defined as a wing-like shape or a body-like shape. The exact method to determine previously mentioned values is largely similar.

$$C_D = C_{D_0} + C_{D_i} \tag{6.8}$$

$$C_{D_0} = \sum_{i=1}^{N} \frac{K_i \bar{C_{f_i}} S_{wet_i}}{S_{ref}} \tag{6.9}$$

First, the skin friction coefficient is determined by the Prandtl-Schlichting formula, correcting for laminar flow and surface roughness (Equation 6.10). The Reynolds number, is calculated for design point 1 using Equation 6.11 with the mean aerodynamic chords for wings and total length for bodies. Then the wetted area is determined and the form factor K is obtained from literature by Shevell [17]. A summary of the values and the result of the zero-lift drag estimation are given in Table 6.4. Values in parentheses are components used for the IFS drag estimation. The total value will zero-lift drag will be added to the lift-induced drag from AVL, to provide a total drag estimate for the aerodynamic polars.

$$\bar{C_f} = \frac{0.455}{(\log_{10} Re_L)^{2.58}} - \frac{1,700}{Re_L} \quad (6.10) \qquad Re_L = \frac{\rho_\infty U_\infty l}{\mu_\infty} \quad (6.11)$$

Table 6.4: Estimation of zero-lift drag coefficients.

Surface	Type	l [m]	Re_L ($\times 10^6$) [-]	$\bar{C}_f$ [-]	K [-]	S_{wet} [m^2]	C_{D_0} [-]
Wing	Wing-like	1.95	0.824	0.00307	1.230	48.968	0.00648
Vertical Tail	Wing-like	1.97	0.832	0.00306	1.200	14.894	0.00192
Horizontal Tail	Wing-like	1.29	0.546	0.00318	1.180	15.300	0.00202
(Vertical Wings (2))	Wing-like	(1.34)	(0.566)	(0.00318)	(1.140)	(2.614)	(0.00068)
(Upper Wing)	Wing-like	(1.34)	(0.566)	(0.00318)	(1.225)	(19.375)	(0.00264)
Fuselage	Body-like	14.00	5.913	0.00240	1.140	62.809	0.00603
Nacelles (2)	Body-like	2.70	1.140	0.00296	1.500	6.955	0.00217
Total							**0.01872 (0.02204)**

6.3 Verification & validation

In this section, the verification and validation of the aerodynamic analysis will be discussed. First the verification of the code will be treated, followed by the verification of the model. Then an acceptance test will be discussed as a validation of program used for the aerodynamic analysis. Finally, the models used for the simulation will be validated.

6.3.1 Code verification

As mentioned earlier, a script was written in MATLAB to produce the input file (xxx.avl) for AVL. This code was first verified by checking for errors in the compiler. After this, the AVL input file was visually checked to confirm the correct syntax was used for the file to work with AVL. Any other errors found during the code verification were corrected.

6.3.2 Model verification

After importing the model to AVL, it was plotted to verify its geometry and grid. The geometry was checked for any discontinuities and anomalies. A test run was performed for which the loads were plotted on the aircraft. Figure 6.7a shows an anomaly found at boundary between the winglet and main wing tip. This anomaly was attributed to the grid spacing. The model was originally set up with a coarse spacing at the root of a section, refining toward the tip. Since the induced velocity is inversely proportional to the cube of the distance between a control point and any arbitrary horseshoe vortex, the induced velocity will go towards infinity as the distance gets smaller (Equations 6.12 and 6.13).

$$\mathbf{dV} \propto \frac{1}{\mathbf{r}^3} \quad (6.12) \qquad \lim_{\mathbf{r}\to 0} \frac{\Gamma}{4\pi} \frac{\mathbf{dl} \times \mathbf{r}}{|\mathbf{r}|^3} = \infty \quad (6.13)$$

To deal with this anomaly, the grid was changed from a varying spanwise spacing to a constant spacing. A simulation was once again run. Figure 6.7b shows the anomaly has indeed been resolved by the new spanwise spacing.

6.3.3 Program validation

A software acceptance test was performed to validate AVL. In 1947, Sivells [2] performed wind tunnel tests on a simple wing with a NACA 65-210 profile at the Langley 19-foot pressure tunnel. An overview of the geometry can be found in Figure 6.8.
This exact wing was also modelled in AVL as seen in Figure 6.9. With the pressure, Reynolds and Mach number known for the wind tunnel test, the free stream speed and density were determined to be $V = 64.94$ m/s and $\rho = 2.249$ kg/m^3 using Equations 6.14 through 6.16. Since the air in the wind tunnel was compressed, these numbers are feasible.

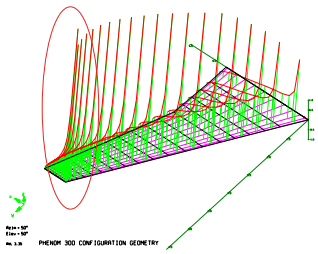

(a) Wing with varying spanwise grid, with anomaly indicated by a circle.

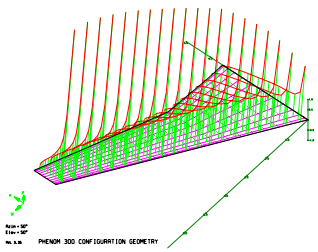

(b) Wing with constant spanwise grid.

Figure 6.7: Evolution of the wing model in AVL.

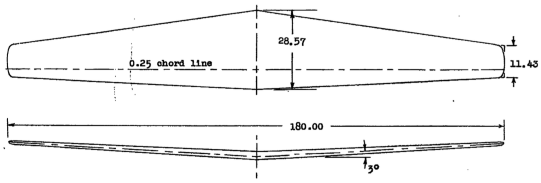

Figure 6.8: Wing geometry used by Sivells [2].

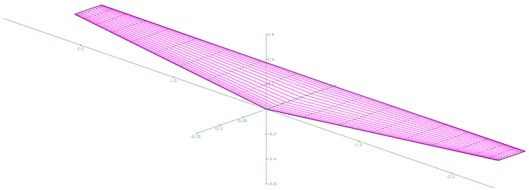

Figure 6.9: AVL model of the wing used by Sivells [2].

$$V = \frac{Re \cdot \mu}{\rho \cdot \bar{c}} \qquad (6.14) \qquad M = \frac{V}{\sqrt{\gamma \cdot R \cdot T}} \qquad (6.15) \qquad P = \rho \cdot R \cdot T \qquad (6.16)$$

AVL simulation runs were then executed for angles of attack ranging from -5 to 15 degrees. The results of the simulation and wind tunnel tests were plotted as seen in Figure 6.10. Overall the data agrees quite well in the linear region of the lift polar. The data obtained from AVL however does not reflect the stalling of the wing.

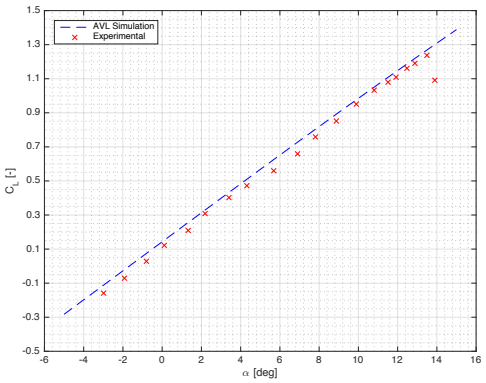

Figure 6.10: Comparison of wing lift polar diagrams for $Re = 4.4 \cdot 10^6$, $M = 0.17$.

6.3.4 Model validation

As mentioned in subsection 6.2.2, the aircraft were modelled with and without non-lifting surfaces. Data on the reliability of modelling the fuselage as two planar surfaces is not readily available. Therefore, lift- and moment polars were created for the standard Phenom 300 model, both with and without non-lifting surfaces. The result is seen in Figure 6.11.

Since the fuselage and nacelles were modelled as non-lifting surfaces, their contribution to the total lift coefficient is negligible. This can be seen in the graph as the lift polars are very similar. Comparing the moment polars or the different components to those of the Cessna Citation seen in Figure 6.12, it can be seen that the moment polars are also similar in sign and magnitude. That is, the fuselage and nacelles have a destabilizing effect, whilst lifting surfaces have a stabilizing effect.

Whilst the above results look very promising, during runs at low angle of attack, the models with fuselage produced negative values for induced drag. Off course this is not within the realm of possibilities. Therefore, the Phenom 300 and IFS models with only lifting surfaces will be used.

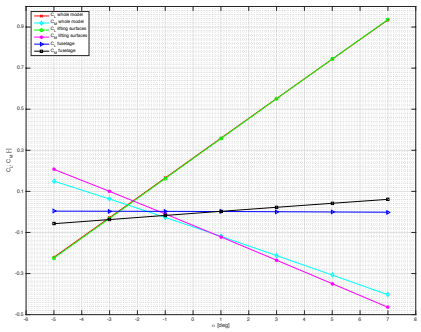

Figure 6.11: Lift and moment polar of the Embraer Phenom 300.

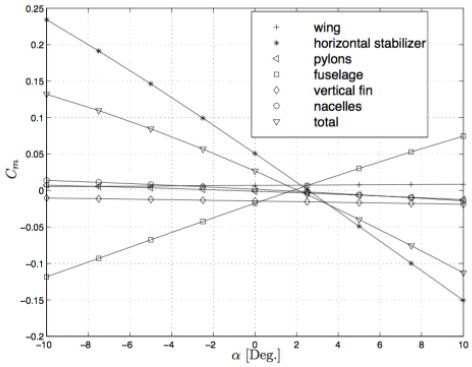

Figure 6.12: Moment polar of the Cessna Ce500 Citation.

6.4 Analysis results

In this section the results of the aerodynamic analysis will be treated. First, the aerodynamic polars for both the Phenom 300 and IFS will be shown and discussed, followed by the stability derivatives and the discussion of said derivatives. Where possible, the results will be compared with data of the Cessna Ce500 Citation.

6.4.1 Aerodynamic polars

The aerodynamic polars for the Phenom 300 are shown in Figures 6.13a through 6.13c. As previously mentioned, viscous effects are not taken into account in AVL. Looking at Figure 6.13a, the IFS has a higher zero-lift angle-of-attack than the Phenom 300. This can be attributed to the negative incidence angle of the upper wing. Due to this additional lifting surface, it does have a higher lift-curve slope.

The addition of the upper wing also has an impact on the longitudinal stability. As can been seen, the IFS has a steeper, negative moment-curve slope. This can be attributed to the fact that the upper wing is mounted behind the center of gravity, providing an additional nose-down moment with increasing angle of attack.

Though not clearly visible in Figure 6.13a, the addition of the vertical and upper wings has an effect on the drag. This reduction in performance is more clearly observed in both Figures 6.13b and 6.13c. In clean configuration, the vertical wings contribute to the drag in the form of parasitic drag. The contribution of the upper wing consists of both parasitic and lift-induced drag.

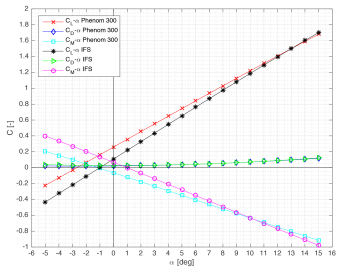

(a) $C_L, C_D, C_M - \alpha$- curves.

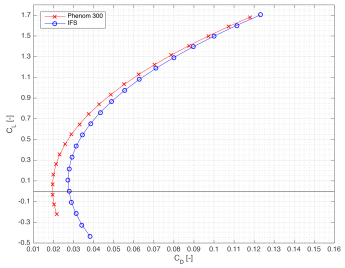

(b) $C_L - C_D$- curve.

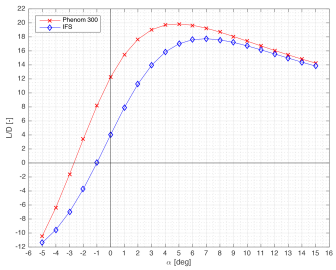

(c) L/D $- \alpha$- curve.

Figure 6.13: Comparison of lift, drag and moment curves w.r.t. AoA of the Phenom 300 and the IFS.

6.4.2 Stability derivatives

The results of the simulation are seen in Tables A.2 and A.3. Since the models used in AVL should be considered as a rough representation of reality, the stability derivatives will not be compared in terms of exact numbers, but only in terms of magnitude and sign. As can be seen in the tables, not all values could be determined by AVL. The non-dimensional inertia terms should be separately calculated. For the symmetric coefficients, most values were found, for the asymmetric coefficients, all values were found. The calculated difference in percentage for these results is presented in Table 6.5.

Since all derivatives for the IFS were made non-dimensional with a larger reference area, a reasoning will only be provided for differences of more than 35% . Derivatives with respect to u (marked with '*') are very rare, since these are mostly determined in steady flight. These derivatives should therefore be considered with care. Control derivatives (marked with '**') obtained from AVL are in the wrong order of magnitude. A reason for this could not be accounted for. These values should also be considered with care.

Table 6.5: Comparison of stability derivatives between the original Phenom 300 and the IFS.

Derivative	Difference	Reasoning
C_{X_u}*	-50%	Due to increased drag by the modifications.
C_{X_q}	-8%	
$C_{X_{\delta_e}}$**	25%	
C_{Z_u}*	12%	
C_{Z_q}	20%	
$C_{Z_{\delta_e}}$**	25%	
C_{m_u}*	42%	Due to upwards shift in c.g., the moment arm of the thrust gets smaller, moment gets smaller.
C_{m_α}	35%	This value should be discarded, since the slope of the moment curve in Figure 6.13a is clearly more steep.
C_{m_q}	21%	
$C_{m_{\delta_e}}$**	24%	
C_{Y_β}	-42%	A larger sideforce per degree of sideslip is produced by the addition of the vertical wings.
C_{Y_p}	263%	Due to the addtion of the upper wing, an additional sideforce is created during rolling.
C_{Y_r}	10%	
$C_{Y_{\delta_a}}$**	90%	This value should be discarded. The difference is accounted for by the change in order of magnitude. Since the absolute order of magnitude is small, this value could be considered zero.
$C_{Y_{\delta_r}}$**	-33%	
C_{l_β}	33%	
C_{l_p}	-13%	
C_{l_r}	2%	
$C_{l_{\delta_a}}$**	12%	
$C_{l_{\delta_r}}$**	-24%	
C_{n_β}	-9%	
C_{n_p}	-54%	The forward swept wing provides a positive rolling moment in addition to the negative moment created by the main wing.
C_{n_r}	14%	
$C_{n_{\delta_a}}$**	-398%	This value should be discarded. The difference is accounted for by the change in order of magnitude. Since the absolute order of magnitude is small, this value could be considered zero.
$C_{n_{\delta_r}}$**	30%	

6.5 Conclusion & recommendations

As expected, the IFS causes a decrease in overall aerodynamic performance. This can be accounted for by the addition of the modifications. The stability derivatives obtained from AVL generally have the right sign. Their magnitude in most cases remains questionable however. As such, a more thorough analysis with respect to the stability characteristics is recommended using CFD analysis.

7 | Stability & Control Analysis

Compliant with its requirements, the IFS will be certified with the modifications (boxwing). Therefore it is needed to analyze the effects of these modifications on the original airplane. Modifications inside and outside of the fuselage will change the mass and mass distribution over the aircraft. The new center of gravity will be calculated in section 7.1 whereas the assessment of the new center of gravity range is done in section section 7.2.

After having checked the static stability and controllability characteristics with these values, the augmented flight will be analyzed. The four main test cases (direct lift up, direct lift down, side-force and high drag) will be described in detail with free body diagrams and relevant equations in section 7.3.

Based on these cases assumptions will be made so that more extensive sets of equations of motion can be stated. These EOMs will be in matrix format and feature extended input vectors to account for new control surfaces section 7.5.

Scripts will be used throughout the flight dynamics analyses and most quantities will be treated as variables both to account for later changes and to enable sensitivity evaluations when needed.

7.1 New center of gravity location

In order to determine the center of gravity of the IFS, the mass and center of gravity of the unmodified Embraer Phenom 300 will be used. Thereafter the mass increments of the modification design from the different sub-groups and their moment arms will be accounted for in order to calculate the center of gravity of the IFS.

The aircraft is assumed to fly with maximum fuel. The Basic Empty Weight (BEW), the Maximum Fuel Weight (MFW) and their corresponding moment arms have been retrieved from the flight manual [25]. The impact the boxwing on the mass and center of gravity of the IFS can be found in section 8.4, the same is done for the drag chute in section 5.4 and lastly the summary of the contributions of the ergonomics, sensors and actuators is provided in subsection 9.2.4. An overview of the used parameters and their values for the weight and balance computations performed for the IFS can be found in Table 7.1. All locations are taken w.r.t. the aircraft's nose.

Table 7.1: An overview of the masses and moment arms of the IFS.

Lumped mass	**Mass** $[kg]$	**Moment arm** $[m]$
BEW	5,150.00	7.77
MFW	2,420.00	7.09
Boxwing	92.29	9.32
Drag chute	5.99	13.0
Ergonomics, sensors and actuators	-131.88	6.37

The center of gravity of the IFS was determined to be 7.59 meters, whereas it would have been at 7.55 meters without the modifications applied. The impact of this shift will be discussed in section 7.2. This section covers the longitudinal stability of the aircraft. Note that the resulting mass difference from the modifications altogether is a negative one, since altogether the modifications will make the IFS 78.41 kilograms lighter than the original Embraer Phenom 300. Requirement **IFS-SYS-04** states that the weight of the IFS shall not exceed the MTOW of the unmodified aircraft, hence this requirement is met.

7.2 Longitudinal stability

Having adjusted the aircraft, the IFS should be assessed on its longitudinal stability. It is most important to make sure that after a change in angle of attack due to a disturbance of any kind, the aircraft returns to its original state, and will not continue to pitch up [26]. When this would happen, the aircraft could reach a too high angle of attack causing the IFS to stall. Equation 7.1 defines this statement in symbols, with pitch up defined as positive.

$$C_{m_\alpha} < 0 \tag{7.1}$$

To check if Equation 7.1 holds for the IFS, the main moments w.r.t. the aircraft center of gravity are assessed, see Figure 7.1. As one can see there are three main forces acting on the longitudinal balance of the aircraft. These forces are coming from the main wing, the upper wing and the tail.

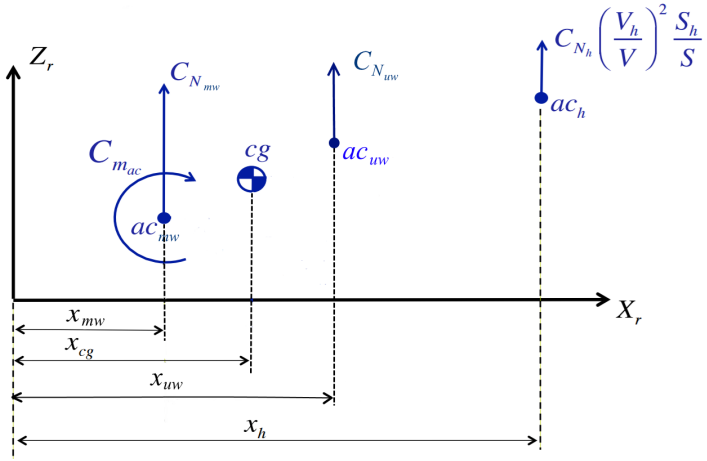

Figure 7.1: The free body diagram for the assessment of the longitudinal stability of the IFS.

The first step is to examine the moment coefficient of the original aircraft. For the original Embraer Phenom 300 only the main wing and horizontal tail are assumed to be contributing to the moment equation shown in Equation 7.2 [27]. In Figure 7.1 a few assumptions are made. The contribution of the engine thrust is thought to be quite small since it has a small moment arm and only works in the horizontal direction. The force it generates is quite large though, but will not vary with a change in angle of attack and so will not contribute to the C_{m_α} eventually. Also the tangential (drag) components of the wing and horizontal tail are neglected because of their small moment arm. The airfoil of the horizontal stabilizer is assumed to be symmetric so it will not generate an aerodynamic moment around its aerodynamic center.

$$C_m = C_{m_{mw}} + C_{m_h} = C_{m_{ac}} + C_{N_{mw}} \frac{x_{cg} - x_{mw}}{\bar{c}} + C_{N_h} \left(\frac{V_h}{V}\right)^2 \left(\frac{S_h}{S}\right) \frac{x_{cg} - x_h}{\bar{c}} \tag{7.2}$$

For the IFS the upper wing is taken into account for the longitudinal stability as well, which added a factor into the conventional equations. For the upper wing the effects of speed reduction w.r.t. the free-flow are ignored, since these are expected to be very small. The tangential component (drag) is neglected. Since the chosen airfoil for the upper wing is symmetric (as explained in section 5.2) this surface does not generate an aerodynamic moment around its pressure center, meaning that it can basically be treated as a wing. The moment that this upper wing creates is expressed and made dimensionless in Equation 7.3.

$$C_{m_{uw}} = \frac{\frac{1}{2}\rho V^2 S_{uw} C_{N_{uw}} (x_{cg} - x_{uw})}{\frac{1}{2}\rho V^2 S \bar{c}} = C_{N_{uw}} \frac{x_{cg} - x_{uw}}{\bar{c}} \frac{S_{uw}}{S} \tag{7.3}$$

Adding Equation 7.3 to Equation 7.2 leads to the moment coefficient equation for the IFS shown in Equation 7.4.

$$C_m = C_{m_{mw}} + C_{m_{uw}} + C_{m_h} = C_{m_{ac}} + C_{N_{mw}} \frac{x_{cg} - x_{mw}}{\bar{c}} + C_{N_{uw}} \frac{x_{cg} - x_{uw}}{\bar{c}} \frac{S_{uw}}{S} + C_{N_h} \left(\frac{V_h}{V}\right)^2 \left(\frac{S_h}{S}\right) \frac{x_{cg} - x_h}{\bar{c}} \tag{7.4}$$

Using Equation 7.2 and Equation 7.4 the change of the moment coefficient with respect to the angle of attack can be computed for both the original Embraer Phenom 300 and the IFS, as can be seen in Figure 7.2. Using these graphs it can be checked if the stability requirement in Equation 7.1 is met by examining the slope of the $C_m - \alpha$. As expected both $C_m - \alpha$ slopes are negative, meaning that the aircraft is longitudinally stable for the position of the center of gravity calculated in section 7.1. Also, it can be seen that the slope of the curve for the IFS is steeper, resulting in more pitch up moment at small and negative angles of attack and more pitch down moment at higher angles of attack. This is due to the fact that the aerodynamic center of the upper wing is located behind the center of gravity. Hence at a large angle of attack, while generating positive lift, a pitch down moment is generated. To counteract this moment, the elevator is deflected to such an angle that in horizontal flight the C_m is zero. In Figure 7.2 it can be seen that the two lines intersect each other at an angle of attack of 5.5 degrees. The incidence angle of the upper wing is -5.5 degrees, which means that at this point the upper wing does not generate any lift. This causes the C_m of the IFS at this point to be the same of that of the original Embraer Phenom 300. It should be noted that for plotting this curve only the linear part of the C_{L_α} curves for the main wing, upper wing and

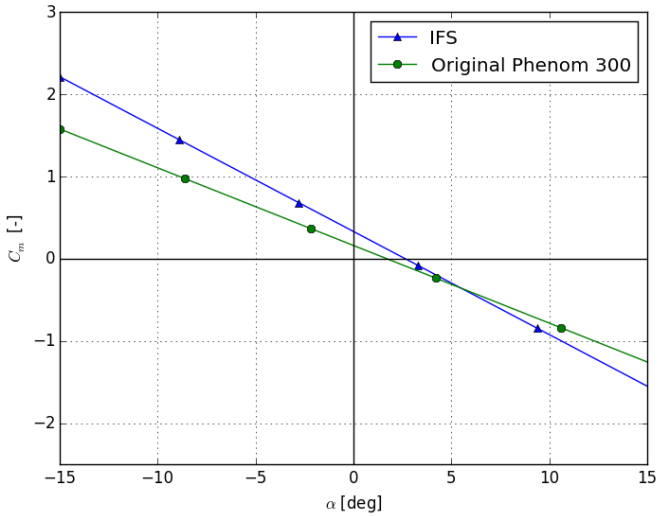

Figure 7.2: The $C_m - \alpha$ curve for both the original aircraft (line with circles) and the IFS (line with triangles).

horizontal stabilizer is used, implying that for the angles of attack that are not on this linear part the $C_m - \alpha$ curve in Figure 7.2 is not accurate.

7.2.1 Center of gravity range

For the examination of stability, a center of gravity is calculated. To determine the range that this center of gravity can be in, a C_{m_α} over X_{cg} plot is computed. To generate the plot the moments present in Equation 7.4 are differentiated over the angle of attack leading to Equation 7.5 [27]. The downwash effect ($\frac{d\varepsilon}{da}$) on the upper wing is neglected in this equation. Also, the moment coefficient around the aerodynamic center of the main wing does not return in this equation since it is not dependent on the angle of attack.

$$C_{N_{mw_\alpha}} \frac{x_{cg} - x_{mw}}{\bar{c}} + C_{N_{uw_\alpha}} \frac{x_{cg} - x_{uw}}{\bar{c}} \frac{S_{uw}}{S} + C_{N_{h_\alpha}} \left(1 - \frac{d\varepsilon}{da}\right) \left(\frac{V_h}{V}\right)^2 \left(\frac{S_h}{S}\right) \frac{x_{cg} - x_h}{\bar{c}} < 0 \qquad (7.5)$$

In Equation 7.5 the most important variable is the location of the center of gravity x_{cg}. The left part of the equation will attain a higher value when x_{cg} increases i.e. shifts to the back and will eventually reach a value of zero. At this point neutral stability is reached. This means that when the aircraft experiences a disruption in angle of attack, it will continue to pitch up or down with the same rate as was imposed. The value of the center of gravity x_{cg} in this condition coincides with that of the neutral point, e.g. the point where the force that is created by the change in angle of attack acts. Since these points coincide in this situation, there is no moment created to counteract the pitching motion introduced. More specifically, the so called stick-fixed neutral point is indicated here, since the $C_{N_{h_\alpha}}$ is not changed by deflecting the elevator of the tail.

In order to guarantee a longitudinally stable aircraft it should be checked where this most aft center of gravity can be located. Input values for this check follow from the aerodynamic analysis performed in chapter 6. The result can be found in Figure 7.3, where C_{m_α} is calculated for both the original aircraft and the IFS over a range of center of gravity positions, starting at the leading edge of the MAC. As one can see the C_{m_α} values of the IFS at all center of gravity positions are greater in magnitude, meaning its $C_m - \alpha$ curves will be steeper. It actually allows a further backward travel of the center of gravity than the original aircraft. This is due to the fact that the vertical force that is generated by the change in angle of attack is located behind the center of gravity, causing the aircraft to be more stable longitudinally.

Analysis of the aft center of gravity position

For the original aircraft at maximum take-off weight the most aft allowed position of the center of gravity is at 7.54 meters from the datum [25], shown as the left vertical line in Figure 7.3, this leaves margin to where C_{m_α} is actually equal to zero. This difference is present due to estimations and assumptions but also due to a stability margin between the maximum allowed position of the aft center of gravity and the neutral point. This margin is used by the aircraft manufacturers ans usually is 5 to 15 percent of the MAC. This is to make sure that other factors that may determine the maximum allowable aft travel of the center of gravity are met as well. These are

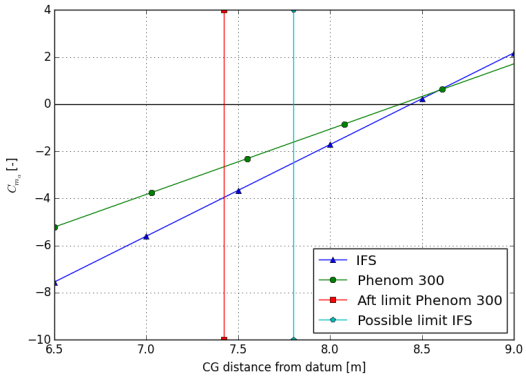

Figure 7.3: C_{m_α} over various center of gravity positions.

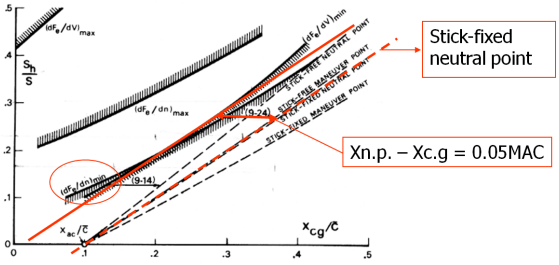

Figure 7.4: Various limiting factors on the aft center of gravity. [3]

factors like the stick free neutral point, stick fixed manoeuvre point and the stick free manoeuvre point (as shown in Figure 7.4) [15].

At this point the margin in C_{m_α} is a little smaller than 3. If the same margin is taken for the IFS, the center of gravity would be allowed to be positioned at 7.8 meters, as is indicated by the right vertical line in Figure 7.3. The value of the new center of gravity location is 7.59, so this is within the new margin. Also, the weight at which this center of gravity is located is less than the maximum take-off weight. A lower weight allows for a more aft center of gravity, making the margin even larger. Also in the center of gravity calculations in section 7.1 passengers are not included. Since these will be seated in the front part of the aircraft, the center of gravity is expected to shift forward a bit, again creating a larger margin w.r.t. the aft limit. This will also give a margin on the original aircraft calculations, in which the calculated center of gravity if close to the limit stated in the flight manual. It can be concluded that the boxwing causes the center of gravity to shift backwards, but also makes the aircraft more stable allowing for a more aft limit. This means that it is now shown that the IFS is longitudinally stable for the linear part of the C_{N_α} curves.

Forward center of gravity position in the landing configuration

For conventional aircraft the forward center of gravity in flight is limited by the controllability of the aircraft. The aircraft must be trimmable, so not needing a constant stick force, for the range of angle of attacks that the aircraft uses to operate. Usually the conditions during landing are most critical in this [3]. In landing conditions the aircraft flies with its HLDs deployed, causing the center of pressure to move more aft and creating a large aerodynamic moment around the aerodynamic center of the main wing. This results in a highly negative (pitch down) moment as indicated in Figure 7.5. To compensate for this the tail generates a large amount of negative lift (so a positive moment) to keep C_m equal to zero. Since the Embraer Phenom 300 is a certified aircraft, the tailplane fitted is able to produce this amount of negative lift probably even with some margin. When looking at Figure 7.5 one can see that the aerodynamic center of the upper wing is also located behind the center of gravity. In landing conditions the aircraft flies at a higher angle of attack than the incidence angle of -5.5 degrees of the upper wing. This means the upper wing will create a positive lift force and so a negative moment around the center of gravity. This moment has to be counteracted by the horizontal tailplane as well.

Since it is decided not to modify the tailplane, to still guarantee a stable aircraft during landing conditions other measures have to be taken. One of those measures is to limit the forward center of gravity travel. To determine this limit the properties of the aircraft during landing have to be assessed, which will not be necessary since there is an easier more convenient solution. The control surfaces of the upper wing can be deflected upward during landing, decreasing the amount of lift generated by the upper wing. So to not have extra limitations in the forward center of gravity position, the deflection angle of the control surface during the landing approach should be such that no lift is generated by the upper wing. The system that will perform this is discussed in section 9.8. The calculated center of gravity from section 7.1 is well aft off the forward center of gravity limit and will thereby comply with controllability on this case. As can be seen in Figure 7.5 the upper wing will also create a small drag force and thereby a moment around the center of gravity. Although this is neglected as in other calculations present in this section it will be a favourable moment during landing since it is positive (pitch up).

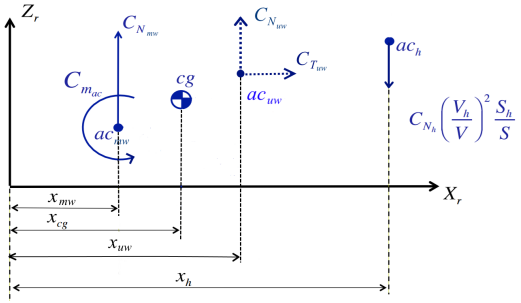

Figure 7.5: The orientation of moments during the landing phase, note the negative moment contribution of $C_{m_{ac}}$ and the possible presence of $C_{N_{uw}}$.

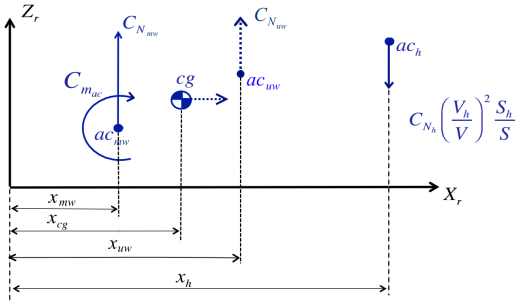

Figure 7.6: The longitudinal stability during the lift manoeuvre.

Forward center of gravity position during the lift manoeuvre

When the aircraft performs the manoeuvre in which an instant lift force is generated, this force is coming from the upper wing. Since the aerodynamic center of this upper wing is located behind the center of gravity, as can be seen in Figure 7.6, this implies a pitch down moment. This moment will be quite large since both the force and moment arm have considerable numbers as can be read in subsection 7.3.1. This negative moment has to be counteracted by a positive moment generated by the horizontal tail. Since the horizontal tail will not be modified, it has to be checked if the already existing tail can generate enough downward lift to prevent the aircraft from pitching down during the instant lift manoeuvre. If this is not the case with the current most forward center of gravity allowed, this limit should be adjusted. This is because a backward shift of the center of gravity as indicated in Figure 7.6 causes a decrease in the distance between the center of gravity and both the upper wing and the horizontal tail. This happens with an arm ratio that is increasingly favourable for the horizontal stabilizer, since it will have a relatively longer moment arm. The need for this adjustment is checked in subsection 7.3.1.

7.3 Simulation cases

The driving requirements of the aerodynamic subsystem are as follows:

- **IFS-SYS-08-AERO-01** The IFS shall be able to generate a side force induced acceleration of 0.5 m/s^2 at 61.7 m/s CAS.
- **IFS-SYS-08-AERO-02** The IFS shall be able to reach a L/D ratio of 4.
- **IFS-SYS-08-AERO-04** The IFS shall be able to generate a direct ΔC_L of +/- 0.15.

As decided, the forces that will make the IFS meet requirements **IFS-SYS-08-AERO-01**, **IFS-SYS-08-AERO-02** and **IFS-SYS-08-AERO-04**, will be generated by the vertical wing fins, the drag chute and the flaps on the upper wing, respectively. The fact that these forces do not necessarily act through the center of gravity, makes that stability has to be taken into account. This section contains the examination on stability for the cases as described by the requirements. Sections 7.3.1, 7.3.2 and 7.3.3 describe the boundary conditions of stability and their impact on the design for direct lift variation, side force induced acceleration and low L/D flight, respectively. Before working out the three cases, general assumptions have been made. These general assumptions are used except for when the opposite is explicitly stated. The assumptions are as follows:

- All maneuvers shall be feasible while flying with the aircraft's MTOW of 8,150 kilograms.
- The gravitational acceleration is assumed to be 9.81 m/s^2, independent of the altitude.
- The velocities of the airflow that are experienced by the main wing, upper wing, horizontal tailplane and drag chute are assumed equal to the free stream velocity.
- Corrections for compressibility on lift and moment coefficients have been done according to Equations 7.6 and 7.7. [1]
- The thrust of the aircraft is assumed not to have a moment contribution.
- The drag of the aircraft is assumed not to have a moment contribution.
- Interactions between lifting surfaces such as downwash are neglected.

[1] http://aerostudents.com/files/aerodynamicsC/subsonicCompressibleFlowOverAirfoils.pdf [cited 17 January 2017]

- Moment arms of lifting surfaces are assumed not to be affected by the aircraft's AoA and thus vehicle reference frame coordinates can be used as moment arms in moment equations.
- Aerodynamic coefficients of the IFS's lifting surfaces are assumed as in Table 7.2.
- Locations of points of engagement of forces are assumed as in Table 7.3, where the datum for x-coordinates is at the nose (positive to the rear), while the datum for z-coordinates is in the center of the fuselage (positive upwards).

$$C_L = \frac{C_{L_{incomp.}}}{\sqrt{1-M^2}} \tag{7.6}$$

$$C_M = \frac{C_{M_{incomp.}}}{\sqrt{1-M^2}} \tag{7.7}$$

Table 7.2: Aerodynamic parameters assumed for stability calculations.

Parameter	Unit	Main wing	Upper wing	Hor. stab.
C_{L_α}	-	4.90	6.19	4.70
α_0	deg	-3.00	0	0
$C_{M_{ac}}$	-	-0.30	0	0
AR	-	4.80	10.60	-
e	-	0.74	0.91	-

Table 7.3: Locational parameters in meters assumed for stability calculations.

Parameter	CG	Main wing	Upper wing	Vertical wing	Hor. stab.	Vert. stab.	Drag chute
x-coordinate	7.59	7.32	10.64	8.66	15.06	14.00	14.39
z-coordinate	-0.44	-	-	-0.12	-	1.54	0.30

7.3.1 Direct lift

The definition of direct lift, is that it is not generated by changing the angle of attack. Thus, the angle of attack of the aircraft w.r.t. the airflow will not change. In order to prevent the aircraft from pitching, this means that the moment around the aircraft's center of gravity has to remain equal to zero.

Since fast response times are favored, the increment in lift is assumed to be provided by the electrically actuated upper wing flaps. In order to make sure the equilibrium is preserved, the elevator on the horizontal tailplane will respond accordingly. The free body diagram is shown in Figure 7.7, while the equations for the total sum of the forces in the Z-direction and the sum of the moments around the Y-axis for this case are provided in Equations 7.8 and 7.9.

$$\sum F_Z = W - L_{mw_1} - (L_{uw_1} + \Delta L_{uw}) - (L_{h_1} + \Delta L_h) = -\Delta L \tag{7.8}$$

$$\sum M_Y = M_{mw_{ac}} + L_{mw_1}(x_{cg} - x_{mw}) + (L_{uw_1} + \Delta L_{uw})(x_{cg} - x_{uw}) + (L_{h_1} + \Delta L_h)(x_{cg} - x_h) = 0 \tag{7.9}$$

The forces with subscript 1 indicate the forces of the initial condition. The initial condition does not influence the increments of the lift force generated by the upper wing and the horizontal tailplane that are needed for the required ΔC_L. Since the aircraft is assumed to be in steady symmetric horizontal flight in the initial condition, Equations 7.8 and 7.9 can be rewritten to Equations 7.10 and 7.11.

$$\sum F_Z = \Delta_{L_{uw}} + \Delta_{L_h} = \Delta L \tag{7.10}$$

$$\sum M_Y = \Delta L_{uw}(x_{cg} - x_{uw}) + \Delta L_h(x_{cg} - x_h) = 0 \tag{7.11}$$

Since ΔL is not explicitly stated in requirement **IFS-SYS-08-AERO-4**, while only the dimensionless ΔC_L is provided, an interpretation had to be found on how to scale this coefficient. The decision has to be made to scale it with the main wing of the Embraer Phenom 300, according to Equation 7.12.

$$\Delta L = \Delta C_L \tfrac{1}{2} \rho V^2 S_{mw} \tag{7.12}$$

Now Equations 7.10 and 7.11 can be solved for, using the x-locations of the center of gravity and the relevant control surfaces as shown in Table 7.3 and the center of gravity location as calculated in section 7.1. This yields in a total ΔL of 9,968 N, provided by a ΔL of 16,835 N by the upper wing, and a ΔL of 6,867 N by the horizontal tailplane, in the opposite direction. These the magnitudes of these forces are influenced by the center of gravity location, which is influenced by adaptations to original aircraft. In order to examine the sensitivity, the lift increments of both surfaces that is needed in order to provide the total ΔC_L of 0.15 is plotted against center of gravity locations in Figure 7.8.

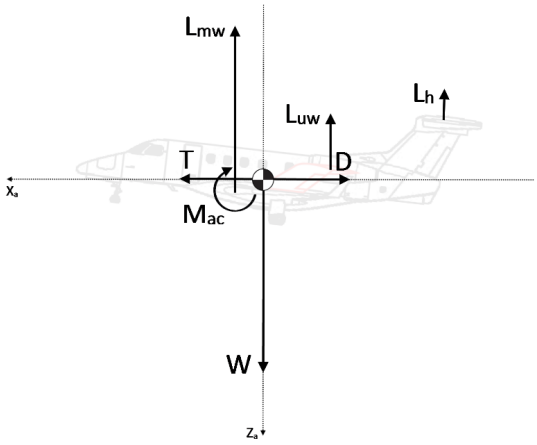

Figure 7.7: Free body diagram of the direct lift case.

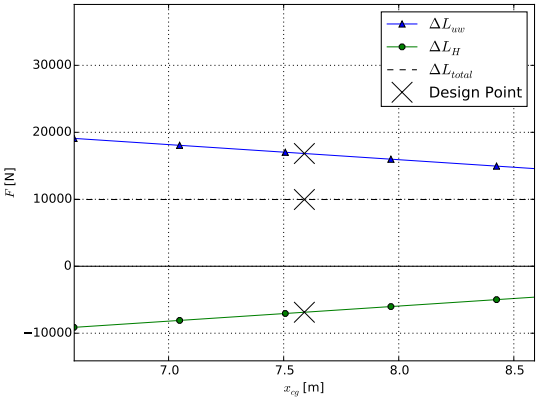

Figure 7.8: Sensitivity of lift increment needed from the upper wing and horizontal tail per c.g. location.

Since the magnitude of these forces is considerable, their feasibility has been examined. The amount of ΔL that is available, depends on the initial condition of the aircraft. The forces per lifting surface for this initial condition are determined by solving Equations 7.13, 7.14, 7.15, 7.16, 7.17 and 7.18, using the aerodynamic coefficient estimates as provided in Table 7.2.

$$\sum F_Z = W - L_{mw_1} - L_{uw_1} - L_{h_1} = 0 \tag{7.13}$$

$$\sum M_Y = M_{mw_{ac}} + L_{mw_1}(x_{cg} - x_{mw}) + L_{uw_1}(x_{cg} - x_{uw}) + L_{h_1}(x_{cg} - x_h) = 0 \tag{7.14}$$

$$M_{mw_{ac}} = C_{M_{mw_{ac}}} \tfrac{1}{2}\rho V_{mw}^2 S_{mw} \bar{c}_{mw} \tag{7.15}$$

$$L_{mw} = (\alpha - \alpha_{mw_0})\, C_{L_{mw_\alpha}} \tfrac{1}{2}\rho V_{mw}^2 S_{mw} \tag{7.16}$$

$$L_{uw} = (\alpha + i_{uw})\, C_{L_{uw_\alpha}} \tfrac{1}{2}\rho V_{uw}^2 S_{uw} \tag{7.17}$$

$$L_h = (\alpha + i_h)\, C_{L_{h_\alpha}} \tfrac{1}{2}\rho V_h^2 S_h \tag{7.18}$$

In order to solve Equations 7.16, 7.17 and 7.18, estimated values for the C_{L_α} of the main wing, upper wing and horizontal tailplane have been used. The angle of incidence of the upper wing, i_{uw}, is determined in subsection 5.3.3. The angle of incidence of the tail is a variable input, since the aircraft is assumed to be trimmed at the initial condition. These equations yield an angle of attack of the main wing of 10 degrees, and a lift force by the main wing, upper wing and horizontal tailplane of 75,200, 12,589 and -7,864 Newton, respectively. Now the initial condition is determined, the feasibility of the ΔC_L generation by the combination of upper wing and horizontal tailplane can be examined. For the negative ΔC_L, the required lift of the upper wing shall be the lift provided by the upper wing during the standard condition minus the maximum ΔL of the upper wing of 16,835 Newton. This yields a negative lift force of -4,247 Newton. According to calculations made by the aerodynamic sub-department, the flaps of the upper wing can make the upper wing provide a negative lift force up to -5,553 Newton. This means that the maneuver is proven to be feasible. At the same time the horizontal tail will provide 4,028 Newton of force

downward. The subdivision of ΔL contributions by the upper wing and horizontal stabilizer per ΔC_L for this case is shown in Figure 7.9.
For the positive ΔC_L, the required lift of the upper wing shall be the lift provided by the upper wing during the standard condition plus the maximum ΔL of 16,835 Newton. This yields a positive lift force of 29,424 Newton. According to calculations made by the aerodynamic sub-department, the flaps of the upper wing cannot provide a larger upward lift force than 22,355 Newton under the described flight condition. This means that the lift contribution of the combination upper wing and horizontal tail plane will not suffice. For this reason, the flaps of the main wing will be partially deflected. The increment in lift will be attained by Equation 7.20 and the moment equilibrium will be maintained according to Equation 7.20, where $\Delta L_{uw_{max}}$ is the maximum lift increment that can be created by the upper wing during flight in the initial condition.

$$\Delta L = \Delta L_{mw} + \Delta L_{uw_{max}} + \Delta L_h \tag{7.19}$$

$$\Delta L_{mw}(x_{cg} - x_{mw}) + \Delta L_{uw_{max}}(x_{cg} - x_{uw}) + \Delta L_h(x_{cg} - x_h) \tag{7.20}$$

A graphical representation of the subdivision of ΔL contributions by the upper wing, horizontal stabilizer and main wing per ΔC_L is provided in Figure 7.10.

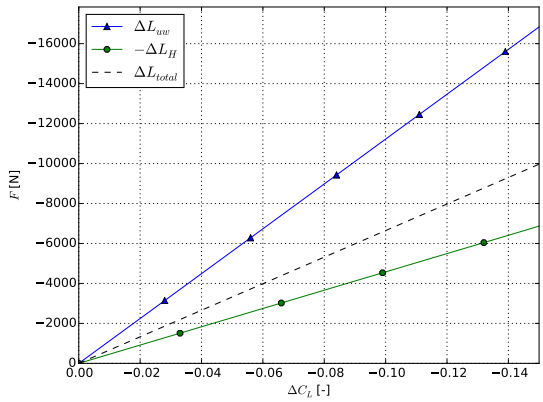

Figure 7.9: Increment in lift generation per lifting surface for a negative ΔC_L.

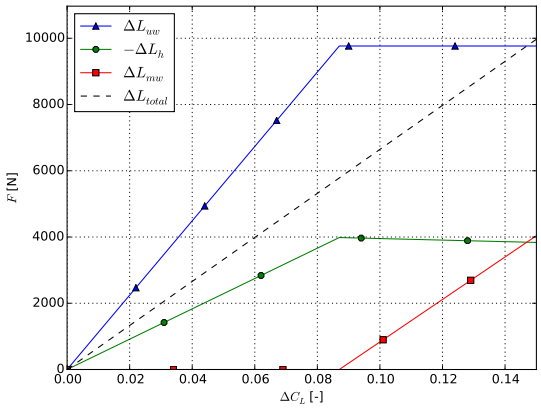

Figure 7.10: Increment in lift generation per lifting surface for a positive ΔC_L.

7.3.2 Sideforce

The IFS will have the ability to introduce a side force without rolling, by means of using its vertical wings that are part of the boxwing installation. However, as was the case for the lift increment case, the generation of side force will introduce moments on the aircraft. The vector is assumed to be parallel with the Y-direction of the body reference frame, but since it does not exactly act through the center of gravity of the aircraft, it will introduce a yawing moment and a rolling moment. The compensation of the yawing moment will be done by the rudder on the vertical stabilizer, introducing an even higher rolling moment. The entire rolling moment resulting from these deflections will be compensated by the ailerons on the main wing. A visual representation of this case can be found in the free body diagrams in Figures 7.11 and 7.12.
The equations that can be derived from the free body diagrams in 7.11 and 7.12, can be found in Equations 7.21, 7.22 and 7.23.

$$\sum F_Y = \Delta F_{vw} + \Delta F_{vs} = M \cdot a_Y \tag{7.21}$$

$$\sum M_Z = \Delta F_{vw}(x_{cg} - x_{vw}) + \Delta F_{vs}(x_{vs} - x_{cg}) = 0 \tag{7.22}$$

$$\sum M_X = \Delta F_{vw}(z_{vw} - z_{cg}) + \Delta F_{vs}(z_{vs} - z_{cg}) + \Delta M_a \tag{7.23}$$

Using the x- and z-locations of the center of gravity and the relevant control surfaces as shown in Table 7.3, the force required from the vertical wings is determined to be 4,891 Newton. This is higher than the total force required in this side direction, since the rudder on the vertical stabilizer will counteract this moment with a force of -816

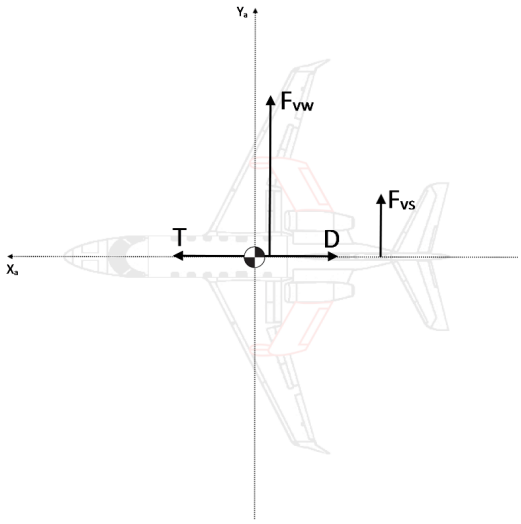

Figure 7.11: Free body diagram for the side force case (XY-plane).

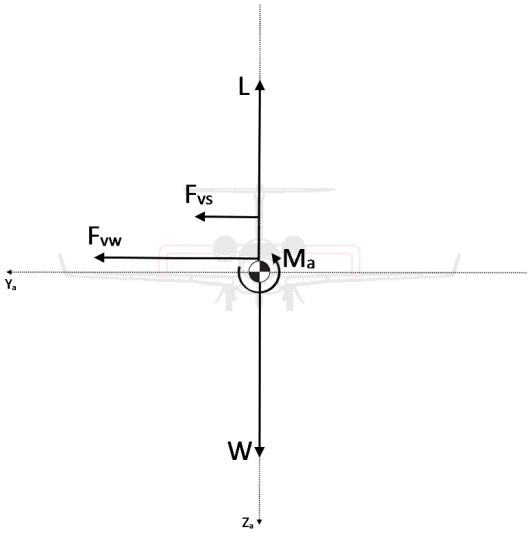

Figure 7.12: Free body diagram for the side force case (YZ-plane).

Newton. The moment provided by the ailerons to prevent the IFS from rolling is only 50 Nm. The lift on the vertical wings is designed for in subsection 5.3.2, while the forces on the vertical tailplane and ailerons can be generated by the Embraer Phenom 300's unmodified control surfaces.

7.3.3 Low L/D flight

In order to achieve a low L/D of 4, a drag chute can be deployed together with the aircraft's spoilers to increase the drag considerably. This 're-entry mission' is a descending flight starting at 40,000 ft. with a velocity of 144 m/s, and ending at sea level with a velocity of 61.7 m/s as defined in subsection 5.4.1. Since thrust counteracts the drag, the thrust setting is considered zero in order not to overdesign the IFS and the associated drag chute. This yields an FBD of this flight condition as shown in Figure 7.13.

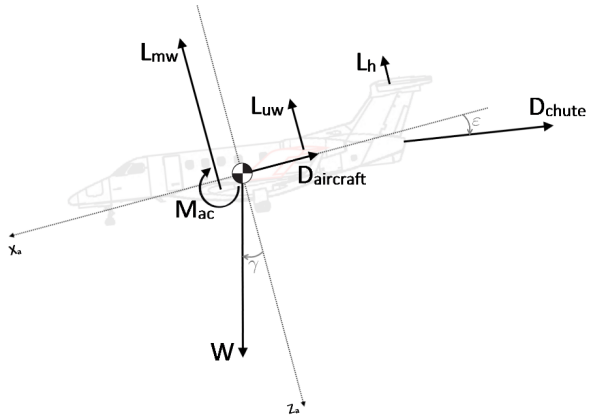

Figure 7.13: Free body diagram of the re-entry simulation case.

Although over the full descent the velocity and AoA of the IFS will change considerably, the IFS is assumed to fly under equilibrium conditions at every instant during the descending flight as described in Equations 7.24 and 7.25. The equations for the lift of the main wing and upper wing as a function of the AoA have previously been described in Equations 7.16 and 7.17 whereas the equation for the lift of the horizontal stabilizer as a function of the angle of incidence of the horizontal stabilizer and the AoA has been provided in 7.18. Note that the lift provided by the horizontal stabilizer will not be taken into account in Equation 7.24. The reason for this is that it makes the set of equations more easily solvable, while the force is very small relatively to the lift provided by the main wing.

$$\sum F_Z = W\,cos(\gamma) - L_{mw} - L_{uw} = 0 \tag{7.24}$$

$$\sum M_Y = M_{mw_{ac}} + L_{mw}(x_{cg} - x_{mw}) + L_{uw}(x_{uw} - x_h)$$
$$+D_{chute}\left((z_{chute} - z_{cg})\, cos(\alpha - \varepsilon) + (x_{cg} - x_{chute})\, sin(\alpha - \varepsilon)\right) = 0 \tag{7.25}$$

The x- and z-location of the attachment point of the drag chute are given in Table 7.3. It is assumed to be attached to the most aft point of the fuselage, since it provides the necessary clearance for the chute and the cable under a wide range of angles of attack.

The values for the descent angle (γ) and the drag of the drag chute can be found in Equations 7.26 and 7.27, respectively. The value for L/D is explicitly stated in requirement **IFS-SYS-08-AERO-02**. The drag coefficient of the the drag chute has been estimated in section 5.4. In the same chapter, the area of this chute is determined.

$$\gamma = \arctan\left(\frac{D}{L}\right) \tag{7.26}$$

$$D_{chute} = C_{D_{chute}} \tfrac{1}{2}\rho V_{chute}^2 S_{chute} \tag{7.27}$$

Equation 7.27 yields a drag force of the drag chute of 17,438 N at the start of the re-entry simulation (144 m/s, 40,000 ft) and a drag force of 10,774 N at the end of the descent (61.7 m/s, sea level). Since the force of the drag chute on the aircraft is this high and the distance between the attachment point of the drag chute and the center of gravity is high as well, the moment introduced by the drag chute can be considerable. For this reason, the effect of the AoA on the moment arm will be taken into consideration, and the estimated effect of downwash from the aircraft's main wing on the drag chute will be examined according to Equation 7.28.[2]

$$\varepsilon = \frac{C_{L_{mw}}}{\pi \cdot AR_{mw}} = \frac{(\alpha - \alpha_{mw_0})\, C_{L_{mw_\alpha}}}{\pi AR_{mw} e_{mw}} \tag{7.28}$$

Since the effects of downwash vary per location after the wing, while the distance between the main wing and the drag chute is not being taken into consideration in Equation 7.28, the expected downwash angle is assumed to be somewhere between 0 and ε as determined using Equation 7.28. In order to have a look at its influence, calculations on the drag chute will be performed using both extremes.

For the effect of the AoA and downwash angle on the moment arm of the drag of the chute, the small angle approximation has been used, since the angles are relatively small. The approximation is performed by substituting the sine and cosine terms in Equation 7.25 in radians by their approximations as given in Equations 7.29 and 7.30.

$$sin(\alpha - \varepsilon) \approx \alpha - \varepsilon \tag{7.29}$$

$$cos(\alpha - \varepsilon) \approx 1 - \frac{(\alpha - \varepsilon)^2}{2} \tag{7.30}$$

Solving for this re-entry case yields the results as shown in Table 7.4.The angle of incidence of the horizontal tailplane that is needed to maintain a moment equilibrium does not fall within the range from 2° to -13° that is possible for the unmodified Embraer Phenom 300. [3] Nevertheless, the differences are so small, that only a small deflection of the upper wing flaps will be enough to account for this small shortage. Lastly, the effects of downwash on the drag chute decrease its moment contribution, making the aircraft even more easily controllable.

Table 7.4: Outcome of the re-entry simulation stability calculations, all angles are in degrees.

Angle	**40,000 ft, 144 m/s**		**Sea level, 61.7 m/s**	
	w/o downwash	**w downwash**	**w/o downwash**	**w downwash**
α	4.81	4.81	9.00	9.00
i_α	-6.30	-5.92	-13.79	-13.20
ε	-	3.82	-	5.22

7.4 General performance

Because of the modifications to the original Embraer Phenom 300 the figures relative to range and endurance need to be updated. Even though the MTOW did not change, the addition of upper and vertical wings creates more drag in all flight conditions, so that more power needs to be generated by the engines that, in turn, will burn more fuel. The fuel tanks on the Embraer Phenom 300 were not modified to account for this, resulting in reduced endurance

[2] http://www.dept.aoe.vt.edu/ lutze/AOE3104/airfoilwings.pdf [cited 16 January 2017]
[3] http://janes.ihs.com/JAWADevelopmentProduction/Display/1344700 [cited 22 January 2017]

and range. First the difference in drag between the original aircraft and the IFS was calculated, using Equation 7.32 at MTOW (8,150 kilograms), 191.8 m/s and 40,000 ft (12,192 meters) in ISA conditions. The total zero-lift drag coefficient for the IFS was calculated as 8.937 $\times 10^{-4}$ in with Equation 7.31, while the original Embraer Phenom 300 has a C_{D_0} of 7.684 $\times 10^{-4}$.

$$C_{D_0} = C_{D_{0\,mw}} + C_{D_{0\,uw}} \frac{S_{uw}}{S_{mw}} + C_{D_{0\,vw}} \frac{S_{vw}}{S_{mw}} \tag{7.31}$$

$$C_L = \frac{2W}{\rho V^2 S} \quad ; \quad D = \frac{1}{2}\Big(C_{D_0} + \frac{C_L^2}{Ae\pi}\Big)\rho V^2 S \tag{7.32}$$

The change in drag at cruise from 7,271 to 7,291 Newton represents a 0.27 % increase. Because this value is very small the new fuel consumption was calculated assuming it to be linearly related to the new drag force, as described in Equation 7.33, resulting in a fuel consumption of 631 liters per hour.

$$f.c._{IFS} = \frac{D_{IFS}}{D_{original}} \cdot f.c._{original} \tag{7.33}$$

It was also assumed that the extra drag would have the same relative effect on fuel consumption in all flight conditions, allowing the calculation of IFS max range and endurance as linear functions of the original Embraer Phenom 300 ones as described in Equation 7.34.

$$R_{max,IFS} = \frac{f.c._{original}}{f.c._{IFS}} \cdot R_{max,original} \quad ; \quad E_{max,IFS} = \frac{f.c._{IFS}}{f.c._{original}} \cdot E_{max,original} \tag{7.34}$$

The maximum range and endurance of the original Embraer Phenom 300 are 3,650 km and 5 hours respectively, while fuel consumption at cruise is 166 gal/hour, or 629 liters per hour [4]. Using these values in Equation 7.34 the new values for the IFS are nearly identical, with a maximum range of 3,640 km and a maximum endurance of 4 hours and 58 minutes.

As stated the stock aircraft has an fuel consumption of 629 liters a hour, or $1.74 \cdot 10^{-4} m^3/s$. Requirement **IFS-SYS-24** states that an average fuel use of the IFS shall not exceed $3.15 \cdot 10^{-4} m^3/s$ with 4 approaches. It is not likely that the fuel consumption will increase with 45% while performing the 4 approaches also with the added drag this is uncertain, so the fuel use is within the limit and complying with requirement **IFS-SYS-24**. Looking at the trade of matrix in the Baseline Report [9] it can be seen that the stock Embraer Phenom 300 has one of the lowest fuel consumptions of the possible aircraft that met the trade-off requirements. Having one of the lowest fuel consumptions, requirement **IFS-SH6-01** is met.

The landing distance is influenced mainly by mass and braking efficiency. Because the MTOW, the landing gear and the spoilers were not modified in the IFS it is safe to conclude that the stopping performance after touchdown will not change w.r.t. the original Embraer Phenom 300, with a BFL of 1059 meters [5], thereby satisfying requirement **IFS-SYS-07**. The airport of Rotterdam The Hague has a runway of 2,200 $\times$ 45 meters [6], making it one of the feasible basing options for the IFS. The fact that it will be able to operate from this airport fulfills requirement **IFS-SH1-01**.

Requirements **IFS-SYS-08-AERO-05** to **IFS-SYS-08-AERO-13** asses the manoeuvrability of the IFS. The purpose of these requirements is to make sure the IFS is able to reproduce the characteristics of other aircraft. However, the IFS will only be used to simulate other aircraft of similar or bigger proportions. The manoeuvrability of these aircraft will not be higher than of the IFS. Besides this requirement **IFS-SYS-08-AERO-03** states a maximum lift coefficient that must be achievable, however the boxwing adds direct lift devices to the aircraft, which ensures that the maximum lift coefficient will not be lower than the original aircraft. As a result of this all these requirements do not add value to the design of the modification hence are dropped.

7.5 Equations of motion

The exact motion of an aircraft can be described with Newton's laws if an inertial Frame Of Reference (FOR) is used as a basis for all equations. Even though higher level frames exist, the J2000 frame of reference is considered an inertial one for aerospace applications close to Earth. Its origin is in the center of the Earth with X-axis directed towards the Vernal Equinox, the Z-axis collinear with the axis of rotation and the Y-axis according to the right-hand rule. Ultimately all forces acting on an aircraft can be brought back to this frame reference through static

[4] http://www.embraerexecutivejets.com/en-us/jets/phenom-300/pages/performance.aspx [cited 19 January 2017]
[5] http://www.jetrequest.com/private_aircraft/light_jet/6/embraer_phenom_300/92 [cited 19 January 2017]
[6] http://www.ais-netherlands.nl/aim/2016-11-24-AIRAC/eAIP/html/eAIP/EH-AD-2.EHRD-en-GB.html [cited 19 January 2017]

and dynamic transformations that account for relative positions, linear and angular motions and accelerations. Intermediate frames can be the Earth-centered/Earth-fixed (ECEF) FOR, the vehicle-carried Earth-normal FOR, the body-fixed FOR and the aerodynamic FOR. All these transformations are needed when a space vehicle motion has to be described, with speeds of thousands of kilometers per hour, significant Earth-relative angular velocities and a force of gravity that varies substantially with distance from Earth.

In the case of an aircraft some assumptions can be made, eliminating the need for some of the transformations. In particular the Earth is assumed not to be rotating, its surface to be flat, the force of gravity to be constant with respect to altitude, the local wind intensity to be zero, the atmosphere to be described by the ISA model and the aircraft itself to be a rigid body. The body-fixed FOR was adopted, so that only two direct transformations were needed to express every external force involved. The force of gravity, acting along the Z-axis of the vehicle-carried Earth-normal FOR, is brought in the body-fixed FOR by rotation through the attitude angles ψ, θ and φ (yaw, pitch and roll angles respectively). The forces created by the airflow around the aircraft, acting in the aerodynamic reference frame, are brought in the body-fixed FOR by rotation through the freestream angles α and β (angle of attack and sideslip angle respectively). Once the reference frame and the related transformations have been determined it is possible to set up the equations of motion for the general case with six degrees of freedom.

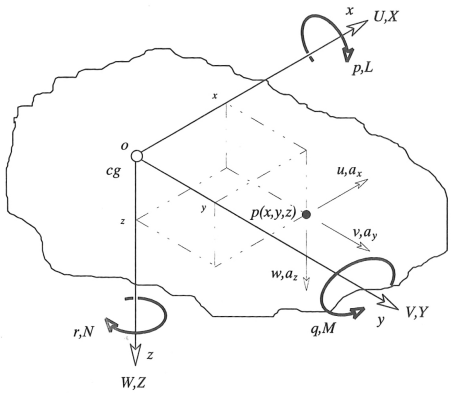

Figure 7.14: Motion referred to generalized body axes [4].

7.5.1 Linearized equations of motion

The procedure followed is the same as presented in Cook [4], where calculation of forces and moments around the three axes are grouped together in a six-equation system that is applicable to any case. Equations 7.35, 7.36 and 7.37 apply Newton's second law $F = m \cdot a$ to the three body axes, while Equations 7.38, 7.39 and 7.40 relate inertias and moments around the same three axes.

$$m(\dot{U} - rV + qW) = X \tag{7.35}$$

$$m(\dot{V} - pW + rU) = Y \tag{7.36}$$

$$m(\dot{W} - qU + pV) = Z \tag{7.37}$$

$$I_x\dot{p} - (I_y - I_z)qr - I_{xz}(pq + \dot{r}) = L \tag{7.38}$$

$$I_y\dot{q} + (I_x - I_z)pr + I_{xz}(p^2 - r^2) = M \tag{7.39}$$

$$I_z\dot{r} - (I_x - I_y)pq + I_{xz}(qr - \dot{p}) = N \tag{7.40}$$

Every right-hand term in Equations 7.35 to 7.40 is the sum of all forces (X,Y,Z) and moments (L,M,N) acting on the aircraft. These sum terms can be detailed based on the origin of such forces, as presented in Equation 7.41 with forces along X-axis due to aerodynamic effects (X_a), force of gravity (X_g), control surfaces (X_c), engine power (X_p) and atmospheric disturbances (X_d).

$$X = X_a + X_g + X_c + X_p + X_d \tag{7.41}$$

Another series of assumptions can be made to simplify and linearize the system. No wind was previously assumed, causing all airstream disturbance terms to drop out. Furthermore steady horizontal flight is assumed, setting angular velocities equal to zero and omitting the angle of sideslip. The velocity components are expressed with respect to

the total velocity vector plus disturbances terms. Products and powers of small quantities are neglected, removing most of the terms related to u, v, w, p, q anr r. The effects of the force of gravity in the moment equations is zero because the reference frame origin is the center of mass. The resulting system is presented in Equations 7.42 to 7.47.

$$m(\dot{u} + qW_e) = X_a + X_g + X_c + X_p \tag{7.42}$$

$$m(\dot{v} - pW_e + rU_e) = Y_a + Y_g + Y_c + Y_p \tag{7.43}$$

$$m(\dot{w} - qU_e) = Z_a + Z_g + Z_c + Z_p \tag{7.44}$$

$$I_x\dot{p} - (I_{xz})\dot{r} = L_a + L_c + L_p \tag{7.45}$$

$$I_y\dot{q} = M_a + M_c + M_p \tag{7.46}$$

$$I_z\dot{r} - I_{xz}\dot{p} = N_a + N_c + N_p \tag{7.47}$$

Linearization is performed with Taylor series truncated after the first non-constant term, so that every dimensional parameter can be expressed as a constant value plus its derivatives with respect to each variable times the change in the variable itself. A side effect of linearization is that multiplied derivatives were assumed small and are therefore neglected. An example of this linearization is given in Equation 7.48 for the forces along the X-axis. The same approach is used for the control surface terms as presented in Equation 7.49 for the pitching moment with constant term $M_{c_e} = 0$ due to the trimmed flight assumption. The new control surfaces on the IFS have been added, with upper wing flap κ, vertical wing rudder σ and drag chute χ. The sign convention used is the same as the standard one, with positive deflections causing negative moment contributions around the axis closest to the hinge line, as presented in Figure 7.15.

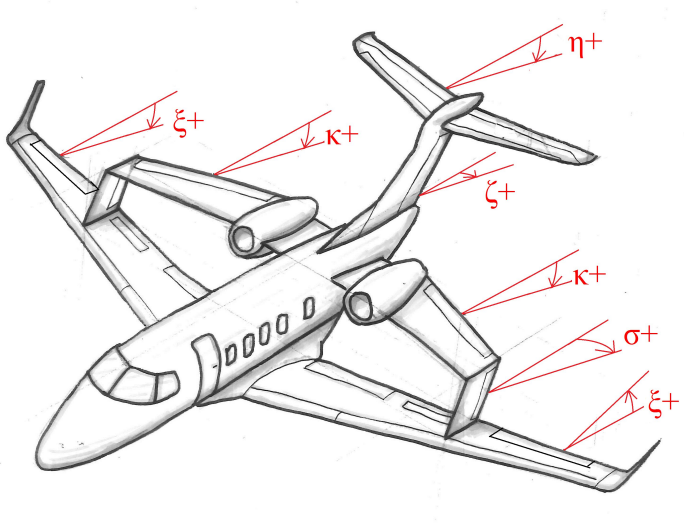

Figure 7.15: Sign convention of the IFS control surfaces.

$$X_a = X_{a_e} + \frac{\delta X}{\delta u}u + \frac{\delta X}{\delta v}v + \frac{\delta X}{\delta w}w + \frac{\delta X}{\delta p}p + \frac{\delta X}{\delta q}q + \frac{\delta X}{\delta r}r + \frac{\delta X}{\delta \dot{w}}\dot{w} \tag{7.48}$$

$$M_c = \frac{\delta M}{\delta \xi}\xi + \frac{\delta M}{\delta \eta}\eta + \frac{\delta M}{\delta \zeta}\zeta + \frac{\delta M}{\delta \kappa}\kappa + \frac{\delta M}{\delta \sigma}\sigma + \frac{\delta M}{\delta \chi}\chi \tag{7.49}$$

The resulting system, not presented here because of its complexity, can be found in Cook [4]. It describes aircraft motion in all six degrees of freedom, however at the cost of not being solvable because all equations are fully coupled and the number of variables greatly exceeds the number of equations. This system is used as basis to create new reduced sets of EOMs that are uncoupled and thus solvable. The two most used sets are the longitudinal and the lateral ones, also called "symmetric" and "asymmetric", that are described in sections 7.5.1 and 7.5.1.

Longitudinal motion EOMs

The main assumption for the longitudinal set is that disturbances act on the XZ-plane which is also the symmetry plane of the aircraft, leaving three of the six equations standing: forces along the X-axis (Equation 7.42), forces along the Z-axis (Equation 7.44) and moments around the Y-axis (Equation 7.46). Further simplifications can be made as there is no lateral motion. Some of the control terms can be neglected and the level flight causes θ to be small enough to be neglected. The resulting system, still containing dimensional terms, is presented in Equations 7.50 to 7.52, re-arranged to have control and thrust terms on the right side. For clarity the derivative terms like $\delta X/\delta u$ in Equation 7.48 and Equation 7.49 are written with simplified notation X_u. The terms with subscripts κ and χ are related to upper wing flap and the drag chute respectively.

$$m\dot{u} - X_u u - X_{\dot{w}}\dot{w} - X_w w - X_q q + mg\theta = X_\eta \eta + X_\kappa \kappa + X_\chi \chi + X_\tau \tau \tag{7.50}$$

$$- Z_u u + (m - Z_{\dot{w}})\dot{w} - Z_w w - (Z_q + mU_e)q = Z_\eta \eta + Z_\kappa \kappa + Z_\chi \chi + Z_\tau \tau \tag{7.51}$$

$$- M_u u - M_{\dot{w}}\dot{w} - M_w w + I_y \dot{q} - M_q q = M_\eta \eta + M_\kappa \kappa + M_\chi \chi + M_\tau \tau \tag{7.52}$$

Lateral motion EOMs

For the lateral set of EOMs the main assumptions are absence of longitudinal and vertical motions, thereby reducing the degrees of freedom to movement along the Y-axis (Equation 7.43), rotation around the X-axis (Equation 7.45) and around the Z-axis (Equation 7.47). Some terms are considered small and are neglected, like multiplied derivatives and coupling derivatives. Equations 7.53 to 7.55 make up the lateral set of EOMs, re-arranged to have control terms on the right side. The terms with subscript σ are related to the rudders of the vertical wings.

$$m\dot{v} - Y_v v - Y_p p - (Y_r - mU_e)r - mg\varphi = Y_\xi \xi + Y_\zeta \zeta + Y_\sigma \sigma \tag{7.53}$$

$$- L_v v + I_x \dot{p} - L_p p - I_{xz}\dot{r} - L_r r = L_\xi \xi + L_\zeta \zeta + L_\sigma \sigma \tag{7.54}$$

$$- N_v v - I_{xz}\dot{p} + I_z \dot{r} - N_r r = N_\xi \xi + N_\zeta \zeta + N_\sigma \sigma \tag{7.55}$$

7.5.2 Non-dimensional equations

The general EOMs presented in this chapter have been de-coupled in section 7.5.1. They feature forces, moments, masses, inertias, velocities and accelerations related to a specific aircraft in a particular flight condition. These values in the EOMs change significantly when the flight condition or aircraft is altered. To achieve a more general formulation a standard approach was used to make the equations dimensionless, that is by dividing them with physical quantities representative of both aircraft and flight conditions. Force equations (7.50, 7.51 and 7.53) were divided by $\frac{1}{2}\rho V^2 S$, longitudinal moment equation (7.52) by $\frac{1}{2}\rho V^2 S\bar{c}$ and lateral moment equations (7.54 and 7.55) by $\frac{1}{2}\rho V^2 Sb$. This division is presented in Equations 7.56 through 7.61.

$$\frac{m\dot{u}}{\frac{1}{2}\rho V^2 S} - \frac{X_u u + X_{\dot{w}}\dot{w} + X_w w + X_q q}{\frac{1}{2}\rho V^2 S} + \frac{mg}{\frac{1}{2}\rho V^2 S}\cdot\theta = \frac{X_\eta \eta + X_\kappa \kappa + X_\chi \chi + X_\tau \tau}{\frac{1}{2}\rho V^2 S} \tag{7.56}$$

$$\frac{m(\dot{w} - U_e q)}{\frac{1}{2}\rho V^2 S} - \frac{Z_u u + Z_{\dot{w}}\dot{w} + Z_w w + Z_q q}{\frac{1}{2}\rho V^2 S} = \frac{Z_\eta \eta + Z_\kappa \kappa + Z_\chi \chi + Z_\tau \tau}{\frac{1}{2}\rho V^2 S} \tag{7.57}$$

$$\frac{I_y \dot{q}}{\frac{1}{2}\rho V^2 S\bar{c}} - \frac{M_u u + M_{\dot{w}}\dot{w} + M_w w + M_q q}{\frac{1}{2}\rho V^2 S\bar{c}} = \frac{M_\eta \eta + M_\kappa \kappa + M_\chi \chi + M_\tau \tau}{\frac{1}{2}\rho V^2 S\bar{c}} \tag{7.58}$$

$$\frac{m(\dot{v} + U_e r)}{\frac{1}{2}\rho V^2 S} - \frac{Y_v v + Y_p p + Y_r r}{\frac{1}{2}\rho V^2 S} - \frac{mg}{\frac{1}{2}\rho V^2 S}\cdot\varphi = \frac{Y_\xi \xi + Y_\zeta \zeta + Y_\sigma \sigma}{\frac{1}{2}\rho V^2 S} \tag{7.59}$$

$$\frac{I_x \dot{p} - I_{xz}\dot{r}}{\frac{1}{2}\rho V^2 Sb} - \frac{L_v v + L_p p + L_r r}{\frac{1}{2}\rho V^2 Sb} = \frac{L_\xi \xi + L_\zeta \zeta + L_\sigma \sigma}{\frac{1}{2}\rho V^2 Sb} \tag{7.60}$$

$$\frac{I_z \dot{r} - I_{xz}\dot{p}}{\frac{1}{2}\rho V^2 Sb} - \frac{N_v v + N_r r}{\frac{1}{2}\rho V^2 Sb} = \frac{N_\xi \xi + N_\zeta \zeta + N_\sigma \sigma}{\frac{1}{2}\rho V^2 Sb} \tag{7.61}$$

Adoption of new symbols for stability and control derivatives allows to make Equations 7.56 through 7.61 more readable, resulting in a new set of EOMs as presented in Equations 7.62 through 7.67. For example, the coefficient of the forces along the Z-axis w.r.t. the angle of attack α is renamed in C_{Z_α}, and the other coefficients follow the same naming rule.

$$2\mu_c D_c\hat{u} - C_{X_u}\hat{u} - C_{X_{\dot{\alpha}}}D_c\alpha - C_{X_\alpha}\alpha - C_{X_q}D_c\theta - C_{Z_0}\theta = C_{X_\eta}\eta + C_{X_\kappa}\kappa + C_{X_\chi}\chi + C_{X_\tau}\tau \tag{7.62}$$

$$2\mu_c(D_c\alpha - D_c\theta) - C_{Z_u}\hat{u} - C_{Z_{\dot{\alpha}}}D_c\alpha - C_{Z_\alpha}\alpha - C_{Z_q}D_c\theta = C_{Z_\eta}\eta + C_{Z_\kappa}\kappa + C_{Z_\chi}\chi + C_{Z_\tau}\tau \tag{7.63}$$

$$2\mu_c K_Y^2 D_c\left(\frac{q\bar{c}}{V}\right) - C_{m_u}\hat{u} - C_{m_{\dot{\alpha}}}D_c\alpha - C_{m_\alpha}\alpha - C_{m_q}D_c\theta = C_{m_\eta}\eta + C_{m_\kappa}\kappa + C_{m_\chi}\chi + C_{m_\tau}\tau \tag{7.64}$$

$$2\mu_b\left(D_b\beta + 2\frac{rb}{2V}\right) - C_{Y_\beta}\beta - C_{Y_p}\left(\frac{pb}{2V}\right) - C_{Y_r}\left(\frac{rb}{2V}\right) - C_L\varphi = C_{Y_\xi}\xi + C_{Y_\zeta}\zeta + C_{Y_\sigma}\sigma \tag{7.65}$$

$$4\mu_b\left(K_X^2 D_b\frac{pb}{2V} - K_{XZ}D_b\frac{rb}{2V}\right) - C_{l_\beta}\beta - C_{l_p}\left(\frac{pb}{2V}\right) - C_{l_r}\left(\frac{rb}{2V}\right) = C_{l_\xi}\xi + C_{l_\zeta}\zeta + C_{l_\sigma}\sigma \tag{7.66}$$

$$4\mu_b\left(K_Z^2 D_b\frac{rb}{2V} - K_{XZ}D_b\frac{pb}{2V}\right) - C_{n_\beta}\beta - C_{n_r}\left(\frac{rb}{2V}\right) = C_{n_\xi}\xi + C_{n_\zeta} + C_{n_\sigma}\sigma\zeta \tag{7.67}$$

7.5.3 State-space formulation

Equations from subsection 7.5.2 can be expressed in a multi-dimensional vector space (the *state space*) to allow analysis of the dynamic response of the aircraft to airflow disturbances. The starting point is to define a set of variables that fully describes the state of the aircraft, called the state vector $x(t)$. Typical values used in the state vector are Earth-attitude angles, airspeed and body angles and rates of roll, pitch and yaw. The state vector $x(t)$ is a function of time as its values are expected to change after the disturbances are encountered.

The second step is to identify all the means through which the aircraft can be controlled. In the case of the IFS they include the original Embraer Phenom 300 control surfaces and engine power setting plus the new upper wing flaps, the vertical wing rudders and the drag chute. The final step is to describe the rate of change of the state variables as a function of the current state and the inputs given through the aircraft control means. This generates a system of linear, time-invariant differential equations that can be evaluated numerically. Two matrices **A** and **B** are added to this system, as described in Equation 7.68, to account for the characteristics of the particular aircraft, with state matrix **A** accounting for the sensitivity to changes in the state variables and input matrix **B** expressing the efficiency of the control methods in affecting the aircraft behaviour.

$$\dot{x}(t) = \mathbf{A}x(t) + \mathbf{B}u(t) \tag{7.68}$$

In Equation 7.69 the state vectors for the longitudinal and lateral set of EOMs are presented, showing no difference of the IFS with respect to other airplanes. Equation 7.70 instead describes the new input vectors for the IFS, with original deflections of ailerons ξ, elevators η and rudder ζ plus deflections for upper wing flap κ, vertical wings rudders σ and deployment of drag chute χ. For χ the only possible values are '0' and '1', as the chute is a binary device that can only be 'on' or 'off'. The engine power setting was dropped in the longitudinal set of EOMs because engine spool-up times are typically larger than the time-spans over which aircraft response is investigated.

$$x(t)_{longitudinal} = \left[\,\hat{u},\ \alpha,\ \theta,\ \frac{q\bar{c}}{V}\right]^T \quad ; \quad x(t)_{lateral} = \left[\,\beta,\ \varphi,\ \frac{pb}{2V},\ \frac{rb}{2V}\right]^T \tag{7.69}$$

$$u(t)_{longitudinal} = [\,\eta,\ \kappa,\ \chi\,]^T \quad ; \quad u(t)_{lateral} = [\,\xi,\ \zeta,\ \sigma\,]^T \tag{7.70}$$

A second system of equations can be added when precise measurement of state variables is not possible. A set of output variables is chosen (output vector $y(t)$) and their values obtained as a function of current state and input vectors as shown in Equation 7.71. Again two matrices are added to account for the particular aircraft characteristics with output matrix **C** and direct matrix **D** acting as multipliers of the vectors $x(t)$ and $u(t)$. This second system is however not used on the IFS as the installed sensors allow precise measurement of the state variables. By choosing the state one $x(t)$ as output vector $y(t)$ the whole system simplifies to an identity, thereby Equation 7.71 was not used.

$$y(t) = \mathbf{C}x(t) + \mathbf{D}u(t) \tag{7.71}$$

Population of the state matrix **A** and input matrix **B** is achieved using the longitudinal or the lateral set of EOMs. The final objective of this approach is to use linear algebra to evaluate the dynamic stability of the aircraft, and for this purpose matrix **A** needs to be square, with as many equations as state variables. Matrix **B** is not analyzed for stability and has no requirement to be square, with as many columns as variables in the input vectors (Equation 7.70).

Longitudinal motion EOMs

The longitudinal set of EOMs consists of three equations while the state vector (Equation 7.69) has four variables, creating the need for an extra equation relating attitude angle θ and its rate of change q to the aid of differential operator D_c. Equation 7.72 presents the state-space formulation of the longitudinal set of EOMs.

$$\begin{bmatrix} 2\mu_c D_c - C_{X_u} & -C_{X_{\dot{\alpha}}} D_c - C_{X_\alpha} & -C_{X_q} D_c - C_{Z_0} & 0 \\ -C_{Z_u} & 2\mu_c D_c - C_{Z_{\dot{\alpha}}} D_c - C_{Z_\alpha} & -2\mu_c D_c - C_{Z_q} D_c & 0 \\ 0 & 0 & D_c & -1 \\ -C_{m_u} & -C_{m_\alpha} D_c - C_{m_\alpha} & -C_{m_q} D_c & 2\mu_c K_Y^2 D_c \end{bmatrix} \cdot \begin{bmatrix} \hat{u} \\ \alpha \\ \theta \\ \frac{q\bar{c}}{V} \end{bmatrix} = \\ = \begin{bmatrix} C_{X_\eta} \\ C_{Z_\eta} \\ 0 \\ C_{m_\eta} \end{bmatrix} \eta + \begin{bmatrix} C_{X_\kappa} \\ C_{Z_\kappa} \\ 0 \\ C_{m_\kappa} \end{bmatrix} \kappa + \begin{bmatrix} C_{X_\chi} \\ C_{Z_\chi} \\ 0 \\ C_{m_\chi} \end{bmatrix} \chi \quad (7.72)$$

Because q is the time rate of change of θ it is possible to shift some of the terms of the third column of the right matrix in Equation 7.72 to the fourth column and drop the differential operator D_c. Furthermore the EOMs were re-arranged so that remaining differential terms are in a new matrix that multiplies the time-derivative of the state vector, making the system more similar to Equation 7.68 as presented in Equation 7.73.

$$\frac{\bar{c}}{V} \cdot \begin{bmatrix} 2\mu_c & -C_{X_{\dot{\alpha}}} & 0 & 0 \\ 0 & 2\mu_c - C_{Z_{\dot{\alpha}}} & 0 & 0 \\ 0 & 0 & 1 & 0 \\ 0 & -C_{m_\alpha} & -C_{m_q} & 2\mu_c K_Y^2 \end{bmatrix} \cdot \begin{bmatrix} \dot{\hat{u}} \\ \dot{\alpha} \\ \dot{\theta} \\ \frac{\dot{q}\bar{c}}{V} \end{bmatrix} = \\ = \begin{bmatrix} C_{X_u} & C_{X_\alpha} & C_{Z_0} & C_{X_q} \\ C_{Z_u} & C_{Z_\alpha} & 0 & 2\mu_c + C_{Z_q} \\ 0 & 0 & 0 & 1 \\ C_{m_u} & C_{m_\alpha} & 0 & C_{m_q} \end{bmatrix} \cdot \begin{bmatrix} \hat{u} \\ \alpha \\ \theta \\ \frac{q\bar{c}}{V} \end{bmatrix} + \begin{bmatrix} C_{X_\eta} & C_{X_\kappa} & C_{X_\chi} \\ C_{Z_\eta} & C_{Z_\kappa} & C_{Z_\chi} \\ 0 & 0 & 0 \\ C_{m_\eta} & C_{m_\kappa} & C_{m_\chi} \end{bmatrix} \cdot \begin{bmatrix} \eta \\ \kappa \\ \chi \end{bmatrix} \quad (7.73)$$

The system in Equation 7.73 is of type $\mathbf{P}\dot{x}(t) = \mathbf{Q}x(t) + \mathbf{R}u(t)$, so it is necessary to pre-multiply the right-side terms by the inverse of the matrix on the left side (assumed invertible), obtaining the desired $\dot{x}(t) = \mathbf{A}x(t) + \mathbf{B}u(t)$ formulation. Because of this last manipulation a new set of symbols is used to improve readability, with x terms and subscripts in the **A** and **B** matrices, as presented in Equation 7.74.

$$\begin{bmatrix} \dot{\hat{u}} \\ \dot{\alpha} \\ \dot{\theta} \\ \frac{\dot{q}\bar{c}}{V} \end{bmatrix} = \begin{bmatrix} x_u & x_\alpha & x_\theta & x_q \\ z_u & z_\alpha & 0 & z_q \\ 0 & 0 & 0 & \frac{V}{\bar{c}} \\ m_u & m_\alpha & 0 & m_q \end{bmatrix} \cdot \begin{bmatrix} \hat{u} \\ \alpha \\ \theta \\ \frac{q\bar{c}}{V} \end{bmatrix} + \begin{bmatrix} x_\eta & x_\kappa & x_\chi \\ z_\eta & z_\kappa & z_\chi \\ 0 & 0 & 0 \\ m_\eta & m_\kappa & m_\chi \end{bmatrix} \cdot \begin{bmatrix} \eta \\ \kappa \\ \chi \end{bmatrix} \quad (7.74)$$

Lateral motion EOMs

The lateral set of EOMs also consists of three equations while the state vector (Equation 7.69) is composed by four variables. The extra equation is again a simple relation between roll angle φ and its rate of change p using the differential operator D_b. The state-space formulation of the longitudinal set of EOMs can be found in Equation 7.75 [28].

$$\begin{bmatrix} 2\mu_b D_b - C_{Y_\beta} & -C_L & -C_{Y_p} & -C_{Y_r} \\ 0 & D_b & -1 & 0 \\ -C_{l_\beta} & 0 & 4\mu_b K_X^2 D_b - C_{l_p} & -4\mu_b K_{XZ} D_b - C_{l_r} \\ -C_{n_\beta} & 0 & -4\mu_b K_{XZ} D_b & 4\mu_b K_Z^2 D_b - C_{n_r} \end{bmatrix} \cdot \begin{bmatrix} \beta \\ \varphi \\ \frac{pb}{2V} \\ \frac{rb}{2V} \end{bmatrix} =$$

$$= \begin{bmatrix} C_{Y_\xi} \\ 0 \\ C_{l_\xi} \\ C_{n_\xi} \end{bmatrix} \xi + \begin{bmatrix} C_{Y_\zeta} \\ 0 \\ C_{l_\zeta} \\ C_{n_\zeta} \end{bmatrix} \zeta + \begin{bmatrix} C_{Y_\sigma} \\ 0 \\ C_{l_\sigma} \\ C_{n_\sigma} \end{bmatrix} \sigma \quad (7.75)$$

As done with the longitudinal set it is possible to re-arrange the equations of the lateral set and obtain a system of type $\mathbf{P}\dot{x}(t) = \mathbf{Q}x(t) + \mathbf{R}u(t)$. Because p is the time rate of change of γ it is possible to move terms in the second row of the right matrix of Equation 7.76. The terms were also separated in three groups: one acting on the state vector, one acting on its time derivative and a last one acting on the input vector.

$$\frac{b}{2V} \cdot \begin{bmatrix} 2\mu_b & 0 & 0 & 0 \\ 0 & 1 & 0 & 0 \\ 0 & 0 & 4\mu_b K_X^2 & -4\mu_b K_{XZ} \\ 0 & 0 & -4\mu_b K_{XZ} & 4\mu_b K_Z^2 D_b \end{bmatrix} \cdot \begin{bmatrix} \dot{\beta} \\ \dot{\varphi} \\ \frac{\dot{p}b}{2V} \\ \frac{\dot{r}b}{2V} \end{bmatrix} =$$

$$= \begin{bmatrix} C_{Y_\beta} & C_L & C_{Y_p} & C_{Y_r} \\ 0 & 0 & 1 & 0 \\ C_{l_\beta} & 0 & C_{l_p} & C_{l_r} \\ C_{n_\beta} & 0 & 0 & C_{n_r} \end{bmatrix} \cdot \begin{bmatrix} \beta \\ \varphi \\ \frac{pb}{2V} \\ \frac{rb}{2V} \end{bmatrix} + \begin{bmatrix} C_{Y_\xi} & C_{Y_\zeta} & C_{Y_\sigma} \\ C_{l_\xi} & C_{l_\zeta} & C_{l_\sigma} \\ 0 & 0 & 0 \\ C_{n_\xi} & C_{n_\zeta} & C_{n_\sigma} \end{bmatrix} \cdot \begin{bmatrix} \xi \\ \zeta \\ \sigma \end{bmatrix} \quad (7.76)$$

The system was finally pre-multiplied by the inverse of the right matrix in Equation 7.76 to find the $\dot{x}(t) = \mathbf{A}x(t) + \mathbf{B}u(t)$ formulation. After this last manipulation another new set of symbols was used to improve readability, with y terms and subscripts in the **A** and **B** matrices, as presented in Equation 7.77.

$$\begin{bmatrix} \dot{\beta} \\ \dot{\varphi} \\ \frac{\dot{p}b}{2V} \\ \frac{\dot{r}b}{2V} \end{bmatrix} = \begin{bmatrix} y_\beta & y_\varphi & y_p & y_r \\ 0 & 0 & \frac{2V}{b} & 0 \\ l_\beta & 0 & l_p & l_r \\ n_\beta & 0 & 0 & n_r \end{bmatrix} \cdot \begin{bmatrix} \beta \\ \varphi \\ \frac{pb}{2V} \\ \frac{rb}{2V} \end{bmatrix} + \begin{bmatrix} y_\xi & y_\zeta & y_\sigma \\ 0 & 0 & 0 \\ l_\xi & l_\zeta & l_\sigma \\ n_\xi & n_\zeta & n_\sigma \end{bmatrix} \cdot \begin{bmatrix} \xi \\ \zeta \\ \sigma \end{bmatrix} \quad (7.77)$$

7.5.4 Eigenmotions and method validation

The analysis carried out until now is purely theoretical, and requires the estimation of every one of the parameters in Equation 7.73 and Equation 7.76 if the complete dynamics of the aircraft have to be evaluated. A more limited analysis is possible either by simplifying the system and that way obtain a direct solution or by creating a time-step simulation based on initial conditions and step/pulse control inputs. The first method makes use of additional assumptions to reduce the number of EOMs and the dimensions of the **A** matrix so that a direct solution can be obtained (with Laplace transforms) in the $a_1 e^{\lambda_1 t} + a_2 e^{\lambda_2 t}$ exponential form. The second method uses simulation software to calculate the aircraft response to a specific disturbance, usually a control deflection. It was decided to apply the second method and create a program in Python 3.5.2 for this purpose, using the external packages NumPy, SymPy, Control and sub-package Matlab. A test session with data from the Cessna Ce500 Citation (Table A.1) provided validation of the program, as presented in Figure 7.16a and 7.16b where stable phugoid and slightly unstable spiral modes are clearly visible.

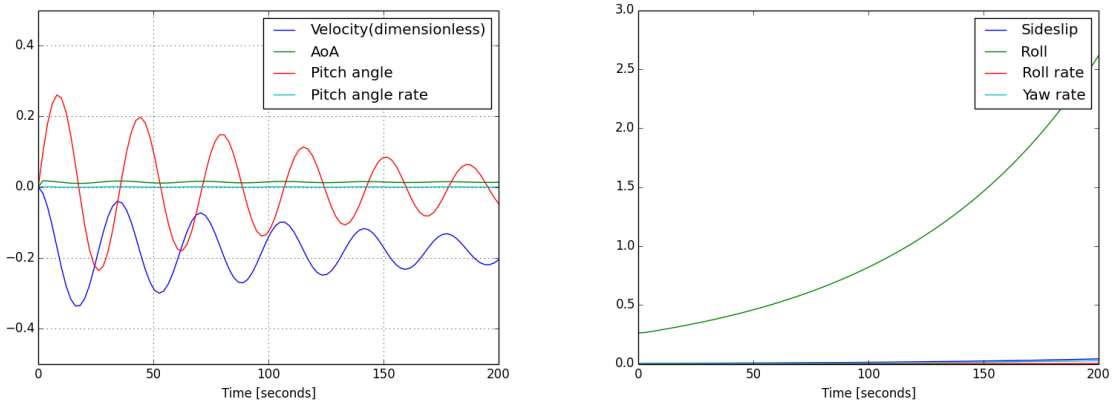

(a) Long-period longitudinal motion.

(b) Long-period lateral motion.

Figure 7.16: Longitudinal and lateral motion diagrams of the Cessna Ce500 Citation.

The geometric properties, flight conditions and stability derivatives of the original Embraer Phenom 300 and the IFS were then implemented in the software, using data from chapter 6 as summarized in Appendix A. Before the simulation was run a sanity check of the coefficients of the three airplanes was done, indicating a large discrepancy between the Cessna Ce500 Citation figures and the two Embraer Phenom 300 and IFS data, as also reported about in subsection 6.4.2. It was decided to run the simulation anyway for the IFS configuration and evaluate the results, leaving further corrections and iterations to following design phases as described in section 11.4. In the longitudinal EOMs of the IFS a clear result is the unstable phugoid motion, as shown in Figure 7.17a and 7.17b. This motion develops with a 30 second period over a time span large enough to be controlled manually by the pilot, or by the auto-pilot, thereby posing a piloting comfort problem but not a direct safety risk.

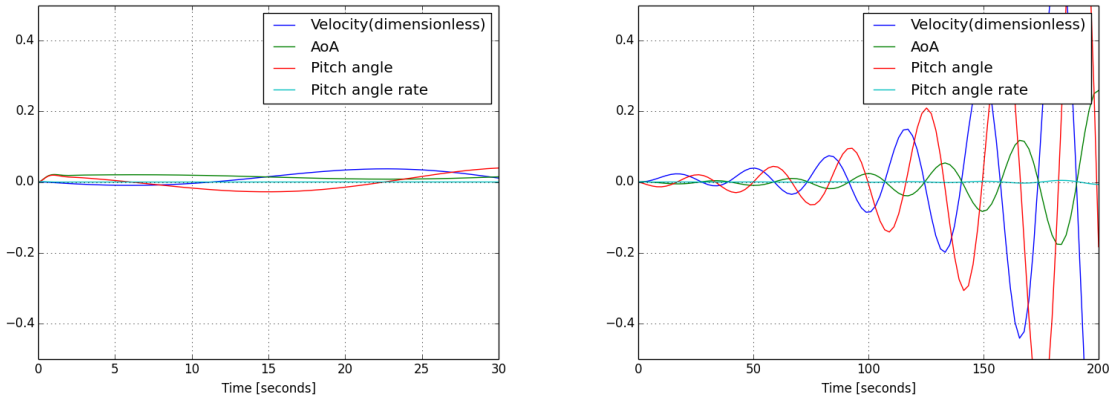

(a) Short-period motion.

(b) Long-period motion.

Figure 7.17: Longitudinal motion diagrams of the IFS.

In the lateral EOMs case the results were not acceptable, as the short and long period responses have similar divergent shapes even though the time-span is very different, as shown in Figure 7.17b and 7.18b. This could indicate the non-convergence of the calculations, raising doubts about the AVL parameters for this case (inertias in particular, Table A.3). Because of this issue the lateral EOMs analysis did not produce usable results. In both the longitudinal and lateral cases the controls' effectiveness parameters for the IFS appear to be too small, with very little motion in the short period (Figure 7.17a and 7.18a). Evidently not all of these motions and rates would have to be shown to indicate the fact that the IFS is unstable, but they are included for the sake of completeness.

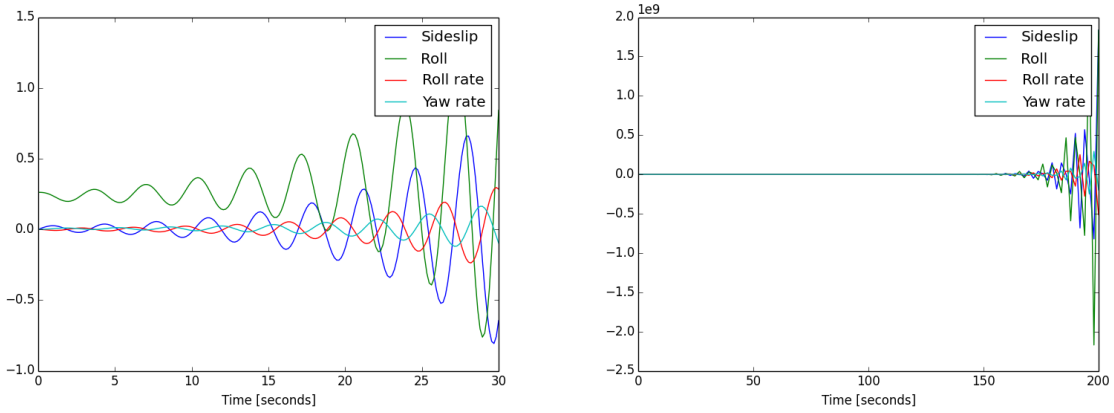

(a) Short-period motion.

(b) Long-period motion.

Figure 7.18: Lateral motion diagrams of the IFS.

Eigenvalues of the **A** state matrices were also calculated with package LinAlg as shown in Table 7.5. A negative real part is always desirable, as in this case the eigenmotion will converge to a constant solution. If the real part is positive the motion amplitude will diverge and the aircraft will become uncontrollable. Presence of an imaginary part indicates if the motion, either convergent or divergent, also features oscillations. In Table 7.5 the Cessna Ce500 Citation shows convergent longitudinal motions (short period and phugoid having real parts -3.038 and -0.008), while for the lateral motions the short-period one is stable (real part -0.807) and the spiral one is moderately divergent (real part +0.012). In the longitudinal case the IFS has a short-period stable motion (real part -1.802) and a moderately unstable phugoid behaviour (real part is +0.023). However in the lateral case the IFS shows a dangerous lateral instability denoted by the +0.127 real part eigenvalue.

Table 7.5: Eigenvalues of the state matrices for Cessna Ce500 Citation and IFS.

Set of EOMs	Aircraft	Eigenvalues		
Longitudinal	Cessna Ce500	-3.038 $\pm$ 2.861 i	-0.008 $\pm$ 0.176 i	
Lateral	Cessna Ce500	-0.807 $\pm$ 3.047 i	-9.49	+0.012

7.5.5 Conclusions

In subsection 7.5.4 it was determined that the IFS is laterally unstable, and this means that it is dangerous (if not impossible) to fly it without artificial stability as any gust introducing a β disturbance would rapidly put the aircraft out of control. Furthermore the whole certification process is not possible, preventing the IFS from even entering the in-flight simulation market. However, because of the uncertainties regarding the input values used in the calculations, the results of this analysis are not conclusive and the rest of the report does not account for them. Further iterations of the calculations done in this chapter will have to be completed before the manufacturing process of the IFS can begin, as described in section 11.4.

7.6 Variable stability

The equations of motion derived in section 7.5 apply to the IFS on a general level, as they feature the original aircraft parameters and the new control surfaces. The original Embraer Phenom 300 was modified with the addition of an upper wing and vertical wings, and this new configuration is represented in Equations 7.74 and 7.77 by the **A** matrices, that describe the IFS behaviour when control surfaces are not used. The main purpose of the IFS is to change this behaviour and simulate specific test cases, as described in section 7.3, and different aircraft dynamics, as stated in block *1.10 design variable stability transfer functions* of the FBS. **A** and **B** matrices in Equation 7.68 are representative of physical characteristics of the IFS like wing surface and mass distributions, therefore it is not possible to change them during flight. The new flight control system (FCS) can only act on the deflections of the control surfaces and the power settings to influence the IFS behaviour. This is explained in Equations 7.78 and 7.79, where the aircraft state at $t + \Delta t$ is a function of actual state $x(t)$, matrices **A** and **B** and input vector $u(t)$.

$$x(t + \Delta t) = x(t) + \dot{x}(t) \cdot \Delta t \tag{7.78}$$

$$x(t + \Delta t) = x(t) + \mathbf{A} \cdot x(t) \cdot \Delta t + \mathbf{B} \cdot u(t) \cdot \Delta t \tag{7.79}$$

During safe-flight mode the safety pilot is in control of the aircraft, with surface deflections directly and linearly connected to the safety pilot station. This means that the added upper and vertical wings are still present but their control surfaces are put in a fixed position, as described in Equation 7.80 where channels κ, χ and σ are all zero. This configuration is applicable to takeoff, landing, ferry and safe recovery flight phases.

$$u_{long} = [\ \eta_{pilot}\ ,\ 0\ ,\ 0\ ]^T \quad ; \quad u_{lat} = [\ \xi_{pilot}\ ,\ \zeta_{pilot}\ ,\ 0\ ]^T \tag{7.80}$$

During augmented flight phases the FCS becomes active positioning itself between the test pilot commands and the control surfaces deflections, as outlined in Equation 7.81. The FCS uses pilot inputs, actual flight conditions and desired aircraft behaviour to calculate the required deflections to be applied. The input vector u is then also a function of the state vector, becoming $u(t, x)$. Presence of algorithms in the FCS turns the IFS in a sort of "servo-mechanism" with a human pilot in-the-loop.

$$u_{long} = [\ \eta_{FCS}\ ,\ \kappa_{FCS}\ ,\ \chi_{FCS}\ ]^T \quad ; \quad u_{lat} = [\ \xi_{FCS}\ ,\ \zeta_{FCS}\ ,\ \sigma_{FCS}\ ]^T \tag{7.81}$$

7.6.1 Standard test cases

The four basic cases described in section 7.3 can be reproduced by the FCS by bringing the airplane in new trim conditions, applying sets of pre-determined gains and deflections to the basic flight deflections. This change in the EOMs is described in Equation 7.82.

$$\dot{x}(t) = \mathbf{A}x(t) + \mathbf{B}u(t) \quad \rightarrow \quad \dot{x}(t) = \mathbf{A}x(t) + \mathbf{B} \cdot \left(\mathbf{K_0} + \mathbf{K_1}x(t) + \mathbf{K_2}u(t)_{pilot}\right) \tag{7.82}$$

These parameters are determined by analysis of the four test cases and calculation of new trim conditions using forces and moments equations from section 7.3. Because of the multiple control surfaces available in both the longitudinal and lateral motion EOMs, the solutions are not unique, but constitute solution spaces. For example a particular acceleration in Z-axis can be achieved by deflecting the upper wing flaps and/or the elevators on the horizontal tail, resulting in a 2-dimensional solution space. Motions along the Y-axis or around the Z-axis can also be obtained by deflections of the vertical wing rudders and the original tail rudder, again creating a 2D solution space. Choice of the actual solution is made by the FCS following the principle of maximization of the stability margins, and to this purpose the forces and moment equations described in section 7.3 are used again. Most optimization techniques used on aircraft prioritize overall drag reduction for better fuel efficiency, however this is not the case for the IFS because simulation fidelity and maneuvering safety are more important aspects.

7.6.2 Aircraft imitation

Simulation of different aircraft uses a different approach from subsection 7.6.1. The first step is to obtain state and input matrices of the to-be-simulated aircraft ($\mathbf{A}_{sim}$ and $\mathbf{B}_{sim}$) using data and capabilities external to the IFS project. In the case of an existing aircraft it is expected that this data is available from wind tunnel and flight testing campaigns. If the aircraft is still in design phase the data will come from software tools that use theoretical or CFD techniques to predict them, an example being the AVL program used in chapter 6. The FCS on-board the IFS uses $\mathbf{A}_{sim}$ and $\mathbf{B}_{sim}$ to understand the effect that the pilot inputs would have on the to-be-simulated airplane (Equation 7.83), that is by calculating the state vector time-derivative $\dot{x}_{sim}(t)$. The 'sim' subscript is used for parameters related to the simulated aircraft, 'act' is used for those related to the actual IFS aircraft, 'pilot' for the test pilot's inputs and 'FCS' for the deflections commanded by the FCS.

$$\dot{x}_{sim}(t) = \mathbf{A_{sim}} \cdot x(t) + \mathbf{B_{sim}} \cdot u_{pilot}(t) \quad ; \quad \dot{x}_{act}(t) = \mathbf{A_{act}} \cdot x(t) + \mathbf{B_{act}} \cdot u_{FCS}(t) \tag{7.83}$$

To maximize simulation fidelity this value has to matched by the IFS so that resultant time-derivatives $\dot{x}(t)$ are the same. The FCS uses the same state vector in both calculations, so there is no 'mapping' or 'obfuscation' of the state variables themselves, meaning that the test pilot will see real instrument readings at all times. By solving Equation 7.84 the FCS will continuously determine the inputs u_{FCS} needed to imitate the simulated aircraft.

$$\begin{aligned} \dot{x}_{sim}(t) = \dot{x}_{act}(t) \quad \rightarrow \quad \mathbf{A_{sim}} \cdot x(t) + \mathbf{B_{sim}} \cdot u_{pilot}(t) = \mathbf{A_{act}} \cdot x(t) + \mathbf{B_{act}} \cdot u_{FCS}(t) \quad \rightarrow \\ \rightarrow \quad \mathbf{B_{act}} \cdot u_{FCS}(t) = (\mathbf{A_{act}} - \mathbf{A_{sim}})x(t) - \mathbf{B_{sim}} \cdot u_{pilot}(t) \end{aligned} \tag{7.84}$$

The multiplicity of control surfaces causes solution of Equation 7.84 to be a 2D solution space both in the longitudinal and lateral sets of EOMs. As explained in subsection 7.6.2 the actual solution (which is a combination of deflections) is determined by the FCS to maximize stability margins. After calculation of the solution the actual deflections are applied to the control surfaces by the FCS.

8 | Structural Analysis

In this chapter, the structural design of the implemented modifications is presented. The design is based on inputs from the boxwing design described in chapter 5, and complies with restrictions set by the stability characteristics as determined in chapter 7. Furthermore, the resource allocation as done in section 4.4 needs to be taken into account, wherein a maximum mass of the structural modifications of 224 kg was assigned, and a maximum cost of €450,000. At the end of this chapter, a detailed overview will be established of the loads acting on the structure, the stresses as a result of these loads and the required sizing of the structural elements that have to cope with these stresses. The final result will be a wingbox for the upper wing and main wing that will carry all of the loads introduced by the forces acting on the modifications. In the process of creating the structural design, the chapter follows the chronological steps taken during the calculations that produced the results. This means that it first describes a general overview of the approach (and assumptions) set up in the initial phases of the design in section 8.1. Based on this approach, a program was set up to compute the design characteristics of a wingbox structure. The layout of the program and the theory used in it are described in section 8.2. The validity of the program is described in section 8.3. The results and a discussion thereof are presented in section 8.4. These results include the complete mass-optimized wingbox geometry with all of its structural properties, such as spar location and number of stiffeners. The chapter is concluded with sections on additional design properties not included in the program in section 8.5. Recommendations for future research are made in chapter 16.

8.1 Approach to structural design

Before the start of the actual structural analysis, a few aspects of the analysis were considered. First, the coordinate system in which the wing box was analyzed was set up. The coordinate system used for the structural analysis is the body-fixed frame of reference, as was explained in section 7.5. This coordinate system applied to the IFS is shown in Figure 8.1. A right-handed coordinate system with the X-axis placed parallel to the fuselage of the airplane and the Z-axis placed positive in the upward direction, the Y-axis is perpendicular to these axes such that the outward direction to the left wing is positive. Next, several assumptions and limitations that were implemented to simplify the analysis will be explained.

The first simplification that was made to make the analysis easier is that the upper wing and the vertical wing were analyzed separately (without ignoring the influence that the two parts of the modifications have on each other). That is also why Figure 8.1 shows two separate origins: one for the analysis of the vertical wing placed at the leading edge of the vertical wing where it meets the main wing and one for the analysis of the upper wing placed at the leading edge of the upper wing where it meets the engine nacelle.

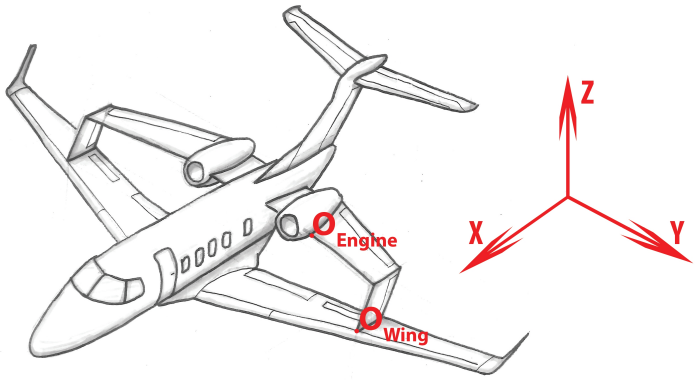

Figure 8.1: The coordinate system used in the structural analysis of the modifications.

Another important assumption is that the structure is assumed to possess only hinged connections. The upper wing will be connected to the engine nacelle by means of a hinge, the upper wing will be connected to the vertical wing using a hinge and the vertical wing is mounted on the main wing using a hinge. This means that there will be no moments around the previously defined X-axis that are transmitted from one structural element to another, which will positively affect the stresses in the upper and vertical wings. The design of these hinges will not be incorporated into the program, but will be discussed in section 8.4.

Additionally, some limitations were set on the structural design. First, the wingbox was assumed to have only two spars: one at the front end of the wingbox and one at the aft end of the wingbox. This was done primarily to reduce the amount of variables that would have to be iterated. Based on existing wingbox structures in lifting surfaces of aircraft that are in service today, this starting point would pose no problems for the structural integrity of the modifications. A final limitation was that the wingbox was assumed to be made of AL T6-7075, which is a very common aerospace grade aluminum [29]. The material properties used for this metal are shown in Table 8.1. [1]

Table 8.1: The material properties of AL T6-7075.

Parameter	Value	Unit
ρ	2700	kg/m^3
E	72	GPa
v	0.32	-
σ_{yield}	460	MPa
τ_{max}	330	MPa

To conclude the framework in which the structural design was created, Table 8.2 summarizes the key dimensions that were set earlier on in the design process. This includes the flap dimensions from the aerodynamic design as seen in chapter 5 and actuator dimensions as calculated in section 9.8. All of these dimensions, together with the assumptions made earlier on in this section represent the foundation and most basic input for the program described in the next section.

Table 8.2: The geometrical dimensions of the added surfaces.

(a) Flap dimensions.

Parameter	Value	Unit
$(c_f/c)_{uw}$	0.46	-
$(c_f/c)_{vw}$	0.38	-
$Clearance_{flap,uw}$ (each side)	0.213	m
$Clearance_{flap,vw}$ (each side)	0.2	m

(b) Actuator properties.

Parameter	Value	Unit
$Mounts_{uw}$	6	-
$Mounts_{vw}$	4	-
$Clearance_{act,uw}$	0.09	m
$Clearance_{act,vw}$	0.0497	m

(c) Global dimensions.

Parameter	Value	Unit
b_{uw}	3.53	m
b_{vw}	0.96	m
c_{uw}	1.34	m
c_{vw}	1.34	m
Λ_{uw}	-28	deg

8.2 Content of the program

The program that was set up to calculate the structural behaviour of different design options will be explained in this section. The language used for the program was Python 3.5.2. The main purpose during the development of the program was to maximize its flexibility while still complying with the limitations set in section 8.1. The general layout of the program is shown in Figure 8.2. From top to bottom, this shows the step-by-step execution of the code written during the course of the project. As can be seen in the image, the two very first steps deal with aligning the program with variables that were either presented in other chapters or set according to limitations discussed in section 8.1. After this was done, certain boundaries were applied to limit the amount of iterations and therefore computing time. This initialization phase is further described in subsection 8.2.1. After this first phase, a large loop is initiated that iterates over all of the possible design options for the structural elements that can be created within the iteration limits set before. This loop calculates all stresses occurring in each design option and then checks them for several failure modes before adding them to the resulting design options. This process is further described in subsections 8.2.2 through 8.2.7. From the options that did not fail according to the checks built into the loop the program then selects the option adding the least amount of weight and wraps up the entire process by storing the viable options in an Excel file and creating both stress and loading diagrams of the chosen structural design. This process is briefly described in subsection 8.2.8.

[1] http://www.makeitfrom.com/material-properties/7075-T6-Aluminum [cited 13 January 2017]

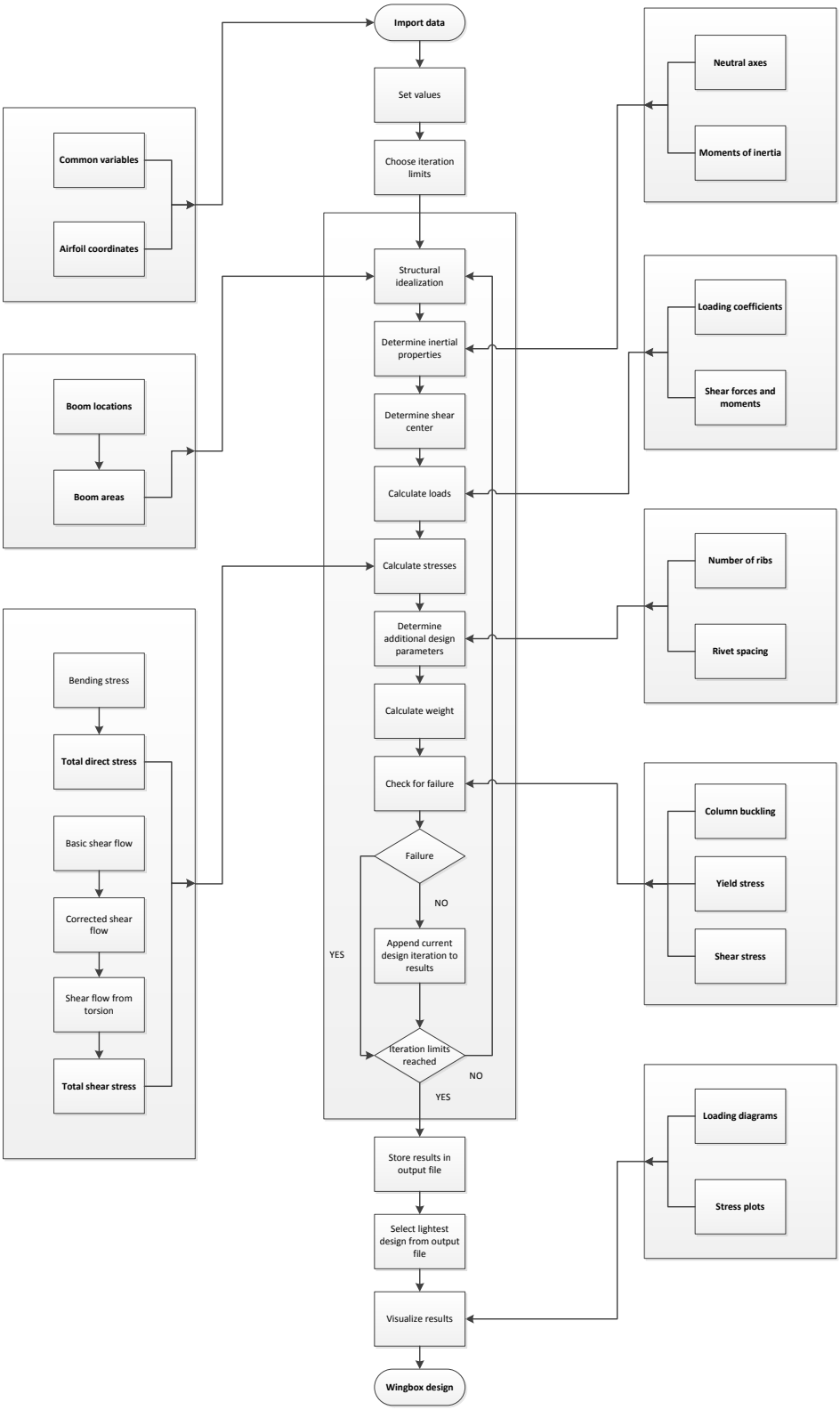

Figure 8.2: The layout of the program written to optimize the wingbox structure present in the modifications.

8.2.1 Initialize program

As discussed in the introduction of section 8.2, the first step that the program takes is importing data and setting some initial values determining the rest of the design process taking place in the lines of code in the core of the program.

Import data

First and foremost, every aspect of the design that was previously defined was imported. This does not only include the properties already mentioned in Table 8.1 and Table 8.2, but also basic data on the coordinates of the airfoil used on the upper and vertical wings. These airfoil data for the NACA0008 and NACA0012 profile as they were selected in chapter 5 consisted of 200 data points representing the coordinates of the airfoil [2]. Next to this, these initial steps involved importing useful Python packages including NumPy, SciPy, Math, Pandas, XLSWriter and Matplotlib.

Setting iteration limits

Another important step in the start-up phase of the program was the initialization of a few variables. These variables included parameters affecting the accuracy of the program (the section width used during discretization of the wingbox), variables affecting the reliability of the final design (the safety factor SF used to multiply the loads with) and a variable indicating which part of the modifications was analyzed (indicating either the upper or the vertical wing). Next to these very general indicators, limits were set for the number of iterations that generate the optimal design. These variables included limits on the thickness of the skin, the area of the stiffeners, the number of stiffeners and the thickness of the spars. The location(s) of the stiffeners was calculated automatically by the program, assuming an even distribution over the chord length of the wingbox. The location of the two spars could be directly calculated from the chord ratio of the flaps and the clearance needed for actuation of the flaps. The limits for the other variables were chosen using basic engineering knowledge and involved an educated guess on the manufacturing limits and practical limits of the wingbox construction. The limits used when coming to the final design are presented in section 8.4. It should be noted that the number of iterations was kept as high as possible to keep the highest number of design options for the wingbox.

8.2.2 Constructing and idealizing the wingbox

After the initialization of the program, the idealization procedure was started. The first step of this procedure is to create a wingbox in the program based on the design parameters defined in the current loop within the bounds of the iteration limits. The wingbox is then idealized to simplify the structural analysis. In this process, several assumptions and equations are used that will be described here. All equations that are mentioned in this part are directly taken or derived from equations stated in Megson [30].

The very first step in the idealization process is the construction of a workable model for the wingbox. This means that the the wingbox is divided in individual sections, which are then assigned a location and idealized individually. The coordinates of each section can be expressed as shown below. These coordinates define the position of the leading edge of each wing box section in the coordinate system defined in section 8.1. The sectionlength in these equations is defined in the coordinate system governing the program and directly influences the accuracy of the calculations:

$$x_{i,uw} = \tan(\Lambda_{uw}) \cdot i \cdot sectionlength \qquad x_{i,vw} = 0$$
$$y_{i,uw} = i \cdot sectionlength \qquad y_{i,vw} = 0$$
$$z_{i,uw} = 0 \qquad z_{i,vw} = i \cdot sectionlength$$

Next to the leading edge coordinates of each section in the global coordinate system, each boom in the wingbox section was given a coordinate. These coordinates were determined using the already calculated coordinates of the leading edges of the wingbox sections, combined with airfoil coordinates of the selected airfoil downloaded from an online airfoil database as described in subsection 8.2.1. After the determination of the positions of all the elements and the booms therein, the areas of the booms were determined. Before starting the idealization of the wingbox structure, a few simplifying assumptions have to be made:

- In a normal aircraft structure, the skin of a wingbox carries the largest part of the shear stresses originating from shear loads and torsional moments. The stiffeners attached to the structure mostly carry direct stresses from bending. For this idealization, the stiffeners are assumed to carry all of the direct stress, and the skin is assumed to carry all of the shear stress.

[2] http://airfoiltools.com/airfoil/naca4digit [cited 20 December 2016]

- The stress in the skin will vary slightly throughout the thickness. In this case, however, this variation is neglected.
- The neutral axis of the stiffeners is assumed to coincide with the neutral axis of the skin that it is attached to. This assumption can be made since the dimensions of the stiffeners are relatively small when compared to the dimensions of the overall wingbox. Although the wingbox is smaller than wingboxes used in standard wings, this is true since the stiffeners are also reduced in size.

Now that these assumptions are made, booms can be defined. These booms include the area of stiffeners present, but the area is also modified to include the area of the skin. By doing so, the assumption that the booms carry all of the direct stress can be implemented. This idealization is done in such a way that the same moments are present in the idealized structure as in the original structure. The general equation that is derived for the calculation of the area of a boom B_1 with a stress of σ_1 which is attached to a skin element of thickness t_D and length b with another boom B_2 and corresponding stress σ_2 is shown in Equation 8.1.

$$B_1 = \frac{t_D b}{6}\left(2 + \frac{\sigma_2}{\sigma_1}\right) \tag{8.1}$$

In the case of the wingbox of the upper wing and vertical wing, the bending stress is assumed to be the dominant stress in the wingbox. This means that the direct stresses in the wingbox can be assumed to vary linearly with the vertical distance from the neutral axis. Since the equation shows that only the stress ratio determines the boom area, the equation can be rewritten to include this relation as a simple ratio of distance with respect to the neutral axis.

$$B_1 = \frac{t_D b}{6}\left(2 + \frac{z_2}{z_1}\right) \tag{8.2}$$

In the wingboxes designed in this project, however, there are no booms that are attached to only one skin element. Therefore the equation for the boom area is rewritten to include all of the adjacent skin elements.

$$B_1 = \sum_{j=0}^{n} \frac{t_{D_j} b_j}{6}\left(2 + \frac{z_j}{z_1}\right) \tag{8.3}$$

Finally, the area of the stiffeners present at some of the boom locations has to be included in the calculations. Since these areas carry only direct stresses they can be directly added to the equation calculating the boom areas. This results in the final equation shown in Equation 8.4 giving the boom areas of the booms used in the discretization of the wingbox structure.

$$B_1 = \sum_{i=0}^{m} A_{stiffeners,i} + \sum_{j=0}^{n} \frac{t_{D_j} b_j}{6}\left(2 + \frac{z_j}{z_1}\right) \tag{8.4}$$

The process of boom idealization creates a boommatrix for the wing that is being analyzed. Throughout the program, several loops are used that iterate over the individual booms. Therefore the booms are numbered. The numbering system used is shown in Figure 8.3. The matrix that is defined is first used to calculate several inertial properties, as is explained in subsection 8.2.3.

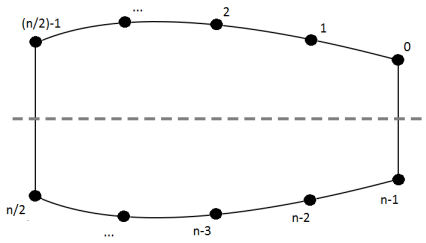

Figure 8.3: Boom numbering system of the idealized boxwing.

8.2.3 Calculation of inertial properties

Once the boommatrix has been generated, it is possible to calculate the various stresses resulting from the shear forces, moments and torsion acting on the wingbox. The basis for all the stress calculations are the location of the centroid and the area moment of inertia of the cross section. These two properties are explained in the following two sections. Once these inertial properties have been determined one can proceed with calculating the relevant stresses.

Computation of centroid coordinates

The centroid of a cross-section is the point about which the area of the section is evenly distributed. It is also a point on the neutral axis, which is the intersection line between the cross-section and the plane in which direct stresses are zero. Because the stresses are zero at this point it is very convenient to use it as an origin in stress calculations. The equations for obtaining the x and z coordinate of the centroid for each section are shown in Equation 8.5 and Equation 8.6. The variables A_i, x_i and z_i are taken from the boommatrix. The coordinates of the centroid are stored in a two-dimensional matrix with the number of rows equal to the number of sections and two columns for each one of the coordinates. Since the cross-section has an axis of symmetry $\bar{z}$ is equal to 0.

$$\bar{x} = \frac{\sum_{i=i}^{n-1} A_i x_i}{\sum_{i=1}^{n-1} A_i} \tag{8.5}$$

$$\bar{z} = \frac{\sum_{i=1}^{n} A_i z_i}{\sum_{i=1}^{n} A_i} \tag{8.6}$$

Computation of area moment of inertia

The next step is to determine the Area Moment of Inertia (MOI). This property of a cross-section is a measure for resistance against bending. If a geometry has a high MOI the structure is very stiff and thus will develop less stresses than a structure with a low MOI. The magnitude of the MOI is depended on the amount of area and its distance from the centroid. When considering bending moments, stiffeners are the most used structural elements in many aerospace applications because they add area to the structure at a large distance from the centroid. Since bending can happen around two axes, two MOIs need to be determined. Equation 8.7 and 8.8 are used to calculate the MOI of the cross-section of the wingbox. Since the booms have small areas with relatively low distances from their own centroids compared to distance to the centroid of the wingbox, the MOI of the separate booms around their own centroid can be neglected. Only the contribution from the so-called Steiner's theorem is taken into account when calculating the MOI of a boom. In this way, the MOI is determined by multiplying the area of each boom with the squared distance to the centroid. The results per section are stored in a two-dimensional matrix with the number of rows equal to the number of sections and two columns for each one of MOI's.

$$I_{xx} = \sum_{i=1}^{n} A_i (z - \bar{z})^2 \tag{8.7}$$

$$I_{zz} = \sum_{i=1}^{n} A_i (x - \bar{x})^2 \tag{8.8}$$

8.2.4 Shear center

The location of the shear center is necessary to properly compute the forces and stresses acting on the wingbox. When computing the shear flows in subsection 8.2.6, it is assumed that the shear forces causing these shear flows act through the shear center. If a force has to be translated to the shear center there has to be accounted for an additional torque. A good example is the lift produced by the flaps the upper and vertical wing. The lift acts as a shear force on the wingbox. Since the lift is acting outside the wingbox it has an arm with respect to some point in the wingbox and thus is also creating a torque.

To determine the shear center, an artificial force with a known magnitude is exerted on the cross-section, with an unknown distance ξ from the shear center. This shear force will create a shear flow in the cross-section. If the shear force would have act through the shear center, the shear flows would generate no moment about any random point. Since this is not the case in this problem, the moment the artificial shear force makes will be equal to the moment caused by the shear flows. The basic equation is shown in Equation 8.9. It equates the torque created by the shear force to the basic shear flow integrated over the circumference together with the torque from the constant shear flow. Since the cross-section has a horizontal axis of symmetry, the shear center will be positioned on that axis. So only the horizontal position need to be determined, resulting in a distance of the applied shear force perpendicular to the Z-axis.

$$S_z \xi_{sc} = \oint_s p q_b ds + 2A q_{s0} \tag{8.9}$$

$$q_{s0} = -\frac{\oint_s q_b ds}{\oint_s ds} \tag{8.10}$$

In this equation S_z is the vertical shear force, ξ_{sc} the unknown distance of the shear force to the shear center, A the enclosed of the cross-section, q_{s0} the constant shear flow, p the arm from the shear flow to the point around which the moments are taken and q_b the basic shear flow found by making a cut in the cross-section. The latter is explained in subsection 8.2.6, q_{s0} can be calculated with the Equation 8.10. The coordinates of the shear center are stored in a two-dimensional matrix with the number of rows equal to the number of sections and two columns for each one of the coordinates.

8.2.5 Determination of the loads acting on the structure

The determination of the loads on the structure can be split into three parts: the determination of the load cases, the calculation of the forces from the C_p-distribution and the actual calculation of forces that form the basis for the loading diagrams. All of these aspects will be elaborated in this section, thereby contributing to the fulfillment of requirement**IFS-SYS-18**.

Defining the load cases

The loads acting on the wingbox structure are primarily defined by the flight conditions of the IFS. Within these flight conditions, the IFS will be able to take on different configurations using, for example, different flap settings. The latter is the variable which was the prime concern in the structural design since it largely determines the distribution, magnitude and direction of the forces acting on the wingbox. It was found with the XFLR5 program that the load cases for the flight at testing conditions with maximum flap deflections were higher than the load cases for cruise conditions in clean configuration. The flap deflection at speeds higher than the speed at the testing conditions will be limited. Besides, it was clear that for the upper wing the load case for a downwards deflected flap was higher than for an upwards deflected flap because the angle of attack at testing conditions is positive and thus generates a higher lift coefficient in the first mentioned flap setting as was found in subsection 5.3.3. For the analysis of the wingbox at testing conditions two load cases with different flap deflections were considered. The variables governing the two load cases are summarized in Table 8.3.

- **Load case 1:** the flap of the upper wing is deflected downward by 20 degrees, the flap of the vertical wing is deflected outward by 20 degrees. This creates a compressive force in the upper wing and a tensile force in the vertical wing.
- **Load case 2:** the flap of the upper wing is still deflected downward by 20 degrees, the flap of the vertical wing is deflected inward by 20 degrees (giving a flap deflection angle of -20 degrees). This creates a tensile force in the upper wing and a retains the tensile force in the vertical wing.

Table 8.3: The variables describing the two load cases analyzed.

(a) First load case.

Parameter	Value	Unit
$\delta_{flap,uw}$	20	deg
$\delta_{flap,vw}$	20	deg

(b) Second load case.

Parameter	Value	Unit
$\delta_{flap,uw}$	20	deg
$\delta_{flap,vw}$	-20	deg

(c) Shared flight conditions.

Parameter	Value	Unit
ρ_∞	1.225	kg/m^3
V_∞	61.7	m/s
Re_{uw}	4265749	-
Re_{vw}	5471740	-

Calculation of the force coefficients

In order to calculate the forces introduced in the wingbox, a C_p-distribution was imported from the XFLR5 analysis performed in chapter 5. By means of this distribution the force coefficients could be calculated. Before these calculations, a short inventory was taken of the available theory on pressure distributions. This resulted in the following assumptions:

- The pressure distribution can be split up in two parts: one part giving the coefficients for the non-flapped part of the wing in which the wingbox is placed and one part for the flapped part of the wing. The coefficients calculated for each of these parts were assumed to follow the chord lines of the individual parts (i.e. the normal coefficient for the flapped part is perpendicular to the deflected chord line). An illustration of this division is given in Figure 8.4.
- For the non-flapped part of the wing, the force coefficients act in the quarter chord point, since for symmetrical airfoils this equals both the aerodynamic center and the center of pressure [1]. The same reasoning was followed for the flap.

Now that the theory on the pressure distribution is defined, the coefficients can be calculated using basic aerodynamic equations from Anderson [23]. These equations were used to calculate both the tangential force coefficient (parallel to the chord lines of the wingbox or the chordline of the flap) and the normal force coefficient (for the forces acting perpendicular to those axes).

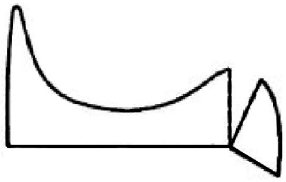

Figure 8.4: A qualitative representation of the pressure distribution over the flapped wing sections.

$$c_n = \frac{1}{c}\left[\int_0^c (C_{p,l} - C_{p,u})\,dx + \int_0^c \left(c_{f,u}\frac{dy_u}{dx} + c_{f,l}\frac{dy_l}{dx}\right)dx\right] \tag{8.11}$$

$$c_t = \frac{1}{c}\left[\int_0^c \left(C_{p,u}\frac{dy_u}{dx} - C_{p,l}\frac{dy_l}{dx}\right)dx + \int_0^c (c_{f,u} + c_{f,l})\,dx\right] \tag{8.12}$$

The skin friction coefficients $c_{f,u}$ and $c_{f,l}$ for the upper and lower side of the airfoil are calculated using Equation 8.13. The Reynolds numbers were adjusted to match the Reynolds numbers of the upper and the vertical wings [31].

$$c_f = 0.074 \cdot Re^{-0.2} \tag{8.13}$$

These coefficients calculated in Equation 8.11 and Equation 8.12 result in the force coefficients per unit span of the chosen airfoil. This means that in order to get to the force created in either normal or tangential direction, the coefficients still have to be multiplied by a the dynamic pressure that is dependent of the flight conditions. This factor is calculated in Equation 8.14. The example calculation for the normal force per unit span is shown in Equation 8.15 [23]. A similar calculation can be done for the tangential force per unit span. Note that these forces will vary over the span of the wings, since the flaps that are implemented on the modifications do not cover the entire length of the modification wings. The safety factor sf included in Equation 8.15 is set to 1.5.

$$q_\infty = \frac{1}{2}\rho_1 V_1^2 \tag{8.14}$$

$$F_{n,perunitspan} = sf \cdot c_n \cdot c \cdot q_\infty \tag{8.15}$$

Load calculations

Having calculated the forces per unit span, the forces and moments acting on each section can be calculated using the coordinates of each section from the boommatrix. The results can be found in Appendix B in Figure B.1 and Figure B.2. These diagrams are created by first calculating the reaction forces and moments at the engine mount, the hinge intersection and the wing mount. For the calculation of the reaction forces, basic static analysis equations were used. Since the upper wing and vertical wing are both constrained at two sides, the calculation of the end moments was done using the equation calculating the fixed end moments for beams under a certain loading P as shown in Equation 8.16 [32]. The L in this equation stands for the length of the beam over which the moment should be generated. The weight of the wingbox, flaps and actuators is not taken into account in these load calculations. The effect of this is that the loads in the structure will be higher than in reality, since the weight of the wings would result in bending relief. Furthermore the weight of the wingbox is negligible compared to the aerodynamic forces. Therefore the wingbox will be designed for a higher loading case which decreases the possibilities even more.

$$M_{end} = \frac{PL}{8} \tag{8.16}$$

When looking at, for example, the loading diagram created for the shear force in the X-direction of the upper wing in the first load case (as shown in Figure B.1a) it is easy to see how the forces are introduced. It can be seen that at the engine mount (where Y equals zero) there is already a reaction force. The first small part of the graph then shows the force generated by the non-flapped part of the wing. The slope of this part indicates the distributed loading. In a similar way, the flapped part of the wing generates another distributed loading which is seen between the jumps in the remainder of the graph. These jumps are there because of the way the flap is attached to the wingbox. As mentioned in Table 8.2, there is a finite number of mounts that comprise the connection between the flap and the wingbox. This means that the forces created by the flapped part are not included in the diagrams as

a distributed loading, but as a discrete loading that when summed up equals the total force generated by the flap. The mounts were assumed to be evenly spaced over the entire flapped length of the upper and vertical wings. The same line of reasoning was used to create the other shear load diagrams.

The loading diagrams that represent the shear force in the sections were then used to create the moment diagrams. A good example of this is seen when looking at the relation between the shear force in the Z-direction and the moment around the X-axis in Figure B.1a. The end moments around the X-axis are zero because of the hinged connections, and the moments in between the ends are formed by using the shear force diagram as its slope. The moment diagrams around the other axes are formed in a similar way.

In the diagrams, one can also see the relation between the upper wing and the vertical wing. When looking at the magnitude of the shear force in Y-direction of the upper wing in Figure B.1 and the shear force at the end of the vertical wing in the Y-direction shown in Figure B.1b, one can see that these forces are of the same magnitude. This makes sense, since the shear force created in the Y-direction in the vertical wing is directly taken up by the upper wing as a compressive force in the Y-direction. Similar relations can be seen for the reaction forces and moments that are transmitted at the hinge intersection.

The loads calculated in this part of the program are also used in section 9.8 to size the actuators of the flaps. These forces were $F_n^{flap,uw} = 4,548N$ and $F_n^{flap,vw} = 670N$ for the normal forces on the flapped surfaces of the upper and vertical wings, and $F_t^{flap,uw} = 4008N$ and $F_t^{flap,vw} = 574N$ for the tangential forces on these surfaces.

8.2.6 Determination of stresses

Now the area of the structure is idealized into booms, the moments and shear forces calculated from the C_p-distribution can be applied to the structure. These forces will introduce stresses into the wingbox. The maximum stress must not exceed certain limits, since the wingbox will not be able to carry all the loads if these criteria are not met. This is checked in subsection 8.2.7. By varying the cross-sectional geometry the stresses in the wingbox can be controlled. For instance, if a stiffener is attached to the skin, the stress due to bending will decrease because the moment of inertia increases.

When determining the stresses in the wingbox, the calculations can be split up in two different parts, namely direct stress and shear stress. The direct stress consists of bending stress and axial stress. The shear stress consists of shear flow due to the shear forces and shear flow due to torsion. The equations used in these sections are taken from Megson [30].

Bending stress

As stated in the text above, the direct stress of the wingbox is a combination of stress due to bending of the wingbox and stress due to an axial force. To determine the bending stress Equation 8.17 has been used.

$$\sigma_{y_{bending}} = \left(\frac{M_z I_{xx} - M_x I_{xz}}{I_{xx} I_{zz} - {I_{xz}}^2}\right) \cdot (x - \bar{x}) + \left(\frac{M_x I_{zz} - M_z I_{xz}}{I_{xx} I_{zz} - {I_{xz}}^2}\right) \cdot (z - \bar{z}) \tag{8.17}$$

In this equation, M_x and M_z are the moments acting on the particular cross-section, I_{xx}, I_{zz} and I_{xz} the MOIs of the cross-section, x and z the coordinates of the specific boom and $\bar{x}$ and $\bar{z}$ the coordinates of the centroid. These values can be retrieved from the various matrices generated by the program that were discussed in previous sections. Because the airfoil is symmetric it is assumed that the geometry has one axis of symmetry, thus I_{xy} is equal to zero. Therefore Equation 8.17 can be reduced to Equation 8.18.

$$\sigma_{y_{bending}} = \left(\frac{M_z}{I_{zz}}\right) \cdot (x - \bar{x}) + \left(\frac{M_x}{I_{xx}}\right) \cdot (z - \bar{z}) \tag{8.18}$$

By inserting all the values from the different matrices, the bending stress for each boom is calculated. The resulting bending stress for each boom is stored in a matrix that has a number of rows equal to the number of sections and a number of columns equal to the number of booms.

Axial stress

Furthermore there is a contribution of the axial force to the direct stress. This axial force comes from the fact that the vertical wing and upper wing are connected to each other. For instance, a deflection of the flap on a vertical wing causes a lift force in positive or negative Y-direction. This force is then transferred via the hinge to the upper wing. Thus a shear force for the vertical wing becomes an axial force in the upper wing. This axial stress is computed with Equation 8.19. In this equation S_y is the axial force exerted on the wingbox and A is the combined areas of all the booms in the boommatrix.

$$\sigma_{y_{axial}} = \frac{S_y}{A} \tag{8.19}$$

After these results are stored in a matrix, they are combined with the computed bending stresses in a matrix holding the total direct stress for each boom. The values from this matrix will be plotted on a three dimensional surface, as shown in Appendix B in Figures B.3a, B.3c, B.4a, and B.4c.

Shear flow due to shear force

Since the wingbox is a thin-walled structure, the shear forces are introduced in the structure as a shear flow. To make use of the shear flow equations, the calculations of the shear flow must be split up into two parts. The first part calculates a so-called basic shear flow by assuming an open cross-section. Therefore an artificial cut has to be made in order to make the closed wing cross-section open. After the basic shear flow is calculated the cut is removed again and a constant shear flow can be determined. This can be done by making use of Equation 8.9. The two shear flows combined represent the actual shear flow in the structure. All these steps will be explained in this section.

The results of these calculations will be stored in several matrices. The basic shear flow matrix has a number of rows equal to the number of sections and a number of columns equal to the number of booms, where the position of boom i in the matrix is describing the shear flow from boom i to $i+1$. The constant shear flow matrix has a number of rows equal to the number of sections and a number of columns equal to one. At last, the two matrices will be summed up to acquire the total resulting shear flow.

As stated before, the first step is to calculate the basic shear flow. In order to do that, the program assumes that the aft spar of the cross-section is cut in the middle. This is the line between booms 0 and $n-1$ in Figure 8.3. By making a cut the basic shear flow in the vertical wall of the wingbox is 0. Therefore, the basic shear flow at the two adjacent booms is also 0. The general formula for calculating the basic shear flow for a cross-section with booms is Equation 8.20.

$$q_b = -\left(\frac{S_x I_{xx} - S_z I_{xz}}{I_{xx} I_{zz} - {I_{xz}}^2}\right) \cdot \left(\int_0^s t_D x ds + \sum_{i=1}^{n} A_i (x_i - \bar{x})\right) - \left(\frac{S_z I_{zz} - S_z I_{xz}}{I_{xx} I_{zz} - {I_{xz}}^2}\right) \cdot \left(\int_0^s t_D z ds + \sum_{i=1}^{n} A_i (z_i - \bar{z})\right) \tag{8.20}$$

Since there is assumed that the cross-section has an axis of symmetry and the skin only carries shear, I_{xz} and t_D are assumed to be zero. Equation 8.20 is therefore simplified to Equation 8.21.

$$q_b = \frac{S_x}{I_{zz}} \cdot \sum_{i=1}^{n} A_i (x_i - \bar{x}) - \frac{S_z}{I_{xx}} \cdot \sum_{i=1}^{n} A_i (z_i - \bar{z}) \tag{8.21}$$

As stated before, the shear flow before boom 0 is equal to 0. To calculate the shear flow after boom 0, the specific area A_i and the distance to the centroid of that boom must be filled in. Each time a boom is passed the area and the coordinates have to be added to the equation. This means that the calculation of the shear flow after the last boom concerns the areas and coordinates of all booms. Though because there is an artificial cut after the last boom, this basic shear flow is equal to 0.

Now the basic shear flow is known one can calculate the constant shear flow. Therefore the artificial cut is removed from the cross-section. Since the shear forces act through the shear center and the basic shear flow is constant between booms, Equation 8.9 can be reduced to Equation 8.22.

$$q_{s0} = -\frac{\sum_{i=0}^{n-1} p_i q_{b_i} s_i}{2A} \tag{8.22}$$

The symbol s is the length of the element between the booms, p is the arm the specific element has with respect to the centroid, q_b the basic shear flow acting on the element and A the enclosed area of the cross-section, which can be determined with use of the boom coordinates. Adding these two shear flows will result in the actual shear flow on each segment of the cross-section induced by the shear force(s).

Shear flow due to torsion

Besides the shear flow generated by the shear forces, torsion is also creating shear flow in the structure. A torque results in a constant shear flow in the shear bearing members of the cross-section and has to be added to the shear flow matrix discussed above to determine the final shear flow acting on the cross-section. Equation 8.23 is used to compute this shear flow and has similarities with Equation 8.9.

$$T = 2Aq_{s0} \tag{8.23}$$

Shear stress

In order to check if the structure does not fail under the applied loads, the shear flow has to be converted into shear stress to compare the values with the shear strength of the material used. Since the structure is thin-walled, it is assumed that the shear stress is constant through the thickness of the segment subjected to shear flow. Therefore Equation 8.24 can be used to calculate the shear stress for each segment. The shear stress is stored in a matrix that has a number of rows equal to the number of sections and a number of columns equal to the number of booms. The values from this matrix will be plotted on a three dimensional surface, as shown in Appendix B in Figures B.3b, B.3d, B.4b, and B.4d.

$$\tau = \frac{q_s}{t_{skin}} \tag{8.24}$$

8.2.7 Check structure for failure

Before the set of parameters describing the structure such as stiffener area or skin thickness is stored as a valid result, the stresses calculated for the wingbox have to be checked if they do not exceed the limit stresses of the material. If the proposed wingbox parameters exceed the yield stress, the program discards the current set of parameters and start the calculations again with a new set of parameters having a higher moment of inertia. If it does meet the requirements, the parameters will be stored in a results matrix after the weight of the wingbox is calculated using those parameters. After all sets of parameters have been analyzed, the program will filter the result with the lowest weight from the results matrix.

There are five types of checks in the program. The first three, namely yield strength, shear strength and column buckling, only check if the structure meets the requirements. The last two, namely plate buckling and inter-rivet buckling, will determine the spacing of ribs and rivets so that the structure will not fail for those requirements.

Yield strength

The yield strength of a material is the amount of tensile or compressive stress the structure is capable to withstand without deforming plastically. After the structure is plastically deformed, it is less stiff and has a lower buckling strength. In order to check for yielding, the program compares the maximum value of the total direct stress matrix with the yield strength value.

$$\sigma_{max_{wingbox}} < \sigma_{yield} \tag{8.25}$$

Shear strength

The structure also has to be evaluated on maximum shear strength. This is done by taking the maximum value of the shear stress matrix and compare it to the maximum shear stress of the material (Equation 8.26). Especially the ribs are sensitive of failing due to shear stress, since they are perpendicular to the lift force.

$$\tau_{max_{wingbox}} < \tau_{max} \tag{8.26}$$

Column buckling

If a column is subjected to a compressive force it can deflect out of its plane if the force is high enough. Once a column buckles it loses all its load-carrying abilities. Since the horizontal and upper wing are connected with a hinge, negative lift from the from the upper wing will cause a compressive force in the vertical wing and vice versa. The column buckling criterion is checked with Equation 8.27 [30]. Since the MOI around the X-axis is much lower than the MOI around the Z-axis, I_{xx} will be used for the calculations.

$$P_{max} < P_{cr} = \frac{\pi^2 E I_{xx}}{L^2} \tag{8.27}$$

In this equation, E is the Young's modulus, I_{xx} the MOI around the X-axis and L the length of the column.

Plate buckling

Since the wings will bend under the loads they produce, the top and bottom skin will be either in compression or tension. The stress due to tension is checked against the yield strength, while the skin subjected to compression must be checked for buckling. The critical stress on which plate buckling occurs is determined with Equation 8.28. The critical buckling stress is mainly dependant on the number of stiffeners and ribs attached to the plate [33]. By adding stiffeners and ribs the number of half waves in which the plate can buckle is increased and thereby the critical buckling stress is increased.

$$\sigma_{max} < \sigma_{cr} = \frac{D\pi^2}{tb^2}\left(\frac{mb}{a} + \frac{n^2 a}{mb}\right)^2 \tag{8.28}$$

$$D = \frac{Et^3}{12\left(1-\nu^2\right)} \tag{8.29}$$

In Equation 8.28 t is the thickness of the skin, b the width of the wingbox, a the length of the wingbox and m the number of ribs + 1, n the number of stiffeners + 1. For Equation 8.29, E is the Young's Modulus and ν is the Poisson's ratio. With this equation the combination of stiffeners and ribs is determined, with the number of stiffeners initially governed by the number already added to increase the moment of inertia.

Inter-rivet buckling

The last parameter that needs to be determined is the inter-rivet spacing. If the rivets are placed too far apart, the skin will buckle in between rivets because they provide not enough support. The inter-rivet spacing can be determined with Equation 8.30 [34].

$$s_{ir} < s_{ir_{cr}} = \frac{t}{\sqrt{\frac{\sigma_{ir}}{0.9cE}}} \tag{8.30}$$

8.2.8 Storing results and determination of best solution

Only results that meet all of the criteria given in subsection 8.2.7 and have a realistic number of ribs and rivet spacing are stored in a results matrix. This results matrix contains the skin thickness, the number of stiffeners, the area of a stiffener, the thickness of the spar, the number of ribs and the rivet spacing for each wingbox.

Now all the information about the different wingboxes that are able to withstand the stresses on the structure is known, the weights of the options can be analyzed. This weight is the most important parameter of the wingbox, because the design should have the least amount of weight. When the wight is calculated in the iteration over the different design options it is assumed that the skin thickness of the wingbox is equal to the skin thickness of parts outside the wingbox, such as the parts at the leading- and trailing edge. Therefore the area of the skin is calculated by multiplying the circumference of the airfoil by the skin thickness. To get to the total area per section the number of stiffeners is multiplied by the area of a single stiffener. The cross-sectional area of the spar is calculated by multiplying the height of the spars multiplied by their thickness. Finally, the weight of the wingbox without ribs is calculated by multiplying the total area by the length of the wings and then multiplying by the density of the material. To include the weight of the ribs, the number of ribs has to be multiplied with the cross-sectional area and thickness and then added to the weight of the wingbox without ribs. The actuators are not taken into account in this weight calculation, but since they are equal for all the wingbox options this does not affect the end-result. Furthermore, the extra weight of the rivets is not taken into account as well, because weight is also removed by drilling holes.

From the results matrix, the program will pick the wingbox with the lowest weight. To check whether the program worked properly, the entire results matrix is also stored in an Excel file. This gives a more graphical representation and the results can be interactively sorted for instance based on weight or number of ribs. It is possible that a situation occurs where the second-best option is a few grams heavier but much more easy to manufacture. This is very hard to check by a program but can easily done by hand.

Once the best design has been chosen, the program will make several two- and three dimensional diagrams of the loading cases and stress distributions on the wingbox. These results can be found in Appendix B and will be discussed in section 8.4.

8.3 Code verification

To verify the part of the program that calculates all the stresses and analyzes the structural integrity of the wingbox construction, a comparison was made between the results of the program and analytical solutions calculated by hand. In this process, the same equations as explained in section 8.2 are used.

First, a very simple coordinate system was set up to create a simple test case that could also be calculated by hand. This coordinates system is then used to place booms at the original coordinates. Loads will be applied to the idealized section to verify the results of the stress calculations. This coordinate system is shown in Figure 8.5. The assumed skin thicknesses and loads that are applied to the test case are shown in Table 8.4.

Table 8.4: Skin thickness and loads used for verifying the structural analysis program.

Parameter	Size	Unit
t_{skin}	0.01	m
S_x	20	N
S_y	0	N
S_z	20	N
M_x	10	Nm
M_y	0	Nm
M_z	0	Nm

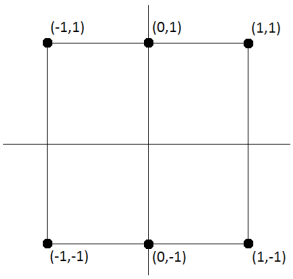

Figure 8.5: Coordinates used for verifying the structural analysis program.

The moment is taken around the X-axis, since this represents bending which is the dominant moment in the actual structure. Going counterclockwise the booms are numbered from 0 at the top right coordinate to 5 at the bottom right coordinate. The coordinates are all in SI Units. This simple coordinate system was fed into the program together with artificial moment- and shear force matrices. This simplicity ensured that it was possible to verify the code with an analytical solution. The results for the calculation of the boom areas is shown in Table 8.5. The values match perfectly and verify this part of the program. Next step in the verification of the output is to check the stresses arising in the booms when the loads mentioned in Figure 8.5 are applied to the cross-section. The results of this analysis are shown in Table 8.6.

Table 8.5: Verification of the boomareas.

Parameter	Analytical	Program	Unit
B_0	0.008333	0.008333	m^2
B_1	0.01	0.01	m^2
B_2	0.008333	0.008333	m^2
B_3	0.008333	0.008333	m^2
B_4	0.01	0.01	m^2
B_5	0.008333	0.008333	m^2

Table 8.6: Verification of the resulting stresses.

Parameter	Analytical	Program	Unit
x_{sc}	0	$6.2 \cdot 10^{-5}$	m
τ_{max}	187.5	187.5398	Pa
τ_{min}	-1,187.5	-1,187.546	Pa
σ_{max}	187.5	187.557	Pa
σ_{min}	-187.5	-187.556	Pa

As can be found in the table, the results from the analytical solution were almost identical to the results from the program. However, it should be noted that this test case was only performed on one section. When the entire wingbox would be analyzed, the small errors that occur in each section can add up to a significant deviation from the actual load case. Therefore the program behaviour was monitored for different section lengths. It was seen that if the section length was taken smaller than 0.01 m the deviation of the end result became insignificant. Above this length the results became slightly different because of round-off errors and inaccuracy of the discrete representation of the loading diagrams. Therefore the decision was made to have a section length of 0.001 m, obtaining an error in the order of 10^{-3}. Although this could be decreased even further, the amount of extra computing power does not match the change in outcomes.

After verification has been performed, the program also has to be validated in order to use the results. Since it was very hard to obtain reliable validation data, validation has been postponed to later stages of the design process.

8.4 Results and discussion

After all of the equations and iteration limits mentioned in section 8.2 were implemented the program was started. The iteration limits used for the final run that determined the structural design of the wingbox are shown in Table 8.7a. The results of the final run are displayed in Table 8.7b for both the upper and vertical wing. The resulting plots of the stresses in the wings are shown in Figure B.3 and Figure B.4 in appendix B. The number of stiffeners mentioned in these tables is the number of stiffeners on one side of the wingbox of one wing. This means that for the two upper wings, there is a total of 28 stiffeners and for the two vertical wings there is a total of 20 stiffeners. The spacing of the stiffeners is such that they are evenly divided along the upper and lower surfaces.

Table 8.7: Iteration limits and results for the two additional wings.

(a) Iteration limits.

Parameter	Value	Unit
$t_{skin,low}$	0.0005	m
$t_{skin,high}$	0.002	m
$t_{skin,step}$	0.0001	m
$t_{spar,low}$	0.001	m
$t_{spar,high}$	0.01	m
$t_{spar,step}$	0.001	m
$A_{stif,low}$	0.00001	m^2
$A_{stif,high}$	0.00008	m^2
$A_{stif,step}$	0.00001	m^2
$n_{stif,low}$	1	-
$n_{stif,high}$	20	-

(b) Iteration results for the upper and vertical wing.

Parameter	Value upper wing	Value vertical wing	Unit
m	77.2	15.09	kg
x_{cg}	9.44	8.7	m
y_{cg}	0	0	m
z_{cg}	0.39	-0.88	m
t_{skin}	0.0013	0.0009	m
t_{spar}	0.002	0.002	m
$(x/c)_{frontspar}$	0.1	0.1	-
$(x/c)_{rearspar}$	0.45	0.57	-
A_{stiff}	0.00001	0.0001	m^2
n_{stiff}	7	5	-
$(x/c)_{stiff}$	0.14, 0.19, 0.23, 0.28, 0.32, 0.36, 0.41	0.18, 0.26, 0.34, 0.41, 0.49	-
n_{ribs}	23	6	-
s_{rivet}	0.036	0.034	m

The masses shown in the table represent the combined masses of upper and vertical wings on both sides of the aircraft. The number of ribs is mentioned for each wing and they will be spaced evenly over the span. The values that are given for the location of the c.g. concerns the combination of both wings and are directly used in the stability calculations.

Now the masses of the wings are known, requirement **IFS-SYS-18-STRUC-01**, which stated that the structure shall withstand a load factor of 4.5 g_0, can be checked. The total load due to additional load factor for a single

upper wing is $36.8 \cdot 4.5 g_0 = 1,704.2N$. Looking at the shear force in X-direction of the main wing, the structure is designed to handle 3,850 N. This is more than double the maximum load due to the load factor. The same rationale also holds for the load on the vertical wing due to a load factor of 4.5, where the difference is even more than double. Therefore it can be concluded that **IFS-SYS-18-STRUC-01** is met.

Next to the parameters already mentioned in Table 8.7 the dimensions and shape of the stiffeners are an important factor in the design. The dimensions shown in Table 8.8 are chosen to match the area given in Table 8.7. The stiffener is made larger in width than in height to ensure that the rivets used will not compromise the structural integrity by being too large compared to the stiffener width and therefore introducing a vulnerability to cracks. The L-shape of the stiffeners is primarily chosen to decrease the complexity of manufacturing. A graphical representation of the design of the stringer can be found in Figure 8.6.

Table 8.8: Stiffener dimensions final wingbox design.

Parameter	Size	Unit
$t_{stiffeners}$	0.001	m
$h_{stiffeners}$	0.004	m
$b_{stiffeners}$	0.007	m

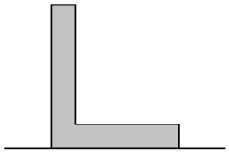

Figure 8.6: Stiffener shape final wingbox design.

8.5 Additional design considerations

Apart from the wingbox design based on the static load case, other design aspects have to be treated as well. The dynamic loading from a change in flap deflection has been taken into account in the safety factor. Moreover, due to the limited capabilities of actuators the flap cannot be deflected instantly and therefore this situation can be treated as quasi-static. Furthermore, loads due to gusts, flutter instability and the design of the attachment points to the aircraft are discussed in this section.

8.5.1 Gusts

During flight, aircraft can experience turbulent flows or gusts. These gusts can cause a temporary increase in airspeed of the incoming airflow or increased angle of attack. If this is not properly analyzed, a gust can cause structural failure due to excessive loading of the wings. Therefore a never-exceed speed V_{NE} is given by the manufacturer. Since the boxwing is not clamped to the nacelle and attached to the main wing, the main wing has to cope with additional stresses on top of the extra loading due to the gust, because the extra lift generated by the boxwing due to the gust is partially transferred to the main wing. Because the loading of the main wing will be increased, the never-exceed speed must be lowered in order make sure the structure will not fail when experiencing a gust. If one wants to keep the never-exceed speed the same, structural modifications to the wingbox of the main wing have to be made in order to be able to cope with the additional loads. This is a very expensive operation. Another explanation is that a part of the lift produced at V_{NE} is not produced by increasing the airspeed to the old V_{NE}, but by adding an additional lifting surface on the wing.

Because the never-exceed speed of the Phenom 300 is unknown, a qualitative explanation is given. The reduction of V_{NE} can be found with Equation 8.31. The ΔV_{NE} must then be subtracted from the original never-exceed speed to get the new V_{NE}. This new airspeed should also be implemented in the relevant instrumentation in the cockpit, FCS and SCS.

$$\Delta V_{NE} = \sqrt{\frac{\Delta L_{uw}}{\frac{1}{2} C_L \rho S}} \tag{8.31}$$

8.5.2 Flutter instability

Classical flutter of an aircraft is described as a divergent oscillation of a structure because of coupled flexural and torsional modes. It is mainly found on structures subjected to large aerodynamic forces, such as wings. Due to this divergent oscillation the loads on the structure increases, which in the end can lead to structural failure. The flexural mode is linked to the bending of the aircraft, while the torsional mode is linked to the incidence angle of the wing with respect to the incoming airflow. Flutter instability occurs when the bending of the wing and the incidence angle have a 90 degree phase angle. This means that when the deflection of the wing is maximum, the incidence angle is 0 and when the deflection of the wing is 0, the incidence angle of the wing is maximum. When the wing is bend upwards, the stresses in the structure will try to decrease that deflection and thereby producing a downwards acceleration until the wing reaches the neutral position. However, at this neutral position the incidence angle is maximum, producing an extra downwards acceleration. Because of this extra downwards acceleration the deflection of the wing downwards will be larger than the previous one, inducing more stresses and therefore a larger acceleration to the neutral position. Until a certain airspeed this oscillation is damped by the structure. Above this airspeed, which is called V_f, the destabilizing effects become greater than the stabilizing forces. One possibility to increase V_f is to make use of mass balancing, making the center of gravity coincide with the so-called flexural axis.

When looking at flutter instability with respect to the boxwing design, the conclusion can be drawn that the boxwing is not subjected to flutter instability. Since the Phenom 300 is already certified according to EASA specifications, the V_f of the aircraft must be higher than the never-exceed speed. Furthermore, the wings of the boxwing are smaller and more constrained than the main wing of the aircraft. It can therefore be assumed that no additional modifications have to made with respect to flutter instability [35].

8.5.3 Hinge design

Now the two wings have been designed, they must be integrated with the aircraft. As stated before, hinges will be used to connect the wings to each other and to the aircraft. Aircraft with hinge points in the wing are mostly used on aircraft carriers, since they require to use the least amount of space. In these applications however, the hinges are only used when the aircraft is grounded. During flight, the hinge is not used and the sections are clamped to each other. These are very complicated systems, since they are placed in the middle of the wing. This means they need to transfer all shear forces and moments, but also electrical wires, hydraulics, de-icing and other system components normally running through the wing.

The hinges in the boxwing design can be made much more uncomplicated, since they are simple load-transferring hinges positioned at the end of the separate wings. Furtermore, by using hinges there is a possibility to detach the entire boxwing from the aircraft relatively easy. An example of a hinge that can be used for the design is shown in Figure 8.7. Such a single hinge, made of stainless steel, is 0.23 m long and can transfer up to 6,671 N [3]. It features a low resistance, low wear core and grease fitting for easy lubrication possibilities. Since the chord of the upper and vertical wing is 1.34 m five hinges can be placed. This would result in a load-transferring capability up to 33,355 N. Looking at the shear and moment diagrams displayed in Figure B.1, this would be more than enough to cope with the maximum forces that the structure is able to generate.

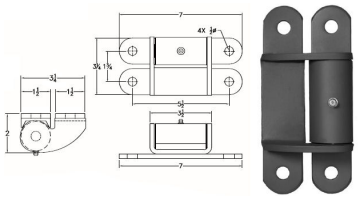

Figure 8.7: Hinges for connecting the boxwing.

To reduce the amount of drag generated by the hinges, flexible fairings can be placed around the hinges. Besides obtaining drag reduction, the fairings also protect the hinges against dirt or corrosion due to exposure of the weather and thereby increase their lifespan and lowering the maintenance interval. Finally, it is advised to use shear bolts to attach the boxwing to the aircraft. If, for some reason, the boxwing cannot handle the forces acting on it, the boxwing will detach from the aircraft without damaging the wingbox of the main wing or engine nacelle.

[3] http://www.hardwaresource.com/hinges/specialty-hinges/heavy-duty-hinges/heavy-duty-gate-hinges-1 [cited 23 January 2017]

9 | Control and System Layout

The IFS needs to be properly equipped, controllable and safe, both in normal and augmented flight. Several of these properties are partially assessed in the previous chapters. This chapter finalizes this assessment by looking at the entire aircraft, taking into account communication between systems.

The Ergonomics, Sensors and Actuators department includes several different systems and to be able to keep track of the bigger picture, the chapter is split up into two parts. The chapter starts with an overview of these systems in sections 9.1 and 9.2. Sections 9.3 to 9.10 explain the different parts of this system more in depth.

Sections 9.1 and 9.2 explain respectively the communication layout and the complete aircraft layout. Section 9.3 explain the change in the ergonomics, explaining the different IFS stations, followed by the hardware diagram in section 9.4. Next the complete flight control system is elaborated on in section 9.5, including the Aircraft Control System, Simulation Control System and control-loaded stick. After this the layout of the control devices and actuators is shown in 9.6, followed by the in-depth analysis of the sensors on the aircraft in section 9.7. The chapter continues with section 9.8 on actuator section, which goes in depth in the system actuators, including types, attachment and safety. The chapter is concluded with a power and cost assessment of all the subsystems of the ESA department in respectively section 9.9 and section 9.10.

9.1 Communication layout

In order to get a complete overview of the sensors, controls and actuators, the communication diagram and aircraft layout are explained in this section.

9.1.1 Communication diagram

The communication diagram in Figure 9.1 shows the communication lines between different systems. The diagram was created at an earlier step in the process of the design. The solid lines indicate commanding data flows, whereas the dotted lines indicate non-commanding data flows. A basis for this diagram lies in the N^2 chart as stated in the Mid-Term Report [10]. The communication flow diagram however, deals with actual data flows and not just with interaction. Furthermore, interactions such as feedback from the actuators and the engines are added. The electrical power system is included as well. Lastly, it is shown how the safety trip system deals with the three different modes: simulation mode, safety pilot mode and back-up FBW mode. The communication flow diagram is updated. The main changes are that the most data will be redistributed by the flight control system, this main system will distribute the sensor data and commands around the aircraft in sub section 9.5.1 the layout of the Flight control system will be explained.

9.1.2 Aircraft communication layout

The aircraft's physical communication lines are displayed in Figure 9.2. The lines are projected on the physical top view of the aircraft. The solid lines indicate new communication lines that will be added to the aircraft. These lines will go to the new actuators, sensors and ergonomic systems. The dotted lines indicate the original communication or controlling lines. It can be seen that the Aircraft Control System(ACS) works with the original actuators and collect data from the original sensors. In subsection 9.5.1 the communication and layout of the Flight Control System(FCS) will be explained. The location of the sensors, actuators, FCS and the test station will be discussed below.
Sensors will be installed on the aircraft in order to get the correct air data and aircraft state data. Heavier systems such as the test engineer station influence the c.g. and can be placed in the location that is preferred by the flight dynamics department (chapter 7), keeping in mind that it is preferable to have it as close to the cockpit as possible for communication to the pilots. The cockpit layout will be given in section 9.2.

- **Sensors:** the additional sensors will be placed in the position where they will perform the best. In section 9.7 the additional sensors will be discussed in more detail. The main added sensors are the syncros, these will measure the deflection of the control surfaces. These deflections will be used to get an understating of the behaviour of the aircraft during the simulation. The Embrear phenom 300 has a lot of stock systems which will be used to collect data and to run the simulation. Because these sensors are placed all around in aircraft it is placed in the middle of the aircraft.

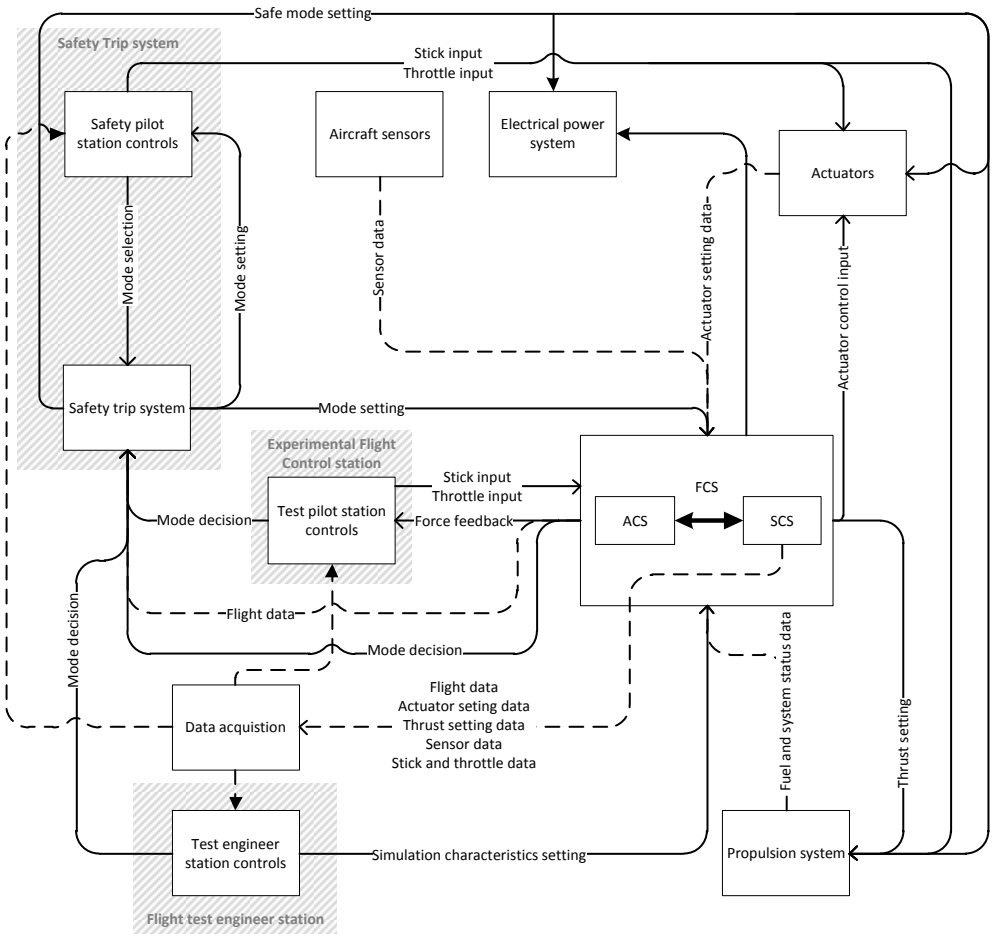

Figure 9.1: Communication flow diagram of the IFS.

- **Actuators:** the original actuators will be converted to be operated electronically (fly by wire) for the test pilot. The conversion to a fly by wire system will be elaborated upon in section 9.6. The additional actuators will be placed in the boxwing. The added actuators and the clutch system will be controlled by the SCS.
- **FCS:** the FCS will collect all the data from the sensors and actuators. The FCS will be divided into two systems, Aircraft Control System(ACS) and the Simulation Control System (SCS). The SCS will be placed on a different position then the FCS because the Simulation Control System is an addition to the aircraft the possibility of easy instalment and maintenance is desirable. The connection of the ACS and the Simulation Control System will be discussed in section 9.5. The location of the ACS will be elaborate on in subsection 9.2.3. The implementation of a SCS ensures that the IFS has a fully programmable flight control system, hence requirement **IFS-SYS-10-EXP-09** is met.
- **Test stations:** two test stations are added to the aircraft, pilot test station and the test engineer station. The aircraft is certified for single operation on the left side, hence the test pilot station will be located at the right of the cockpit to maintain the single operation certification. The test engineer station will be placed near the cockpit for easy offline communication if needed. A more elaborate explanation of both stations is given in section 9.3.

9.2 Layout changes

Changing the interior of the aircraft will change the handling of the aircraft. Removing or adding weight will cause a c.g. shift. Some aircraft can compensate for this change by redirecting fuel to different parts of the aircraft. It is however preferred that the c.g. is affected as little as possible by the changes to the aircraft. As stated by the flight dynamics department in chapter 7, the c.g. is preferred to be shifted as little as possible from the original location.

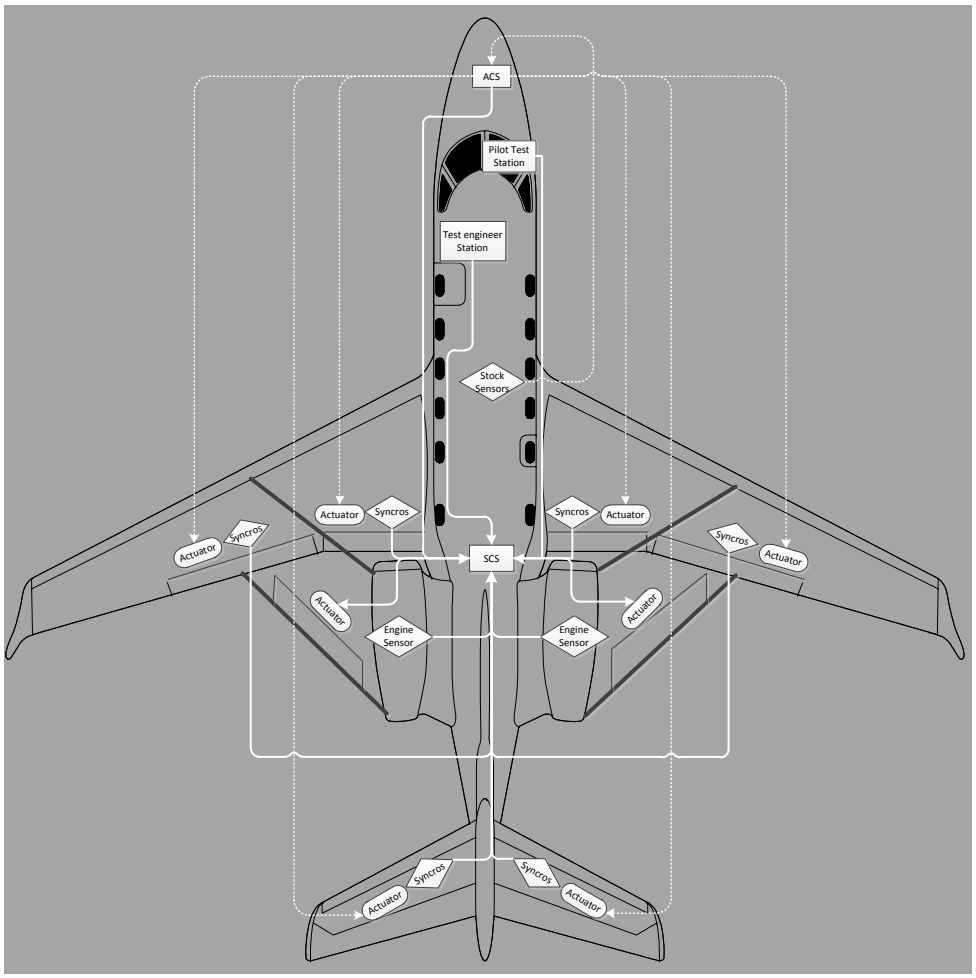

Figure 9.2: Physical layout of communication.

The boxwing and the drag chute system will add weight behind the c.g., shifting it backwards. Removing interior and placing the stations in forward locations will compensate for this shift. This section addresses the change in c.g. and starts with the removed and added systems. Secondly the location of the major components is explained and lastly, a total overview of the sub-system weights and location is given, together with the corresponding total c.g. location.

9.2.1 Removed systems

In order to create more design freedom the luxury seats will be removed from the aircraft. This will influence the c.g. location. In the Mid-Term Report [10] the weights are stated of different removable parts of the aircraft. Also the cabinets will be removed from the aircraft. In the old configuration there are two cabinets installed, one on the left front side and right front side. The weights of both cabinets are estimated in shown in the list below.

- Luxury seat weighs 27 kg.
- Simple seat weighs 15 kg.
- Lavatory weighs 24 kg.
- Side-facing seat weighs 15 kg.
- Left front cabinet weighs 25 kg.
- Right front cabinet weighs 15 kg.

The aircraft contains 7 luxury seats, these seats will all be removed and replaced by two simple seats, one for the test engineer and one for the passenger/second test pilot. The lavatory will also be removed to save extra weight and will be replaced by lavatory bags. The total weight saving will be 268kg. The location of the new systems will be shown in subsection 9.2.3.

9.2.2 Added systems

There will be a lot of systems added to the aircraft to make it an IFS. The boxwing will be at a fixed location. The ESA department will add these extra systems:

- **Test engineer station:**
  - pilot monitor weighs 3.5 kg.[1]
  - 2 laptops weigh 3.4 kg together.[2]
  - table weighs 10 kg.
  - logger weighs 0.250 kg.[3]
  - simple seat weighs 15.0 kg.
- **SCS:**
  - computer weighs 2.00 kg.
  - communication bus weighs 2.00 kg.
  - data acquisition weighs 1.25 kg.
  - computer rack weighs 14.5 kg.[4]
- **Boxwing actuators[5]:**
  - 4 side wing actuators weigh 6.0 kg together.
  - 4 upper wing actuators weigh 36 kg together.
- **Additional:**
  - simulation battery weighs 4.6 kg. [6]
  - drag parachute quick release weighs 18.14 kg.[7]
  - drag parachute sensor weighs 0.480 kg [8]
  - peripheral products weigh 20 kg.
  - 4 lavatory bags weigh 1.00 kg together. [9]
- **Passenger:**
  - Simple seat weighs 15.0 kg.

The list is split up into 5 systems: test engineer station, SCS, boxwing actuators, additional and passenger. The test engineer station and the passenger station are the only systems that can easily be shifted in the aircraft. The passenger station consist of one seat, which will provide the possibility to take an extra test pilot or for example the client. The configuration of these stations will elaborated on in section 9.3. The location of the SCS is fixed and will be placed in the back of the cabin, see section 9.5. The test pilot station is not taken into account in this list, since it assumed there is no net weight change. The FBW actuators and the sidestick will be added, but the complete yoke and attachment will be removed. Also the sensors themselves are not taken into account, since it is assumed they have a negligible weight. The data collection is taken into account and placed in the SCS rack. The actuators will be explained more in depth in section 9.8. Lastly, the additional category contains the simulation battery, explained in section 9.9, and the peripheral products, which contain power cables, data cables and small items such as the flight manual.

Also the drag chute sensor (section 9.7) and quick release are stated. The quick release system is implemented to make sure the drag chute can be released before landing. A landing with a drag chute attached is possible, making sure it is no single point of failure, however undesired since it makes landing much more difficult. When the landing is not the purpose of the simulation the drag chute will be released using the quick release model TR12[10], which has a safe working load of 15 kN and a breaking load of 75 kN, hence the release is able to withstand the deployment.

9.2.3 Location

Now that the size and the weight of the extra systems are known the cockpit and the cabin space can be equipped. The original aircraft is designed as a business jet, but the simulator does not have to be as luxurious as the original aircraft. Changing the interior is an easy way of reducing the weight and thus increasing the design freedom of the boxwing. In Figure 9.3 the redesign is presented. The original cabin contains 7 luxury seats and two cabinets, for transporting the aircraft to the customer remaining the original interior would be nice but not a necessity.
In Figure 9.3 the redesign of the cabin is shown. The test engineer station is placed on the right side of the cabin. All the luxury seat are removed and replaced by two simple seats. The SCS is placed in the back compartment where the lavatory was originally situated. The layout and specification of the SCS will be discussed in subsection 9.5.1. The last addition is the modification to the cockpit to implement the test pilot station. An active force feedback control system is implemented that will be explained in section 9.5.4.

[1] http://www.philips.co.in/healthcare/product/HC863068/suresigns-vm8-bedside-patient-monitor [cited 19 January 2017]
[2] http://store.hp.com/NetherlandsStore/merch/Product.aspx?id=N9Q76EA&opt=ABH&sel=NTB [cited 19 January 2017]
[3] https://www.kvaser.com/product/kvaser-eagle/ [cited 19 January 2017]
[4] http://wmdllc.com/products/rugged-electronics-racks/index.php[cited 23 January 2017]
[5] http://www.boschrexroth.com/en/xc/ [cited 19 January 2017]
[6] https://www.aircraftspruce.com/catalog/elpages/concorde-rg121-4.php [cited 18 January 2017]
[7] http://www.seacatch.com/models.htm [cited 19 January 2017]
[8] https://www.kistler.com/?type=669&fid=59472&model=document&callee=frontend [cited 19 January 2017]
[9] http://www.cleanwaste.com/products#pop [cited 23 January 2017]
[10] http://www.seacatch.com/models.htm [cited 19 January 2017]
[11] http://www.embraerexecutivejets.com/nva/img/old/jets/phenom/Phenom_300_Light_Executive_Jet_Optional_Cabin_Layout.jpg [cited 18 January 2017]

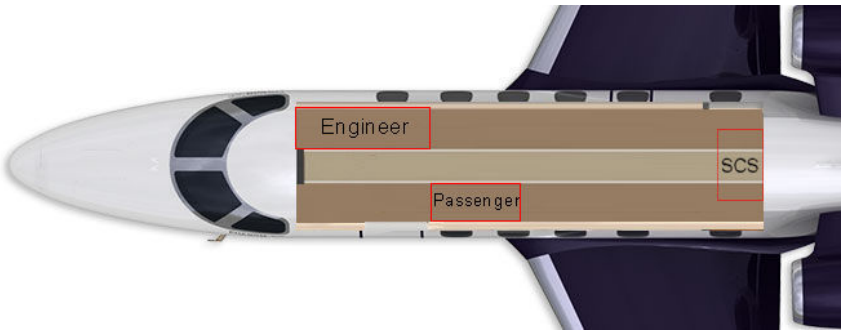

Figure 9.3: Modified interior layout.[11]

9.2.4 Center of gravity change

The c.g. location and weight of the ESA components is shown in Table 9.1. As can be seen the peripheral products do not have an arm, since it is assumed that this category is balanced around the c.g. and any deviation from this is negligible. From this overview the c.g. is found to be at 6.05 m from the nose and the weight addition is -131,88 kg. The weight addition is negative since the removal of all the redundant parts is assumed to be part of the ESA department. The total weight removal is equal to 268 kg and the total weight addition to 136.12 kg.

Table 9.1: c.g. contributions of the systems assessed by the ESA department.

System	Weight (kg)	Arm (m)	System	Weight (kg)	Arm (m)
Removed			*Added*		
Seat 1	-27	4.24	SCS rack	19.75	8.61
Seat 2+3	-54	5.21	Engineer equipment	17.05	4.24
Seat 4+5	-54	6.58	Engineer seat	15	4.24
Seat 6+7	-54	7.76	2nd test pilot seat	15	4.24
Seat side	-15	8.49	Battery sim	4.6	1.21
FL cabinet	-25	3.64	Actuator upper	36	9.95
FR cabinet	-15	3.51	Actuator side	6	9.22
Lavatory	-24	8.49	Lavatory bags	2.72	4.24
			Peripheral products	20	n.a.

9.3 Ergonomics design

The IFS will need to be operated by a crew of a test pilot, safety pilot and a test engineer. This is also stated in the FBS at block *3.2.4*. The three man crew will need to be stationed at various locations. Their individual stations shall be designed so they can perform to their full potential. Also an extra passenger is required to take on board if a mid flight change of test pilots is required. It is more efficient to fly with an extra test pilot than landing the aircraft and needing to switch pilot on ground as described in section 11.1. Below every station will be elaborated, including the subsystems they consist of and what their main purpose is, hence meeting **IFS-SH2-09**. Lastly, it should be kept in mind that the ergonomics design is performed keeping in mind the mass budget of 90 kg and the cost budget of €62,000, as assigned in sections 4.4.2 and 4.4.1.

9.3.1 Test pilot station

If the IFS behaves the same as the to be simulated aircraft but the controls do not feel the same, a part of the training and testing is lost. In order to experience the feeling of other aircraft the cockpit will be adapted. Because the IFS needs to simulate a broad range of aircraft, the cockpit needs to be adaptable in order to feel the same as the to be simulated aircraft and to give feedback the other aircraft would give. Below the different parts of the test pilot station are given.

- **Control loaded stick:** a control load stick will be added to the cockpit in order to let the pilot feel what the aircraft is doing, in sub section 9.5.4 the working of the stick will be elaborated upon. In sub section 9.5.3 the software system behind the control loaded stick is given. Adding a control loaded stick to the cockpit will make it comply to requirement **IFS-SYS-10-EXP-01**. An example is given in Figure 9.5.

- **Control loaded pedals:** the pedals will also have force feedback. The pedals work in the same way as the force feedback stick.
- **Primary flight display:** the screen of the Embraer will be programmed in order display the same gages as the simulation aircraft will have.
- **Safety buttons:** around the test pilot the various safety buttons will be placed in order to engage the safety trip system. Below the location of the buttons will be elaborated upon.
- **Audiovisual feedback:** the aircraft shall provide the test pilot with audiovisual feedback in case of a safety trip.
- **Health monitor:** an additional feature is that the test pilot will be connected to a health monitor, this will monitor the heart rate, blood pressure and the blood saturation. With this data the stress levels can be analysed, this will give an indication of the physical impact of flying the various aircraft. In section 9.7 the health monitor system will be explained.
- **Camera:** in the cockpit their will be an camera implemented to record the behaviour of the pilot during the simulation, see section 9.7, this will give the possibility to look back at images and see how the pilot reacted to certain inputs or behaviour of the aircraft. Together with the health monitor this will give a clear image on the performance of the test pilot.

In Figure 9.4 a graphical representation is given of the test pilot station, The force feedback stick will be placed at '1', which is placed on the right side. The screen on the Embraer, indicated by '2', will be programmed to have the same interface as the simulated aircraft, hence meeting requirement **IFS-SYS-10-EXP-04**. The throttle is reachable, as in a unadapted aircraft, hence requirement **IFS-SYS-10-EXP-07** is met. Also the location of the added safety trip system buttons is shown by the red dots. It can be seen that they are placed in such order that the buttons can be reached without leaving the seat. They also shall be reachable within one arm length in any possible position within the cockpit. For redundancy the test pilot and the safety pilot will be able to reach a minimum of two buttons while seated. If a button is defect the other one can quickly be pressed. The buttons will be placed in such positions that they will not be touched by accident. Therefore requirement **IFS-SYS-10** is met. Also the right yoke is blurred in the picture, to indicated it will not be present in the modified cockpit.

Figure 9.4: Layout of the adapted cockpit.

Figure 9.5: Example of a control-loaded sidestick.[12]

9.3.2 Test engineer station

The simulation needs to be controlled by the test engineer . The test engineer will upload the simulation to the simulation control system,this will be elaborated upon in subsection 9.5.3. He will also give the commands to the test pilot and keep track of the pilots performance by the health monitor. Another function is checking the behaviour of the different aircraft components. He will receive a specific data package. The amount of data he receives from the data acquisition can be set by the customer. In subsection 9.7.3 the data handling is described and how the test engineer receives his data. Below the different components of the test engineer are discussed. By adding the test engineer requirement **IFS-SYS-11** is met.

- **Computer:** the test engineer needs a computer to operate the simulation, since the simulation will not run on the test engineer station. This means that the test engineer needs a computer to look at the data but not for elaborate calculations.

[12] http://www.stirling-dynamics.com/compact-side-stick?format=raw&task=download&fid=48 [cited 23 January 2017]

- **Screen:** the data needs to be shown on screens to give a graphical representation of the data, including both outputs from the SCS and ACS. These screen provide the test engineer the possibility to monitor the aircraft and test pilot, ensuring requirement **IFS-SYS-11-TEST-01** is met.
- **Simulation control panel:** the simulation will be uploaded by the test engineer, see subsection 9.5.3. This will be done from a control panel where he will upload the simulation to the simulation control system. This control panel ensures that the test engineer will always be able to upload changes to the IFS settings, hence requirement **IFS-SYS-11-TEST-04** is met.
- **Safety trip button:** when an emergency happens the test engineer will also be able to engage the safety trip system. Two buttons will be placed within arm reach of the test engineer but not in a position where it will be touched by accident. This function is as stated in the FBS at block *3.2.5.3*.
- **Audiovisual feedback:** the aircraft shall provide the test engineer with audiovisual feedback in case of a safety trip. New warning lights will be added for this. With this feedback, requirement **IFS-SYS-17-SAFE-05** is met.
- **Logger:** the final addition the station is a logger, where the handling of the test engineer will be stored. This system is redundant because all data will be stored in a logger in the data handling system, see subsection 9.7.3. But when the connection breaks, it will be possible to check what the last inputs of the test engineer station were on the system and trace back where the system crashed.

9.3.3 Safety pilot station

The safety pilot station is next to the pilot. Because the Embraer phenom 300 is certified for single pilot operation the safety pilot can take full control without any problem and even the fly the plane under normal conditions. His main purpose is being a back up if something goes wrong with the simulation and the safety trip system will give full control the the safety pilot. Implementing a safety pilot station will mean that requirement **IFS-SYS-12** is met. Below the safety pilot systems are stated.

- **Safety buttons:** the safety pilot also needs to have safety trip buttons, a minimum of two, in order to shut off the simulation, these will be placed in arm reach. This provides the possibility for the safety pilot to always take over flight, ensuring compliance to requirement **IFS-SYS-17-SAFE-01**.
- **Audiovisual feedback:** the aircraft provides the pilot with audiovisual feedback in case of a safety trip.
- **Screen:** the safety pilot will have an additional screen where he can see how the simulation is going and what inputs the test engineer gives to the test pilot.

9.3.4 Passengers station

An additional passenger station will be added to the aircraft during flight, this passenger can switch places with the test pilot during flight. Changing a pilot mid air can safe time and money because the aircraft does not need to land and pick up another pilot. Looking at Figure 9.4 it can be seen that their is enough room that it will not be a problem to switch the pilot. Therefore requirements **IFS-SYS-13** and **IFS-SYS-14** are met.

9.4 Hardware diagram

In Figure 9.6 the hardware diagram of the IFS is shown. The diagram is made up of eight different blocks, each representing a system that will be added to the aircraft. In this block diagram only the systems that will be added or altered are shown. As can be seen in the figure the SCS is at the center of the system, so all other components communicate with the SCS Since the SCS will be the brain of the IFS, each system is linked to it. Below, each block will be explained on how it works and what input and output it gets from what system.

- **Test engineer station:** the test engineer station will control the simulation. The systems of the test engineer station are elaborated in section 9.3. He will send the control commands and the flight simulation dynamics. He also has a safety trip system. All these commands are first send to the SCS. The station receives data from the ACS, SCS, test pilot sensors and flight data. How the data will be handled will be elaborated upon in subsection 9.7.3.
- **Safety pilot:** during the simulation the safety pilot is the back up pilot for in case the simulation goes wrong. In section 9.3 the functions are elaborated upon. The main systems are the safety trip system and the flight data overview. The latter is present to have clear impression on what happens to the aircraft.
- **Test pilot station:** as explained above in section 9.3 the test pilot flies during the simulation. The main inputs are the force feedback and instructions. The main output is the control input to the SCS. From the SCS the controls will be distributed to the control actuators and the ACS as shown in the image. How the control inputs will be converted to actual aircraft movement will be discussed in section 9.5.3.

- **ACS:** the aircraft control systemACS is the original control system of the aircraft. During the simulation the SCS will control the ACS in order to let the aircraft behave as required. In section 9.5.1 the communication between the ACS and the FCS is explained in more detail. The main output is the original flight sensor data to the SCS, because they are needed for the simulation. The main input is the control input for the original aircraft. The original systems, such as communication, will be kept original.
- **Drag chute:** a drag chute is added to generate an L/D of 4, as explained in section 5.4. This drag chute will be controlled via the SCS. It will contain a quick release for safety and a deployment system that will deploy the drag chute in flight. In the system itself there will also be a tension sensor. This sensor however is stated under the sensors block. The drag chute sensor will be elaborated upon in subsection 9.7.3.
- **Actuators:** all the additional actuators need to be controlled. This is done by the SCS as can be seen in the diagram. The SCS will control the boxwing actuators, the fly by wire conversion actuators and the clutches. The output will be actuator data such as their position.
- **Sensors:** sensors will be added to the aircraft in section 9.7. What sensor will be added and how the sensor data is handled will be explained.
- **SCS:** in the center of the system is the SCS. It is the main component in the system, all the different systems are linked to the SCS. Having all of the data at a single system will mean that data handling and actuator control will be at a central location. This is convenient since otherwise every system needs to be linked to all the components. Instead the systems are linked to one system and the SCS will distribute it in the aircraft. How the SCS works in detail will be elaborated in section 9.5.1. As can be seen in the hardware diagram the SCS sends control commands to all added actuators and is able to send control inputs to the ACS. This control input is, in normal conditions, only present during augmented flight and comes from the test pilot. In this way the SCS is able to control the aicrafts' drag devices, side force devices and control surfaces, ensuring the compliance with requirements **IFS-SYS-10-EXP-05**, **IFS-SYS-10-EXP-06** and **IFS-SYS-10-EXP-08**. Lastly the SCS has a logger and a data storage of 2 Tb. The data storage will consist of a simple Solid-State Drive, which is preferred over a Hard-Disk Drive since it has no moving parts. Hence it is less sensitive to the vibrations and maneuvers of the aircraft. The Samsung 850 EVO 2TB[13] is chosen, which is able to write data at 520 mb/s. This sufficient for the amount of data which will be gathered by the SCS. The implementation of this drive ensures compliance to requirement **IFS-SYS-11-TEST-03**. The functions of the SCS will comply to the function as stated in the FBS at block *3.3*.

9.5 Control system

The complete control system itself consist mainly of the cockpit controls and the FCS. First the split up of the FCS is explained and hereafter the simulation control system software diagram. The last subsection is on the force feedback the test pilot receives. The control subsystem as a whole is assigned a mass budget of 70 kg in subsection 4.4.2, while the cost assigned to this part of the design is €160,000 as stated in subsection 4.4.1.

9.5.1 Flight control system

The FCS will be dived in two parts: the ACS and the SCS. The ACS will control all the parts of the stock aircraft. The system for the simulation and the original aircraft are separated for safety reasons. The SCS will control the simulation that the aircraft needs to perform. This simulation can be of experimental aircraft. The SCS makes the aircraft into a programmable variable stability platform, hence complying to requirements **IFS-SYS-08**, **IFS-SH2-05** and **IFS-SH2-06**. In the section 4.3, at block *3.2.3.2* of the FBS, is stated that the IFS shall provide computing power. The different sub blocks will be explained in more detail below.
The development of experimental aircraft can be in an early stage and risks needs to be brought to a minimum. If the simulation does not work as desired, the SCS can be switched off completely This can be done both manually and via an automatic safety trip system, ensuring the aircraft will go back to the original controls of the Phenom 300. Having this safety trip system ensures that the IFS complies with requirements **IFS-SH2-03**, **IFS-SH7-01** and **IFS-SYS-17**. Both the SCS and ACS systems will have different responsibilities and tasks.

[13] https://www.ssdcenter.nl/product/632004/samsung-ssd-850-evo-2-tb.html [cited 23 January 2017]

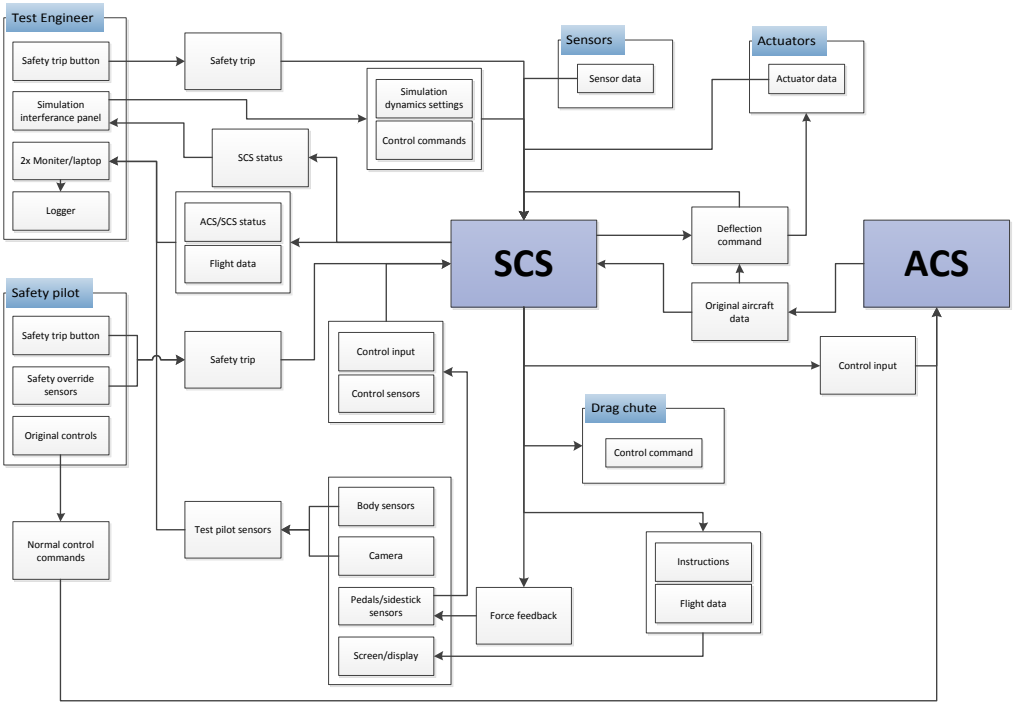

Figure 9.6: Hardware diagram of the IFS.

The main functions for the different systems are as follows:

Aircraft control system:
- controls the stock aircraft
- controls stock actuators
- forwards data to SCS

Simulation control system:
- computes simulation
- handles (additional) data
- controls actuators in box wing
- operates clutches
- controls ACS during simulation
- manages force feedback

In Figure 9.7 the communication flow between the two systems is shown. The solid lines indicate one way communication, the dotted lines indicate two way connections. Also the input and output of the FCS is given and connected by the ACS or SCS depending on which system is responsible.

9.5.2 Simulation control system

The simulation control system will be a separate system from the ACS. This additional computer will be added into the cabin space, for easy maintainability. The communication of the SCS with the ACS is described in Figure 9.7. The SCS contain the following parts.

- **Computer system:** the SCS needs to contain a computer that has enough computing power to run the simulated flight. This computer will be able to translate the movements of the to be simulated aircraft into the actual movements of the control surfaces. Below the software diagram will be shown where the simulation will be explained. The simulation calculations will be performed by the computer system.
- **Communication bus:** the communication bus is responsible for communicating the flight controls to the FCS and the boxwing actuators. It will get its commands from the computer and distributes it to the actuators and the ACS. The communication bus will tell the ACS which stock control surfaces need to be operated.
- **Data acquisition and distribution:** all the extra sensor data also needs to be gathered and processed. The sensor data will be uploaded to the data communication bus. All the gathered data will be send to an additional air data computer, dedicated for augmented flight. This data will be sent to the test engineer station, the test pilot

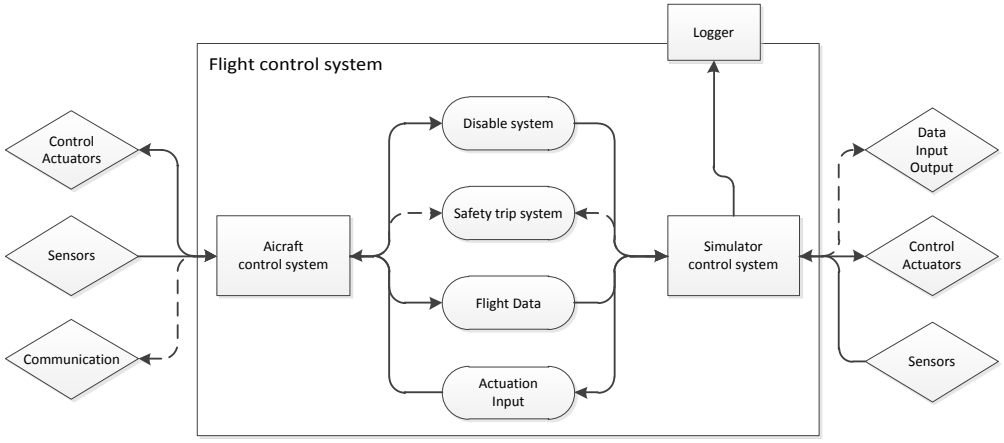

Figure 9.7: FCS communication flow diagram.

and to several loggers, which will be located at the test engineer station and at the SCS.

- **Structural rack:** the system above need to be mounted in a rack. This rack must be easy to maintain and shall be strong enough to be certified. The certification of the rack means that it needs to withstand a force of 18g forward and 4.5 g sidewards[14]. In order to meet this requirement a rugged electronic rack has been chosen which can withstand the 18G loading [15]. Choosing a rack that can cope with the 18G loading means that the the requirement **IFS-SYS-18-STRUCT-02** has been met for the SCS.
- **Safety trip system:** to be able to ensure safe flight, a safety trip system is implemented in the IFS. This safety system has two different modes, namely safety mode and back-up mode. The safety mode can be engaged both manually and automatically. The manual trip of this system can be engaged by the test pilot, test engineer or safety pilot. The automatic safety trip can be triggered for several reasons of which the most important are when the aircraft comes within 5% of it's flight envelope and when not enough electrical power is available to power all system. The automatic safety trip and safety margin ensure compliance to requirements **IFS-SYS-17-SAFE-02** and **IFS-SYS-17-SAFE-03**. When the safety mode is activated, all controls go to the safety pilot and the clutches via which the test pilot controls the aircraft will be disengaged.
  However it might happen that the safety pilot is incapacitated and is not able to fly the aircraft. In such a case the test pilot should be able to take over normal flight and the back-up mode will be activated. The clutches on the primary controls will be engaged again and the test pilot is then able to control the aircraft in a limited way. The boxwing control surfaces will be set in a predetermined (landing) setting and the sidestick will directly control the primary flight controls. This back-up mode ensures compliance to requirement **IFS-SYS-17-SAFE-06**.
  Both modes will have their own warning sounds and lights, hence complying to requirement **IFS-SYS-17-SAFE-04**. The implementation of the safety trip system adds to the compliance to requirements **IFS-SH7-01** and **IFS-SYS-17**.

9.5.3 Simulation control system software diagram

In the previous subsection it is explained which systems the SCS contains and what their functions are. One major component is the computer system. This system will calculate the simulation and give commands to the communication. It also receives data from the data gathering system which needs to be analysed for the simulation. The internal software layout will be elaborated uoon below. In Figure 9.8 the block diagram of the software structure is shown.

The diagram is divided in four blocks: behaviour simulation, translation simulation to aircraft, aircraft control and feedback. The blocks all have a different part in the simulation and need to work together in order to let the aircraft behave as the to be simulated aircraft. Below, the four blocks will be explained using the diagram as reference.

[14] http://www.kilohotel.com/rv8/index.php?option=com_content&view=article&id=536:placards-2&catid=29&Itemid=101 [cited 12 January 2017]

[15] http://wmdllc.com/products/rugged-electronics-racks/index.php [cited 12 January 2017]

- **Behaviour simulation:** the behaviour system has two main inputs in order to operate it namely the stick input of the test pilot and the flight dynamics profile of the to be simulated aircraft. The test engineer will upload the behaviour of the simulated aircraft to the computer, this meets the stated function *1.8 design for easy adjustment of in-flight simulator* of the FBS. The computer will analyse the data in order to compute what a certain stick input would have on the aircraft, it will also check if the input will not create unsafe flying conditions, as stated in the FBS at block *3.2.5.2*. After the stick input is analysed the behaviour of the simulated aircraft is calculated. This works the same as in a normal aircraft simulation on your computer, with the computed behaviour of the system the deflections in the simulation are calculated. With these deflections the force feedback is computed and the test pilot feels the behaviour of the simulated aircraft. The first block(behaviour simulation) works essentially the same as an aircraft simulator that can be found on the ground. The test pilot thus gets feedback before the translation to the Embraer has been made, the computer system will be fast enough that the latency cannot be felt by the pilot. The next step is to calculate the deflections the real aircraft should have in order to match the feeling of the simulated aircraft.
- **Translation simulation to aircraft:** the translation simulation to aircraft block will convert the simulated aircraft to the Embraer flight behaviour. An input to the block is the digital behaviour of the Embraer with the added control surfaces. With the known behaviour of the Embraer a comparison is made between the wanted behaviour and the standard behaviour of the Embraer. From the comparison a translation matrix is made to know how the Embraer should fly in order to behave as the simulation. With knowing the behaviour that is needed of the Embraer the needed deflections can be computed in the next block. With all the deflections calculated it will give a command to the communication bus in the next block, the aircraft control.
- **Aircraft control:** the final control block will control the aircraft. As discussed in subsection 9.5.1 the computer system will not communicate with the different systems because in that case too many functions will be operated by one system. So the computer system will give the communication bus the deflections that are needed in order to perform the simulation. The communication bus will distribute and control the extra actuators and also signal the ACS what original fly by wire control surfaces need to be controlled. The original aircraft control systems will be handled by the ACS, but the actuators that are added in order to make it fly by wire will be directly be controlled by the communication bus. This can be seen in the block *Control added actuators*. Both the original control surfaces and the boxwing control surfaces will influence the flight dynamics (the behaviour) of the aircraft to match the simulation flight dynamics. The flight dynamics states will be measured by the sensors in the aircraft. This data will be used to check if the aircraft's behaviour complies to the wanted behaviour.
- **Feedback:** the last block is the feedback. Herein, the first block contains the sensors that measure flight dynamics. The data from all the sensors will be translated into one flight dynamics profile. This will be compared to the desired flight dynamics of the simulation. If these flight dynamics do not comply a block will change the translation matrix in order to make it fit to the wanted behaviour. In real life situations it is expected that it will not be aligned perfectly the first run. The client will need to fly a calibration run in order to check if the aircraft matches the wanted flight dynamics. The aircraft itself will adjust the translation matrix so that the simulation is correct. The test engineer will receive a signal if the system complies and the real simulation can take place.

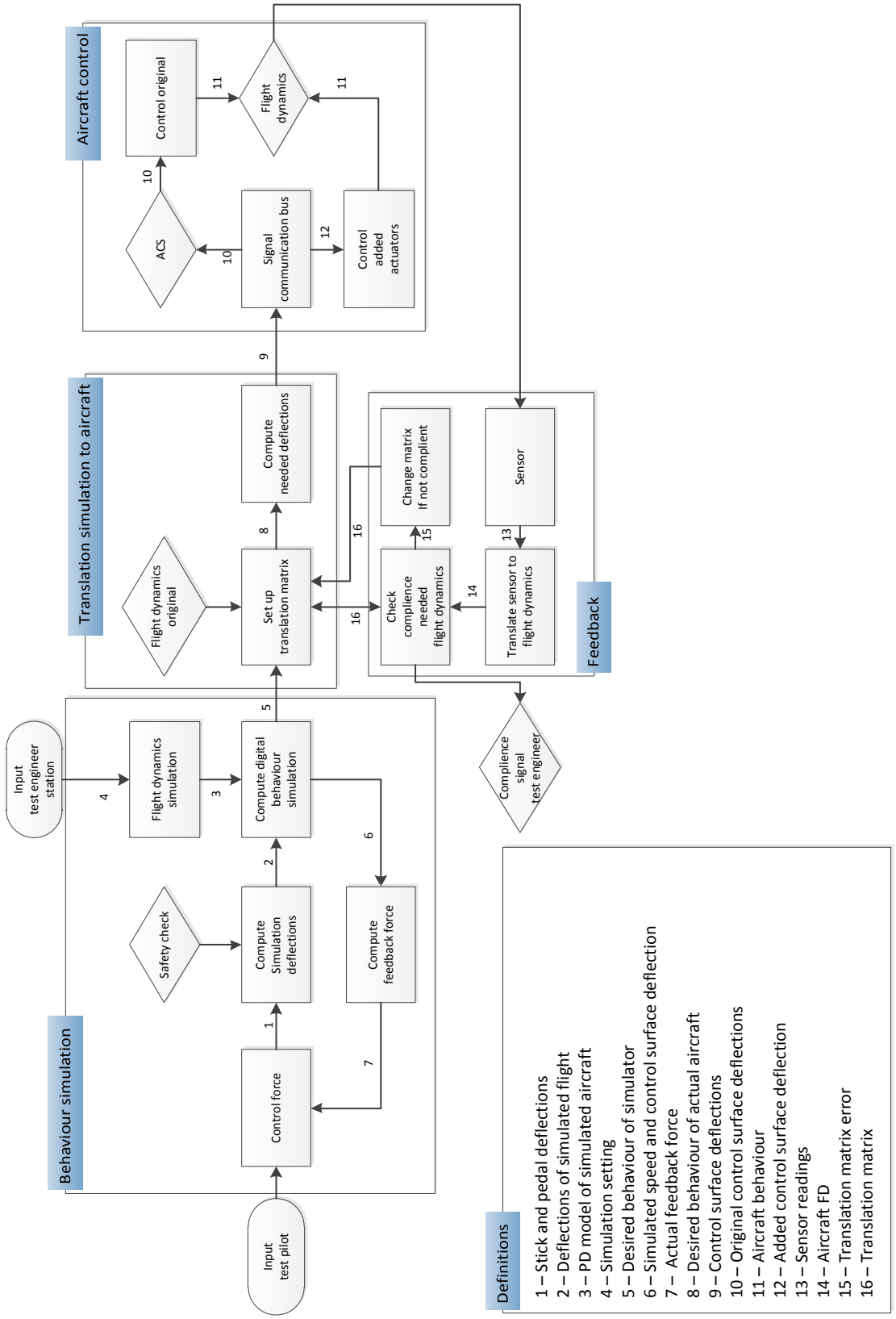

Figure 9.8: Software diagram of the computer system.

9.5.4 Force feedback control

One of the requirements the experimental flight control station should comply with is **IFS-SYS-10-EXP-01** [10], which states that the aircraft should have a force feedback stick. This requirement originates from the fact that there are currently several aircraft that have force feedback to the pilot[16]. To be able to simulate aircraft with this feedback an active force feedback stick should be implemented. For this project a sidestick is chosen over a centerstick since the cockpit of the Phenom 300 is focused on one pilot, the left pilot. The right pilot station does not have all the controls and buttons leaving sufficient room to implement the sidestick without adding structure or removing controls. A new centerstick would need a more extensive modification, since a column should be implemented, while the sidestick can be implemented in the side console, where no buttons are located. A force feedback stick gives the pilot feedback on the aircraft dynamics, next to the visual feedback which can be slightly delayed.

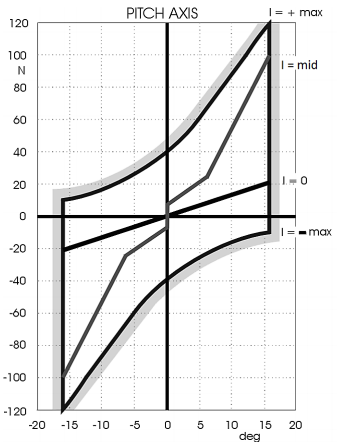

Figure 9.9: Force-deflection envelope for an active sidestick. [5]

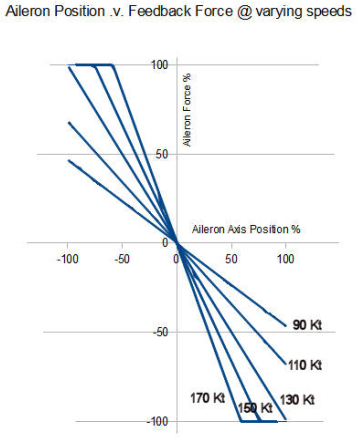

Figure 9.10: Force-speed envelope for an active sidestick.[17]

The current market offers programmable off-the-shelf active force feedback sidesticks[18]. This allows to change the type of force feedback depending on the simulated aircraft. The force the pilot feels from the stick does not directly on the actual force on the control surface, but can be a function of control surface deflection and/or aircraft speed. Also there are different functions on which the stick can give feedback, which are listed next.

- **Initial displacement force:** to give the pilot a feel of the initial/zero-deflection position of the stick an initial force, the breakout force, is needed to move the stick away from the initial position. This is usually a small force but enables the pilot to find the initial position. It also makes sure no unwanted small deflection are created when the stick is in the initial position. An example of the breakout force is given in Figure 9.9. The curve indicated with 'I=mid' shows a jump at 0 degree, which represents the force needed to move the stick. The curve is based on an electro-magnetic sidestick, however the qualitative representation of the graph can be applied to each control-loaded stick.
- **Deflection dependent force feedback:** the force the pilot feels when operating the stick can either be increasing with a constant force change or with a stepwise force change. The constant force change is shown in Figure 9.9 indicated by 'I=0', which shows a linearly changing force depending on the deflection. This is considered to be passive force feedback and represents a spring loaded stick.The stepwise force change is shown in the same figure indicated by 'I=mid', which shows a kink around 7 degrees to indicated that more force is needed to deflect the stick further. The amount and placement of these steps can be programmed.
- **Speed dependent force feedback:** besides a deflection also a speed dependent feedback can be given, as shown in Figure 9.10. The graph represents the stick force needed to move an aileron to a certain position dependent on different speeds, however again the graph is primarily used to give a qualitative representation. The graph shows that at higher speeds more force is needed to move the stick for an equal aileron deflection. This corresponds to the fact that higher speeds require larger actuator forces than low speeds, based on the same surface control deflection.

[16] http://www.boeing.com/commercial/737ng/ [cited on 9-1-2017]
[18] http://www.stirling-dynamics.com/training-simulation/active-controls [cited 9 January 2017]
[18] http://bffsimulation.com/FFB-Yoke-2/Ail_Stiffness.jpg [cited 14 January 2017]

- **Safety feedback:** a control-loaded stick can also be used to make the test pilot aware of safety issues. Force feedback, like shaking the stick, can be given in case of exceeding the flight envelope or to give a stall warning. It is also possible to limit the stick deflection when a gear is locked up and thus the use of a control surface is limited or locked.

Also the yaw control by the test pilot, with rudder pedals, should be mechanically decoupled. This is due to the fact that the pilot does not directly control the rudder, but rather the simulated rudder from the aircraft which is being simulated. Hence the simulated rudder deflection can be a combination of deflections of the vertical control surfaces on the boxwing and of the rudder. Also it might be needed to operate the rudder or the vertical control surfaces on the boxwing without the test pilot giving an input to simulate a characteristic of the simulated aircraft while doing a maneuver.

The control-loaded compact sidestick from Stirling Dynamics[19] that will be used is able to provide a force feedback of 222N, which makes sure it complies with requirement **IFS-SYS-10-EXP-02**. The actuators for yaw control will be off-the-shelf actuators[20] with a gearbox, which ensure the pedals comply to requirement **IFS-SYS-10-EXP-03**.

9.6 Controls and actuators layout

To make sure all control and actuator parts work together well and safety measures are implemented at the correct places, a detailed overview of the actual systems is created and explained in this section. First the system layout will be presented and after that the physical implementation will be elaborated on.

9.6.1 System layout

A general lay-out of the adapted system is shown in Figure 9.11. As can be seen the original control system for the safety pilot is left intact, with no interruptions added. The whole additional system is connected to this original system with a clutch to always be able to disconnect in case of a safety trip. This safety trip will be engaged in several occasions, which will be explained throughout the chapter. The implementation of this safety trip system makes sure the IFS complies to requirement **IFS-SYS-17**.

Next to this there will be a clutch and motor for the rudder, elevator and aileron control. The motor after each clutch will be used to control the regular controls during augmented flight, making the augmented flight completely FBW.

Another additional system part is a power trip system, which will restore the original controls and disengage all augmented flight controls when an engine fails and not enough power can be delivered to run both the regular flight systems and the augmented flight systems. Also an important fact is that the test pilot control will be FBW and all links to the controls go through the FCS and Simulation Control System.

Lastly the power supply as indicated in Figure 9.11 consists of the generators from the engines. The engine generators of the aircraft[21] are able to deliver 28V DC each rated at 400A. During flight the standard aircraft uses 390A (peak-load) of this 400A. In the aircraft computers, sensors, sensor data handling devices and extra actuators are added, which will all need electricity to operate. To be able to be able to operate all these systems two measures are taken. At first the passenger electronics, such as passenger tv-screens, are taken out. However this will not be enough, hence when purchasing the aircraft it is needed to implement stronger generators connected to the engines. This will not compromise the ability of the aircraft to function as IFS since the engines are very power-full for this aircraft. A more complete overview of the power usage of the aircraft will be given in section 9.9.

[19] http://www.stirling-dynamics.com/compact-side-stick?format=raw&task=download&fid=48 [cited 20 January 2017]

[20] http://www.boschrexroth.com/dcc/Vornavigation/VorNavi.cfm?Language=EN&Variant=&VHist=g97568%2Cg96068&PageID=p201894 [cited 23 January 2017]

[21] https://www.phenom.http://phenom.aero/resources/library/Phenom300_QuestionBank.pdf [cited 13 January 2017]

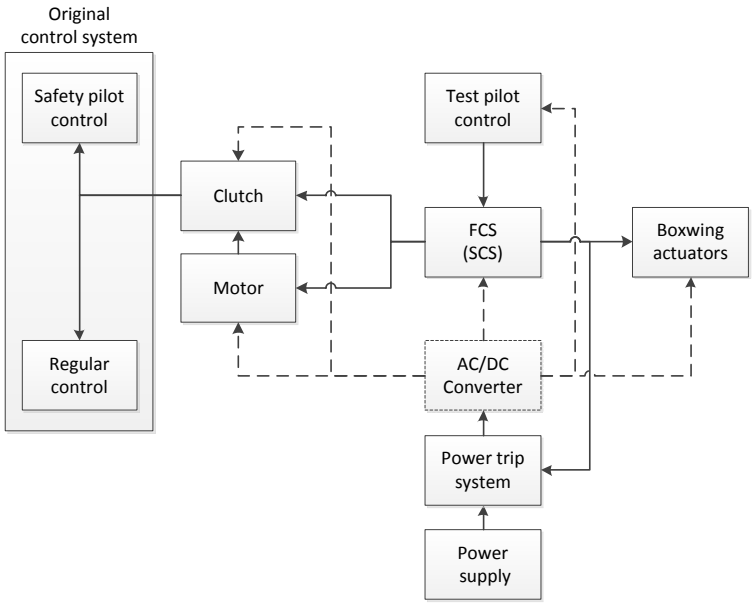

Figure 9.11: Controls and actuator layout.

9.6.2 Physical implementation

For the physical implementation of the system several parts are assessed. The first part treated in this section is the motor and clutch that connects the additional system to the original system. An options that is considered is to use the actuators from the autopilot, since these are already in the system and certified. However this is probably not feasible since these motors are not made to perform duringthe more extreme maneuvers, which the IFS will perform.Besides this the clutches used for the autopilot are friction clutches, hence do not allow operations that need a high torque. For these reasons it is chosen to implement a different motor and clutches system. Since the aircraft is certified for single pilot operations[22] the right pilot station can be adapted without having the re-certify the whole control system. Since a control-loaded stick needs to be implemented the right yoke will be removed. The original yoke control system in the cockpit of the Embraer Phenom 300 is shown in Figure 9.12, the yoke control system with the right yoke removed is shown in section Figure 9.13.

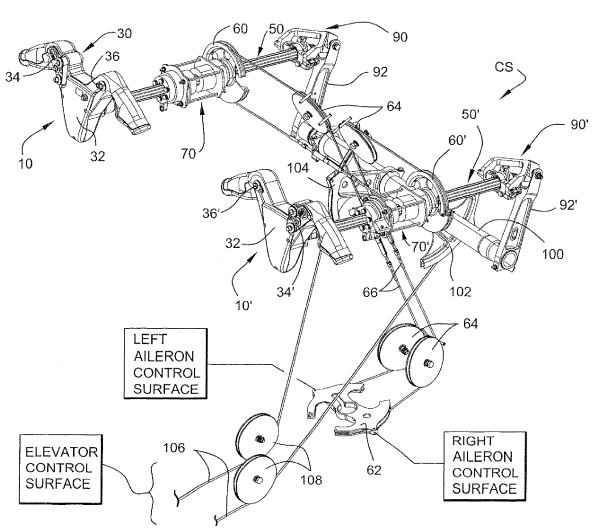

Figure 9.12: Control system Embraer Phenom 300.[23]

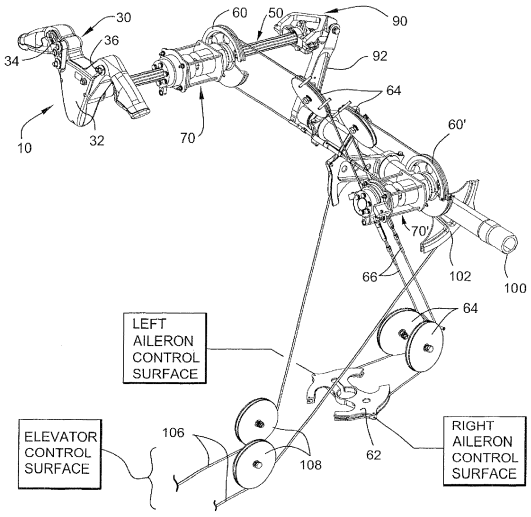

Figure 9.13: Control system with center yoke removed.[24]

[22] http://www.flightrun.com/embraer-phenom-300/single-pilot [cited 12 January 2017]

As can be seen in Figure 9.13, some space has been created by removing the yoke which can be used to install the clutch and motor control for both pitch and roll. The motor and clutch for roll control can be implemented at position $60'$ and for pitch control at position 100. The second part of the system is the adapted test pilot control. The main parts are a control-loaded side stick and control-loaded pedals. The latter option is not a direct result from the requirements, however to be able to make the yaw control FBW the cables will be removed from the test pilot station and are replaced by either springs or actuators to give the pilot a more realistic feeling. The control-loaded devices will be explained more in depth in subsection 9.5.4. The third part is the FCS and the SCS, which is the core of the additional systems. A more detailed description of these systems is given in subsection 9.5.1. The last part of the additional system is the power supply which is described in section 9.9.

9.7 Sensors design

The sensors of an aircraft are of vital importance to monitor the flight and for post research. The Embraer Phenom 300 is equipped with a large set of sensors which will be explained in the first section. After this the sensors that need to be added are elaborated on. The section concludes with the explanation of the data handling diagram. During the design of the additional sensors and data handling, the assigned mass of 30 kg and cost of €80,000 have to be taken into account, as decided in section 4.4.

9.7.1 Standard sensors

Most sensors that are needed are present on the Embraer Phenom 300 already. The aircraft is equipped with SmartProbe®[25] that combine multi-function probes (sensing probes and pressure sensors) with a small air data computer. The SmartProbe® is a system which is under development since 1998 and can measure some extra data which is not usually measured such as the angle of sideslip. Next to this the Embraer is equipped with several accelerometers, gyros and GPS. An overview of the most important data that is measured is given in Table 9.2.

Table 9.2: Sensor data available on the Embraer Phenom 300.

Aircraft state	θ, ϕ, ψ, p, q, r, N_x ,N_y ,N_z
Air data	α, β, V, P_s, Q_s, RoC, T
Additional	GPS

Next to these a lot of sensors are on the aircraft that are of minor importance to this project and hence are not mentioned. Examples of these sensors are icing sensors and fuel flow sensors.

9.7.2 Added sensors

There are two categories of sensors that will be added, those of vital importance to correctly performing augmented flight and those that are used for research purposes only. There are several sensors that need to be added to the aircraft to be able to perform augmented flight but most sensors are already present on the aircraft.

- **Control surface deflection:** the deflection of both the existing and added control surfaces need to be known. The deflections of the boxwing control surfaces can be taken directly from the motors that will be installed, which will be explained in section 9.8. However to implement redundancy in the system some extra sensors are implemented. To measure the deflections synchros[26] are used, which are low weight transformer-like devices that measure angular position and/or velocity. These sensors will be placed at one end of the corresponding control surface, as close to the fuselage as possible to keep the amount of wires to a minimum.
- **Engine sensors:** extra sensors will be added to monitor the engines. Since the aircraft is likely to be operated close to its limits, such as during the low L/D simulation, the engines will be monitored closely to observe any abnormal behaviour. These attributes will be measured: N1, N2 sensors (turbine and compressor rpm)[27], exhaust gas temperature [28] and engine pressure ratio[29]. All these sensors will be placed in or very close to the engine.

[24] https://www.google.com/patents/US7740207 [cited 13 January 2017]
[24] https://www.google.com/patents/US7740207 [cited 13 January 2017]
[25] http://utcaerospacesystems.com/cap/systems/sisdocuments/Air%20Data%20Products%20and%20Systems/SmartProbe(R)%20Air%20Data%20Systems.pdf [cited 12 January 2017]
[26] https://www.aea.net/AvionicsNews/ANArchives/synchrosOct04.pdf [cited 12 January 2017]
[27] http://www.ameteksensors.com/Products/Speed-Sensors.aspx [cited 19 January 2017]
[28] http://www.ameteksensors.com/Products/Temperature-Sensors.aspx [cited 19 January 2017]
[29] http://www.ameteksensors.com/Products/Pressure-Transducers.aspx [cited 19 January 2017]

- **Electric sensors:** an additional power system will be added to the aircraft and better generators installed. To be able to operate safely any failures in this electric system should be detected instantaneously. In case the IFS is simulating an other aircraft the augmented flight should be aborted. The back-up system for the boxwing actuators should monitored closely as well, since in case of a generator failure the actuators still need to be able to move to a safety configuration. To monitor the system the following attributes will be measured: system overload[30], generator failure, actuator power[30] and battery state of charge[31]. The system overload sensors will be placed at multiple location in the system, namely after each generator and after each battery. Generator failure sensing is included in the BMS (explained in section 9.9), hence is located close to the batteries. Actuator power sensors will be placed close to the actuators. Lastly, the state of charge sensors are placed at the battery locations.
- **Boxwing sensors:** two types of sensors are added to the boxwing itself. The first are temperature sensors on the actuators. The electric actuators should not exceed a certain temperature else performance can go down and wear can increase. This will be elaborated on in section 9.8. The second type of boxwing sensors are icing sensors[32], which are installed to early detect icing on the boxwing. The temperature sensors of the actuators will be placed at each actuator. The temperature sensors to check for icing of the bowxwing are placed close to the leading edge, distibuted over the entire width (for the upper wing) and height (for the side wing).
- **Drag chute cable tension:** to determine the actual drag of the drag chute, a tension sensor[8] is placed on the drag chute cable. To be able to measure the force correctly an amplifier is needed[33]. The whole system will be placed in the tail of the aircraft.

Besides these a lot of sensors can be added that could add to the research value of the aircraft. A basic set of extra sensors that will be added is described below. Off course several more sensors can be added, but this will only be done if the customer desires this.

- **Pilot stress:** the pilot will be monitored by the test engineer using a Philips health monitoring system[1]. This system can give an indication of the stress levels of the test pilot. The most important quantities the system can measure are the following: heart-rate, saturation and blood pressure. The sensors connected to the system will be placed on the test pilot while the monitor is part of the test engineer station.
- **Human interface:** human interface includes the action the pilots do. Most of the aircraft is FBW, hence these values can be extracted from the ACS. The primary control still happens via a pulley system, hence synchros[26] will be implemented to measure the input of these deflections: yoke deflections and rudder pedal deflections. Both deflections will be measured in the cockpit, as close as possible to the actuators that are implemented on the primary flight controls (which are installed to provide a FBW system for the test pilot). In this way the modification will be close to each other, simplifying maintenance on these systems.
- **Cameras:** lastly, two cameras will be implemented, namely one external to monitor the drag chute[34] and one internal to monitor the test pilot[35]. The drag cute needs to be monitored by a camera, since else no visual feedback is present. The test pilot is monitored for research purposes.The test pilot camera will be mounted in the front ceiling of the cockpit, so in facing the test pilot. The drag chute camera will be mounted externally at the tail of the aircraft.

By adding all the aforementioned sensors the requirements **IFS-SH2-04** and **IFS-SYS-15** are met. Requirements **IFS-SYS-15-SENS-01** to **...-SENS-03** will be elaborated on. In these requirements it is stated that <TBD> air data, <TBD> IFS states and <TBD> control forces will be measured. However the actual sensors will not be determined within one requirement since this would result in a requirement with several parts. Hence the requirement is split up into the next requirements:

- **IFS-SYS-15-SENS-01 group**
  - **IFS-SYS-15-SENS-01-A:** the sensor subsystem shall measure the angle of attack.
  - **IFS-SYS-15-SENS-01-B:** the sensor subsystem shall measure the angle of side slip.
  - **IFS-SYS-15-SENS-01-C:** the sensor subsystem shall measure the velocity.
  - **IFS-SYS-15-SENS-01-D:** the sensor subsystem shall measure the static pressure.
  - **IFS-SYS-15-SENS-01-F:** the sensor subsystem shall measure the impact pressure.
  - **IFS-SYS-15-SENS-01-G:** the sensor subsystem shall measure the attitude rate.
  - **IFS-SYS-15-SENS-01-H:** the sensor subsystem shall measure the temperature.

[30] http://www.robotshop.com/en/hall-effect-voltage-current-sensor-100a.html[cited 19 January 2017]
[31] http://www.manzanitamicro.com/products?page=shop.product_details&flypage=flypage.tpl&product_id=76&category_id=23 [cited 19 January 2017]
[32] http://www.dtic.mil/dtic/tr/fulltext/u2/a266273.pdf [cited 19 January 2017]
[33] https://www.kistler.com/?type=669&fid=55760 [cited 19 January 2017]
[34] http://www.ad-aero.com/external_cameras.php [cited 19 January 2017]
[35] http://www.ad-aero.com/internal_cameras.php [cited 19 January 2017]

- **IFS-SYS-15-SENS-02 group**
  - **IFS-SYS-15-SENS-02-A:** the sensor subsystem shall measure the pitch attitude.
  - **IFS-SYS-15-SENS-02-B:** the sensor subsystem shall measure the roll attitude.
  - **IFS-SYS-15-SENS-02-C:** the sensor subsystem shall measure the yaw attitude
  - **IFS-SYS-15-SENS-02-D:** the sensor subsystem shall measure the pitch rate.
  - **IFS-SYS-15-SENS-02-E:** the sensor subsystem shall measure the roll rate.
  - **IFS-SYS-15-SENS-02-F:** the sensor subsystem shall measure the yaw rate.
  - **IFS-SYS-15-SENS-02-G:** the sensor subsystem shall measure the longitudinal acceleration.
  - **IFS-SYS-15-SENS-02-H:** the sensor subsystem shall measure the lateral acceleration.
  - **IFS-SYS-15-SENS-02-I:** the sensor subsystem shall measure the vertical acceleration.
- **IFS-SYS-15-SENS-03 group**
  - **IFS-SYS-15-SENS-03-A:** the sensor subsystem shall measure the elevator deflections.
  - **IFS-SYS-15-SENS-03-B:** the sensor subsystem shall measure the aileron deflections.
  - **IFS-SYS-15-SENS-03-C:** the sensor subsystem shall measure the rudder deflections.
  - **IFS-SYS-15-SENS-03-D:** the sensor subsystem shall measure the flap deflections.
  - **IFS-SYS-15-SENS-03-E:** the sensor subsystem shall measure the spoiler deflections.
  - **IFS-SYS-15-SENS-03-F:** the sensor subsystem shall measure the upper wing deflections.
  - **IFS-SYS-15-SENS-03-G:** the sensor subsystem shall measure the side wing deflections.

All these data are measured with the existing and new sensors, hence all these requirements are fulfilled. Lastly, requirement **IFS-SYS-15-SENS-04** should be considered. This requirement states an accuracy for the sensors in general, which is not useful, since each sensor has its own accuracy. Therefore this requirement is dropped.

9.7.3 Data handling diagram

In order to get a clear representation on the communication of all the sensors a data handling diagram is made, it also is stated as a needed function in the FBS, at block *3.2.3.2.4*. In Figure 9.14 the data handling diagram is presented. The diagram consist of 8 different sub parts that are connected to the communication bus. This communication bus is a data gathering bus where all the data can be sent to. The convenience of this bus is that you do not need to make all the connections to the data acquisition system, but there only need to be two cables for redundancy. These then go through the aircraft where all the systems can be connected to and the data acquisition will collect the data from this bus. The system looks like the CAN bus interface, a CAN bus interface is an interface that can work without a host computer that needs to distributes the data to the different components. The SCS does not need to have a direct link to every sensor. This will reduce the amount of cables that need to be added to the aircraft. Connecting new sensors is really simple because they need to be connected to the bus and the data acquisition system will sense that new parameters are send on the bus and will collect them. This means that the costumer can connect new sensors to the system without adding any new cables trough the aircraft and the data acquisition system will recognise the sensors and store the data. The sample frequencies given in Figure 9.14 are the minimum recommended frequency for the components, it is not advised to lower these frequencies. The sample frequency can be adjusted to a higher frequency by the customer if the sensor allows a higher frequency. The eight sub parts will be elaborate below. Why certain sample frequencies are chosen, how the communication flows and this data will be handled was described in section 9.7.

- **Syncros control surfaces:** to all the original control surfaces of the aircraft syncros will be added, they will measure the deflection of the surfaces. The data will be sent with a rate of 60Hz [27]. The sensors cannot have a higher data frequency. In the diagram all the needed syncros are presented.
- **Engine sensors:** the engine will also contain sensors to monitor its performance. All have a data frequency of 10 Hz, this is the sample frequency of the temperature sensor [28]. This will be sufficient because its general performance will be measured so 10 data points per second is sufficient. The sample frequencies within this block all have the same frequency because all the data points will be combined and would be redundant if some sensors have more data. This extra data can not be compared to the other relevant data, so the slowest sensor determines the data frequencies for the engine sensors.
- **Electric sensors:** the electric sensors measure three parts: the power overload and generator failure, the power usage of all the actuators and the State Of Charge(SOC) of the batteries. The state of charge does not need to be monitored at a high frequency because the battery will be constantly charged by the generator so in real life it shall not drop to a really low state, it works as a buffer. If it slowly drops, which can be seen at a rate of 1 Hz, the system used more energy than the generators can provide. The data of the power actuator will be sampled

at 200Hz as stated for the motors.[36] Because the motors will draw most of the electrical power the chance that an electrical overload is caused by the electric motors is most likely. Because of that reason the overload sensor will be sampled at a minimum frequency that is the same as that of the motor, 200Hz. The generator failure will also be sampled at 200Hz to have the same amount of data points for the whole system.

- **Pilot sensors:** the status of the pilot will be monitored to see the physical affects of the simulation and what the inputs of the pilots are on the system. The Philips suresigns-VM8 samples the pilot vitals at a frequency of 40Hz[1]. His inputs will also be sampled at this frequency, so the customer can see if the vitals of the pilot have a direct influence on the way he will control the aircraft. This is a good way to see if how stress-full it is to fly the simulated aircraft. The inputs of the pilot will also be used to check if the aircraft will behave the way the pilot intended.
- **Camera:** the aircraft will contain cameras that keep track of the pilot and the drag chute. The sample frequency is 60Hz because standard imaging is 30 frames per second and we want to slow down the images in order to analyse the images in more detail. Especially for the drag chute this is preferred, because the deployment of the drag chute can then be analysed in more detail.
- **Boxwing sensors:** the boxwing sensors consist of two main sensors: the temperature sensors and the icing sensors. Both these sensors will be sampled at a frequency of 1Hz because the temperature will not rise so fast that within one second the actuators will be overheated. The icing sensors are sampled at the same frequency because ice does not build up so fast that it needs to be sampled faster than once per second.
- **Drag chute:** the drag chute consist of one sensor that measures the tension in the cable. Because with gust the amount of drag can change in an instance the sensor is sampled at the maximum frequency of 200Hz [8]. When the tension exceeds the tension it was designed for it needs to be detached by the safety system in order to prevent more damage to the aircraft.
- **ACS:** the ACS collects all the data from the stock aircraft and will upload the sensor data to the communication bus. It will deliver this data at a sample rate of 200Hz in order to mach the highest sample rate performed by the simulation system.
- **Data acquisition:** with all the data uploaded on the communication bus it needs to be extracted from the bus in order to store the data, which is done by the data acquisition system. The data acquisition system will collect all the data. The data conversion system will convert the data, apply correct labels and order the sensor data and bundle the data needed for every station so it can be sent in data packages to the stations, this is done by the data distribution system. This data packaging is done in order to minimize the data overflow to the stations. All the data can still be accessed by the test engineer station, but the station will receive a standard data packed that the customer wants to receive. All the data will be stored in a logger and can be used for research on the ground. The SCS will also receive the data needed to compute the simulation of the aircraft.

When looking at the data handling diagram it can be seen that the highest data sample frequency is 200 Hz. The data acquisition system will be chosen such that it at least can comply to this data rate, hence it will be able to send the data at a rate of 200 Hz or higher. This ensures compliance to requirement **IFS-SYS-11-TEST-02**. The rate of incoming and outgoing data of the SCS is also at least 200 Hz, hence requirement **IFS-SYS-10-EXP-10** is also met.

[36] https://www.boschrexroth.com/country_units/america/united_states/sub_websites/brus_dcc/documentation_downloads/ProductDocumentation/CurrentProduct [cited 19 January 2017]

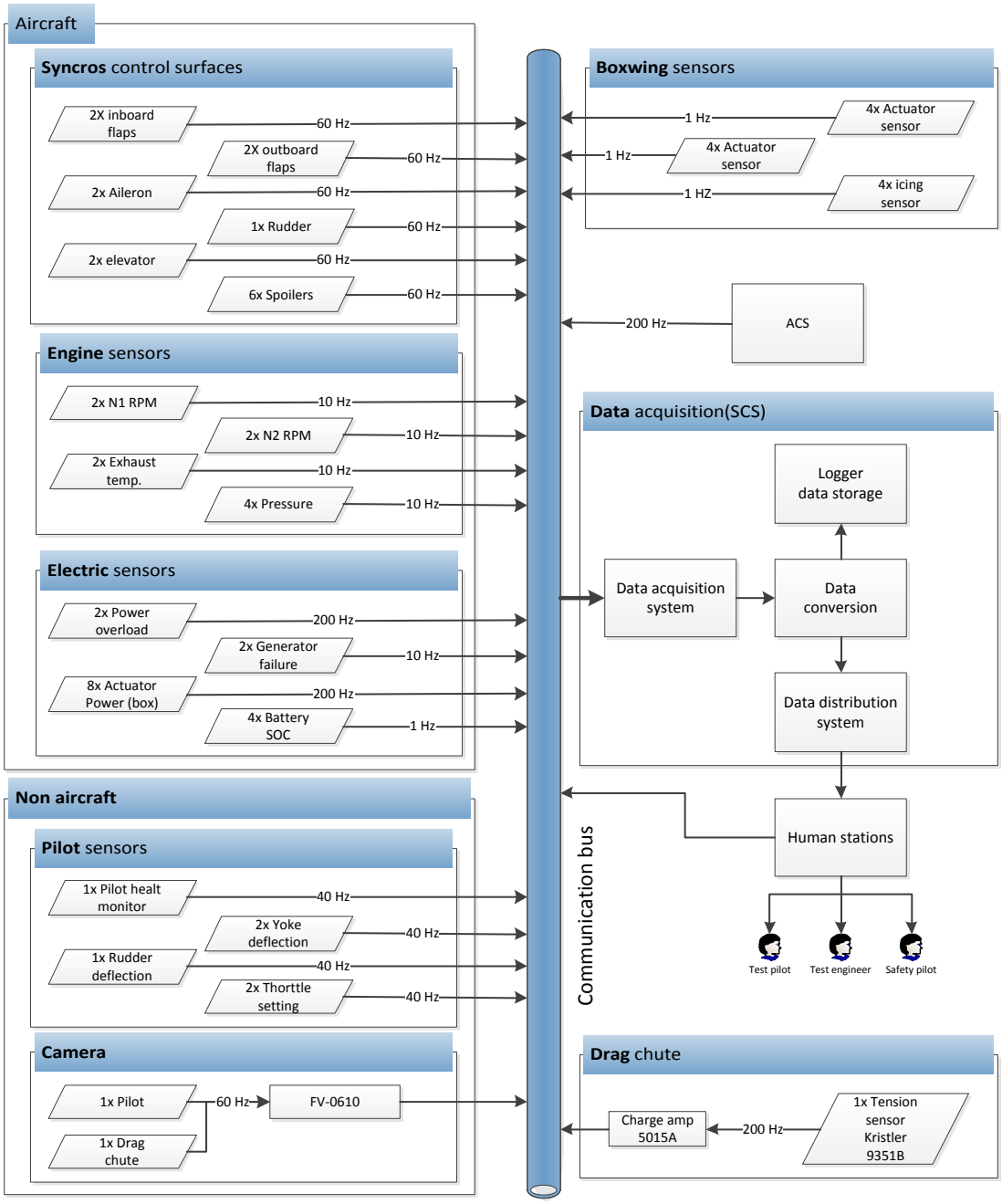

Figure 9.14: Data handling diagram.

9.8 Actuators design

In this chapter, actuator types will be argued and an actuator type will be selected. Following from actuator type, the exact actuator will be chosen. Also the connection to the aircraft will be explained, as well as a fail safe to return the actuators to the desired position in case of failure. As shown in Figure 9.2 actuators will be placed on the added wings. More information on how the lift requirement will be met can be found in subsection 5.3.2 and subsection 5.3.3 where pressure distributions have been plotted in Figure 5.6 and subsequent figures.

9.8.1 Actuator types

There are many different actuator types available, but not all are considered viable for aircraft. For example, piezoelectric actuators will be ignored as the forces are negligible with respect to the size of the control surfaces. When discussing actuator types, accuracy and repeatability are considered. Accuracy is a measurement of how much error in position the motor will reach. Repeatability is the measure of how well the position can be reached time and time again. High repeatability will mean a predictable performance.

- **Pneumatic linear actuator:** pneumatic actuators are actuated by pressurized air, producing linear motion. Pressure is added from an external compressor to the cylinder to force a piston through the hollow cylinder. The cylinder can be returned to its original position either with a spring force or by adding fluid on the other side of the piston[37]. Pneumatic actuators are simple designs and they are cheap, durable and lightweight. Pneumatic actuators do however need to compress air with an electric to pneumatic conversion efficiency loss. A compressor must also run continuously, regardless of whether or not the rod is moving.
- **Hydraulic linear actuator:** Hydraulic actuators are actuated by incompressible liquids. Hydraulic actuators can produce forces up to 25 times greater than pneumatic cylinders of equal size and can have the pumps placed at a considerable distance from the actuator with minimal power loss. Hydraulic actuators will however leak fluid, leading to problems with other components and environmental hazards. They also have many companion parts such as fluid reservoir, pumps, motors, valves heat exchangers, noise-reduction equipment. This makes hydraulic actuators large, heavy, maintenance intensive and difficult to incorporate into the design.
- **Electric actuator:** Electric motors convert electricity into torque directly[38,39]. This torque can be changed into a linear motion with a mechanical conversion such as a ballscrew. Electric motor design has many different options are available for accuracy, strength, controllability, speed, size and cost. Electric actuators also offer the highest accuracy and repeatability.
  With the use of backlash free planetary gear boxes or harmonic gear boxes in a rotary actuator, the generated torque can be multiplied for a speed sacrifice. With the use of servo motors, the desired controllability can be achieved. Electric motors have a "rated torque" below the maximum torque. If it operates above the rated torque the motor will generate heat. Using an encoder feedback loop and a synchronous electric motor, a servo motor is able to hold deflection angles regardless of the variable forces acting on it. When considering electric actuators, servo motors are the highest performing options and will thus be added. Choosing and sizing the electric motor will be done by an external party when considering servo motors.

9.8.2 Actuator type selection

A table is made to compare the advantages and disadvantages of different actuator types. This table concludes the arguments of this chapter.

[37] http://machinedesign.com/linear-motion/what-s-difference-between-pneumatic-hydraulic-and-electrical-actuators [cited 23 December 2016]

[38] http://www.kollmorgen.com/uploadedFiles/kollmorgencom/Service_and_Support/Knowledge_Center/White_Papers/Growing%20Trend%20of%20Electrical% [cited 12 January 2017]

[39] http://www.icas.org/ICAS_ARCHIVE/ICAS2006/PAPERS/736.PDF [cited 20 January 2017]

Table 9.3: Advantages and disadvantages of different actuator types.

Actuator type	Advantages	Disadvantages
Pneumatic	• Cheap • High acceleration • High speeds • Durable	• Compressible gasses • Low force • Low controllability • Compressor increases weight and power consumption • Piping increases weight
Hydraulic	• highest force • moderate speed levels • high accelerations • high stiffness	• Can leak hazardous liquids • Requires position feedback • External hydraulic pump necessary • High maintenance • Expensive • Heavy • Electric to hydraulic energy conversion • Low ambient pressure at high altitude
Electric	• Cost efficient • Repeatable • Accurate • Scalable • Position feedback • Identical behavior extending or retracting • Low maintenance • Low part count	• Temperature sensitive • High initial cost • Requires driver

From Table 9.3 and the reasoning discussed in section 9.8 a clear winner emerges; the electric actuator. With high accuracy and repeatability, high design variability, low long term cost and high sustainability, the electric actuator will be used for the IFS. This is to be expected as the aerospace industry is slowly moving towards electric[40,41]. What kind of electromechanical actuator will be chosen and many design options will be discussed in later portions of the chapter.

9.8.3 Actuator - aircraft connection type

Now that an actuator type has been chosen, it is time to decide how to implement it. The actuators have to use the fixed wing structure to push, pull or torque the flap to its desired location. The different options for connecting the actuators will be discussed in this chapter.

- **Linear actuation:** the linear actuator has been used by aircraft in the past many times in the hydraulic format as this linear actuator type is able to generate very large forces at a moment arm. This project however, an electric actuator will be used. Electric actuators are very versatile in design and can reach high forces[42]. Making a linear actuator rotate a flap upwards and downwards can be done inside the wing through the implementation of some compact mechanical systems. One that has been used before in aviation is the hinge triangle configuration as shown in Figure 9.15 where the flap is held at the top hinge and pushed on the bottom hinge by the actuator. There are also other options that are a little more complex such as an articulated hinge system.

[40] http://www.ainonline.com/aviation-news/2006-09-12/upstarts-favor-electric-while-establishment-sits-fence [cited 16 January 2017]
[41] http://www.icas.org/ICAS_ARCHIVE/ICAS2006/PAPERS/736.PDF [cited 16 January 2017]
[42] http://www.actuators-electric.co.uk/electric-linear-actuators-faqs/ [cited 10 January 2017]

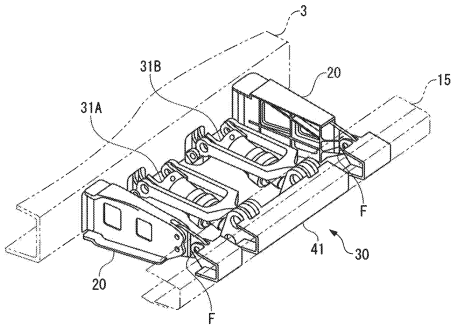

Figure 9.15: Interface between wing and a simple linear flap actuator.[43]

- **Torque connection:** a torque connection can be done with a direct drive for maximum efficiency or with a gearbox connection reducing efficiency and speed but increasing torque. The stator would need to be mounted to the wing box and the rotor to the flap.
- **Belt actuation:** with a belt system torque can be translated while maintaining its axis. This would be useful if the electric motor were placed inside the wing box where there is more space than at the flap connection. A belt would need to run through the wingbox from the motor to the flap hinge. This option is not often used in aviation due to the weight and the moving parts.
- **Gearbox addition:** adding a gearbox to an electric motor can increase the torque output by factors of 100 or more. Usually, factors of more than 30 are undesirable for backlash reasons. Types of gearboxes commonly used are planetary gearboxes and harmonic gearboxes. Harmonic gearboxes are able to have zero backlash with higher ratio conversion but with a factor 10 reduced life span and have a much higher cost. For these two reasons planetary gearboxes are often preferred. Harmonic gearboxes are still a relative new concept (1957[44]) so there is still room for improvement in this technology in the future.
- **Fairings:** these can be added underneath a wing if space is too sparse for the required force. In commercial aviation fairings are often used to accompany the complex flap systems that are required to deflect multiple flaps in only one direction.

9.8.4 Safety mechanism

Safety is always the number one priority in designing aircraft systems. The additional control surfaces will be electrical actuated. This means that if the aircraft loses electrical power or the circuit trips the extra control surfaces can not be operated. Uncontrollable control surfaces are not preferred during an emergency flight. A back up system is made, in order to prevented single point of failure. The approach and the design of the safety system are done as follows:

- **Occurrence:** In the power diagram in Figure 9.25, it can be seen that if the circuit breaker trips, the actuators lose power and cannot be operated. Actuators can contain locking brakes, so that when the power is cut of, the actuator would stay at their last position. There is a possibility that automatic locking is not preferred, because the dynamic behavior of the aircraft can be influenced if the additional control surfaces are locked in high deflections and safe landing will not be possible. However, without the lock, the surface will just be free moving below the possible motions are described. The actuator itself can also break down and the flap cannot be operated. Both risks will be mitigated in order to comply to the safety requirement **IFS-SYS-16**.
- **Control surface motion:** after the circuit breaker trips all electrical power will be lost in the aircraft, this means that the electrical actuators in the boxwing cannot be operated anymore. Three motion modes are described below that can be implemented if the circuit breaker fails.

[43] https://www.google.com/patents/US20140175216 [cited 10 January 2017]
[43] https://www.google.com/patents/US5388788 [cited 10 January 2017]
[43] https://www.google.com/patents/US5388788 [cited 10 January 2017]
[44] http://machinedesign.com/archive/c-walton-musser [cited 25 January 2017]

- **Fixed:** with fixed position, the control surface will be locked in its last position. The actuators can contain locking brakes if the power is shut off. This motion mode has a big disadvantage that in case the safety system trips when having a high control angle, it would affect the behavior of the aircraft. The advantage is that is really easy to implement, because the actuator locks are already placed on the actuators. But because of the unwanted dynamic behavior, this mode is not preferred and will not be accepted.
- **Free moving:** if the circuit breaker trips all power will be switched of and the additional control surfaces can not be operated. With a free moving motion the surfaces will move freely by the wind going over the surfaces. In this case the actuators will not contain the automatics locks, in case of power loss, but will move freely with the airflow. Not knowing how to control surfaces will behave during a safety landing is certainly not preferred and can impair safe operation.
- **Wanted position:** the ideal safety system is that the boxwing control surfaces move to a wanted position even if the main circuit breaker trips. This means adding an additional safety system that can still be operated even when all power is shut off. This motion mode in the wanted motion mode.

With the three possible motions described, it is clear that fixed and free moving control surfaces are not acceptable in order to comply to the safety requirement that there will be no single point of failure. The safe way is the wanted position system, where the control surface will be moved to wanted position of the pilot. In order to move the control surface to a wanted position, a system needs to be designed that can fulfill this need. Below, three design solutions are stated, which shall operate the control surface to the wanted position.

- **Mechanisms:** in order to move the control surface to the wanted control position actuation is needed without the main power supply. Three mechanisms can be chosen in order to get the surface to the neutral position.

  - **Spring:** if the control surface is spring loaded, the spring will bring it back to the wanted position when the power goes off. The problem with a spring system is that the the spring needs to be disengaged in normal operations, otherwise the spring will add an extra load on the actuator, because it needs to overcome the force of the spring and the aerodynamic forces. Another problem is that changing the wanted position is difficult, because a physical change needs to be made to the aircraft in order to change the position op the control surfaces. In this case, the spring system needs to be altered then. In flight this cannot be changed at all.
  - **Battery:** a small battery can be implemented in the boxwing, which can power the actuators for a limited amount of time. If the circuit break is triggered, a sensor will pick up the lack of power and control the the actuators with energy stored in a back-up battery, see section 9.9. In the batteries enough energy is stored to move the surfaces to the wanted position. This option would be highly affective because the position can be set to every position the pilot wants. Depending on the conditions, the safety system can be programmed in flight in case something will happen the pilot will know to what position the flaps go and will have an predictable and controllable aircraft.
  - **Mechanically:** last a mechanical system can be implemented, working with pulleys that can be operated within the cabin of the aircraft. This system will contain cables that are connected to the control surfaces. These wires will run through the wingbox into the cabin. If all power goes off, the test engineer needs to operate these cables manually and set them the the required position. Every flap would need a separate pulley system so the engineer needs to operate all the flaps in case of an emergency. This would introduce the possibility of human error if the engineer is stressed it can set the boxwing control surfaces in the wrong position, or forget is altogether. This system also needs to be disengaged during normal operations or the controls in the cabin will move with the surfaces adding extra force on the actuators.

Considering the three possible design options for the safety system, a trade of has been made, in Table 9.4 the positive and the negative characteristics of the three design options are stated. Looking at Table 9.4 it can be seen that the battery is the most simple system to implement. Because the wing is really thin, the space available is small. Combined with the actuator, the space for a spring system is thus very limited. Also the spring system will need to be disengaged during normal operations of the aircraft. Otherwise, the spring will influence the force that the actuators needs to deliver. This clutch system is hard to implement into the limed space. The mechanism with pulleys will need to be operated from the cabin manual, this would mean that it does not automatically return the control surface to the neutral position this needs to be done by hand. Implementing a system with pulleys will be hard to implement in the original aircraft.

Table 9.4: Advantages and disadvantages of different safety systems.

System	Advantages	Disadvantages
Spring	• Works without power • Automatically operated	• Difficult to implement • Needs to be disengaged during flight • Need to produce a lot of force • No different settings during flight
Battery	• Small dimension • Easy to implement • Controllable	• Batteries can be dangerous • Additional electrical system
Mechanical	• Works without power	• manual operated • difficult implementation in the whole aircraft • Human error

The best choice is implementing the battery system. In Figure 9.16 the layout of the battery system is shown. When the circuit breaker trips, a sensor will measure the lack of power on the main power grid. When a lack of power is measured, it will send power from the back-up battery to the actuators to move them to the neutral position. This system is also shown in Figure 9.25. The systems contains only enough power to move all actuators to the neutral position. In the neutral position the power will be switched off. As stated, the electrical actuators can contain locks for when the actuators lose power. This needs to be implemented in order to stop the control surfaces from freely moving after their are set to the wanted position. The internal brake system of the actuator will engage locking the control axis in place. With locked boxwing control surfaces, the pilot can land the aircraft in a safe manner.
The next risk that needs to be mitigated is sensor failure or safety control system failure. If the sensor or the control system fails, one flap will not be operated. Since the brake works automatically, it will be locked in the last position, which is preferable. In order to reduce the risk, the upper wing control surfaces will be split up. The boxwing will contain four horizontal control surfaces. If in this case one sensor or control system fails, only one control surface will fail. This resultant aerodynamic effect of this failure can be counteracted by the other three surfaces. This will comply the the safety requirement that there shall not be a single point of failure (**IFS-SYS-16**).
The vertical control surfaces are less critical in terms of safety. If one of the vertical wings fails on the flight behaviour, if one fails it can be counteracted with the vertical wing on the other side. This will create more drag then having them in neutral position, but will not endanger the the operations of the aircraft.
As stated in the elaboration on occurrence on page 93, also failure of an actuator can happen. If one actuator breaks down, it will not be a problems, since the horizontal boxwing control surfaces are divided into four parts. As stated, the other surfaces will counteract any unwanted forced that are generated by the broken control surface. Lastly, it will automatically be locked by the locking system on the actuator so it will not be freely moving in the wind.

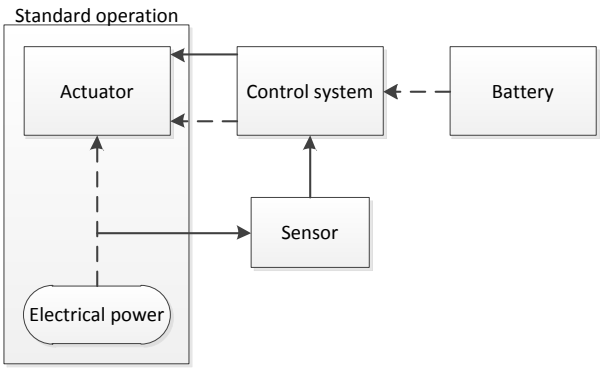

Figure 9.16: Layout of safety battery system.

9.8.5 Actuator sizing

Actuator sizing follows from the values generated in chapter 5 and chapter 8. Actuator systems need to be designed for the upper wings and the vertical wings. The upper wing must carry the greatest load and will present the greatest challenge for design as will be made clear in this chapter. To size the actuators properly, the maximum values have been taken that act on the flap section alone. Information on the lift force is derived from subsection 5.3.2 and subsection 5.3.3 where pressure distributions have been plotted in Figure 5.6 and subsequent figures. This information is then taken and the force acting on the flap is calculated with the procedure mentioned in subsection 8.2.5.

The lift force is located at 1/4 of flap chord location when using the symmetric airfoil [23] for the flap for moment arm calculation purposes. The drag force is assumed to be located on the chord line. The weight of the flap is neglected as the force due to the flap weight is considered small compared to lift and drag. To get the forces which need to be held by the actuator, actuation systems need to be considered. For linear actuation the length of the moment arm is important when used to counteract or generate torque. Due to the limited space available, the arm will be short. A fairing can be placed underneath the wing to accompany an extension of the moment arm reducing the amount of force required.

Table 9.5: List of parameters, measured perpendicular to the trailing edge.

Parameter	Symbol	Upper wing	Vertical wing	Unit
Chord length	c	1,180	1,340	mm
Flap length	c'	543	509	mm
Thickness at flap location	t'	59	78	mm
Maximum flap lift force	L'	4,548	670	N
Maximum flap drag force	D'	4,008	574	N
Maximum flap deflection	δ	20	20	degrees

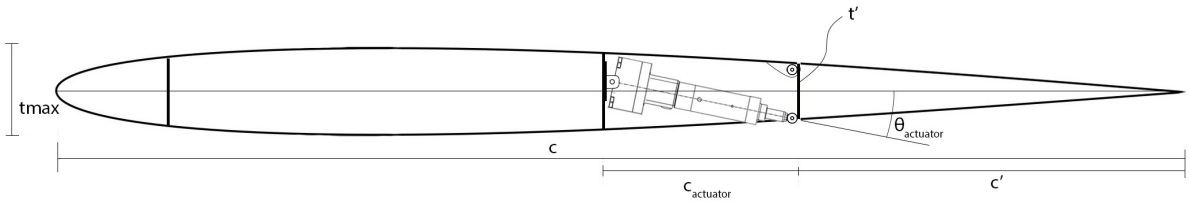

Figure 9.17: Wing and flap structure.

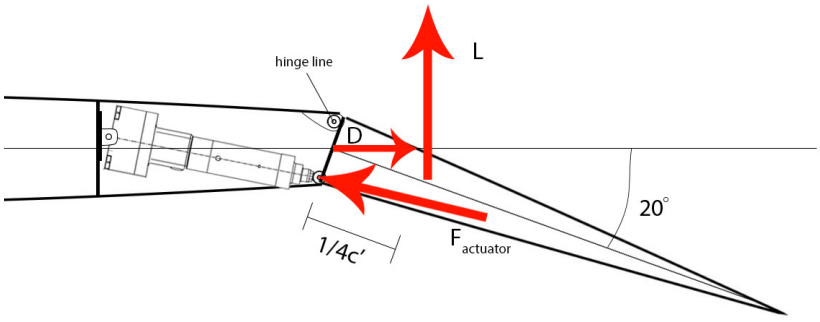

Figure 9.18: Flap load case.

As shown in Figure 9.18, the moments about the hinge line can be expressed with Equation 9.1. A margin of 5% is taken for skin thickness and attachments. A factor of 2 is taken to represent the requirements of a single actuator. Equations can be arranged following from the load case and are shown in Equation 9.1 to Equation 9.4.

$$\sum M_{hinge}^{cw+} = \frac{1}{4} \cdot c' \cdot cos(\delta) \cdot L' + \frac{t' \cdot 0.95}{2} \cdot D' - 2 \cdot F_{actuator} \cdot t' \cdot 0.95 \cdot cos(\theta_{actuator}) = 0 \tag{9.1}$$

Once rearranged and taking the maximum value, the necessary actuator static force can be derived as shown in Equation 9.2.

$$F_{actuator} = \frac{\frac{1}{4} \cdot c' \cdot cos(\delta) \cdot L' + (\frac{t' \cdot 0.95}{2} + \frac{1}{4} \cdot c' \cdot sin(\delta)) \cdot D'}{2 \cdot t' \cdot 0.95 \cdot \cos\theta_{actuator}} \tag{9.2}$$

With a rotary actuator the moments about the hinge axis must be counteracted by the electric motor directly and the hinge line would move to the center, yielding Equation 9.3.

$$\sum M_{hinge}^{cw+} = \frac{1}{4} \cdot c' \cdot cos(\delta) \cdot L + (\frac{1}{4} \cdot c' \cdot sin(\delta)) \cdot D - 2 \cdot T_{actuator} = 0 \tag{9.3}$$

Once rearranged, the necessary actuator static torque can be derived as shown in Equation 9.4.

$$T_{actuator} = \frac{\frac{1}{4} \cdot c' \cdot cos(\delta) \cdot L + (\frac{1}{4} \cdot c' \cdot sin(\delta)) \cdot D}{2} \tag{9.4}$$

Concluding from these equations the following required forces and torques have been determined: For the upper wing a force of 4632N or a torque of 290Nm would be required. For the vertical wing a force of 1318N or a torque of 40Nm would be required.

9.8.6 Actuator selection

When selecting an electric actuator, it is important to consider temperature. An actuator will have two main torques to be analyzed. The first torque is the rated torque, which involves the maximum torque that it can handle without generating any heat accumulation. The second torque is the maximum torque defined as the maximum torque that the actuator can provide while adding heat to the system. This is for dynamic loading capabilities. The generated heat can be cooled off if the actuator operates below the rated torque. Actuators have been sized according to the rated torque. Actuator maximum static torque will not exceed the rated torque so that it will have a natural cooling when operating at maximum conditions. The aircraft will not always operate under maximum loading conditions, so there will be increased cooling during these configurations. Under high dynamic loading conditions such as a storm, it is possible that the actuator will heat up to temperatures that can cause damage to the electric motor and surrounding conditions. In this case, the driver will receive feedback from the actuator positions and torques, from which it will conclude that the electronics are reaching dangerous temperatures and it thus needs to cool down. The cool down time is called dwell time. The IFS can be disengaged for a necessary amount of time until the actuators are cool enough to operate again.

9.8.7 Linear actuator

As follows from extensive research, advice from an expert in the field, Mr. Damman, and many iterations of the design, two options made it to detailed evaluation. An actuator has been chosen from the company "Bosch Rexroth Group" [45] [46] with the apex dynamics AB115-030-S2-P2 gearbox[47] for both cases. The selected electromechanical linear actuator is the EMC-32 with the MSK030 electric motor, a screw drive diameter of 16mm and and screw drive lead of 5mm for the upper wing and a brake extension for safety. This gives an actuator maximum force of 4,500 N and a dynamic force of 12,300 N which is sufficient. This actuator has an accuracy of 0.5% and a repeatability of 0.25% of the operating range. This leads to a total maximum control error of 0.75%, which make sure it complies to requirement **IFS-SYS-09**. This is one of the shortest electromechanical linear actuator available from Bosch Rexroth group. Unfortunately, this option is not short enough to fit into the wing without placing the actuator inside the wingbox or reducing the chord-wise size of the wingbox considerably. Because of maintenance issues, a decision has been made to place the actuator between the flap and the wing box. This eliminates the possibility of using a linear actuator due to the limited size.

[45] http://www.boschrexroth.com/various/utilities/mediadirectory/index.jsp/?publication=NET&remindCcat=on&search_action=submit?&ccat_id=11680&search_
GB [cited 18 January 2017]

[46] http://www.boschrexroth.com/various/utilities/mediadirectory/index.jsp/?publication=NET&remindCcat=on&search_action=submit?&ccat_id=11680&search_
GB [cited 18 January 2017]

[47] https://www.apexdyna.nl/nl/design-tool [cited 18 January 2017]

9.8.8 Rotary actuator

Another appropriate option that has presented itself after many iterations of flap size, airfoil type and force applied to the flap is the electromechanical rotary actuator. A rotary actuator, a fitting electric motor and gearbox will be able to achieve the required torque at a high enough speed. The chosen electric motor-gearbox combination is the MSM041B-0300 electric motor for the upper wing with an AB115-030-S2-P2[48,49] planetary gearbox. This actuator also has an accuracy of 0.5 % and a repeatability of 0.25 % of the operating range, which ensures that this actuator choice also complies to requirement **IFS-SYS-09**. Using the rotary actuator option would require a torque of 290 Nm. The chosen actuator and gearbox combination will provide a rated torque of 310 Nm and a maximum torque of 558 Nm and have a brake extension for safety. This will generate 20 Nm more than maximum static operating conditions which is considered beneficial for cooling purposes. The gearbox will have a ratio of 30 which is within desirable ratios when considering backlash. Once the final values are reached, it becomes clear that the linear actuator does not fit in this design. For this reason, it was scrapped before starting the sizing of the vertical wing actuators. When designing the vertical wing actuators, only the rotary actuators were considered. Two MSM030B-0300 electric motors will be used for each vertical wing, each with a apex dynamics AB060-030-S2-P2 planetary gearbox resulting in a rated torque of 55 Nm and a maximum torque of 99 Nm. The vertical wing actuators will also need fairings as the available thickness at the hinge location is 78 mm and the gearbox has a diameter of 80 mm. This would result in 1-2 mm of fairings sticking out on each side of the wing. The width of each fairing would be 65 mm. Fairings will be neglected for aerodynamic properties as they are considered small. Clearance space is shown in Table 9.5.

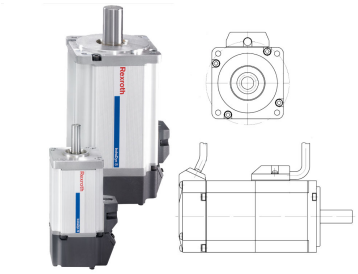

Figure 9.19: Chosen actuator type.

The reason for choosing the aforementioned actuators is that these actuators provide slightly more rated torque than the required static torque for cooling purposes and fit in the available space. While there is a lot of design space for electric actuators, these actuator-gearbox combinations were the only logical choices available. Other options may arise if extensive research is done in actuators provided by companies other than Bosch Rexroth group and Apex Dynamics.

- **Mass:** the chosen rotary actuators have a mass of 9 kg in the upper wing and 1.5 kg in the vertical wing, increasing the total mass of the actuators to 42 kg. This does not include the drivers or the mounts.
- **Actuator lifetifme:** if the actuator is operated within the parameters it is designed for, the life of the actuator will reach 20,000 hours. If the actuator operates above the allowed radial force the service life will be reduced according to Equation 9.5, where L_{10h}, F_{Radial} and $F_{Radial_{act}}$ stand for bearing service life (hours), determined radial force (N) and actual radial force (N), respectively.

$$L_{10h} = \left(\frac{F_{Radial}}{F_{Radial_{act}}} \right)^3 \cdot 20,000 \tag{9.5}$$

  For this reason, radial force will be supported by structures inside the airfoil along the span holding the flap in place by its hinge axis. Radial force defined as the force acting perpendicular to the torque axis as shown in Figure 9.20. More information on the hinge structural support can be found in chapter 8. In order for the electric actuators to forgo any radial forces the motor will be mounted on a connected pendulum system. An example of this mechanism is shown in Figure 9.21 where the actuator is free to move in the z-axis but is still able to hold the torque.

[48] http://www.apexdyna.nl/en/design-tool[cited 16 January 2017]
[49] http://www.apexdyna.com/download/catalog/AFAFR-Eng.pdf [cited 20 January 2017]

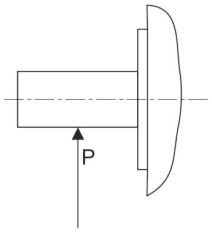

Figure 9.20: Radial force, shown as P.

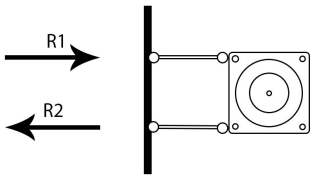

Figure 9.21: Connected pendulum system avoiding radial forces on electric motor shaft.

- **Driver:** a driver is required for each actuator to makes sure that the actuators do not stress themselves beyond their available capacities. Drivers will provide feedback on power consumption and in turn be able to deduce the applied forces on the flaps.
- **Cooling:** electric motors are often not designed to be operated above certain altitudes due to the drop in air density. This drop would decrease the passive cooling of the electric motor substantially in normal operating conditions. The chosen electric motors are not to be used above 4 km for this reason. An inlet system would need to be designed to regulate the temperature of the electric motors. The temperature can be regulated without problems when flying at speeds in the order of mach 0.65.
- **Actuator acceleration:** actuator acceleration is not given in the manual, but can be easily derived from available torque. In Equation 9.6, this acceleration is given. The mass of the flap has not been calculated in other chapters, so a quick estimation will be used to find the acceleration of the flaps.

$$a = \frac{T}{m} \tag{9.6}$$

  The masses of the flaps were taken as a percentage of the wing mass according to the area percentages. This results in rough yet conservative estimates of a mass of 3,9 kg per upper flap, for a total of four flaps, and a mass of 1,67 kg per vertical wing flap, for a total of 2 flaps. When matching each flap with its respective actuator torque values, the accelerations of each flap becomes 40 m/s^2 for four upper wing flaps, and 65 m/s^2 for two vertical wing flaps. According to **IFS-SYS-08-AERO-04** the IFS shall be able to generate direct lift. While the actuators cannot generate direct lift as this would imply an instantaneous deflection, the actuators seem to have the capability to move flaps at excessive accelerations that would likely tear the hinge mount. For calculation purposes a direct lift can be assumed and for practical purposes an adequate acceleration speed would have to be calculated as not to tear the hinge from the flap and structural attachments.
- **Price:** each actuator package has an approximate cost of €2,200. This includes the actuators as well as the gearboxes and drivers. Multiply this by 8 and the total price would add up to €17,600 in total.

9.8.9 Actuator connection

Integrating the electromechanical rotary actuator into the wing will be done by attaching the stationary part of the electric motor, the stator, to the wing box while attaching the rotating part of the electric motor, the rotor, to the flap. The benefit of this location is that the actuator will be connected to the wingbox directly and will have easy access for maintenance without decreasing wingbox strength.

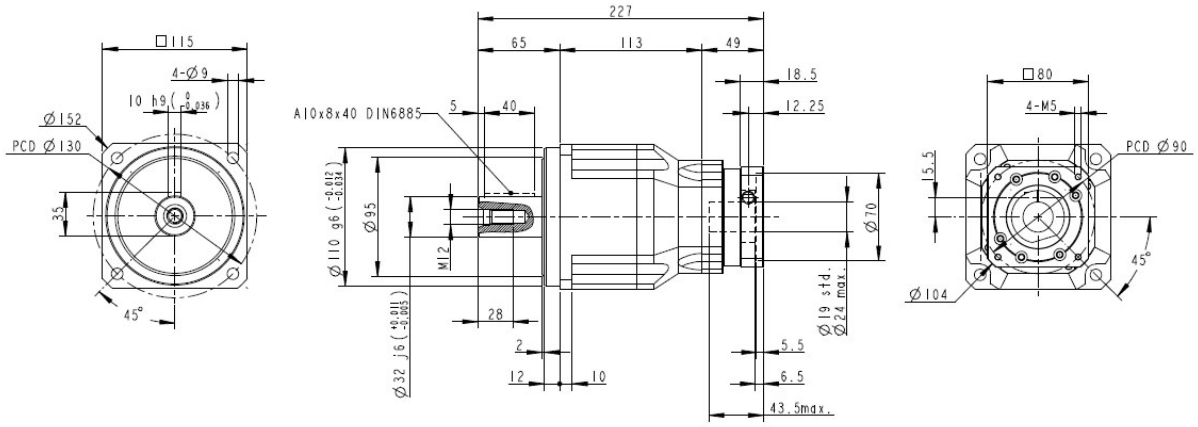

Figure 9.22: Technical drawing of the gearbox.

In Figure 9.22 the dimensions of the gearbox are shown. What is important in fitting the actuator inside the wing is the maximum diameter of the gearbox as these dimensions will need to fit inside the the airfoil in neutral position and while the airfoil is being deflected. It is found that the thickness of the airfoil would have to be incorporate the gearbox dimension of 152 mm while the airfoil thickness is only 129 mm at this location. To fit this design inside the airfoil a fairing will need to be placed around the gearbox. The fairing would stick out of the airfoil by 11.5 mm on each side. In the span-wise direction the gearbox will take up 113 mm. This will need to be taken in by the span-wise thickness of the fairing and will result in four fairings on the upper wing, each 117 mm in the span-wise direction and 12 mm in the thickness direction. Two fairings on the top of the upper wing and two on the bottom. Figure 9.24 shows the fairings with the maximum deflection angle encompassing the gearbox. The electric motor has been chosen to fit inside the airfoil and will not require a fairing as this would greatly increase the span-wise fairing and should be avoided.

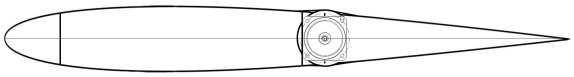

Figure 9.23: Rotary actuator connection.

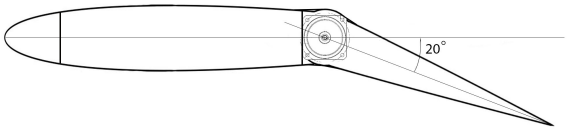

Figure 9.24: Rotary actuator deflected.

9.8.10 Requirements

In this section already some requirements have been fulfilled, however there are several other requirements which still need to be assessed. These are requirements **IFS-SYS-09-SENS-05**, **IFS-SYS-09-SENS-06** and **IFS-SYS-09-SENS-07**, which state the error of the actuators of the original control surfaces. However these actuators will not be replaced and it is assumed the errors of the original actuators will be small enough to provide the desired aircraft behaviour. Therefore these requirements will be dropped. Also **IFS-SYS-09-SENS-08** is dropped since no throttle actuator is present.

9.9 Electrical power distribution

In order to power the added system an additional power system is needs to be implemented to the aircraft, in section 4.3 the FBS is given, at block *3.2.3.1* is stated what systems needs to be powered by the power system that will be implemented.

As mentioned in subsection 9.6.1 the existing generator output will not suffice to power all the extra systems. An overview of all the added system is given in Table 9.6a[2,18,27,1,34,35,50,51,52] and Table 9.6b[52].

Table 9.6: Power load distribution per sub-systems.

(a) Power distribution regarding the simulation battery.

System	#	Power (W)
Sidestick	1	20
Test engineer laptop	2	45
Test pilot monitoring	1	72
Cameras	2	13
Camera recording	1	10
SCS	1	90
Synchros	20	1
Engine sensors	11	5
Power sensors	12	<1
Data computer	1	50
Communication computer	1	50
Basic control actuator	3	201
Drag chute deployment	1	<1
Total power:		1,083

(b) Power distribution regarding the back-up battery.

System	#	Power (W)
Upper wing actuators	4	1,130
Side wing actuators	4	201
Drag chute disengage	1	<1
Total power:		5,321

When there is a dual generator failure the standard aircraft should have electricity for the emergency systems for 45 minutes[53]. The systems on the sim battery do not need to be powered for that same time, however to be able to analyse why the safety system was tripped it is preferred that the sensors and data gathering system will be powered for at least 10 minutes after generator failure. The laptops in the test engineer station will have their own batteries and the basic control actuators will be disengaged straight away. Also the drag chute will not be deployed in case of a failure, leaving a total power needed for the other systems of 418 W. As stated in subsection 9.6.1 the aircraft generators produce 24V DC and given the time power is needed of 10 minutes, the battery will need a capacity of at least 2.9 Ah. An option for this is the Concorde RG-121-4 aircraft battery[6], with a C1 rated capacity of 3.3 Ah, where C1 means that the battery will be able to provide 3.3 Ah for 1 hour until it is discharged completely. This battery has a weight of 4.6 kg and costs €2,140.

The actuators on the boxwing and the drag chute control will be directly powered from a bus that is connected to a generator. The drag chute deployment does not need to be powered when an electric power failure occurs, however the quick release system should be able to immediately release the chute, hence a back-up battery is needed. Also the boxwing actuators should be powered, but only long enough to deflect the boxwing control surfaces to the desired emergency configuration. Both the drag chute release and the control surface configuration can be done in a few seconds. A battery will not be able to discharge fast enough to power the actuators as fast as normal, however almost instantaneous actuation times are not needed. It is assumed that a battery will be able to provide enough electricity to power the actuators for several seconds, but at a lower speed. Both the drag chute deployment and disengagement has a power usage of <1 W, which is due to the fact both mechanism will be either spring or air loaded and the only power usage will be sending the signal to the mechanism.

The overview of the power system is given in the electric block diagram in Figure 9.25. The components described above will be shortly mentioned again to explain their placement in the diagram. The electric system is powered by two generators, both connected to a battery management system. Each generator has two battery management systems, which in turn are connected. This connection is used in case of a generator failure, so one generator is able to power all the necessary buses. The original system is not changed and consist of 2 batteries (battery 1 and 2), a DC/AC converter and 2 buses (one AC and one DC). Two additional batteries will be added for

[50] http://www.ad-aero.com/video_servers.php [cited 19 January 2017]

[51] http://avionics-networking.com/av_vn0601_en.html?gclid=CjwKEAiA79zDBRCgyf2FgeiY-CESJABzr0BMq0Ty_fM9f6T-tDfm_Dp_q1bPXMqt3I98PI7N2r5ZaxoCl4jw_wcB [cited 19 January 2017]

[52] http://www.apexdyna.nl/en/design-tool [cited 17 January 2017]

[53] http://phenom.aero/resources/library/Phenom300_QuestionBank.pdf [cited 18 January 2017]

the IFS, each connected to a HOT bus and a normal bus. The HOT buses will power the sensors, data gathering and drag chute release. In case of electric power failure also the boxwing actuator will be powered via this bus. In normal operation the boxwing actuators will be powered directly via the battery management system. The 24V DC power from the generators will directly by transformed in 37V AC power which is the voltage input of the actuators. This is done as close to the generators as possible, since this will lower the amperage and thus smaller cables are required. Based on the total power need (Table 9.6b) and a voltage of 37V, the amperage is still 72A per side. Given the actuators are placed close to the generators , since the upper wing draws the most power but is situated closest to the engine/generators, the additional weight of thick cables is negligible in comparison to regular power cables.

There is a requirement on the maximum electrical power consumption, namely **IFS-SYS-03**. This requirement will be dropped because of the fact new generators will be added to the aircraft engines. The requirement was made with the idea that the added electrical system would run on the already available generators, however this is in no way possible. To overcome this problem new generators will be implemented, which do not yet have a maximum power output.

The current power output of the aircraft is 19,200 W, based on 2 generators which provide 24V rated at 400 A. The extra needed power will be around 6,400 W, which is an increase of 33 percent. It is assumed the new generators will be powerful enough to provide this increase in power demand since the engines are relatively powerful for the Embraer Phenom 300. The heavier generators will lower the thrust output of the engines, which makes it impossible to meet requirement **IFS-SYS-01-PROP-01**. This requirement states that the thrust output of the IFS shall be at least equal to the base aircraft. However the engines are powerful enough to power the aircraft, even with a slightly lower thrust output. Besides this it can be investigated in future research whether it is a possibility to fit the aircraft with a different engine version of the PW500 series[54]. For example the Embraer Phenom 300 is fitted with the PW535, while the PW545 delivers 15% more thrust. As a result from this it can be concluded that the requirement is partially met, since the aircraft has enough thrust to operate. However it is not equal to the thrust of the base aircraft.

[54] http://www.pwc.ca/en/engines/pw500y [cited 24 January 2017]

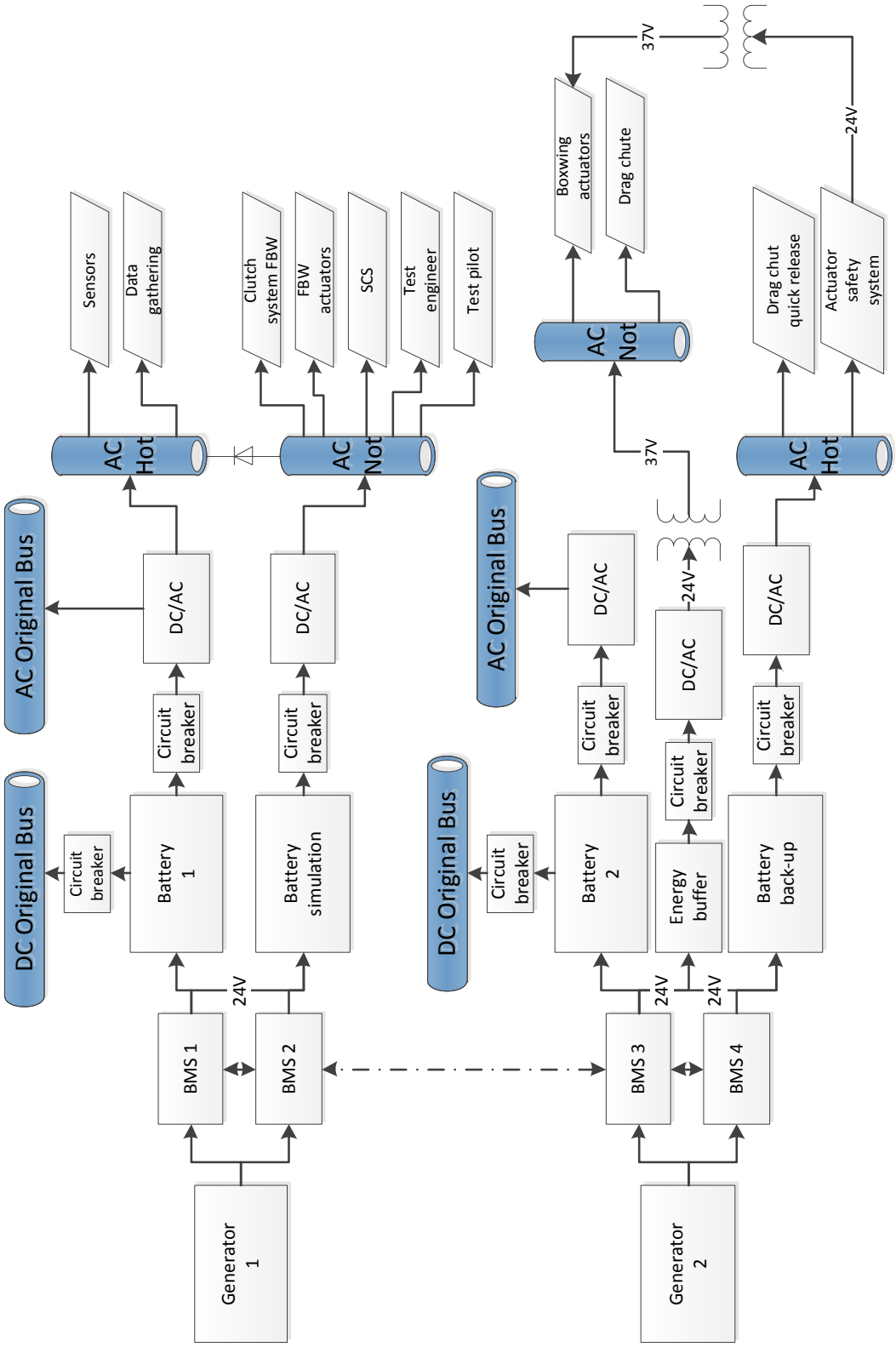

Figure 9.25: Electric block diagram.

9.10 Cost of components

In this section an overview is given of all the costs of the components discussed in the ESA chapter. The overview as displayed in Table 9.7[1,2,3,6,26,35,34,50,55] is based on reference data, estimates and telephonic/mail contact with the producing companies. All components for which exact prices have been found, a footnote is added with the reference. All prices indicated with a '*' are prices which are based on estimates. These product prices are not commercially available and the companies are not willing to provide pricing information. These estimates are based on comparable or secondhand products. Lastly the products indicated by '**' are based on telephonic/mail contact with the companies that produce or distribute the products. As can be seen in Table 9.7 the total cost of the ESA is €101,351. It should also be noted that the amount of laptops for the test engineering station is equal to 4, whil only 2 are needed. This is done since the computing components should be able to be operative for 10 years according to requirement **IFS-SYS-25**. The laptops are estimated to have a lifespan of 5 years, hence a replacement for both is included in the cost. All other computing components will be aircraft grade and it is assumed they will have a lifespan of at least 10 years. This fulfills the requirement.

Table 9.7: Cost division per sub-system regarding the ESA department.

System	#	Cost (€)	Notes
Sidestick	1	15,000	*
Test engineer laptop	4	769	
Test pilot monitoring	1	7,138	
Internal camera	1	300	*
External camera	1	500	*
Camera recording	1	1,000	*
SCS	1	10,000	*
Synchros	20	300	
Engine sensors	11	300	*
Power sensors	12	300	*
Data computer	1	1,000	*
Communication computer	1	1,000	*
Primary control actuator	3	2,200	**
Drag chute deployment	1	10,000	*
Drag chute quick release	1	4,882	
Data logger	2	740	
SCS rack	1	5,585	
Actuators side	4	2,200	**
Actuators upper	4	2,200	**
Simulation battery	1	2,128	
Total cost:		**101,351**	

[55] http://www.seacatch.com/prices.htm [cited 23 January 2017]

10 | System Characteristics

Following the trade-off presented in the Baseline Report [9] and the initial design considerations presented in the Mid-Term Report [10], the Embraer Phenom 300 is used as a base for the IFS. It is a light business jet featuring low sweptback wings with winglets, a T-tail and two rear-mounted Pratt & Whitney PW535E turbofans. The aircraft's main dimensions are given in table Table 10.1a. The fact that a light business jet that is currently in production is chosen as a platform directly satisfies requirements **IFS-SYS-22** and **IFS-SH4-01**. This chapter serves to outline all of the system characteristics of the IFS and will refer to the modification designs made elsewhere in this report. In section 10.1 will be presented some key parameters defining the system and section 10.2 will present technical drawings to clarify the configuration and layout of the IFS. The planform is also shown in section 5.1.

10.1 System characteristics of the IFS

The cockpit of the Embraer Phenom 300 provides space for two pilots, the cabin normally provides space for up to 8 people. The aircraft is certified to be operated by a single pilot [1]. Both the cockpit and the cabin are completely rearranged in the IFS. The layout of the individual stations built in the new system and their integration into the existing aircraft is discussed in section 9.3. The manner in which the individual stations are used in normal operations is described in chapter 11. The change in operational costs is discussed in section 12.1.

The modifications on the Embraer Phenom 300 only have a minor impact on the general performance of the aircraft, as explained in section 7.4. Therefore it can be assumed that both the ceiling and maximum airspeed of the aircraft are within 5% of the Phenom 300 values. The original values, stated in the Mid-Term Report [10], are far above the required values, namely a ceiling of 13,716 m versus a required value of 10,668 m from requirement **IFS-SYS-02** and a maximum airspeed of 0.78 M versus a required value of 0.65 M from requirement **IFS SYS-01**. The new system values are shown in Table 10.1b.

Given the fact that the useful service life of aircraft is generally assumed to be 20 years or more [2], it is expected that the developed system will be able to operate safely for at least 20 years. This is supported by the proven structural design of the modifications presented in sec:results and the substantial funds allocated for maintenance during the operational life of the IFS. Following from these system characteristics is the conclusion that **IFS-SH5-01** and **IFS-SYS-23** have been met. Following this, several other system characteristics can be defined [3,4] [36] [37]:

- **Avionics:** originally equipped with three 1280x800 pixel WXGA displays, two PFD one MFD controlled with 2 touch-screen controllers, dual integrated solid-state AHRS, dual integrated RVSM-compliant digital air data computers, EICAS, integrated Class-B TAWS and integrated Mode S transponder. Additions to these systems are given in section 9.4 until section 9.8.
- **Environmental control system:** pressurization to 0.65 bar, air-conditioning and two-zone temperature control.
- **Power system:** present are a MG103 generator and two lead-acid batteries. There is no APU pre-installed. Section 9.9 describes the additions made in the IFS design.
- **Fuel system:** consists of one tank per wing connected by cross-feed They have a total capacity 3,052 L. Fuel usage is discussed in section 7.4.
- **Hydraulics system:** pressure at 207 bar, powered by two engine-drive pumps.
- **Aerodynamic surfaces:** next to the ailerons, spoilers and flaps already present on the Embraer Phenom 300, there were some additional aerodynamic added to create the variable stability aircraft. These surfaces are discussed in section 5.3 and section 5.4
- **Control and stability:** using a renewed location of the center of gravity calculated in section 7.1, control and stability characteristics of the system were explored in chapter 7. Characteristics such as the balanced field length are elaborated upon in section 7.4.
- **Safety measures:** stick pushers and SPWS. Two fire extinguishers, one in the cockpit and one in the cabin. Smoke detectors in the luggage compartments. Oxygen masks for emergency use available to all occupants.

[1] http://www.embraerexecutivejets.com/Brochures/brochura_phenom_300.pdf [cited 9 December 2016]
[2] https://www.iata.org/publications/Documents/Airline-Disclosure-Guide-aircraft-acquisition.pdf [cited 24 January 2017]
[3] https://janes.ihs.com/Janes/Display/1344700 [cited 7 December 2016]
[4] http://phenom.aero/resources/library/Phenom300_QuestionBank.pdf [cited 7 December 2016]

Table 10.1: Embraer Phenom 300 dimensions and performance parameters.

(a) Key dimensions.

Parameter	Value	Unit
Length	15.64	m
Height	5.10	m
Wingspan (with winglets)	15.91	m
$\Lambda_{0.25C}$	25	deg
S	28.5	m^2
A	8.9	-
Cabin length	4.50	m
Cabin height	1.50	m
Cabin width (max)	1.55	m

(b) Key performance parameters.

Parameter	Value	Unit
Fuel consumption	662.36	L/h
MTOW	8,150	kg
Take-off distance	956	m
Ceiling	10,668	m
Maximum airspeed	0.65	Mach

10.2 Configuration and layout of the IFS

A basic CAD model of the Phenom 300 was constructed in CATIA. According to the design presented in chapter 5 and chapter 8, a detailed model was constructed of the boxwing structure. The model of the boxwing was then implemented in to the model of the Phenom 300. The technical drawing shown in Figure 10.1 provides some general dimensions, with a focus on the dimensions of the vertical and upper wings and flaps. The planform of the added wings is described in more detail in chapter 5, the specific dimensions of the wingbox structure is explained in section 8.4 and the dimensions and types of the additions done by the ESA department are described in full detail in chapter 9.

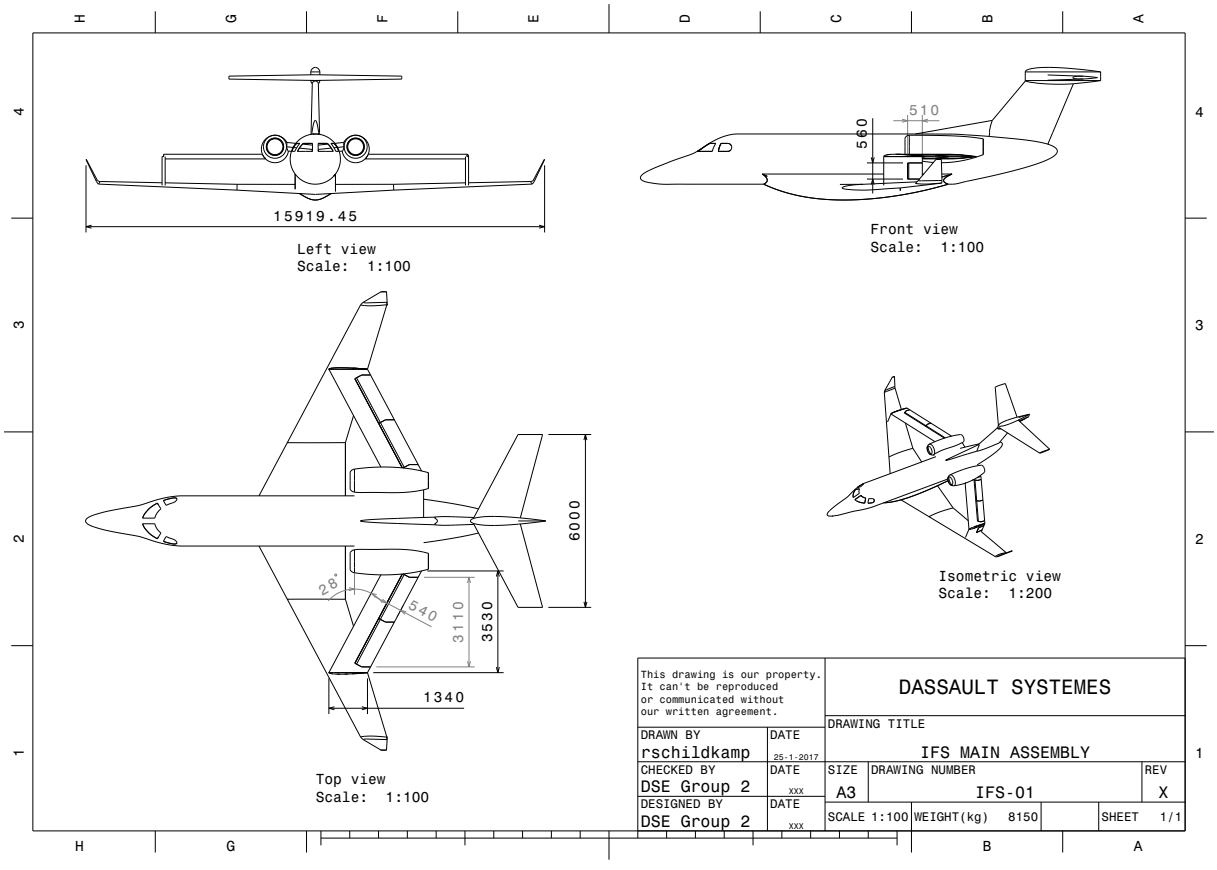

Figure 10.1: Technical drawing of complete IFS.

11 | Operations and Logistics

The operations and logistics concerning the IFS will be covered in respectively sections 11.1 and 11.2 of this chapter. Well defined operational procedures and proper logistic operation are boundary conditions for the product to become successful. Again, as explained in chapter 2, a division is made between the developer and the operator. The operations part of this chapter will cover the way in which the customer for the IFS, so the operator, will work. The logistics part will treat both the developer as the operator of the IFS.

11.1 Aircraft operations

The way the IFS is operated has an influence on the design. Also, a well-designed product is worthless, if one does not know how to operate it. For these reasons, this section will elaborate on the major aspects of the operations of the IFS for the party buying the system. This includes customer contact, the simulation procedures and maintenance [38].

11.1.1 Customer contact

Independent of the type of simulation, the contact between the operator and end user starts with a thorough description of the needs of the customer. Hereafter, it will be sorted out whether these needs can be fulfilled straightaway, or if a modification of the IFS is necessary. If a modification is necessary, its implications will be taken into account in the planning and cost estimation that will follow. An elaboration on the possibility of IFS modification is given in subsection 11.1.2.

In the preliminary planning phase, all actions required to successfully fulfill the customer's needs will be quantified in terms of time. It will be taken into consideration whether actions need to be performed sequential or whether they can be done at the same time. Meanwhile, the cost of the project needs to be determined. If both the time planning and the cost estimate are accepted, agreements in the form of contracts can be made and the project will be performed according to these agreements.

A more detailed planning and a more precise cost analysis will be performed and delivered to the client directly after the agreement has been made. Moreover, the client will be kept up-to-date on the overall progress.

11.1.2 Modification

As stated in section subsection 11.1.1 there is a possibility the aircraft has to be modified internally or externally to meet the client's demands. For the two different segments as described in chapter 2, variable stability training and the testing of new aircraft handling characteristics, different prepareations have to be done. This mostly considers modifying the SCS as described in section 9.5. For the training of pilots with variable stability a standard configuration can be used, while new aircraft characteristics will require a tailored implementation into the SCS. Most of these modifications will take some time to implement and certify on the aircraft, but the modifications consist mainly of programming. The IFS is designed in such a way that programming changes to the SCS will not have to be certified. This also can be done anywhere and send to the location where the aircraft is located. Then it can be uploaded into the SCS so that the aircraft does not have to be relocated.

A larger modification would be to remove the boxwing from the IFS. This is possible since hinges are used for the attachment of the boxwing to the Phenom 300 as described in chapter 8. There are two cases for which this could be wanted. The first one is that for some reason the end user would not want to test their aircraft characteristics with the boxwing attached. Since it will not make renting the aircraft cheaper, one would only possibly preferring flying without the boxwing to have a more accurate simulation for some cases. Aside of the removal of the boxwing also the SCS has to be reprogrammed for this configuration. The other case is that the boxwing would be detached for relocation purposes. This scenario is further described in subsection 11.2.2. In this case the original FCS will provide to control the aircraft.

11.1.3 Simulation procedure

This chapter describes the procedures that has to be executed for the different possible stages of a simulation mission.

Before test flight
Before a typical flight with the IFS, a pre-flight procedure is performed. Since in this case it involves a test or training flight, the briefing beforehand will be elaborate. The mission profile will be treated as well as the safety procedures. After this the aircraft is inspected and the simulation systems are tested [38].

Test flight
As already described there are two different missions the IFS is designed for. They will be described separately since both segments will have a different flight profile, that can be determined by the operator or the client. They will both start with a take-off with the simulation system switched off however. Also their duration is estimated to be around 2.5 hours on average. Connecting this to the 750 operating hours a year, it is estimated 300 take-offs and landings are performed per IFS each year.

High quality simulation for new aerial vehicles
To test aircraft handling characteristics, the client that will most likely be an aircraft manufacturer would provide their own test pilot to asses the characteristics the IFS is able to simulate. The operating company will provide an experienced safety pilot and a flight test engineer. Also an extra passenger from the client can be taken along for the flight. After take-off the predefined test profile will be flown within the operating limits of the IFS. In the event the drag chute is used to simulate the L/D of 4, this stage of the flight is performed in a clear area close to the airfield. The drag chute can then be dropped and picked up for re-use afterwards. Duration of these flights will be around 2 to 3 hours, but less for a drag chute flight since only one approach can be done.

Variable stability simulation and training of flight test pilot
The training flights will be performed with 3 or 4 people on board: one test pilot instructor, two test pilot trainees that will interchange the position in the cockpit during flight and a flight test engineer provided by the operator. After take-off a training mission profile will be flown by the student test pilots. Being able to let two students fly during one flight is economically attractive, since a more fuel consuming landing and take-off can be skipped, and allows them to learn from each other. The drag chute procedure is the same as that for the simulation of new characteristics mentioned earlier. Since two student pilots have a maximum effective learning time of about 1.5 hours, also these flights will take around 2-3 hours.

After test flight
After the IFS has landed, the data recorded during flight can be transferred by the flight engineer. This data is then used to let the test pilots evaluate on the characteristics of the tested aircraft or their own performance. Also this data can be used to improve the characteristics of the IFS.

11.1.4 Maintenance

In order to ensure safe flight, a viable maintenance program will be in place. Generally, this implies following the original equipment manufacturer (OEM) recommendations and guidelines, as well as those from the engine manufacturer, which are respectively Embraer and Pratt & Whitney.[1] An integral part of this consists of standardized pre- and post-flight inspections. These are described in the aircraft flight manual (AFM). The recommendations and guidelines as well as the AFM will be changed when modifications to the aircraft will be made. [38]

11.2 Aircraft logistics

To be able to perform operations, one has to get both (ground)crew and the IFS in the right place at the right time. This applies to the production, aircraft relocation and maintenance part. A more in depth description about this follows in this section.

[1] http://www.embraerexecutivejets.com/en-us/about-embraer/pages/phenom100-phenom300.aspx [cited 30 November 2016]

11.2.1 Production logistics

To get to the actual product, two main production phases can be distinguished. The first one is the production of the aircraft itself. Since the base aircraft is bought off-the-shelf from Embraer with the minimum amount of interior, this part is not further elaborated on. Although Embraer is a Brazilian company, the assembly site for the Phenom 300 is located in Melbourne, Florida, USA.[2] After being delivered, the aircraft has to be modified at the modification facility which will probably be located in Europe. Performing a ferry flight between these continents has been done many times before and should not lead to any problems in the production process.[3] After the boxwing is added and the rest of the aircraft is modified, it is relocated to the main base of the operator. Here it will start its operational life.

11.2.2 Aircraft relocation

To be able to reach as many customers as possible, it is important to satisfy their needs. One of these needs can be that the end user wants to fly the aircraft at their own location. In that case the aircraft has to make a ferry flight. Since the Phenom 300 is a light jet aircraft with a relatively large range, reaching clients in Europe can be done with a single flight. Other customers are mostly located in North-America, a trip that will take 2-3 stopovers.[4] This is a reasonable number, so this is certainly a service that can be offered. As already mentioned in subsection 11.1.2 the boxwing could be removed for this purpose. However the detached boxwing will not fit through the door of the aircraft and therefore cannot be taken along with the IFS itself. So if the client still wants to use it with the six degrees of freedom simulation the boxwing has to be transported separately or on its normal position on the IFS generating a small amount of drag (as determined in section 7.4). This drag will however not require as much fuel burn as flying with a separate transport aircraft.

11.2.3 Maintenance logistics

To keep the aircraft airworthy, sometimes spare parts will be needed to be able to perform repairs and maintenance. With modern day logistics receiving these parts will not take long after ordering them, so operations will not suffer from waiting long for spare parts. The same applies for when the aircraft requires a repair or maintenance when it is located at the customer's location. When it involves a more complicated repair for example on one of the modifications, a specialized mechanic can be supplied by the operator.

11.3 Manufacture and assembly plan

In order to manufacture the IFS a structured plan is needed. A manufacturing plan and an assembly plan is made to give an estimation on how to build the IFS. In this chapter first the location will be discussed, where the assembly take place and the production of small components. Then the product acquirement will be discussed, how different components will be obtained. Lastly the assembly will be discussed how the various components will be put together and how it will serviced during its lifespan.

11.3.1 Location

In order to produce the aircraft a location is needed where the assembly can take place. This location will be also be the main base from where the aircraft shall be delivered to the customer. Ideally the manufacturing location will be near an airport for easy operation and test possibilities. At the location there needs to be room for a hanger in which the IFS can be assembled and if needed in which it can be stored. Because the engineers are Dutch a location in the Netherlands is preferred because it will enable quick face to face communication and would safe on cost of transporting engineers to a location abroad.

11.3.2 Product acquirement

To build the IFS different components need to be obtained. All the different parts that will be added to the aircraft need to be bought, build externally or build in house. Depending on the location of different manufactures transportation is an issue in order to get the different parts safe and on time in the assembly location.

[2] http://www.ainonline.com/aviation-news/2014-08-26/approval-imminent-embraer-legacy-450/500-us-plant [cited 29 November 2016]
[3] http://www.rocketroute.com/blog/ferry-flights-from-usa-to-europe-via-greenland-and-iceland [cited 29 November 2016]
[4] http://performanceflight.com/charter/range_map [cited 29 November 2016]

Stock products

Not all products will be custom made for the modification of the Embraer, if their is a product on the market that is suitable for the application it is preferred to by that product instead of design it in house. This will safe time and money because no effort has to be made in the design of the products. In the list below an estimation is made on the products that will be purchased externally.

- Sidestick
- Test engineer laptop
- Test pilot monitoring
- Recording devices
- Sensors
- Aircraft computers
- Data gathering
- Drag chute mechanism
- Drag chute
- SCS rack
- Lavatory bags
- Actuators
- Batteries

External production

Some components can not be purchased stock and need to be specifically made for the IFS. In order to reduce cost it is preferred to make the parts internal, but if the expertise or the time is not available it will be made on an external location. The parts that are externally produced are the added boxwing, including wingbox, flaps, attachment hinge and actuator attachment and the drag chute.

- **Wingbox:** the entire wingbox will be made off-site, building an wingbox is an specialized job that takes time and experts to do it right. Building the wingbox in house would mean that personnel needs to be trained that can make wingboxes. Training personal would be costly and would take a long time. Building the wingbox internally would also mean that all the equipment for forming the material will also need to be purchased. Because the amount of airplanes that will be build is limited the investment cost of these machines will not be earned back. Ordering the part externally and assembling internal would still mean that personnel need to be trained, costing money and time.
- **Drag chute:** the drag chute will be produced by an external company. The specifications of the drag chute will be supplied. Because the drag chute will not be used frequently it would not be cost efficient to train a whole team that are able to build drag chutes. That is the main reason that an external company is used.

Internal production

Internal production is the production of parts on site and by the IFS company employees themselves. Building products by the employees themselves means that they need to by schooled and certified to be able to safely build the various components. Because the number of aircraft being build is limited schooling the employees would cost a lot of money in relevance to the amount of aircraft. It is expected that their will not be a return of investment in this schooling. That is why all the components will be produced externally. The employees will only assemble the IFS.

Transport

All the components will be shipped to the assembly plant where the IFS shall be build. This will be done by commercial moving companies.

11.3.3 Assembly

The assembly will be done in house. All the parts will be manufactured externally but will added to the aircraft in the IFS workshop. The assembly will be split up in different components and assembly types complying in the FBS to block *1.7*. The two main types of assembly which can be established are mechanical and electrical. With mechanical is meant bolting and fastening all the new components to the aircraft, attaching the wingbox to the original aircraft and changing the interior. The other main assembly is electrical, this is connecting all the electrical components the the aircraft. Safety is not only concerned on the design but also will be met during the assembly of the IFS in order to comply to requirement **IFS-SH2-03**. To introduce safety and organization to the workspace the 5S method will be introduced to the workspace, seiri, seiton, seiso, seiketsu and shitsuke. Meaning, sort, set in order, shine, standardize and sustain.

- **Sort:** when building the IFS only the necessary tools and product will be in the premises, all obstacles will be removed from the workspace. This die-culturing of the workspace will create a clean environment where the employees can safety work without being distracted by unwanted material.

- **Set in order:** al the products will be ordered according to their use in the aircraft. If the wingbox will be implemented first all the other components will be out of the way and only the necessary components will be in the workspace. This will keep a clean workshop and an overview on what needs to be assembled first.
- **Shine:** cleaning of the workspace will be regularly done, with a clean workspace mistakes will be reduced and the change of getting clutter into the aircraft will be minimized. This also keeps a safe workspace because employees will not trip over rubbish.
- **Standardize:** with standardizing everything will get a specific place, from tools to parts. With tools being standardized a missing tool can easily be detected and can prevent tools from being a foreign object in the aircraft structure which can have devastating consequences.
- **Sustain:** creating standard procedures on assembling all the systems to the aircraft reduces the risk of having human manufacturing errors of forgetting steps in the process of making them. For the production of the IFS an in dept step to step production plan will be written.

Working with the 5S model will increase the safety and will minimize the hazard of lose debris damaging the aircraft and hurting the employees. In order to minimize waste and reduce the operational cost of manufacturing an lean method will be chosen. With lean manufacturing the waste will be reduced to a minimum, this will also have a positive influence on the sustainability, minimizing for instance the amount of storage will mean less space will need to be heated and maintained, meaning lower assembly plant emissions. The lean approach will be based on the Toyota method with the three pillars, muri, muda and mura. Below the method is described.

- **Muri:** focuses on the waste created by overburden employees. When employees have to much work on their hands in a short period of time they will be prone to stress, having stressed workers will introduce the chance for human error in the assembly of the IFS. Reducing the overburden will be done by having a steady flow of tasks that need to be performed. Below the stages of the assembly will be explained how a structured and even work load will be obtained.
- **Muda:** means minimizing the waste of the manufacturing system. Waste will mean that resources are spend on processes that will not add value. Having a large storage will mean that a storage needs to be maintained. This will cost space and energy because the storage needs to be facilitated. For the IFS most products will be order from external resources, all parts are build to order so a large stock will be minimized.
- **Mura:** takes into account the unevenness of the work load. The unevenness of work will be minimized by creating a structured assembly plan with an even workload, the assembly plan will be elaborated below.

The added components will be categorized in three different parts, type-A, type-B and type-C components. The difference is the possibility to mount the part to the aircraft, a type-C components are really easy to install in the aircraft, such as the laptops. Type B are components that can still be maintained but require the aircraft to be in a workshop to install. And last type A components are the are difficult to change during operation like the entire wingbox structure. Below the order in what parts will be installed will be explained.

- **Type-A:** the production will start with the type-A components, this is the entire wingbox construction that will be added to the aircraft. At the same time the interior of the aircraft will be removed and the wiring will be placed in the aircraft. After the type-A component phase the two main completed parts are all the wiring and the entire wingbox.Type-A components will all be bolted to the original aircraft. Removing these parts will be possible, changing them will be an elaborated process but if needed this is an option, this will comply to requirements **IFS-SH5-03** and **IFS-SYS-26**.
- **Type-B:** the type-B components are all the actuator, sensors, force feedback control, stations and the flight computers. All these components will be reachable (by hatches). All these component can be changed during an update with relative ease, within one day. With the type-b components being able to be implemented in one day a mid-life update will be possible, being able to update the aircraft mid-life will comply to requirement **IFS-SH5-03** and **IFS-SYS-26**. The type-B components will be able to be checked during maintenance, complying in the FBS to block *4.1* and also block *1.6*.
- **Type-C:** the last components are the type-C components, these are laptops, health monitor, all the products that can be changed within one hour.

The Assembly plan will take place from type-A components to type-C components. The wiring and the wingbox are the main parallel parts, after the wiring is done the electrical engineers can switch to connecting all the sensors while the the boxwing engineers will switch to the interior and the placement of the actuators, that the electrical engineers will connect. The type-C components will be placed before the completion of the aircraft. All the specific tasks and the final assembly plan is for future research and will not be presented in this report.

11.4 Project design & development

The design of the IFS is not completed when the DSE ends. The Project Design & Development (PDD) describes all activities to be executed after the DSE. This includes not only completion of the final design stage, but also manufacturing, operating and maintaining the IFS and ultimately dispose of it. Several phases have been identified and will be explained. A graphical visualization of the PDD logic with details of each phase is presented in Figure 11.2.

- **Phase 1 - Wrap-up final design**: the current report presents the final design for the IFS. This design has been verified and validated by several analyses such as the AVL one. For these verifications and validations several assumptions were made to simplify the models. What remains to be done is a thorough CFD analysis to examine the aerodynamic properties and interaction of the boxwing configuration with respect to the original aircraft even better. Next, a FEM analysis has to be performed to find a better approximation for the structural loads that act on the boxwing configuration. A new stability and control analysis will show if the IFS is stable with the more accurate aerodynamic and structural loading cases. Afterwards a more accurate cost analysis can be performed to see if the modification cost stays within bounds. If the IFS complies with all the requirements the final design will be documented, otherwise an iteration of the design process will be done until this is accomplished.

- **Phase 2 - Assembly IFS**: after the product has been completely verified and validated, the assembly phase can be started. The assembly phase starts off by making an inventory of all parts that are needed to assemble the actual IFS. The assembly consists partly of manufacturing parts and partly of buying off-the-shelf parts. The parts that will be manufactured will be first designed in a CAD program to simplify the manufacturing process. Next the parts will be formed mechanically. The COTS components will be bought on the market and then brought together with the manufactured parts and assembled on the IFS. After assembly of the subsystems, the subsystems will be integrated in the original aircraft. The IFS will be thoroughly inspected after integration. Just before the assembly starts, the first steps of the certification process will commence. During the assembly the certification will continue and the procedure will be concluded with a maiden flight of the IFS. Besides, checks will be performed regularly to assure that the IFS is of a high standard.

- **Phase 3 - Operations**: the following stage is the stage at which the IFS is actually operated. The IFS producer will approach potential companies that are willing to operate the aircraft and the IFS will then be sold to external operators. The operator will sub-let the IFS for training and research purposes to end-users. The operator notifies the producer what type of aircraft the end-user desires to simulate and the producer will then provide the software modifications to simulate that certain aircraft. When the IFS is updated by the producer, the test flight will be preceded by an elaborate briefing. After the test flight the recorded data will be transferred by the flight engineer to the end-user.

- **Phase 4 - Maintenance**: during the operational life of the IFS, maintenance is necessary to keep the aircraft safe and flyable. The IFS will be inspected before and after every test flight. Furthermore, the regular A, B, C, and D-checks will be performed in the same manner as stated by the OEM and as is required by the certification of the aircraft. Maintenance can be performed rather easily because the boxwing can be taken apart: the connection points of the vertical wing and upper wing are hinges which makes detachment possible. If a part of the aircraft is broken, the part will be replaced by the producer of the IFS. If a part of the aircraft is worn, the part will be refurbished, thus reducing costs and applying a more sustainable approach.

- **Phase 5 - End-of-life**: when the IFS has reached its end-of-life stage the aircraft will be taken apart. Sustainability has been taken into account during the design process so as many as possible parts can be recycled or redistributed. The other parts will be disposed of as environmentally-friendly as possible.

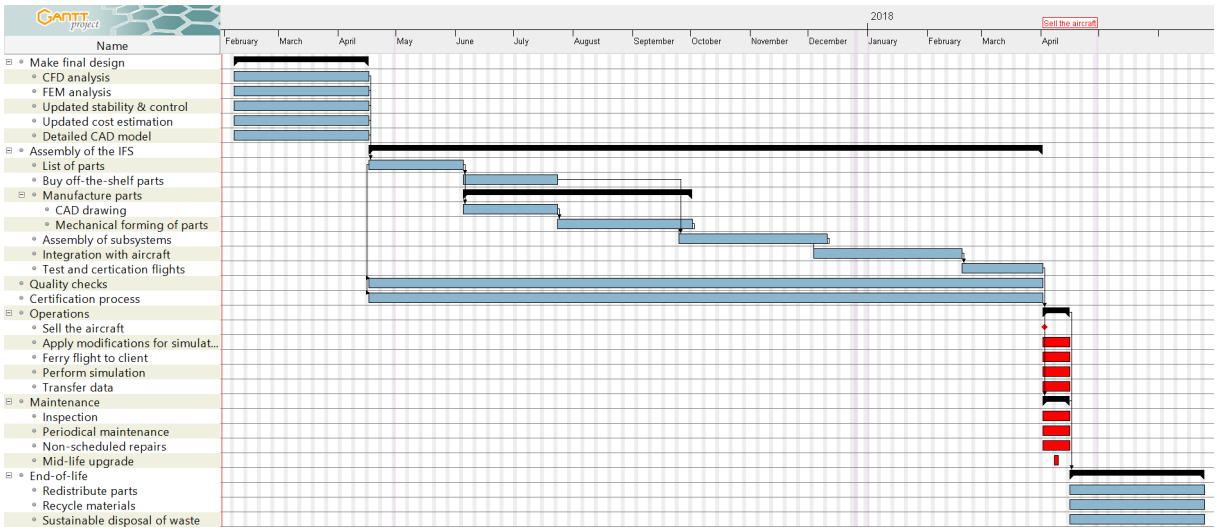

Figure 11.1: Project Gantt Chart.

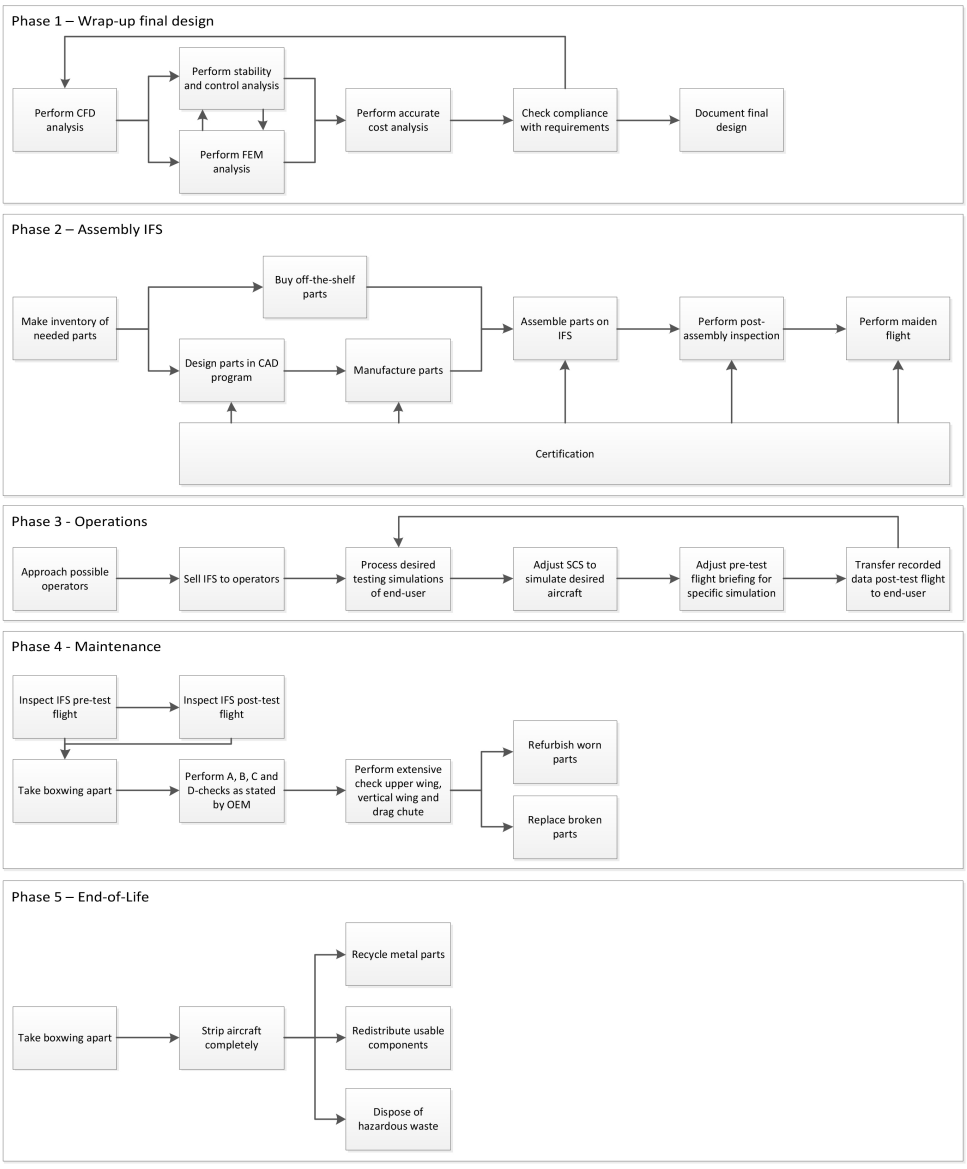

Figure 11.2: Project Design & Development overview.

12 | Cost Analysis

This chapter will provide an in-depth analysis of the total costs for the IFS project from the end of this DSE right until the IFS reaches initial operational capability. This analysis is used to show that the budget breakdown as presented in section 4.4 is not exceeded. The breakdown is the main cost driver during the design phase. A total of €800,000 is available for the modification and certification of the aircraft (requirements **IFS-SH5-04** and **IFS-SYS-20**). Operational costs are limited by requirement **IFS-SH1-02** and **IFS-SYS-21** to a maximum of €4,000 per hour. Section 12.1 presents a top-down approach for the cost estimation. A bottom-up cost estimation is presented in section 12.2. The phases used in the cost estimations are directly linked to the PDD as presented in section 11.4. Part of the data used for the calculations leading to the final cost estimations were based on values derived in subsection 4.4.1 and chapter 2. The link between the phases in the PDD and the individual elements contributing to the costs thereof can be visualized in a Cost Breakdown Structure (CBS) as shown in Figure 12.1. The disposal of the aircraft is assumed to be cost neutral or with a minor profit, therefore no costs were estimated for this phase of the life cycle. A way to achieve this is explained in section 3.3. If necessary, the results of the cost estimations are adjusted for inflation[1] and exchange rate[2].

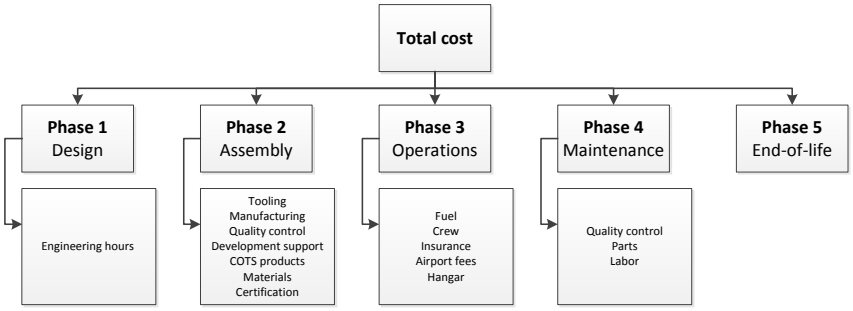

Figure 12.1: A visual representation of the Cost Breakdown Structure.

12.1 Top-down cost estimation

A top-down cost estimation is performed using cost estimation relations provided by Raymer [39]. These relations take input variables like empty weight, maximum velocity and maximum thrust to produce an estimate for required man-hours of different processes and costs of materials and flight tests. The cost estimation is split in two parts, one for the development costs and one for the costs per hour. The results of these estimations can be seen in Tables 12.1 and 12.2. The phases in these tables correspond to the phases in Figure 12.1.

Development cost estimations were made for both the Phenom 300 and the IFS. Subtracting the costs of the Phenom 300 from the IFS provided an estimate for the costs of the structural modifications and flight testing. Certifications costs are based on certification of a *Single Pilot High Performance Aircraft* by the EASA [40] in Europe to comply with requirements **IFS-SH7-02** and **IFS-SYS-27**. A contingency amount of 15% has also been added to account for any unforeseen expenses.

The cost of the crew and maintenance (in parts and labor and quality control) are based on the same CERs from Raymer. Airport handling fees are based on the case presented in subsection 11.1.3 for a projected use of 750 hours and 300 approaches and landings per year at Rotterdam The Hague Airport[3]. The 300 flights follow from subsection 11.1.3.

For the fuel costs, the average fuel consumption of the IFS stated in chapter 10 and current price of jet fuel was used[4].

[1] https://data.bls.gov/cgi-bin/cpicalc.pl?cost1=1.00&year1=1999&year2=2016 [cited 17 January 2017]
[2] http://www.xe.com/currencytables/?from=USD&date=2017-01-18 [cited 17 January 2017]
[3] https://www.rotterdamthehagueairport.nl/content/uploads/2016/03/Summary-landing-fees-04-2016.pdf [cited 24 January 2017]
[4] http://www.iata.org/publications/economics/fuel-monitor/Pages/price-analysis.aspx [cited 24 January 2017]

Table 12.1: Top-down development cost estimation.

Process	Phase	Hours	Cost [€]
Engineering	P1	142	16,500
Tooling	P2	124	15,000
Manufacturing	P2	870	86,000
Quality Control	P2	116	13,000
Development support costs	P2	n.a.	13,000
COTS parts	P2	n.a.	125,000
Materials	P2	n.a.	37,500
Flight Test	P2	n.a.	38,000
Certification	P2	n.a.	196,500
Contingency			81,075
Total		**1,252**	**621,575**

Table 12.2: Top-down operational costs estimation.

Process	Phase	Cost [€/hour]
Parts & Labor	P4	750
Quality Control	P4	90
Fuel	P3	800
Crew	P3	420
Hangar	P3	40
Insurance	P3	40
Airport Handling Fees	P3	330
Total		**2,470**

12.2 Bottom-up cost estimation

Next to the top-down method of estimating costs shown in section 12.1, the costs of the different life cycle phases can also be estimated using a bottom-up approach. Specifically, the assembly phase as seen in the CBS shown in Figure 12.1 can be split up into the individual structural elements comprising the wingbox. S. Castagne [41] provides specific estimation methods for this purpose. These are adapted for the IFS in Equation 12.1 through Equation 12.6.

The bottom-up estimation of the assembly costs makes a distinction between the material costs of the structural elements, the fabrication costs of these elements and the costs for the integration of the elements into a wingbox. The stiffener length and total skin area shown in the equations include a 15% margin to account for material scrapped during production. Ribs are not accounted for in this method, for the integration it is assumed that automatic riveting is used.

$$c_{skin}^{material} = 0.94 \cdot A_{skin} \cdot (0.002303 \cdot t_{skin}) \tag{12.1}$$

$$c_{stiffeners}^{material} = 0.94 \cdot L_{stiffeners} \cdot (0.005969 \cdot A_{stiffener} + 0.0653) \tag{12.2}$$

$$c_{rivets}^{material} = 0.94 \cdot n_{rivets} \cdot 1.0 \tag{12.3}$$

$$c_{skin}^{fabrication} = 0.94 \cdot 13.8 \cdot (0.0001524 \cdot A_{skin} + 56.4) + 0.94 \cdot 11.3 \cdot (0.0001087 \cdot A_{skin}) \tag{12.4}$$

$$c_{stiffeners}^{fabrication} = 0.94 \cdot 10 \cdot (0.02283 \cdot L_{stiffeners} + 151.73) \tag{12.5}$$

$$c_{automatic}^{integration} = 0.94 \cdot n_{rivets} \cdot 10.0 \tag{12.6}$$

Plugging in the values of the chosen structural design results in a material cost of €55,000 for the skin, €15,000 for the stiffeners and €5,000 for the rivets. The fabrication costs came to €80,000 for the skin and €30,000 for the stiffeners. The costs of final integration amounted to €60,000. Adding all of these costs gives a total cost estimation for assembly of €245,000. These values are visualized in Figure 12.2.

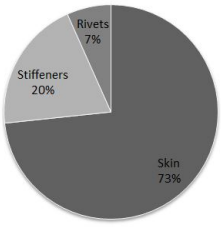

(a) The material cost per category totalling €75,000.

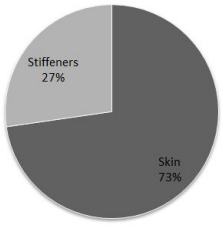

(b) The fabrication cost per category totalling €110,000.

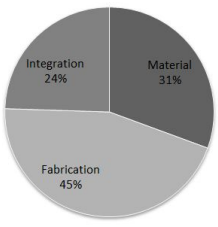

(c) The final assembly costs per phase totalling €245,000.

Figure 12.2: The division of the costs per structural element within the manufacturing process.

This total value for the assembly costs from the bottom-up approach can be compared to the sum of the costs of Tooling, Manufacturing, Quality Control and Materials resulting from the top-down method shown in Table 12.1. The latter totals €151,500. This means that the bottom-up estimation exceeds the top-down estimate for assembly by €93,500. The bottom-up estimation is more precise than the top-down method, therefore it is expected that the costs of the assembly will eventually be closer to the higher estimate than the lower estimate given in section 12.1. Even in this case the total cost add up to €715,075, which is still 10% lower then the total budget.

13 | Risk Assessment

A safe design requires identification of risks before and during the design process. The risks that were identified before the preliminary design process started are reflected upon in section 13.1. Risks that are present for phase 2 to 4 as stated in section 11.4 are elaborated upon in section 13.2. Besides this, a RAMS analysis was performed in section 13.3.

13.1 Baseline and Mid-Term risks review

For the Baseline and the Mid-Term Report risk assessment and mitigation was done on both project and concept level. Some of the planned risk mitigating for the design phase has already been conducted and will be featured in this section.

On the project level, the meetings were structured and improved during the project. Also bad communication was minimized by the application of systems engineering. So far all deliverables were handed in on time including proper resources. Therefore almost all project risks mentioned in the Baseline Report were avoided [9].

In the Mid-Term Report, different risk maps were made for all the generated concepts [10]. Also a risk map that applied to all the concepts was included along with various risk mitigation measures. In the following list a review on how these mitigations were applied in the design is provided [42].

- **1 - Structural failure:** to decrease the likelihood of a structural failure a safety factor of 1.5 was used on the ultimate load case. No further systems were integrated in the wingbox of the boxwing so that its complexity was kept at a minimum and thereby reducing the likelihood of failure. This can be read in chapter 8.
- **2 - Material failure:** as was planned, a certified type of aerospace grade aluminum, AL T6-7075, will be used for the boxwing. This reduces the likelihood of failure since manufacturing impurities are kept at a minimum. The material of the drag chute is not specifically chosen for a low likelihood of failure, but since the impact of a failing drag chute is very low, this is of minor importance. The drag chute will have a safety quick release system, in case a problem occurs with the drag chute during operation. This system is explained in section 9.2.1.
- **3 - Flight control failure:** to reduce the likelihood of flight control failure considering the control surfaces of the added elements, a backup data cable is present for redundancy. Also a backup system in case the power fails is provided in the form of a battery system. This allows the aircraft to set the control surfaces in landing mode, so that the aircraft can land safely and thereby reducing the impact of such a failure.
- **4 - Simulator failure:** to reduce the impact of a failure in the simulation system, a safety trip system was integrated. The safety trip system lets the test pilot or safety pilot terminate the simulation mode directly and return to the normal flight mode. In the cockpit and at the test engineer station safety trip buttons are placed within arm reach of the pilots and the test engineer. A minimum of two buttons are implemented in case of button failure. In section 9.3 the stations are elaborated in more detail. When the safety trip system is engaged the safety pilot will take over controls. All clutches will engaged automatically and the aircraft can fly in normal conditions. Because the pilot will give digital inputs, the computer will check if the wanted input can be performed with the aircraft or if it will lead to jeopardizing the safety of the pilots.
- **5 - Engine failure:** a concept without modifications to the engine was chosen. Since the Embraer Phenom 300 is a widely certified aircraft, the engines can be expected to be very reliable. So not modifying them leads to a very low likelihood of failure. The impact of an engine failure on the IFS is just a bit higher since the boxwing adds drag to the aircraft, decreasing its gliding range a bit.
- **6 - Maintenance failure:** the boxwing design gave the possibility to not use complicated, difficult to maintain systems. So in this way the likelihood of making a mistake in maintenance is limited. Since the boxwing is entirely detachable and not interfering with other aircraft components, it is easy to access and inspect.
- **7 - Actuator failure:** as can be reviewed in section 9.8 several measures were taken to reduce the likelihood of an actuator failure. For static loading the actuators will not exceed their rated torque , preventing heat generation with a margin of 20 Nm. For dynamic loading it might though, but still this will not exceed the maximum torque. In case of bad weather conditions where severe dynamic loading might be introduced, the simulation system will provide for a fixed position, preventing the actuators from eventual failure. In the unlikely event an actuator fails and gets stuck in one position, the other half of the control surface can counteract the lift generated. This is possible due to the decision to split up the control surfaces. Looking back on the initial plan of risk mitigation, these were all used in the actuator system design.
- **8 - Fuel failure:** the fuel system is not modified in the design, thereby the chance of a failure is kept small. Impact is the same as for engine failure as described earlier.

- **9 - Instrumental failure:** in order to mitigate the instrumental failure risk only certified and off the shell sensors and instruments will be added to the aircraft. For the simulation the original flight displays will be used, the Embraer has back up instruments implemented in case the primary flight displays fail. Developing new sensors and instruments will mean that a long testing period will be needed costing a lot of time before these instruments can be implemented in the aircraft, that is why stock en certified instruments will be used. But the original aircraft contain back up instruments to land the aircraft safely.
- **10 - Sensor failure:** the sensors that are in the stock aircraft measure the majority of data that is needed. These sensors are already tested and reliable hence the likelihood of a sensor failure for these sensors are low. The added sensors are divided in two categories, those of vital importance to safely perform flight and those for research purposes only. The sensors for research purposes have a very low impact, since when they fail they do not impact flight safety at all. The sensors which are of vital importance monitor the control surface deflection, the engines and the electric system. The control surface deflection of all added surfaces can also be read from the electric actuators hence these are redundant, reducing the impact. As mentioned earlier, the engines of the Embraer Phenom 300 are very reliable, hence a failure of a sensors will have a low impact, since it is highly unlikely the engine will fail simultaneously. Also each sensors will be installed twice for redundancy. The last category of vital sensors are the electric sensors, which measure data like system overload and generator failure. These sensors will be applied throughout the whole electric system and in case of an electric failure there are several fail saves build in the system, which both reduces the impact of sensors failure.

13.2 Risk management

In the following section first Table 13.1 is presented. This is a risk map based on the risks, displayed with indicators in the map, elaborated on in the three risk subcategories. In these subcategories also mitigation measures are presented. Based on these mitigation measures a new risk map is generated in Table 13.2. Risk is defined as likelihood times impact. So if the likelihood of an event is high and the impact is also high, a high risk is present. The idea is to get risks from the top right corner, where the risk is high, to the bottom left corner. This is done be reducing the likelihood of an event happening, for example by working with a safety factor, and/or reducing the impact, by for instance having backup systems.

Table 13.1: Risk map for the IFS.

Likelihood	Negligible	Low	Medium	Critical	Disastrous
High			I2		
Medium			I4	I1,I5,O5	
Low	E4	O6		E1,E2,E6,O4	I3,O1
Very low		E3,O2	E5		
Close to never		O3			
			Impact		

13.2.1 External technical risks

In this section, risks are mentioned that are implied by external factors. So these can be more difficult to mitigate. They can relate to both technical as organizational risks.

- **E1. - Manufacturing errors:** *Likelihood* - The design features a lot of of-the-shelf products. This reduces the likelihood of failure. The boxwing however, is not. However, the design is kept as simple as possible The boxwing will not be produced in-house but will be outsourced to an external company that is specialised and has a track record of building high quality wingboxes. Only assembly will take place internally with certified and trained personal. In section 11.3 the manufacturing will be elaborated upon and how risks and possible errors will be reduced. *Impact* - The impact of a failure due to a manufacturing error varies a lot per subsystem. So details will be discussed in the separate subsystem risks.
- **E2. - Impurities in used materials:** *Likelihood* - As discussed already, an widely used aerospace grade aluminum is used. This reduces the risk of failure. *Impact* - A material failure basically has the same consequences as a structural failure that will be discussed later on.
- **E3. - Incident during ferry:** *Likelihood* - During the ferry flight the Embraer Phenom is flown from the USA to Europe as described in chapter 11. It is very unlikely something goes wrong during this trip and mitigation consists only of choosing a safe route and waiting for good weather conditions. *Impact* - The aircraft could

be damaged during the ferry flight, but since it is not operational yet, financial consequences are limited. The impact could be reduced by getting an insurance for this ferry trip.

- **E4. - Supply chain mishap:** *Likelihood* - Since the amount of suppliers for the manufacturing phase is limited and parts are mostly of-the-shelf products with a high TRL, chances are small delivery is interrupted. Most suppliers are already chosen, but for the other parts suppliers with a high reliability can be picked to reduce the risk. *Impact* - A mishap in the supply chain can cause a delay in delivery of the IFS to the client. This will mainly have financial consequences.
- **E5. - Bird strike:** *Likelihood* -The likelihood of a bird strike causing a major accident is quite low and it has been estimated that there is only 1 accident resulting in human death in one billion flying hours [1]. Smaller incidents can cause damage to the aircraft however. If one wants to reduce the chances of a birdstrike, the airfield to operate from should be in an area with a minimal amount of large birds. *Impact* - A bird strike is almost never causing the aircraft to crash, but damage can occur. This can keep the IFS on the ground for a longer time, causing financial damage to the operator.
- **E6. - Extreme weather conditions:** *Likelihood* - Depends on the operating airfield location. Since this will most likely be in Europe, extreme weather does not occur often causing the likelihood to be quite small. Chances can be further reduced by studying the weather forecast well in advance of a test flight. *Impact* - Severe turbulence can introduce high loading cases on the IFS. As already mentioned in section 13.1, the structure is designed with a safety factor. Also the actuator system has a mode in which the control surfaces can be fixed to prevent damage.

13.2.2 Internal technical risks

The risks mentioned in this section relate to systems that were designed for the IFS. So no risks for the entire aircraft will be mentioned since the Phenom 300 is a certified aircraft that will have no major risks on itself.

- **I1. - Simulator system failure:** *Likelihood* - Various risks of the simulator system were already discussed in section 13.1. The actuators and layout reduced the likelihood of a failure already. Also the more time spend on designing and testing the entire FCS will make chances of failure smaller. In the end it is considered there is a small chance a failure will occur in the system. *Impact* - Several measures were taken on reducing the likelihood of a failure of the simulation system as already discussed. In the end, every kind of failure that can occur on the simulation system is considered to have at most a low impact on the flight.
- **I2. - Drag chute failure:** *Likelihood* - The drag chute can fail on multiple points. One of the ropes can break, the drag chute can be torn apart itself and it can fail to deploy. To prevent the ropes from snapping a safety factor of 3 was taken for the static load to account for higher loads due to dynamic cases, see section 5.4. *Impact* - A failure of the drag chute will have a low impact since it is meant to be separated safely from the aircraft. So if it fails, it just will be detached and normal flight can be proceeded with. To even further reduce the impact cameras are mounted on the aircraft filming the drag chute and the tension in the cable is measured, as explained in section 9.7. This allows the test engineer to immediately notice the failure and minimal harm is done to the mission.
- **I3. - Structural failure:** *Likelihood* - As mentioned in section 13.1 several measures are taken to reduce the likelihood of a structural failure of the boxwing, such as keeping the design simple and adding a safety factor. *Impact* - In the worst case a structural failure can occur and the boxwing can be ripped of the aircraft. Unless this causes damage to the tailplane of the aircraft, the aircraft will still be able to make an emergency landing. This can be made sure by implementing a scenario in the ACS in which one half of the boxwing is gone, while the other half stabilizes the aircraft. If the horizontal tailplane is hit by debris consequences can be more dramatic, this impact is hard to reduce, but also very unlikely to happen.
- **I4. - Aerodynamic disturbances:** *Likelihood* - With aerodynamic disturbances is meant that the airflow around the IFS does not behave as expected. As mentioned in chapter 6 AVL was used to preliminary assess certain aerodynamic parameters of the aircraft. For the final design a more elaborate aerodynamic analysis as in the form of CFD have to take place to reduce to likelihood of unexpected flow to occur. This will also be implemented in phase 1 of the project development plan described in section 11.4. *Impact* - The main aerodynamic addition to the aircraft is the boxwing. Flows generated by the boxwing will affect the main wing, the aft fuselage and the tail. So it can really affect the flying characteristics of the aircraft. Since these parts will not be modified the impact is not really mitigated on this part. Also the requirements on the different manoeuvres could possibly not be met, although this is considered something with a very low impact on safety.
- **I5. - Stability issues:** *Likelihood* - It is important to keep control of the aircraft stability, since the IFS is designed to have variable stability. The stability was assessed in chapter 7. These preliminary calculations

[1] http://www.int-birdstrike.org/Warsaw_Papers/IBSC26%20WPSA1.pdf [cited 22 January 2017]

indicate no problems. But to reduce the likelihood of stability issues to occur it should be assessed more closely as described in the flight dynamics chapter already. Especially focus should be on assessing the eigenmodes. *Impact* - Unexpected lack of stability can have major consequences. To lower the impact, the aircraft should be tested extensively before delivery to the client. If issues are experienced they will not occur at the after handing over the aircraft to the client.

13.2.3 Operational risks

The following section elaborates on risks that are present during the operational phase of the IFS. These will mainly be related to the operator of the aircraft as explained in chapter 2.

- **O1. - Maintenance error:** *Likelihood* - The boxwing is quite a simple structure on the outside of the aircraft. It can even be detached from the aircraft for closer inspection. Also the actuators and other simulation systems are easy to maintain. So if well qualified maintenance personnel is hired, the likelihood of occurrence of a maintenance error is kept small. *Impact* - In the worst case a material failure can occur and the boxwing can be ripped of the aircraft. With the same consequences as described for the structural failure earlier.
- **O2. - Legal issues:** *Likelihood* - Since the aircraft will be certified, the chance that the IFS is detained from operating by legal issues is very small. *Impact* - Legal issues will mainly have financial consequences and the aircraft might temporarily not be allowed to fly.
- **O3. - Limited operational facilities:** *Likelihood* - Chances the operator of the IFS cannot find a suitable airfield to operate from are low, since many well facilitated airfields are present in Europe and the take-off and landing distances are common. Likelihood can be even further reduced by lowering the standards the airfield should have. *Impact* - Not having a perfect suitable airfield to operate from can affect operations slightly. The impact can be reduced by operating from the airfield the end user wants to use.
- **O4. - Health failure:** *Likelihood* - The chance one of the pilots experiences a medical failure is very small, since the requirements on a medical certificate are quite strict[2]. The further reduction of the likelihood is hardly possible other then picking fitter pilots. *Impact* - The Embraer Phenom 300 is an aircraft that is certified for single pilot operations. So if the pilot is not able to fly the aircraft anymore in that case, impact can be disastrous. In the IFS however, always two pilots will be present during operations. The yoke is removed in the test pilot station as mentioned in section 9.5. So if the safety pilot experiences a health failure, the test pilot either has to land the aircraft with the sidestick or has to change seats with the safety pilot. This will both limit the impact of the failure.
- **O5. - Human error:** *Likelihood* - Flights will only be conducted with a very experienced crew, both pilots and engineer. Due to the nature of its mission profile, that demands a lot from the pilots capabilities, chances are present that one of the pilots makes a mistake during the flight. This is an inevitable fact and risk mitigation will have to take place on the impact aspect. *Impact* - During the critical take-off and landing phase the simulation is not active, so this reduces the possible impact of a human error quite a bit. Also the safety trip buttons present on both pilot stations,see section 9.3, allows both pilots to correct each other if they notice an error.
- **O6. - Organizational failure:** *Likelihood* - The operators of the IFS will be small companies or divisions within companies. Due to the compactness, communication lines are short, reducing the likelihood of an organizational failure. The lack of experience in this small market increases it however. Mitigation can take place in the form of hiring managers with experience in the field test flight operations. *Impact* - Can be disastrous for the business, but as long as maintenance is still performed well, it will induce no risks to the safety of the IFS. Impact can be reduced by hiring an external party to help solve the organizational problem when it is noted.

13.2.4 Mitigated risk map

In Table 13.2 the mitigated risk map is presented. In this map all mitigation measures are implemented that were performed during the design phase, but also those that should be applied further on in the project. Some of these measures are also mentioned in section 11.4. One can see a lot of the risks are moved to the bottom left corner of the map and no high risks are present anymore. Note that not for all risks measures were implemented since they either cannot be reduced or they are already of negligible size.

13.3 RAMS analysis

The RAMS method is a method used to determine the Reliability, Availability, Maintainability and Safety of the IFS. This method focuses on determining which areas are likely to fail and preventing that from happening or reduce the consequences of the failure. Before RAMS is discussed, the definitions will be explained.[3]

[2] https://www.faa.gov/about/office_org/headquarters_offices/avs/offices/aam/ame/guide/standards/ [cited 23 January 2017]

[3] http://www.lr.tudelft.nl/en/organisation/departments/space-engineering/space-systems-engineering/expertise-areas/rams/ [cited 22 January 2017]

Table 13.2: Risk map for the IFS after mitigation.

Likelihood	Negligible	Low	Medium	Critical	Disastrous
High					
Medium					
Low	I2	I1,O5			
Very low	E4	E6,I4,O2,O6	E1,E2,E5,I3,O1,O4	I5	
Close to never		E3,O3	O4		

Impact

- **Reliability:** reliability is the ability to perform required functions under stated conditions for a specific period of time.
- **Availability:** quality of a device or system when needed.
- **Maintainability:** the ease and speed at which an item or equipment can be repaired or restored given a specified amount of time and resources.
- **Safety:** when only Acceptable levels of risk to life,limb or health are present.
- **Failure:** as taken from the TU Delft RAMS explanation, a failure is "A deficiency, defect, nonperformance or non-conformance with specified requirements".

13.3.1 Reliability

A common method for determining reliability in aircraft is to assume failure rates for all the components[4]. This will give a quantitative value to each component which will in turn help determining where to implement changes or improvements as there might be clear outliers that greatly decrease overall reliability.

The general equation for reliability is given in Equation 13.1 where λ is the failure rate. However, the equation most used in conjunction with determining reliability is by Equation 13.2 where reliability is a function of time, given by R(t), a scale parameter θ and a shape parameter β. This is known as the Weibull distribution. It is able to fit the failure curve over time much better than Equation 13.1 and is used throughout engineering for reliability estimation.

$$R(t) = e^{-\lambda \cdot t} \tag{13.1}$$

$$R(t) = e^{-(\frac{t}{\theta})^{\beta}} \tag{13.2}$$

Assuming the reliability of each subsystem can be stacked in series, the following relation in Equation 13.3 can be found. This is the worst case scenario as this assumption means that if only one of the subsystems fail, the whole system will fail to meet the given objective. Noteworthy is that a system does not have to fail completely to have suffered a failure.

$$R_{1-n} = R_1 \cdot R_2 \cdot .... \cdot R_n \tag{13.3}$$

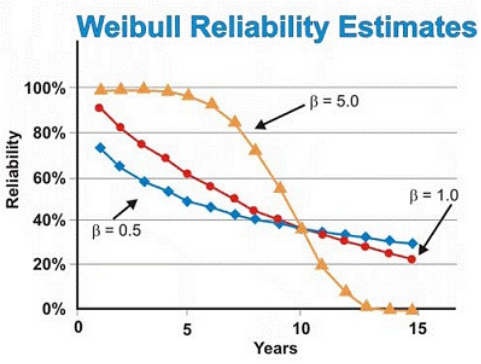

Figure 13.1: Reliability with 3 different β values[5]

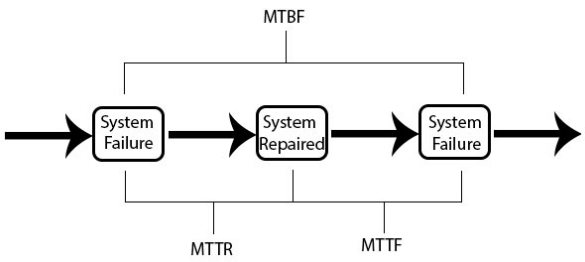

Figure 13.2: MTBF, MTTR and MTTF graphical representation

[4]https://www.faa.gov/aircraft/air_cert/design_approvals/csta/publications/media/risk_analysis_corres_course.doc [cited 22 January 2017]
[5]http://www.reliableplant.com/Read/18693/reliability-engineering-plant [cited 24 January 2017]

When estimating the reliability of the whole system there are three possible outcomes; Increasing ($\beta > 1$), decreasing ($\beta < 1$) or constant ($\beta = 1$) risk over time. All three are plotted in Figure 13.1. There it can be seen that the reliability of the whole system is dependant on any one subsystem failure.

13.3.2 Availability

The most common measurement of availability is he probability that a unit will be operational. An equation for the availability, given as A, can be found in Equation 13.4.

$$A = \frac{t_{operational}}{t_{total}} \tag{13.4}$$

For availability purposes, redundancies will be included. This means that if one subsystem fails, there will be a backup subsystem available, as there will not be any single points of failure. Availability aims at reducing downtime of the aircraft to maximize the it's value.

13.3.3 Maintainability

Factors that influence maintainability include ease and speed as mentioned above but within this definition is also implied safety, cost and accuracy of the maintenance. Maintenance of aircraft is always done at a hangar in between flights. The amount of time required for maintenance often depends on the complexity of the systems being maintained. When a subsystem needs to be maintained also greatly depends on that subsystem. Maintenance is therefore usually measured in time intervals: Mean Time To Repair (MTTR), Mean Time Between Failure (MTBF) and Mean Time To Failure (MTTF). The intervals are shown in Figure 13.2.

$$MTTR = \frac{total\ maintenance\ time}{number\ of\ repairs} \tag{13.5}$$

$$MTBF = \frac{1}{FR_1 + FR_2 + ... + FR_n} \tag{13.6}$$

$$MTTF = \int_0^\infty R(t)dt \tag{13.7}$$

Actual values can be found during later phases of the design phase and will be integrated at that time. For now major considerations concerning maintenance are listed as follows:

- **Software:** software of the aircraft and of the IFS must be updated every time a bug presents itself or every time a new aircraft simulation would be introduced. Updates are done by the test engineer. If software is not working properly and the IFS is put into a dangerous situation, safety measures are available to disengage the software.
- **Tear/crack maintenance:** for safety purposes the weakest spots of structures are given to the maintenance team so that tears and cracks can be detected quickly before they grow large enough to be deemed unsafe. With that information maintenance team will know exactly where to check for cracks or tears due to fatigue or unforeseen dynamic loads. The size of the crack needs to be large enough to be visible to the naked eye long before it is unsafe. Once the tear or crack is detected, appropriate techniques can be applied for maintenance or repair.
- **Part maintenance:** each subsystem or part will have a given maintenance routine or if maintenance is not required, it will be given an amount of operational hours of life time before expected failure. Once it has passed it's operational life time the subsystem or part will need to be analyzed and either extend it's life time due to it's acceptable performance, refurbished to renew it's operational life time or replaced. If the operational life time is extended it will need to be kept in check to make sure it agrees with all safety considerations.

13.3.4 Safety

Safety links with many parts within risk management. Safety is very important in all fields of engineering and must always be taken seriously. For safety concerns one must take into consideration both risks during aircraft operation and risks outside of aircraft operation. Risks during operation and some risks outside of operation are discussed in section 13.2. Risks during maintenance are discussed in subsection 13.3.3.

As discussed above, all risks have been assessed and mitigated. Furthermore, in each chapter the safety measures of the respective systems has been explained. Combined with the fact the aircraft has no single point of failure the following requirements on safety are met: **IFS-SH7-01**, **IFS-SH2-03**, **IFS-SYS-16** and **IFS-SYS-18**.

14 | Sensitivity Analysis

In order to investigate the sensitivity of the IFS design, the result of the decrease and increase of major system parameters will be discussed in this chapter. The effects of varying the different inputs provides insight on the feasibility of the design, since it is considered likely that variables may still be prone to changes in the current phase of the design process.

The parameters of which the sensitivity will thoroughly be examined are at system, namely: the mass of the modifications, the shift of the x-location of the center of gravity and the cost budget of the modifications and certification. Due to the complexity of the system, the change of a single variable eventually has an impact on almost the total set of system characteristics.

Sections 14.1, 14.2 and 14.3 describe the effect of the change of these three major design parameters considering the modifications. Hereafter, section 14.4 qualitatively describes the sensitivity of other performance parameters. Note that even though the varying parameters only consider the modifications, the result of the analysis describes the effect on the IFS system as a whole.

14.1 Total mass of modifications

As summarized in section 7.1, the modifications will cause a mass reduction of 78.41 kg. The impact of adding the boxwing on the mass of the IFS can be found in section 8.4, the same has been done for the drag chute in section 5.4 and lastly the summary of the contributions of the ergonomics, sensors and actuators is provided in subsection 9.2.4.

The mass available for passengers and payload, while flying with the maximum amount of fuel, was 580 kg before the modifications, while the modifications increase this available mass to 652 kg, after adding the payload needed for testing. Assuming the passengers have a payload of 80 kg per person, this means that there will still be a margin of 332 kg taking into account that 4 passengers with a weight of 80 kg are on board of the IFS. This means that an increase in mass even with a quantity of 332 kg will not violate requirement **IFS-SYS-04** on not exceeding the MTOW of the original aircraft.

Looking at maneuvering, an increase in weight will tighten the requirements on the control surfaces, while a decrease makes maneuvering easier. Since all aerodynamic calculations in chapter 6 as well as stability and control analysis in chapter 7 have been performed using the MTOW, the actual performance of the IFS will in practice be better than actually designed for. This implicates that an increase of mass of the modifications up to 332 kg will not effect the design. If, however, this limit would be exceeded, a so called snowball effect will take place, increasing the weight of one modification after another.

14.2 Center of gravity of the modifications

In section 7.1, the center of gravity location of the IFS is calculated to be at 7.59 m from the aircraft's nose, taking into account the masses and centers of gravity per modification. The influence of the center of gravity location on the longitudinal stability of the aircraft is assessed in section 7.2. There, it is concluded that the center of gravity of the IFS cannot be positioned after 7.8 meters, assuring a negative C_{M_α} while taking into account a margin similar to that of the original Phenom 300. Concluded can be that a center of gravity shift to the back of no more than 0.2 m is allowed.

The influence of the center of gravity on the direct lift maneuvers is reviewed in subsection 7.3.1. Here it is shown, that moving the c.g. to the aft is preferable, since it decreases the lift increment that will be needed from the upper wing to produce the increment in lift.

When looking at these conflicting needs for the center of gravity, the longitudinal stability part is considered of the highest importance. Since the boxwing has the highest contribution of the modifications in the c.g. calculation of the IFS, an effect on an increase of the mass of the boxwing is performed. It turns out that an increase of the box wing weight of 100% yields a c.g. shifts to the aft only 0.02 m. This means that it can be concluded that the sensitivity of the center of gravity to changing the mass of the modifications is almost negligible.

14.3 Total costs of modification and certification

The maximum costs budget of the modification and certification from unmodified aircraft to IFS shall not exceed €800,000, as defined in requirement **IFS-SYS-20**. According to the top-down development cost estimation as shown in section 12.1, the total needed budget of the modification and certification are estimated to be €621,575. This amount includes a contingency of €81,075. It can be concluded that the modification is not very sensitive to a change in the budget, since only if the project budget would be decreased by at least 22%, design choices have to be changed in order to maintain contingency.

If the bottom up cost estimation of section 12.2 is used, the needed budget will be €93,500 higher than the previously calculated €621,757. Nevertheless, the project budget should still decrease by at least 11 % in order to have an impact on the design.

14.4 Other performance parameters

Sections 14.4.1, 14.4.2, 14.4.3, and 14.4.4 describe the sensitivity of the designed IFS to weather impact, range, endurance and propulsive efficiency, respectively. Since no direct mathematical expressions have been used to relate the specifications of the design solution to the parameters in this section, a qualitative approach has been chosen. Note that for each case, the sensitivity will only be described for a variance in the concerned parameter that is either negative or positive. An opposite variance of this parameter can be assumed to have the opposite effect.

14.4.1 Drag

The estimated drag parameters of the modified aircraft have been determined to be questionable in section 6.5. The overall drag coefficient of the IFS at cruise condition can be assumed to linearly influence the thrust needed to propel the IFS and therewith the fuel consumption of the system. Meanwhile, the endurance and range of the IFS will decrease.

14.4.2 Propulsive efficiency

The thrust setting of the aircraft is closely related to the drag characteristics, of which not much is known. Nevertheless, it can be said that in case of a lower propulsive efficiency, the fuel consumption will increase, the range and endurance will decrease and the maximum achievable Mach number of the aircraft will decrease.

14.4.3 Range

As stated in the previous sections, the range depends on the drag characteristics and the propulsive efficiency amongst others. It is likely that the IFS will need to be relocated in order to reach customers, as discussed in subsection 11.2.2. These relocation flights will include more stops for refueling in case of a lower range, resulting in higher operational costs.

14.4.4 Endurance

Similar to range, endurance will decrease with an increment in drag or a decrement in propulsive efficiency. In case of a lower than expected endurance, less testing or training can be done per flight, meaning that the operational costs will increase.

15 | Requirements' Compliance

This chapter contains the compliance matrix. It is used to check whether the design meets all the requirements set by the stakeholders. In the first two columns, the requirement ID and description are given. The next column gives the responsible department, followed by the actual compliance of the requirement. The last column shows the part of the report containing the rationale of the compliance. Hyperlinks are provided in this column, so the reader can click on the section to view it. Information on how the requirements are met, what margins are included and (in some cases) why requirements are dropped is included in the respective chapters.

Table 15.1: The requirements' compliance matrix.

Req ID	Req description	Dep.	Compliance			Section
			Full	Partial	None	
IFS-SH1-01	The IFS shall be able to land and take-off at Rotterdam The Hague airport.	FD	✓			7.4
IFS-SH1-02	[KEY] The IFS shall have an operational cost of maximum €4,000 per flight hour.	Gen	✓			12.1
IFS-SH1-03	[KEY] The IFS shall be able to operate safely.	All	✓			13
IFS-SH2-01	The IFS shall be able to land and take-off at Rotterdam The Hague airport.	FD	✓			7.4
IFS-SH2-02	The IFS shall have a range of at least 1,850 km.	FD	✓			7.4
IFS-SH2-03	[KEY] The IFS shall be able to be operated safely.	Gen	✓			13
IFS-SH2-04	[KEY] The IFS shall be able to take additional measurements.	ESA	✓			9.7
IFS-SH2-05	[KEY] The IFS shall be able to simulate variable stability flight characteristics for training purposes.	ESA	✓			9.5
IFS-SH2-06	[KEY] The IFS shall be able to simulate flight characteristics of aircraft for research purposes.	ESA	✓			9.5
IFS-SH2-07	[KEY] The IFS shall be able to simulate flight characteristics of atmosphere reentry vehicles.	Aero	✓			5.4
IFS-SH2-08	The IFS shall have an endurance of at least three hours in non-simulated flight.	FD	✓			7.4
IFS-SH2-09	[KEY] The IFS shall be able to take four passengers including a safety pilot, an experimental pilot, an engineer and one additional passenger.	ESA	✓			9.3
IFS-SH3-01	The IFS shall be certified.	Gen	✓			12
IFS-SH4-01	The unmodified aircraft that forms the basis for the IFS shall currently be in production.	Gen	✓			10
IFS-SH5-01	The IFS shall have an operational lifespan of at least 20 years.	Gen	✓			10
IFS-SH5-02	The return on investment should be high.					12
IFS-SH5-03	A midlife update shall be feasible.	Gen	✓			11.3
IFS-SH5-04	[DRV] The modification cost shall not exceed €800,000.	Gen	✓			12
IFS-SH6-01	The fuel burn shall be low.	FD	✓			7.4
IFS-SH7-01	The IFS shall be able to be operated safely.	Gen	✓			13
IFS-SH7-02	The IFS shall be certified.	Gen	✓			12.1

IFS-SYS-01	The IFS shall be able to fly at a speed of 0.65 M.	Gen	✓			10
IFS-SYS-02	The IFS shall have a ceiling of at least 10,668 m.	Gen	✓			10
IFS-SYS-03	The IFS shall have a maximum electrical power consumption of < TBD > W.	ESA			Dropped	9.9
IFS-SYS-04	[DRV] The weight of the IFS shall not exceed the MTOW of the unmodified aircraft that forms the basis for the IFS.	FD	✓			7.1
IFS-SYS-05	The IFS shall have a minimum endurance of 3.5 hours in non-simulated flight.	FD	✓			7.4
IFS-SYS-06	The IFS shall have a minimum range of 2,000 kilometers in non-simulated flight.	FD	✓			7.4
IFS-SYS-07	The IFS shall have a maximum balanced field length of at most 2,200 m.	FD	✓			7.4
IFS-SYS-08	[KEY] The IFS shall have a variable stability.	ESA	✓			9.5
IFS-SYS-09	The control surface actuators shall have a maximum error of 1 $\%$.	ESA	✓			9.8
IFS-SYS-10	The IFS shall have an experimental flight control station.	ESA	✓			9.3
IFS-SYS-11	The IFS shall have a test engineer station.	ESA	✓			9.3
IFS-SYS-12	The IFS shall have a safety pilot station.	ESA	✓			9.3
IFS-SYS-13	The IFS shall have room for an additional passenger.	ESA	✓			9.3
IFS-SYS-14	The IFS shall provide the possibility to change test pilot during flight.	ESA	✓			9.3
IFS-SYS-15	The IFS shall have additional sensors.	ESA	✓			9.7
IFS-SYS-16	The IFS shall have no single points of failure leading to safety issues.	Gen	✓			13
IFS-SYS-17	The IFS shall have a safety trip system.	ESA	✓			9.5
IFS-SYS-18	The IFS shall provide structural integrity during all predefined missions in its entire lifetime.	Gen	✓			13, 8.2.5
IFS-SYS-19	The unmodified aircraft that forms the basis for the IFS shall currently be in production.	Gen	✓			10
IFS-SYS-20	[DRV] The total costs of modification and certification from unmodified aircraft to IFS shall not exceed €800,000.	Gen	✓			12
IFS-SYS-21	[KEY] The operational costs of the IFS shall not exceed €4,000 per flight hour, based on a projected use of 750 hours per year.	Gen	✓			12.1
IFS-SYS-22	The IFS shall consist of a modified business aircraft.	Gen	✓			10
IFS-SYS-23	The IFS shall have an operational life span of 20 years.	Gen	✓			10
IFS-SYS-24	The average fuel use of the IFS shall not exceed 3.15×10^{-4} m^3/s in a flight with four approaches with descent from 3048 to 0 m, and test sections at 3048 m and 6096 m in which the IFS covers the speed envelope.	FD	✓			7.4
IFS-SYS-25	The computing components shall be operative for 10 years.	ESA	✓			9.10

IFS-SYS-26	A mid-life update shall be feasible.	Gen	✓			11.3
IFS-SYS-27	The aircraft shall be certifiable in Europe.	Gen	✓			12.1
IFS-SYS-08-AERO-01⋆	[DRV] The IFS shall be able to generate a side force induced acceleration of 0.5 m/s^2 at 61.7 m/s CAS.	AERO	✓			5.3
IFS-SYS-08-AERO-02⋆	[DRV] The IFS shall be able to reach an L/D ratio of 4.	AERO	✓			5.3.3
IFS-SYS-08-AERO-03	The IFS shall have a maximum lift coefficient of at least < *TBD* >.	FD			Dropped	7.4
IFS-SYS-08-AERO-04⋆	[DRV] The IFS shall be able to generate a direct ΔC_L of +/- 0.15.	AERO	✓			5.4
IFS-SYS-08-AERO-05	The IFS shall be able to generate a direct ΔC_D of < *TBD* >.	FD			Dropped	7.4
IFS-SYS-08-AERO-06	The IFS shall have a maximum roll rate of at least < *TBD* > deg/s.	FD			Dropped	7.4
IFS-SYS-08-AERO-07	The IFS shall have a maximum pitch rate of at least < *TBD* > deg/s.	FD			Dropped	7.4
IFS-SYS-08-AERO-08	The IFS shall have a maximum yaw rate of at least < *TBD* > deg/s.	FD			Dropped	7.4
IFS-SYS-08-AERO-09	The IFS shall have a maximum roll acceleration of at least < *TBD* > deg/s^2.	FD			Dropped	7.4
IFS-SYS-08-AERO-10	The IFS shall have a maximum pitch acceleration of at least < *TBD* > deg/s^2.	FD			Dropped	7.4
IFS-SYS-08-AERO-11	The IFS shall have a maximum yaw acceleration of at least < *TBD* > deg/s^2.	FD			Dropped	7.4
IFS-SYS-08-AERO-12	The IFS shall have a maximum turn rate of at least < *TBD* > deg/s.	FD			Dropped	7.4
IFS-SYS-08-AERO-13	The IFS shall have a maximum forward acceleration of at least < *TBD* > m/s^2.	FD			Dropped	7.4
IFS-SYS-01-PROP-01	The propulsion system of the IFS shall be able to provide a thrust that is at least equal to the thrust of the base aircraft.	ESA	✓			9.9
IFS-SYS-18-STRUCT-01	The structure of the IFS shall be able to withstand a load factor of 4.5 g_0.	STRUCT	✓			8.4
IFS-SYS-18-STRUCT-02	All installed control equipment of the IFS should be able to withstand their respective loading case in any configuration.	ESA	✓			9.5
IFS-SYS-15-SENS-01	The sensors subsystem shall measure < *TBD* > air data.	ESA			Dropped	9.7
IFS-SYS-15-SENS-01-A	The sensor subsystem shall measure the angle of attack.	ESA	✓			9.7
IFS-SYS-15-SENS-01-B	The sensor subsystem shall measure the angle of side slip.	ESA	✓			9.7
IFS-SYS-15-SENS-01-C	The sensor subsystem shall measure the velocity.	ESA	✓			9.7
IFS-SYS-15-SENS-01-D	The sensor subsystem shall measure the static pressure.	ESA	✓			9.7
IFS-SYS-15-SENS-01-F	The sensor subsystem shall measure the impact pressure.	ESA	✓			9.7
IFS-SYS-15-SENS-01-G	The sensor subsystem shall measure the attitude rate.	ESA	✓			9.7
IFS-SYS-15-SENS-01-H	The sensor subsystem shall measure the temperature.	ESA	✓			9.7
IFS-SYS-15-SENS-02	The sensors subsystem shall measure < *TBD* > the state of the IFS.	ESA			Dropped	9.7

IFS-SYS-15-SENS-02-A:	The sensor subsystem shall measure the pitch attitude.	ESA	✓			9.7
IFS-SYS-15-SENS-02-B:	The sensor subsystem shall measure the roll attitude.	ESA	✓			9.7
IFS-SYS-15-SENS-02-C:	The sensor subsystem shall measure the yaw attitude.	ESA	✓			9.7
IFS-SYS-15-SENS-02-D:	The sensor subsystem shall measure the pitch rate.	ESA	✓			9.7
IFS-SYS-15-SENS-02-E:	The sensor subsystem shall measure the roll rate.	ESA	✓			9.7
IFS-SYS-15-SENS-02-F:	The sensor subsystem shall measure the yaw rate.	ESA	✓			9.7
IFS-SYS-15-SENS-02-G:	The sensor subsystem shall measure the longitudinal acceleration.	ESA	✓			9.7
IFS-SYS-15-SENS-02-H:	The sensor subsystem shall measure the lateral acceleration.	ESA	✓			9.7
IFS-SYS-15-SENS-02-I:	The sensor subsystem shall measure the vertical acceleration.	ESA	✓			9.7
IFS-SYS-15-SENS-03	The sensors subsystem shall measure < *TBD* > control forces.	ESA			Dropped	9.7
IFS-SYS-15-SENS-03-A:	The sensor subsystem shall measure the elevator deflections.	ESA	✓			9.7
IFS-SYS-15-SENS-03-B:	The sensor subsystem shall measure the aileron deflections.	ESA	✓			9.7
IFS-SYS-15-SENS-03-C:	The sensor subsystem shall measure the rudder deflections.	ESA	✓			9.7
IFS-SYS-15-SENS-03-D:	The sensor subsystem shall measure the flap deflections.	ESA	✓			9.7
IFS-SYS-15-SENS-03-E:	The sensor subsystem shall measure the spoiler deflections.	ESA	✓			9.7
IFS-SYS-15-SENS-03-F:	The sensor subsystem shall measure the upper wing deflections.	ESA	✓			9.7
IFS-SYS-15-SENS-03-G:	The sensor subsystem shall measure the side wing deflections.	ESA	✓			9.7
IFS-SYS-15-SENS-04	The < *TBD* > sensors shall have an accuracy of < *TBD* >.	ESA			Dropped	9.7
IFS-SYS-09-SENS-05	The elevator actuator shall have a maximum error of < *TBD* > deg.	ESA			Dropped	9.8
IFS-SYS-09-SENS-06	The aileron actuator shall have a maximum error of < *TBD* > deg.	ESA			Dropped	9.8
IFS-SYS-09-SENS-07	The rudder actuator shall have a maximum error of < *TBD* > deg.	ESA			Dropped	9.8
IFS-SYS-09-SENS-08	The throttle actuator shall have a maximum error of < *TBD* > %.	ESA			Dropped	9.8
IFS-SYS-10-EXP-01⋆	[DRV] The IFS shall include a control-loaded side stick or center stick.	ESA	✓			9.5
IFS-SYS-10-EXP-02	The control-loaded stick shall be able to provide a force feedback of at least 200 N.	ESA	✓			9.5
IFS-SYS-10-EXP-03	The control-loaded pedals shall be able to provide a force feedback of at least 400 N.	ESA	✓			9.5
IFS-SYS-10-EXP-04⋆	The IFS shall include a set of primary flight displays.	ESA	✓			9.3
IFS-SYS-10-EXP-05⋆	The IFS computer shall be able to operate the IFS' drag devices.	ESA	✓			9.3
IFS-SYS-10-EXP-06⋆	The IFS computer shall be able to operate the IFS' side force devices.	ESA	✓			9.3

IFS-SYS-10-EXP-07⋆	The IFS computer shall be able to operate the IFS' thrust.	ESA			Droppped	9.3
IFS-SYS-10-EXP-08⋆	The IFS computer shall be able to operate the IFS' control surfaces.	ESA	✓			9.3
IFS-SYS-10-EXP-09	The IFS computer shall have a programmable flight control system.	ESA	✓			9.1
IFS-SYS-10-EXP-10	The IFS computer shall acquire data at a frequency of 200 Hz.	ESA	✓			9.7
IFS-SYS-11-TEST-01	The flight test engineer station shall have monitoring facilities.	ESA	✓			9.3
IFS-SYS-11-TEST-02	The flight test engineer station shall acquire data at a frequency of 200 Hz.	ESA	✓			9.7
IFS-SYS-11-TEST-03	The flight test engineer station shall have a data storage of 1 TB.	ESA	✓			9.3
IFS-SYS-11-TEST-04	The flight test engineer shall be able to change the IFS settings at any time.	ESA	✓			9.3
IFS-SYS-17-SAFE-01⋆	The safety pilot shall be able to manually take over control at any moment during flight.	ESA	✓			9.3
IFS-SYS-17-SAFE-02	The flight envelope of the simulated system shall have a safety margin of 5% with respect to the flight envelope of the actual aircraft.	ESA	✓			9.5
IFS-SYS-17-SAFE-03	The safety pilot shall automatically take over when the boundaries of the flight envelope of the simulated system are exceeded.	ESA	✓			9.5
IFS-SYS-17-SAFE-04	The aircraft shall give visual feedback when the aircraft is within a 10% margin of the edge of the flight envelope of the simulated system.	ESA	✓			9.5
IFS-SYS-17-SAFE-05	The aircraft shall give visual feedback if the safety pilot takes over the control of the aircraft.	ESA	✓			9.3
IFS-SYS-17-SAFE-06	The experimental pilot shall be able to take control of the aircraft when the safety pilot is incapacitated.	ESA	✓			9.5

16 | Future Work

Having arrived at the end of the project, there are still some parts of the design established for the IFS that will have to be worked out in more detail in a future continuation of the design process [43]. As can be seen in the Project Design and Development logic presented in section 11.4, this work is also accounted for in the post-DSE plan. This chapter will detail the work meant in 'Phase 1 - Wrap-up Final Design'. First, all of the technical parts are explained in section 16.1. The chapter concludes with some general recommendations on non-technical aspects of the IFS design in section 16.2.

16.1 Department recommendations

Aerodynamic design

As mentioned in the conclusion of the chapter on the aerodynamic design in section 6.5, there were still some issues with the stability derivatives that were calculated for the IFS design. These issues can be solved by a more in-depth aerodynamic analysis within the programs currently used (AVL), but this analysis will most likely have to be expanded with a detailed CFD analysis of the IFS. Since the stability derivatives directly influenced the accuracy and level of detail that the stability analysis could achieve, this design aspect of the design can also be improved upon in later design stages. This is explained hereafter.

Stability analysis

As stated in subsection 7.5.5 and section 7.4, the stability analysis showed that the IFS is laterally unstable. However, due to the uncertainty in the aerodynamic stability derivatives that was mentioned above this conclusion could be false. Therefore, the stability analysis will have to be redone after the aerodynamic analysis is refined. Additionally, although the simulator is capable of achieving a low L/D the IFS is not completely designed for re-entry missions. In order to complete the design for re-entry missions, all of its handling, stability and control parameters will have to be explored.

Structural design

Although a detailed design for the wingbox was presented in chapter 8, there were still a few aspects of the structural design remaining that should be researched further:

- **Flap design:** a full design is presented for the wingbox of the non flapped part of the chord. However, the flap itself will also have to resist some loads. Therefore, a more accurate description of this part of the modifications would be desirable.
- **Integration:** due to the time constraint of the project, the structural integration of all of the modifications was not explored in the DSE. This should be done for elements like the engine and wing mounts (including hinges), the wiring through the wingbox and the attachment of the drag parachute.
- **Analysis tools:** instead of the own coding, proven FEM tools could be used to perform structural checks. This includes incorporating a more detailed load case after the more detailed aerodynamic analysis is performed.
- **Maintenance:** it could be that cut outs have to be made in the wingbox for the maintenance of actuators, or that an alternate engine maintenance hatch has to be installed because of the engine mount of the upper wing. These modifications for maintenance will have to be designed before production starts.

Sensors and actuator design

Future improvements in this department mostly involves not buying off-the-shelf products but designing tailored actuation and sensing solution that are both optimized for weight and controllability.

16.2 General recommendations

As mentioned in section 11.4, a more accurate cost estimate should be made during future designing. The cost estimates in chapter 12 can be used as a basis for this. The way to improve the estimates would be to contact the manufacturers directly and implement the values retrieved from their quotes. Also, a pre-mortem analysis should be done to expand on the risks already mentioned in chapter 13.

17 | Conclusion

The purpose of this project was to present a detailed design for a six degrees of freedom, jet powered In-Flight Simulator and show to the stakeholders that such a design is indeed feasible. Currently, simulation options are limited to six degrees of freedom simulations for propeller powered and five degrees of freedom for jet powered aircraft simulations. An IFS being able to provide six degrees of freedom variable stability in a larger flight envelope would generate a lot of interest from parties such as large aircraft manufacturers. For instance, they will be able to train test pilots much faster and thereby increasing their cost effectiveness.

A market analysis was made in advance to confirm if the development of such a IFS would be profitable. From this analysis followed that the design will be able to serve both as a platform to test aircraft handling characteristics and for variable stability training of test pilots. A list of requirements was created that, in case they are met, ensured the IFS to be a success. From that point an extensive analysis of the design was made, which ultimately resulted in the parameters and characteristics stated in this report describing the modifications to the Embraer Phenom 300. Both the Phenom 300 and the final concept, called the IFSix, were chosen by performing an in-depth trade-off in an earlier phase of the project. In the following phases the concept was further worked out into the final design. Not only the technical specifications were generated, but the entire life span of the IFS was thought through in all its aspects.

After analyzing the design options, it was decided to add a vertical and a horizontal wing to the aircraft along with a drag parachute in order to mimic other aircraft as well as contribute to the ability of reaching a low lift-over-drag ratio for simulating re-entry vehicles. These two wings formed the basis of the so called boxwing on which flaps were added to provide direct lift, side force and drag control. The boxwing has a total mass of 92.3 kg, a span of 3.54 meters on each side of the fuselage and a negative sweep angle of -28 degrees. The wings will have an slender symmetrical airfoil since the system must be able to generate forces in all possible directions. The wings will be fitted with simple flaps in order to have fast actuation times and will have a deflection of 20 degrees in both directions. Hinges will be used to attach the boxwing to the engine nacelle and the wingbox of the main wing. The drag chute will have an area of 3.85 m^2, has a mass of 6.5 kg and will be deployed using a quick release system. Also large changes to the way the aircraft is controlled have to be made. The right side of the cockpit of the IFS will contain a test pilot station, equipped with force feedback controls. In the cabin a test engineer will be placed, equipped with a simulation control panel and monitoring screens. These display both data from additional sensors and ACS data. A SCS will run the simulation and includes a safety trip system to restore the unmodified controls of the safety pilot in case of failure. An overview of the whole system is given using diagrams on hardware, software, data handling and the electric systems. All these results are obtained form calculation methods that were verified and validated to the furthest extent as possible.

For this final design it was assessed how viable IFS will be and if it can be really used for operations after all if major risks are mitigated. It turned out that the risks can be fully mitigated or reduced to an acceptable level, making it safe to use. The IFS will be easy to operate with low maintenance effort required. From a market point of view 3 IFSix's are expected to be sold by the developer, with an estimated profit of €3.2 million. Exploiting the IFS is also expected to be viable, with an operating cost far below the expected return.

Having met the requirements stated in the compliance matrix from a technical, simulation and operating point of view, the design has achieved a high potential on the simulation market. Moreover, sustainability has been an important point of attention throughout the designing phase, since society is asking for environmentally friendly products and solutions. This will enable customers to use the IFS without unnecessary harm to the environment. The IFS has more capabilities then the current in flight simulators while being cheaper to operate and maintain. Therefore it is concluded that the IFSix will be the most advanced and cost efficient In-Flight Simulator on the market.

A | Stability and Control Derivatives

Table A.1: Symmetric and asymmetric S&C derivatives for the Cessna Ce500 'Citation' at cruise [7].

V	=	59.5 m/sec	m	=	4547.8 kg	$\bar{c}$	=	2.022 m
S	=	24.2 m^2	l_h	=	5.5 m	μ_c	=	102.7
K_Y^2	=	0.980	x_{cg}	=	0.30$\bar{c}$			
C_{X_0}	=	0	C_{Z_0}	=	-1.1360			
C_{X_u}	=	-0.2199	C_{Z_u}	=	-2.2720	C_{m_u}	=	0
C_{X_α}	=	0.4653	C_{Z_α}	=	-5.1600	C_{m_α}	=	-0.4300
$C_{X_{\dot{\alpha}}}$	=	0	$C_{Z_{\dot{\alpha}}}$	=	-1.4300	$C_{m_{\dot{\alpha}}}$	=	-3.7000
C_{X_q}	=	0	C_{Z_q}	=	-3.8600	C_{m_q}	=	-7.0400
$C_{X_{\delta_e}}$	=	0	$C_{Z_{\delta_e}}$	=	-0.6238	$C_{m_{\delta_e}}$	=	-1.5530
b	=	13.36 m	C_L	=	1.1360	μ_b	=	15.5
K_X^2	=	0.012	K_Z^2	=	0.037	K_{XZ}	=	0.002
C_{Y_β}	=	-0.9896	C_{l_β}	=	-0.0772	C_{n_β}	=	0.1638
C_{Y_p}	=	-0.0870	C_{l_p}	=	-0.3444	C_{n_p}	=	-0.0108
C_{Y_r}	=	0.4300	C_{l_r}	=	0.2800	C_{n_r}	=	-0.1930
$C_{Y_{\delta_a}}$	=	0	$C_{l_{\delta_a}}$	=	-0.2349	$C_{n_{\delta_a}}$	=	0.0286
$C_{Y_{\delta_r}}$	=	0.3037	$C_{l_{\delta_r}}$	=	0.0286	$C_{n_{\delta_r}}$	=	-0.1261

Table A.2: Symmetric and asymmetric S&C derivatives for the Embraer Phenom 300 at Design Point 1.

V	=	61.7 m/sec	m	=	8150 kg	$\bar{c}$	= 1.95 m
S	=	28.5 m^2	l_h	=	7.74 m	μ_c	= 119.7
K_Y^2	=	<tbd>	x_{cg}	=	0.36$\bar{c}$	q_∞	= 2331.7 Pa
C_{X_0}	=	<tbd>	C_{Z_0}	=	<tbd>		
C_{X_u}	=	0.023636	C_{Z_u}	=	-1.464240	C_{m_u}	= -1.049868
C_{X_α}	=	<tbd>	C_{Z_α}	=	<tbd>	C_{m_α}	= -4.655362
$C_{X_{\dot{\alpha}}}$	=	<tbd>	$C_{Z_{\dot{\alpha}}}$	=	<tbd>	$C_{m_{\dot{\alpha}}}$	= <tbd>
C_{X_q}	=	3.143705	C_{Z_q}	=	-16.495266	C_{m_q}	= -36.019611
$C_{X_{\delta_e}}$	=	0.000720	$C_{Z_{\delta_e}}$	=	-0.014299	$C_{m_{\delta_e}}$	= -0.053637
b	=	15.91 m	C_L	=	1.203	μ_b	= 14.7
K_X^2	=	<tbd>	K_Z^2	=	<tbd>	K_{XZ}	= <tbd>
C_{Y_β}	=	-0.368513	C_{l_β}	=	-0.368513	C_{n_β}	= 0.114778
C_{Y_p}	=	0.046947	C_{l_p}	=	-0.486576	C_{n_p}	= -0.175343
C_{Y_r}	=	0.346903	C_{l_r}	=	0.280238	C_{n_r}	= -0.085633
$C_{Y_{\delta_a}}$	=	-0.000833	$C_{l_{\delta_a}}$	=	-0.002485	$C_{n_{\delta_a}}$	= -0.000053
$C_{Y_{\delta_r}}$	=	0.003113	$C_{l_{\delta_r}}$	=	0.000555	$C_{n_{\delta_r}}$	= -0.001189

Table A.3: Symmetric and asymmetric S&C derivatives for the IFS at Design Point 1.

V	=	61.7 m/sec	m	=	8150 kg	$\bar{c}$	= 1.80 m
S	=	37.48 m^2	l_h	=	7.74 m	μ_c	= 98.6
K_Y^2	=	<tbd>	x_{cg}	=	0.38$\bar{c}$	q_∞	= 2331.7 Pa
C_{X_0}	=	<tbd>	C_{Z_0}	=	<tbd>		
C_{X_u}	=	0.011788	C_{Z_u}	=	-1.295419	C_{m_u}	= -0.608433
C_{X_α}	=	<tbd>	C_{Z_α}	=	<tbd>	C_{m_α}	= -3.013017
$C_{X_{\dot{\alpha}}}$	=	<tbd>	$C_{Z_{\dot{\alpha}}}$	=	<tbd>	$C_{m_{\dot{\alpha}}}$	= <tbd>
C_{X_q}	=	2.896320	C_{Z_q}	=	-13.243459	C_{m_q}	= -28.518723
$C_{X_{\delta_e}}$	=	0.000900	$C_{Z_{\delta_e}}$	=	-0.010756	$C_{m_{\delta_e}}$	= -0.040797
b	=	15.91 m	C_L	=	1.203	μ_b	= 11.2
K_X^2	=	<tbd>	K_Z^2	=	<tbd>	K_{XZ}	= <tbd>
C_{Y_β}	=	-0.523167	C_{l_β}	=	-0.245348	C_{n_β}	= 0.105011
C_{Y_p}	=	0.170643	C_{l_p}	=	-0.552195	C_{n_p}	= -0.270083
C_{Y_r}	=	0.381677	C_{l_r}	=	0.287163	C_{n_r}	= -0.073291
$C_{Y_{\delta_a}}$	=	-0.000081	$C_{l_{\delta_a}}$	=	-0.002192	$C_{n_{\delta_a}}$	= -0.000264
$C_{Y_{\delta_r}}$	=	0.002086	$C_{l_{\delta_r}}$	=	0.000420	$C_{n_{\delta_r}}$	= -0.000836

B | Structural Loading Diagrams

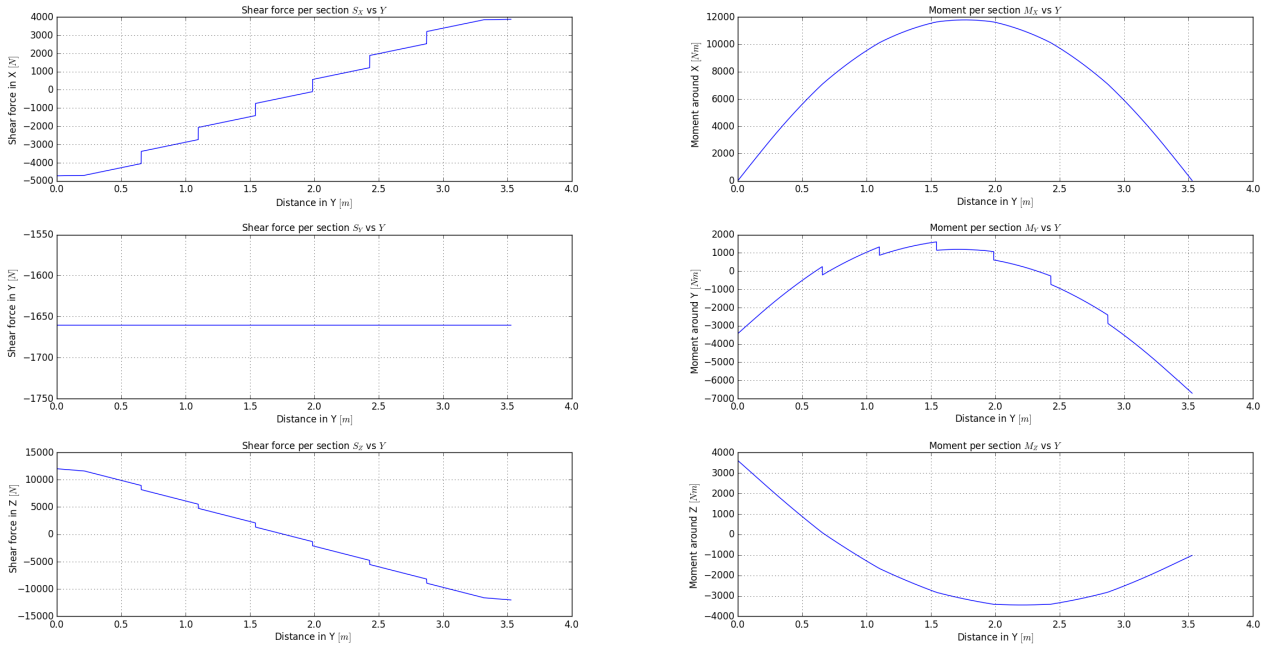

(a) Upper wing load diagrams.

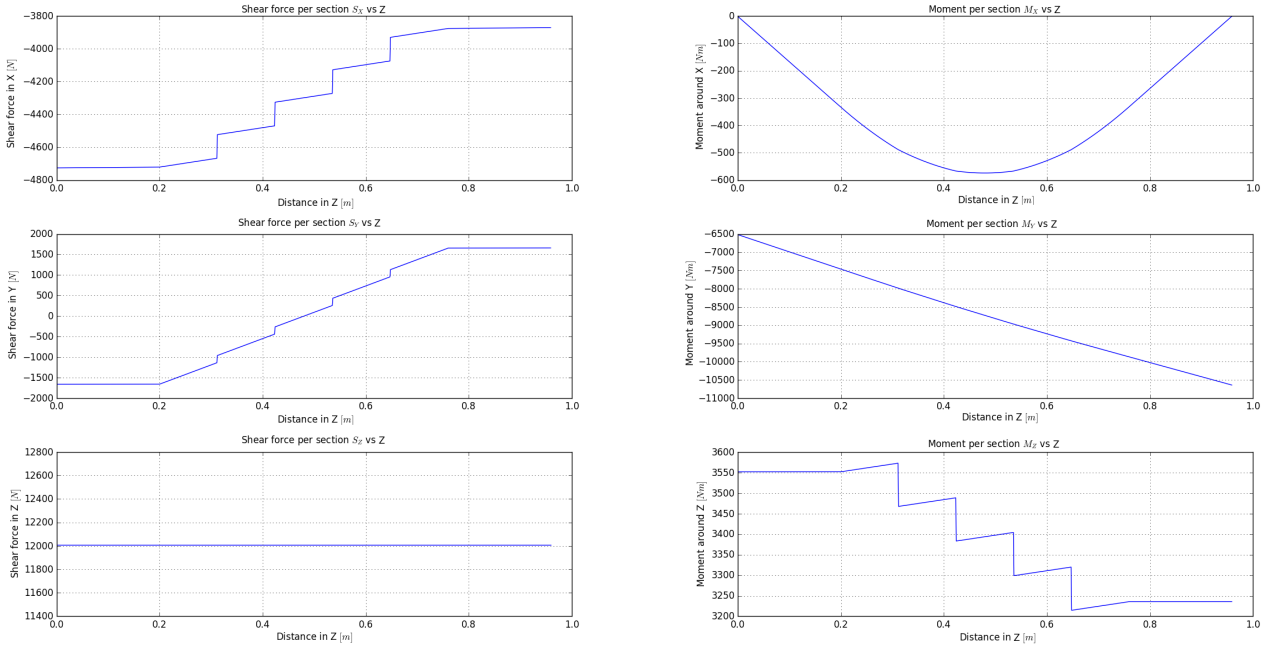

(b) Vertical wing load diagrams.

Figure B.1: Load diagrams for the 1st load case (upper wing in compression, vertical wing in tension).

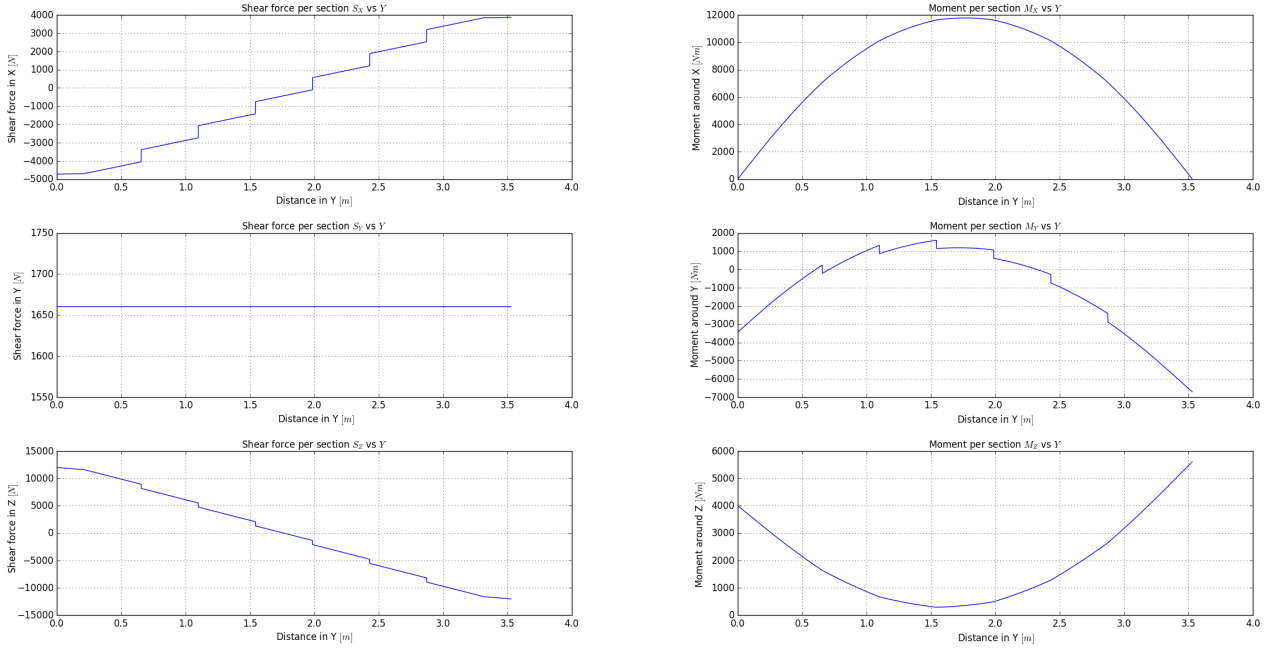

(a) Upper wing load diagrams.

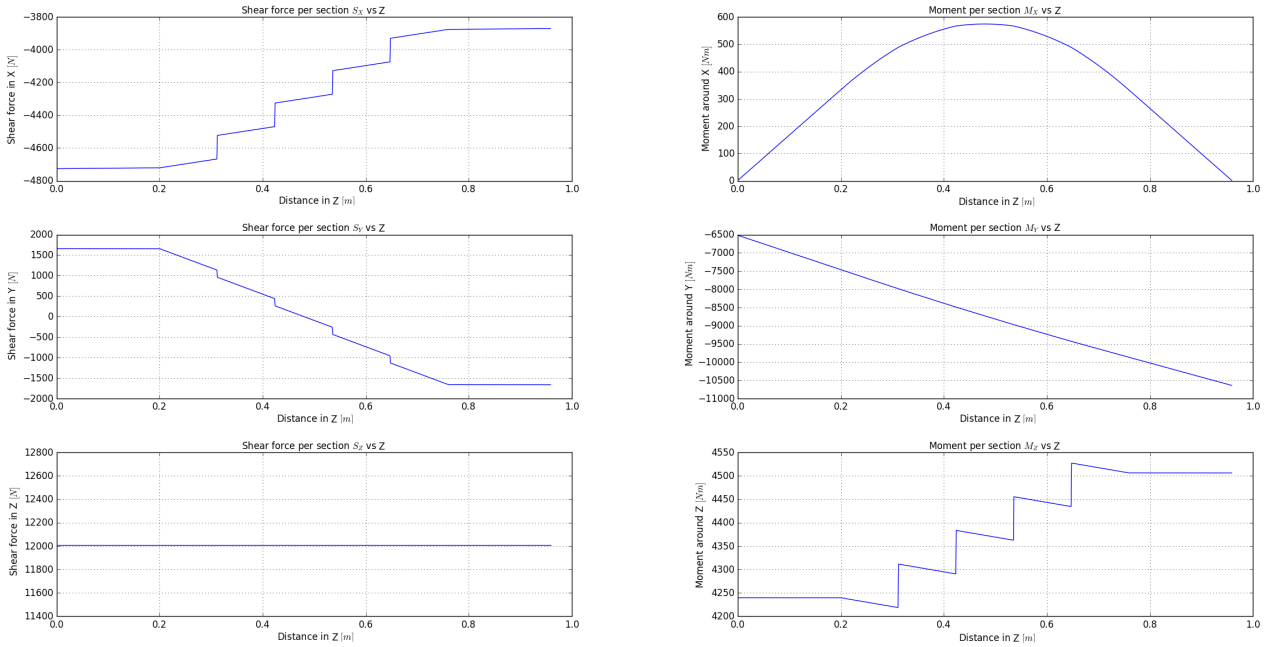

(b) Vertical wing load diagrams.

Figure B.2: Load diagrams for the 2nd load case (upper wing in tension, vertical wing in tension).

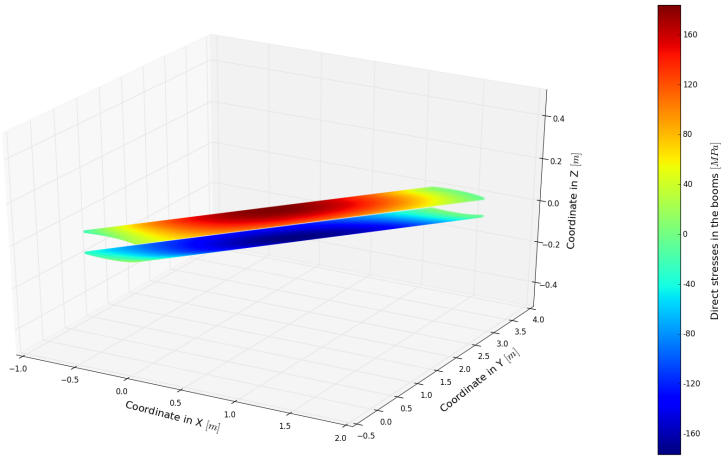

(a) Upper wing direct stress diagram.

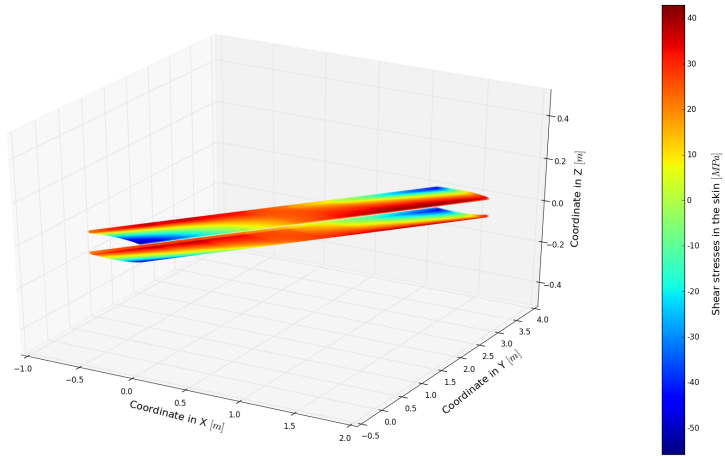

(b) Upper wing shear stress diagram.

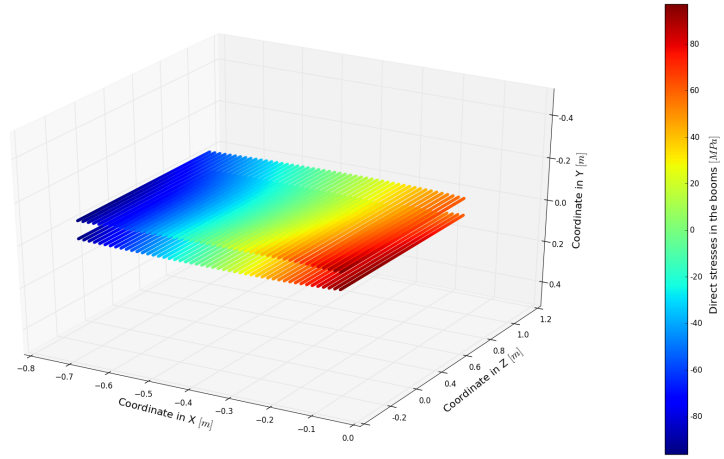

(c) Vertical wing direct stress diagram.

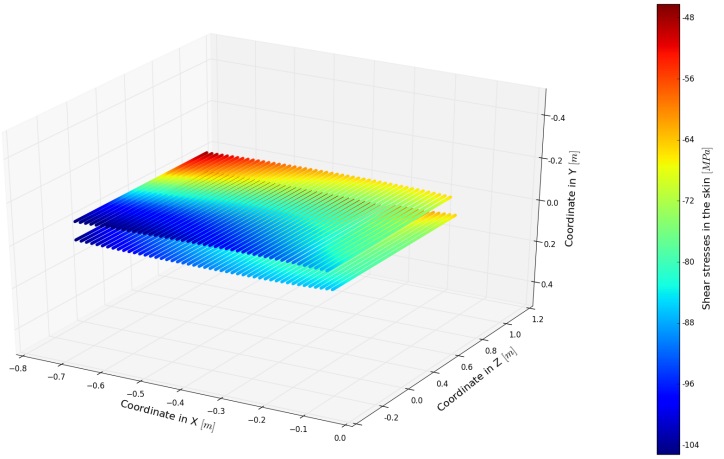

(d) Vertical wing shear stress diagram.

Figure B.3: Direct and shear stress diagrams for the 1st load case (upper wing in compression, vertical wing in tension).

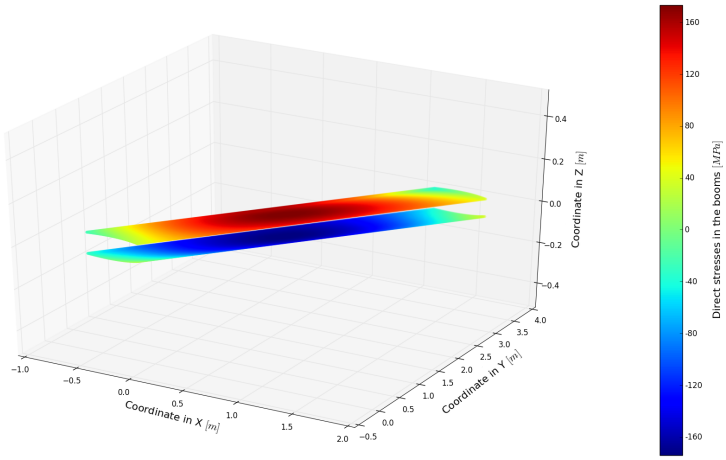

(a) Upper wing direct stress diagram.

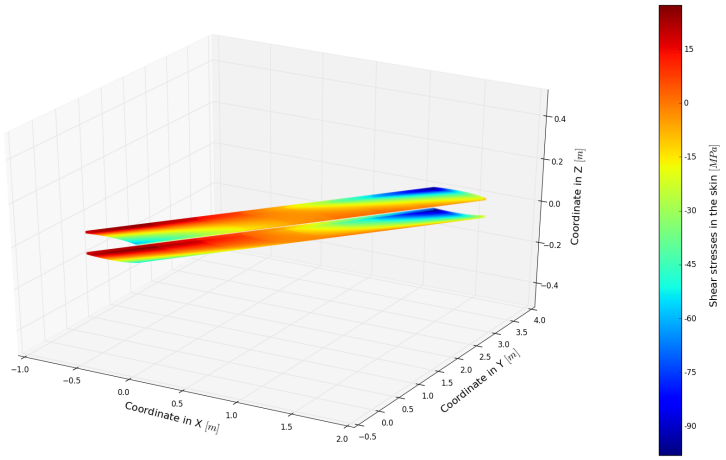

(b) Upper wing shear stress diagram.

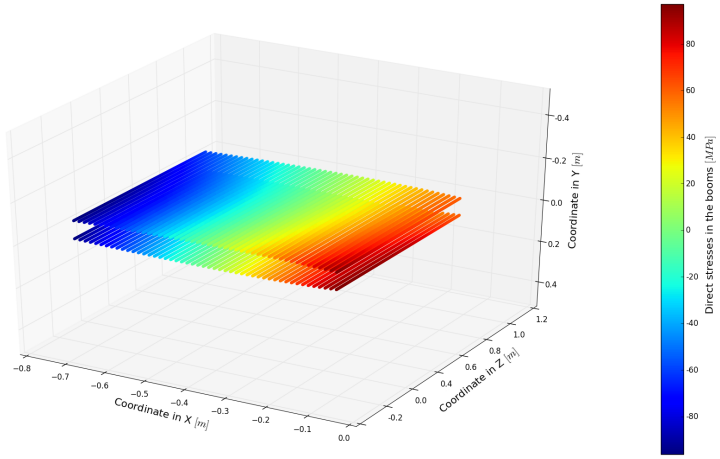

(c) Vertical wing direct stress diagram.

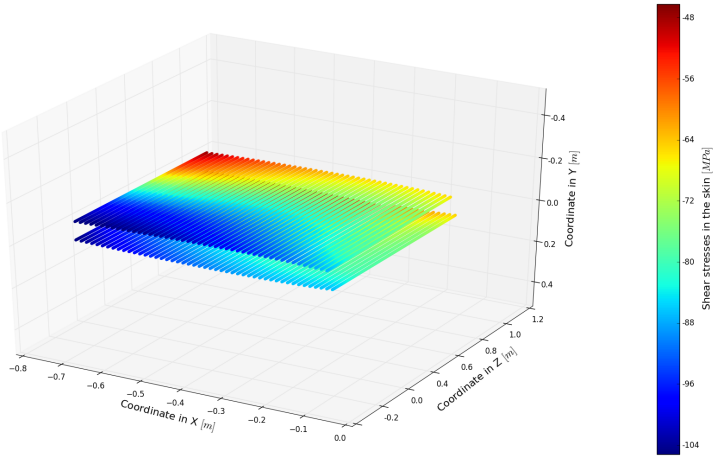

(d) Vertical wing shear stress diagram.

Figure B.4: Direct and shear stress diagrams for the 2nd load case (upper wing in tension, vertical wing in tension).

C | Work Distribution

This appendix provides an overview of the work distribution at section level, as presented in Table C.1. Members responsible for a section are denoted by "R". If one is responsible the team member(s) did the writing of the section and made the calculations, drawings, figures and/or tables if applicable. Members who contributed to a section are denoted by "C". These members were involved in the generation of the section and its content, but were not involved in the whole process. For example, when someone only wrote a subsection of the section, this section will still be checked by the member(s) who is/are responsible. Note that this distribution is of the reporting work only. Tasks such as Quality Control is not included in this distribution.

Table C.1: Work distribution matrix.

Chapter	Section	Tijmen	Jesse	Leo	Menno	Liam	Wessel	Alessandro	Karsten	Roderick	Vincent
Preface	n.a.				R						
Summary	n.a.			C			R				
Introduction	n.a.						R				
Market Analysis	2.1		C								R
	2.2		C								R
	2.3		C								R
	2.4		C								R
	2.5		C								R
Sustainable Development Strategy	3.1		R			C					
	3.2		R								
	3.3		R								
Design Principles	4.1		C						R		
	4.2			C	R	R		C			
	4.3			C	R	R		C			
	4.4			R	R						
Boxwing Design	5.1				R					C	
	5.2				R					C	
	5.3				R					C	
	5.4				R					C	
Aerodynamic Analysis	6.1				C					R	
	6.2				C					R	
	6.3				C					R	
	6.4				C					R	
	6.5				C					R	
Stability & Control Analysis	7.1		R					C			C
	7.2							C			R
	7.3		R					C			
	7.4							R			
	7.5							R			
	7.6							R			
Structural Analysis	8.1						R		R		
	8.2						R		R		
	8.3						R		R		
	8.4						C		R		
	8.5						R		C		

Chapter	Section	Tijmen	Jesse	Leo	Menno	Liam	Wessel	Alessandro	Karsten	Roderick	Vincent
Control and System Layout	9.1	R		C							
	9.2	R		R							
	9.3	R		C							
	9.4	R		R							
	9.5	R		R							
	9.6	R		R							
	9.7	R		R							
	9.8	C				R					
	9.9	C		R							
	9.10	C		R							
System Characteristics	10.1								R	C	
	10.2								C	R	
Operations and Logistics	11.1		C								R
	11.2										R
	11.3	R									
	11.4				R						
Cost Analysis	12.1								C	R	
	12.2								R	C	
Risk Assessment	13.1										R
	13.2					C					R
	13.3					R					
Sensitivity Analysis	14.1		R								
	14.2		R								
	14.3		R								
Requirements' Compliance	15	C		R				C	C	C	
Future Work	16				C		C	C	R	C	
Conclusion	17						R				C
Stability & Control Derivatives	A									R	
Structural Loading Diagrams	B						R		R		
Work Distribution	C	C	C	C	C	C	C	C	C	C	C

Bibliography

[1] I. Abbott, A. Von Doenhoff, *Theory of Wing Sections*. Dover Publications, 1959, p.328.

[2] J. C. Sivells, "Experimental and calculated characteristics of three naca 64-210 and 65-210 airfoil sections," tech. rep., National Advisory Committee for Aeronautics, August 1947. No. 1422.

[3] G. La Rocca, *AE3211-I Systems Engineering and Aerospace Design, Requirement Analysis and Design principles for A/C stability & control (Part 1)*. TU Delft, 2016.

[4] M. V. Cook, *Flight Dynamics Principles*. Arnold, 1997, pp. 55-79.

[5] C. H. D. Hanke, "Active sidestick technology – a means for improving situational awareness," *Éditions scientifiques et médicales Elsevier SAS*, vol. 3, p. 5, 1999.

[6] N. C. Weingarten, "History of in-flight simulation & flying qualities research at Calspan," in *AIAA Atmospheric Flight Mechanics Conference*, vol. 42, (Austin, TX), August 2003.

[7] J. A. Mulder et al., *AE3202 Lecture Notes – Flight Dynamics*. TU Delft, 2013.

[8] T. J. P. Bregt et al., *DSE In-Flight Simulator - Project Plan*. TU Delft, 2016.

[9] T. J. P. Bregt et al., *DSE In-Flight Simulator - Baseline Report*. TU Delft, 2016.

[10] T. J. P. Bregt et al., *DSE In-Flight Simulator - Mid-term Report*. TU Delft, 2016.

[11] J. Howarth et al., *Journal of Cleaner Production*. Elsevier, 2014.

[12] G. Villalba et al., *Ecological Economics*. Elsevier, 2004.

[13] M. H. Sadraey, *Aircraft Design: A Systems Engineering Approach*. John Wiley & Sons, 1st ed., 2012.

[14] D. Steenhuizen, *AE2111-II Aerospace Design and Systems Engineering Elements II - Wing Design*. TU Delft, 2016, p. 44.

[15] E. Torenbeek, *Synthesis of Subsonic Airplane Design*. Kluwer Academic Publishers, 1982, pp.284, 309.

[16] B. Malone, W. Mason, "Multidisciplinary optimization in aircraft design using analytic technology models," *Journal of Aircraft*, vol. 32, 1995.

[17] R. Shevell, F. Bayan, *Development of a method for predicting the drag divergence Mach number and the drag due to compressibility for conventional and supercritical wings*. Stanford, CA, Stanford University, Department of Aeronautics and Astronautics, 1980.

[18] P. Rudolph, *High-Lift Sytems on Commercial Subsonic Airliners*. NASA, 1996.

[19] J. Utreja, "Prediction of the drag coefficient of a 20 degree conical ribbon parachute," *Journal of Spacecraft and Rockets*, vol. 14, 1977.

[20] S. C. Hulteen, "Spiral reefed variable drag parachute," *U.S. Army Patent 3642237 A*, Feb 15, 1972.

[21] E. Obert, *Aerodynamic Design of Transport Aircraft*. IOS Press, 2009.

[22] M. Drela et al., *AVL 3.30 User Primer*. MIT, 2002.

[23] J. D. Anderson, *Fundamentals of Aerodynamics*. McGraw-Hill, 1991, p.26.

[24] R. C. J.J. Bertins, *Aerodynamics for Engineers*. Prentice Hall, fifth edition ed., 2009.

[25] Embraer S.A., *Phenom 300 - EASA - Airplane Flight Manual*. Embraer Technical Publications, 2010.

[26] J. Roskam, *Airplane Flight Dynamics and Automatic Flight Controls*. Design, Analysis and Research Corporation, 1982.

[27] A. in't Veld , *AE3212-I – Aerospace Flight Dynamics and Simulation, Part 3: Static stabililty - course slides*. TU Delft, 2016.

[28] J. Gibson, "Development of a design methodology for handling qualities excellence in fly by wire aircraft," 1999.

[29] W. D. Callister, *Materials Science and Engineering*. John Wiley & Sons, 2014.

[30] T. H. G. Megson, *Aircraft Structures for Engineering Students*. Butterworth-Heinemann, 2012, p.284, p.302, p.309.

[31] R. Monaghan, "A review and assessment of various formulae for turbulent skin friction in compressible flow," tech. rep., 1953, p.11.

[32] R. Hibbeler, *Mechanics of Materials*. Prentice Hall, seventh edition ed., 2008.

[33] D. Rees, *Mechanics of Optimal Structural Design: Minimum Weight Structures*. John Wiley & Sons, Ltd, 2009, p.527.

[34] R. M. Rivello, *Theory and analysis of flight structures*. New York: McGraw-Hill, 1969.

[35] G. D. Vries, "Safeguards against flutter of airplanes," tech. rep., National Advisory Committee for Aeronautics, August 1956, p.2. No. 1423.

[36] D. L. Edwards, *Flight Standardization Board Report EMB-505*. US Federal Aviation Authority, 2013.

[37] Embraer S.A., *EMB-505 Ground Handling & Service Handbook*. Embraer Technical Publications, 2011.

[38] J.R. Cannon, F.D. Richey, *Practical Applications in Business Aviation Management*. Government Institutes, 2012.

[39] D. P. Raymer, *Aircraft Design - A Conceptual Approach*. AIAA, 1992, pp. 263-280, 311, 395-456.

[40] The European Commission, *Commission Regulation (EU) No. 319-2014*. Official Journal of the European Union, 2014.

[41] S. Castagne et al., *A generic tool for cost estimating in aircraft design*. Centre of Excellence for Integrated Aircraft Technology (CEIAT), 2012.

[42] R. Curran, W. Verhagen, "System Engineering and Aerospace Design - Risk Management & Reliability Engineering," pp. 19–34, 2016.

[43] R. T. H. et al., *Requirements for Future Research in Flight Simulation Training: Guidance Based on a Meta-Analytic Review*. The International Journal of Aviation Psychology, 1992.